



Asphalt Research Consortium

Quarterly Technical Progress Report October 31 – December 31, 2009

February 2010

Prepared for
Federal Highway Administration
Contract No. DTFH61-07-H-00009

By
Western Research Institute
Texas A&M University
University of Wisconsin-Madison
University of Nevada-Reno
Advanced Asphalt Technologies

www.westernresearch.org
www.ARC.unr.edu

TABLE OF CONTENTS

INTRODUCTION	1
GENERAL CONSORTIUM ACTIVITIES	3
PROGRAM AREA: MOISTURE DAMAGE.....	5
Category M1: Adhesion.....	5
Category M2: Cohesion.....	14
Category M3: Aggregate Surface	24
Category M4: Modeling.....	33
Category M5: Moisture Damage Prediction System	35
PROGRAM AREA: FATIGUE.....	39
Category F1: Material and Mixture Properties	39
Category F2: Test Method Development.....	82
Category F3: Modeling.....	103
PROGRAM AREA: ENGINEERED MATERIALS.....	125
Category E1: Modeling.....	125
Category E2: Design Guidance.....	162
PROGRAM AREA: VEHICLE-PAVEMENT INTERACTION.....	187
Category VP1: Workshop.....	187
Category VP2: Design Guidance.....	187
Category VP3: Modeling.....	190
PROGRAM AREA: VALIDATION.....	199
Category V1: Field Validation.....	199
Category V2: Accelerated Pavement Testing.....	200
Category V3: R&D Validation	201
PROGRAM AREA: TECHNOLOGY DEVELOPMENT.....	215
PROGRAM AREA: TECHNOLOGY TRANSFER.....	217
Category TT1: Outreach and Databases	217

INTRODUCTION

This document is the Quarterly Report for the period of October 1 to December 31, 2009 for the Federal Highway Administration (FHWA) Contract DTFH61-07-H-00009, the Asphalt Research Consortium (ARC). The Consortium is coordinated by Western Research Institute with partners Texas A&M University, the University of Wisconsin-Madison, the University of Nevada Reno, and Advanced Asphalt Technologies.

The Quarterly Report is grouped into seven areas, Moisture Damage, Fatigue, Engineered Paving Materials, Vehicle-Pavement Interaction, Validation, Technology Development, and Technology Transfer. The format of the report is based upon the Research Work Plan that is grouped by Work Element and Subtask.

This Quarterly Report summarizes the work accomplishments, data, and analysis for the various Work Elements and Subtasks. This report is being presented in a summary form. The Quarter of October 1 to December 31, 2009 is third quarter of the Year 3 contract year. Reviewers may want to reference the Year 3 Work Plan and perhaps the Revised Year 2 Work Plan in order to obtain background information on specific areas of research. The more detailed information about the research such as approaches to test method development, data collection, and analyses will be reported in research publications as part of the deliverables. The Year 3 Work Plan and the Revised Year 2 Work Plan, as well as many other documents are posted on the ARC website, www.ARC.unr.edu.

The previous quarterly reports, Year 1, Revised Year 2, and Year 3 Work Plans, and other related documents and information about the Asphalt Research Consortium can be found at the ARC website, www.ARC.unr.edu.

SUPPORT OF FHWA AND DOT STRATEGIC GOALS

The Asphalt Research Consortium research is responsive to the needs of asphalt engineers and technologists, state DOT's, and supports the FHWA Strategic Goals and the Asphalt Pavement Road Map. More specifically, the research reported here supports the Strategic Goals of safety, mobility, and environmental stewardship. By addressing the causes of pavement failure and thus determining methods to improve asphalt pavement durability and longevity, this research will provide the motoring public with increased safety and mobility. The research directed at improved use of recycled asphalt pavement (RAP), warm mix asphalt, and cold mix asphalt supports the Strategic Goal of environmental stewardship.

GENERAL CONSORTIUM ACTIVITIES

PROGRESS THIS QUARTER

ARC members, Dr. Hussain Bahia, Dr. Elie Hajj, Dr. Peter Sebaaly, and Mr. Michael Harnsberger, attended the RAP Expert Task Group meeting in Seattle, Washington on December 16 & 17, 2009. ARC members presented an update on the construction of the RAP sections in Manitoba and the RAP research being conducted by the ARC.

ARC members Dr. Dallas Little, Dr. Hussain Bahia, Dr. Peter Sebaaly, Dr. Ramon Bonaquist, and Mr. Michael Harnsberger met with AOTR's Dr. Jack Youtcheff and Mr. Eric Weaver at Turner-Fairbank Highway Research Center on December 2, 2009 to discuss the preparation of the Year 4 Work Plan and the planned contract deliverables.

WORK PLANNED FOR NEXT QUARTER

Several ARC members are planning to attend and make presentations at the TRB Annual Meeting in Washington DC during the week of January 13, 2010. ARC members also participate on TRB committees.

A brief ARC advisory board meeting was planned for during the TRB week. The ARC Asphalt Microstructural Modeling team members Mr. Troy Pauli, Dr. Michael Greenfield, Dr. Linbing Wang, and Dr. Jeffrey Bullard planned a meeting during the TRB week to discuss project progress and work plans.

Several ARC members are planning to attend and make presentations at the Binder, Mix & Construction, and Fundamental Properties & Advanced Models ETG meetings in Irvine, California on February 22 – 26, 2010.

PROGRAM AREA: MOISTURE DAMAGE

CATEGORY M1: ADHESION

Work Element M1a: Affinity of Asphalt to Aggregate (UWM)

Work Done This Quarter

In this quarter, a modified procedure based on the Pneumatic Adhesion Tensile Testing Instrument (PATTI) to measure adhesion and cohesion in asphalt-aggregate systems was successfully implemented. The modified procedure can differentiate between the performance of different binder-aggregate interfaces. The effect of binder modifications can be clearly identified with the proposed PATTI procedure.

Also, the moisture susceptibility of the aggregate-binder interface was investigated by means of strain sweep tests in the Dynamic Shear Rheometer (DSR). The rheological properties of a small set of asphalt-aggregate interfaces before and after water conditioning were obtained. The test methodology in the DSR allows the research team to differentiate the susceptibility of aggregate/binder systems to moisture conditions. However, the experimental method poses a major issue in terms of testing time (i.e., seven hours to run one specimen). Although very time-consuming, the strain sweep methodology in the DSR can be used for validation of simplified methods to characterize asphalt-aggregate affinity such as the modified PATTI.

The strain sweep tests in the DSR are performed using a cored rock disk 25 mm in diameter and 5 mm thick as the bottom plate (i.e., substrate). The rock disk and the asphalt binder simulate the asphalt-aggregate interface in the asphalt mixture. In this test, a water cup, specially manufactured for the DSR, is used for water conditioning.

In order to monitor moisture effect on the aggregate-asphalt interface, rheological responses were measured using oscillatory loads with shear strains varying from 1% to 100% at a frequency of 1.6 Hz frequency (i.e., 10 rad/s) and 40 °C, for both dry and wet (using tap water) conditioning. The materials used for preliminary testing are listed in table M1a.1.

Table M1a.1. Materials used to evaluate moisture damage in aggregate-binder interface using the strain sweep DSR.

Mineral Surfaces	Granite
Asphalt Binder	PG 58-28
Modified Asphalt Binder	PG 58-28 + 2% LSBS

LSBS = linear styrene-butadiene-styrene.

A first round of experiments was performed by the research team to investigate the possibility of reducing the conditioning time proposed by Cho (2008). For this set of experiments, the testing

samples in the wet case were conditioned for 6 hours at 40 °C before running the strain sweep test. For dry conditions, the strain sweep was run after only 30 minutes waiting time at 40 °C to ensure a temperature equilibrium state. The results shown in figures M1a.1 and M1a.2 indicate that the wet-conditioned specimens performed slightly better than the dry-conditioned specimens. This behavior is not related to moisture damage but can be explained by steric hardening occurring to the wet samples.

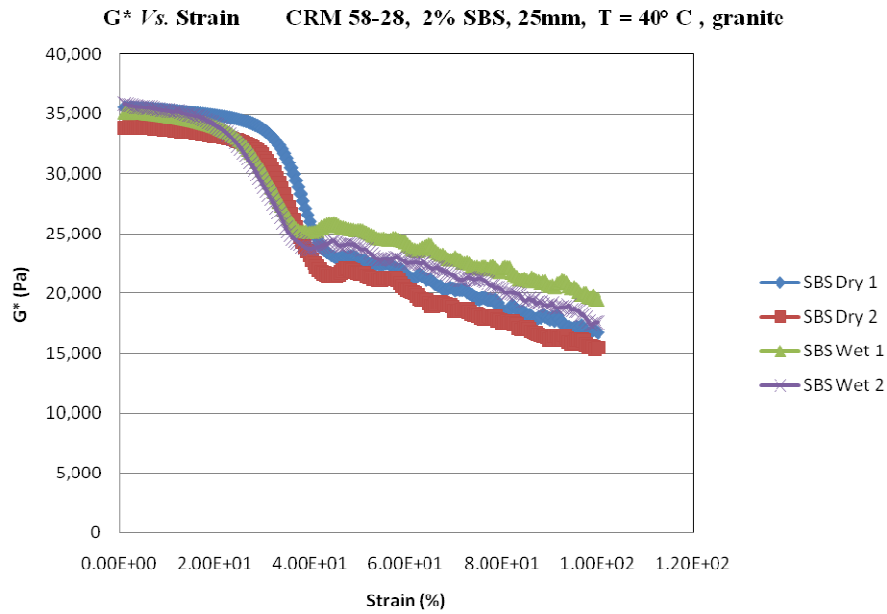


Figure M1a.1. Graph. Complex modulus versus strain for the modified binder (CRM+2% SBS) in both dry and wet conditions. (SBS = styrene-butadiene-styrene.)

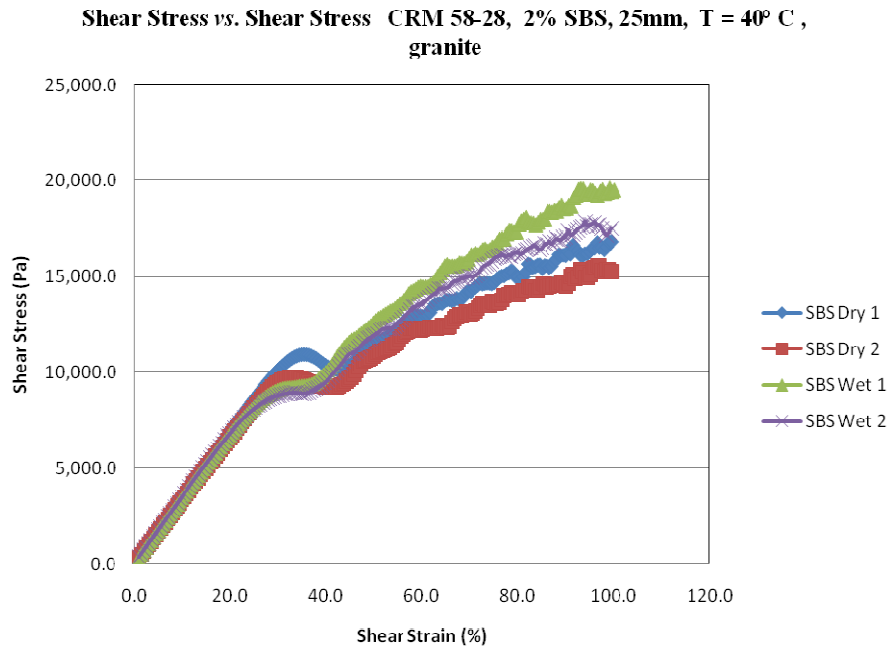


Figure M1a.2. Graph. Shear stress versus strain for the modified binder (CRM+2% SBS) in both dry and wet conditions.

After this preliminary set of experiments, the research team realized that modification of the conditioning time for the dry specimens is very complicated due to steric hardening. Therefore, efforts were focused to determine if strain sweep test with 6 hours of conditioning time for both dry and wet cases can quantify moisture damage in asphalt-aggregate interfaces. It can be seen in figures M1a.3 and M1a.4 that the strain sweep procedure with same conditioning time is able to differentiate performance between wet and dry specimens. The performance of the dry-conditioned specimens is slightly better than the wet-conditioned ones. Furthermore, as it is observed in figure M1a.3, the linear viscoelastic range (LVE) of the material is reduced when moisture is present in the test. The LVE is defined as a range in which the strain depends linearly with the applied stress (Petersen et al. 1994). Within the linear region, the modulus is independent of the stress or strain.

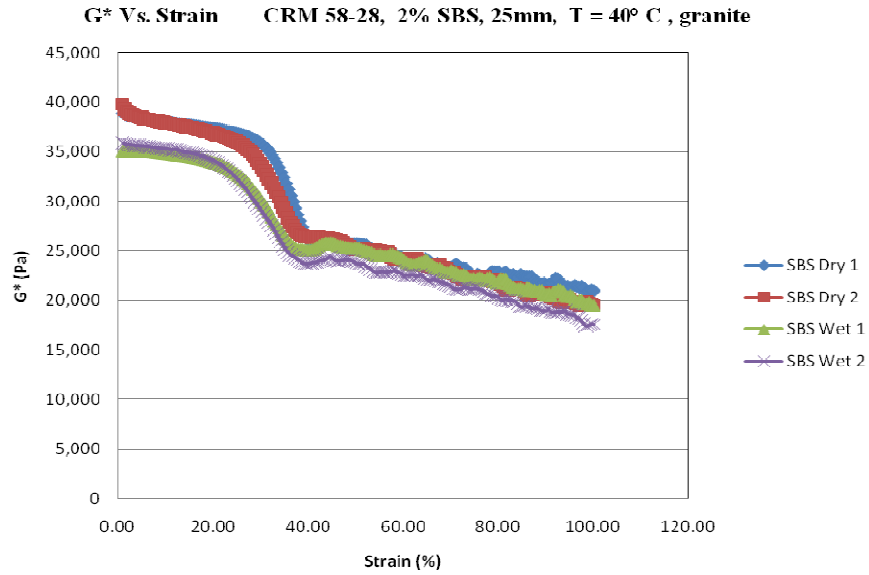


Figure M1a.3. Graph. Complex modulus versus strain for the modified binder (CRM+2% SBS) in both dry and wet conditions.

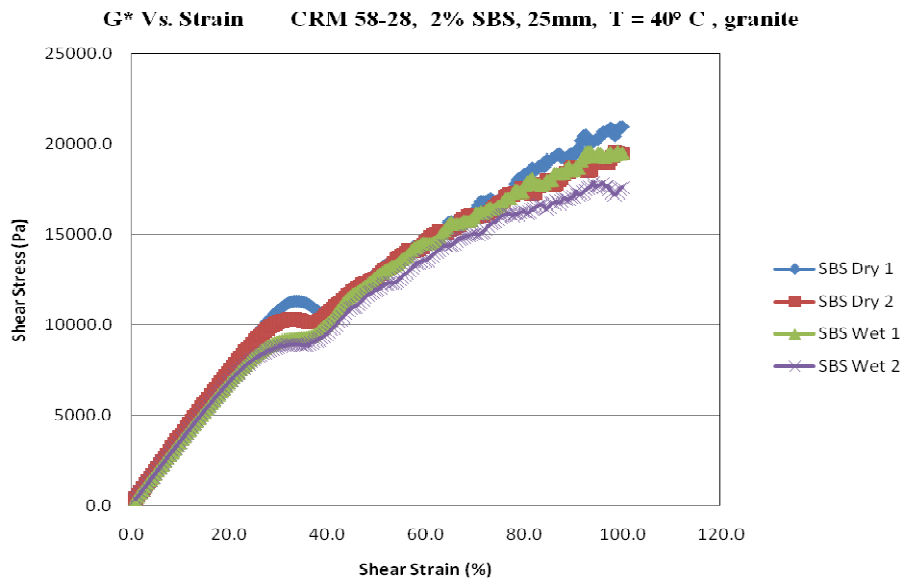


Figure M1a.4. Graph. Shear stress versus strain for the modified binder (CRM+2% SBS) in both dry and wet conditions.

To examine the effects of polymer modification, tests were performed in both modified and unmodified asphalts. It can be observed from figures M1a.5 and M1a.6 that the polymer-modified asphalt performs significantly better than the unmodified asphalt. However, the effect of moisture on the performance of both modified and unmodified asphalts is not significantly different. For both binders, the LVE region is reduced by a similar percentage for the water-

conditioning specimens. It is also observed in figure M1a.6 that the double peak behavior in the stress-strain curves is slightly smoothed for the moisture-conditioned specimens.

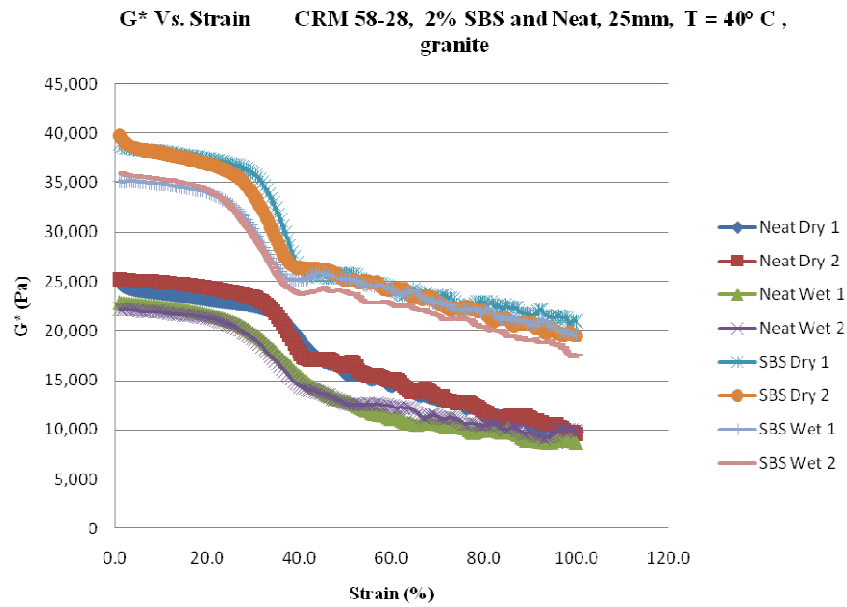


Figure M1a.5. Graph. Complex modulus versus strain for the modified (CRM+2% SBS) and unmodified binder in both dry and wet conditions.

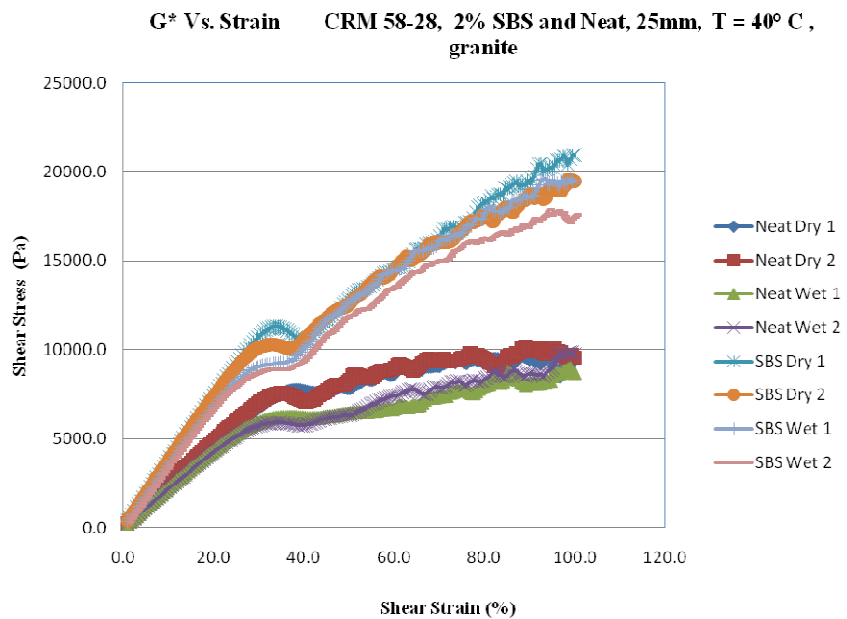


Figure M1a.6. Graph. Shear stress versus strain for the modified (CRM+2% SBS) and unmodified binder in both dry and wet conditions.

Significant Results

The research team obtained promising results regarding characterization of asphalt-aggregate interface by means of a simple-to-perform test (i.e., PATTI). The modified PATTI can be used to investigate moisture susceptibility of different combinations of aggregate-binders systems. The research team used the strain sweep test to successfully differentiate between the performance of dry- and wet-conditioned aggregate-asphalt specimens. However, the modified DSR strain sweep test is time-consuming and will be used only for verification purposes in the next quarters.

Significant Problems, Issues and Potential Impact on Progress

The research team intended to investigate moisture damage of asphalt-aggregate interfaces by means of the Binder Yield Energy Test (BYET) method. However, due to limitations on the torque the machine can apply, the team was not able to successfully run this test using the current aggregate-binder specimen geometry. The team is planning to modify the rate of deformation applied in the BYET to determine the feasibility of the experimental method for moisture damage characterization.

The research team has decided to combine the work elements M1a, Affinity of Asphalt to Aggregate, and M2c, Measuring Thin Film Cohesion and Adhesion Using the PATTI Test and the DSR, due to their similar objectives. All the research activities to be performed in work element M2c will be included in the M1a work element for the following quarters.

Work Planned Next Quarter

Efforts for next quarter will focus on the rationalization of the modified PATTI test. The research team will explain from a fundamental point of view the promising results obtained from the PATTI procedure. An extensive literature review will be performed on the chemical and physical mechanisms driving the moisture susceptibility phenomena of asphalt-aggregate systems. Also, the research team will use finite element modeling to investigate stress and strain distributions during the test and possible damage mechanisms. The team will investigate from the chemical and physical points of view why certain combinations of asphalt-aggregate perform better than others. The research team will also expand the test matrix already completed for the proposed PATTI procedure, and verification of the results will be obtained by using test results from mixtures (e.g., Tensile Strength Ratio) and the strain sweep tests.

Cited References

Cho, D., 2008, *Study of Asphalt-Aggregate Bond in Simple Simulation Using the Dynamic Shear Rheometer*. Ph.D. Thesis, University of Wisconsin–Madison, Madison, Wisconsin.

Petersen, J. C., R. E. Robertson, J. F. Branthaver, P. M. Harnsberger, J. J. Duvall, S. S. Kim, D. A. Anderson, D. W. Christiansen, and H. U. Bahia, 1994, *Binder Characterization and Evaluation, Volume I*. SHRP-A-367, Strategic Highway Research Program, National Research Council, Washington, D.C.

Work Element M1b: Work of Adhesion Based on Surface Energy

Subtask M1b-1: Surface Free Energy and Micro-Calorimeter Based Measurements for Work of Adhesion (TAMU)

Work Done This Quarter

The main goal of this subtask is to provide material property inputs required in other work elements as required. Any data obtained from this subtask will be included in the material properties database. In the last quarter surface free energy of some aggregates and asphalt binders that are being used to develop test methods were measured.

Significant Results

None.

Significant Problems, Issues and Potential Impact on Progress

None.

Work Planned Next Quarter

Work on this subtask will be conducted in conjunction with and as required by other work elements.

Subtask M1b-2: Work of Adhesion at Nano-Scale using AFM (WRI)

Work Done This Quarter

An automated sample thin-film spin-caster has been assembled and tested, figure M1b-2-1. This system will be used to prepare all forms of asphaltic and model compound thin-films to be further studied by nano-mechanical analyses and scanning probe imaging

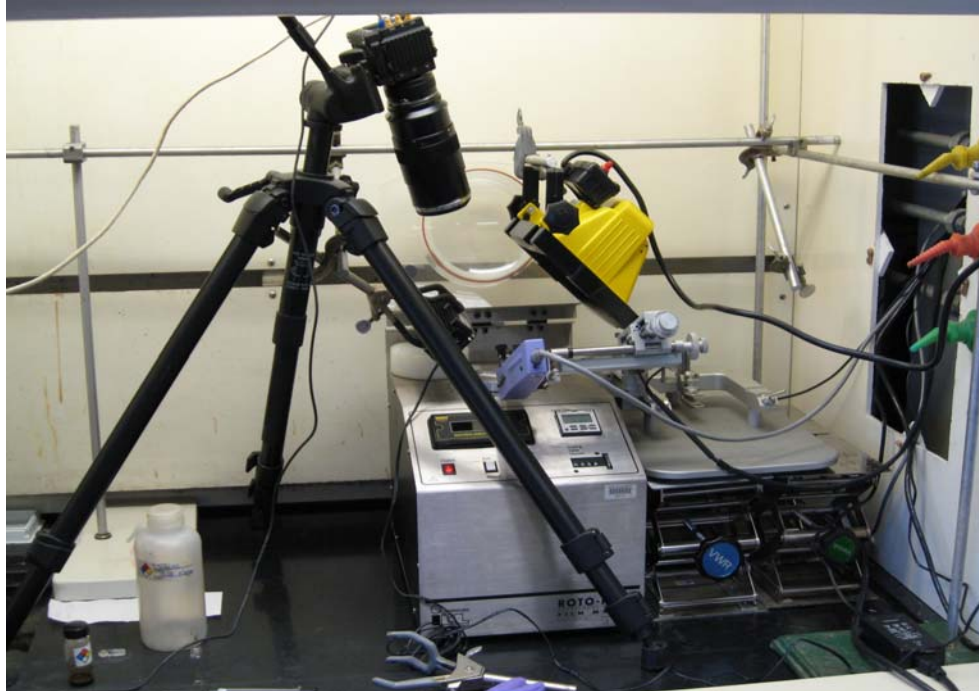


Figure M1b-2-1. Automated sample thin-film spin-caster, equipped with spin-caster, robotic-arm syringe-pump dispenser, and high speed digital camera for film instability control.

The syringe-pump dispenser and high speed digital camera will also be utilized as a pendent-drop tensiometer (Faour et al. 1996; Hansen and Rødsrud 1991).

Significant Results

None.

Significant Problems, Issues and Potential Impact on Progress

None.

Work Planned Next Quarter

Dynamic wetting experiments will be conducted to study the kinetics of adhesion of asphalts and asphalt chromatographic fractions spin-cast on glass microscope slides. These films will be further studied by AFM imaging and nano-mechanics to investigate microstructuring of wax as a function of the compatibility of the asphalt. Preliminary studies will also be conducted to measure interfacial tensions of asphalts in translucent solvents using a pendent-drop approach (Faour et al. 1996; Hansen and Rødsrud, 1991). Acid-Base and van der Waals components of surface tensions will be determined based on this approach.

References

Faour, G., M. Grimaldi, J. Richou, and A. Bois, 1996, Real-Time Pendant Drop Tensiometer Using Image Processing with Interfacial Area and Interfacial Tension Control Capabilities. *J. Colloid Inter. Sci.*, 181: 385–392.

Hansen, F. K., and G Rødsrud, 1991, Surface Tension by Pendant Drop. *J. Colloid Inter. Sci.* 141(1), 1–9.

Subtask M1b-3: Identify Mechanisms of Competition Between Water and Organic Molecules for Aggregate Surface (TAMU)

Work Done This Quarter

This sub task is investigating the mechanisms responsible for adhesion and debonding of model organic compounds (representing functional groups in asphalt binder) to minerals and representative aggregates. We are measuring the heat of reactions of the chemical mechanisms using a dual-mode flow adsorption calorimeter. Differences in molar heats of reaction of different organics bonding to the same absorbent are indicative of differences in the bonding strength of each absorbate with the absorbent of interest.

Work during this quarter focused on continued development of the instrument. We are currently conducting studies to validate the ability of the instrument to differentiate between bonding characteristics of materials produced under different conditions. These materials are known to have variable surface properties depending on the temperature of formation and other environment conditions. Currently we are evaluating the instrument ability to accurately measured changes in surface characteristics as a function of the pH of the aqueous environment.

Significant Results

There are no significant results for this quarter as we focused on aggregate characterizations.

There are no significant issues.

Work Planned Next Quarter

We plan on initiating flow through experiments to measure the molar heat of reaction of the adhesion of model organic compounds that represent asphalt to minerals and aggregates, as well as the molar heats of reactions of water adsorption to organic-coated minerals and aggregates.

Adhesion will be modeled in the flow-through calorimeter by organic sorption from nonaqueous phase solvents. Experimental variables include the chemistry of the model organic, single versus mixtures of model organics, ionic salt content of the nonaqueous phase solvent, and the surface chemistry of the mineral or aggregate.

Competition of water and the model organics for the mineral or aggregate surfaces will be characterized through flow-through experiments that introduce small amounts of water to the systems created during the adhesion studies above.

Work Element M1c: Quantifying Moisture Damage Using DMA (TAMU)

Work Done This Quarter

A new method for preparing Fine Aggregate Matrix (FAM) specimens for the DMA testing was developed. This method aims at preparing FAM specimens that represent the composition and structure of the fine portion of the mixture. FAM specimens were produced using binder content that was determined using the new method as well as the old one. The old method determines the binder content for the FAM mixture based on the binder content in the full mixture and the aggregate batch size. The FAM mixtures that were produced using the new method were easily mixed, compacted and cored compared to the ones that were prepared using the old method.

Significant Results

None.

Significant Problems, Issues and Potential Impact on Progress

None.

Work Planned Next Quarter

A new DMA (ElectroForce 3330 by Bose, Inc.) will be used to test various mixtures that will be prepared using the new method. In addition, software will be developed to analyze the DMA test data with the aim of simplifying the analysis procedure to predict fatigue life and evaluate the moisture susceptibility. This software will be developed using C++ programming language. In this software the user is required to load the DMA test raw data and specify some test information as presented in figure M1c.3.

CATEGORY M2: COHESION

Work Element M2a: Work of Cohesion Based on Surface Energy

Subtask M2a-1: Methods to Determine Surface Free Energy of Saturated Asphalt Binders (TAMU)

Work Done This Quarter

No activity was planned for this quarter.

Work Planned Next Quarter

Work on this task is anticipated to start in year 4 of the project.

Subtask M2a-2: Work of Cohesion Measured at Nano-Scale using AFM (WRI)

Work Done This Quarter

Heating/freezing stages have been incorporated into both the imaging AFM and metrology AFM.

Significant Results

None

Work Planned Next Quarter

Continuation: Work planned for next quarter will include analysis, using the mechanical models described in the previous quarterly report for this task (Quarterly Technical Progress Report, July 2009), of force curve data collected this quarter. Additional force curve data will be collected for a wider selection of asphalt samples. Tests will be conducted to begin to address the effect of temperature and loading/unloading rates with respect to how “fracture” energy is dissipated as indicated by the various parts of the force curve measurements. These measurements should lead to a better understanding of the ductile-brittle transition that takes place as asphalt is cyclically heated and cooled.

Work Element M2b: Impact of Moisture Diffusion in Asphalt Mixtures

Subtask M2b-1: Measurements of Diffusion in Asphalt Mixtures (TAMU)

M2b-2: Kinetics of Debonding at the Binder-Aggregate Interface (TAMU)

Work Done This Quarter

Tests related to the measurement of moisture diffusion using the FTIR, gravimetric measurements and hysteretic effect of moisture diffusivity has been completed using the FTIR. Three different asphalt binders were included in this study. Findings on the measurement of moisture diffusion using FTIR and hysteretic effect on diffusivity were compiled in the form of two journal publications. The detailed procedure for these tests was documented in a doctoral dissertation. The findings and procedures will be formatted per FHWA guidelines as a final report.

Significant Results

As a part of this research study we developed and used a methodology to determine the rate of water diffusion through thin films of asphalt binders using FTIR spectroscopy. Important conclusions and findings from this study are as follows:

- The diffusivity of water through four different asphalt binders was measured. At least one of these binders had a diffusivity that was significantly higher than the other three binders indicating that diffusivity may be an important material variable that influences the rate of moisture damage.
- A dual mode diffusion model was shown to better represent the diffusion of water through asphalt binders. Figure M2b.1 illustrates a typical example of how the dual mode diffusion model better represents the experimental data as compared to the conventional Fickian diffusion. This model suggests that water molecules may diffuse at two different rates within the asphalt binder with the slower rate being associated with interaction between water molecules and polar functional groups within the material. The implication of this mode of diffusion through asphalt binders in terms of performance and asphalt chemistry requires further investigation. However, these results do suggest that future efforts related to modeling of moisture damage should consider the use of a dual mode diffusion model rather than simple diffusion based on Fick's second law. Table M2b.1 lists the values for diffusivities for some of the asphalt binders.

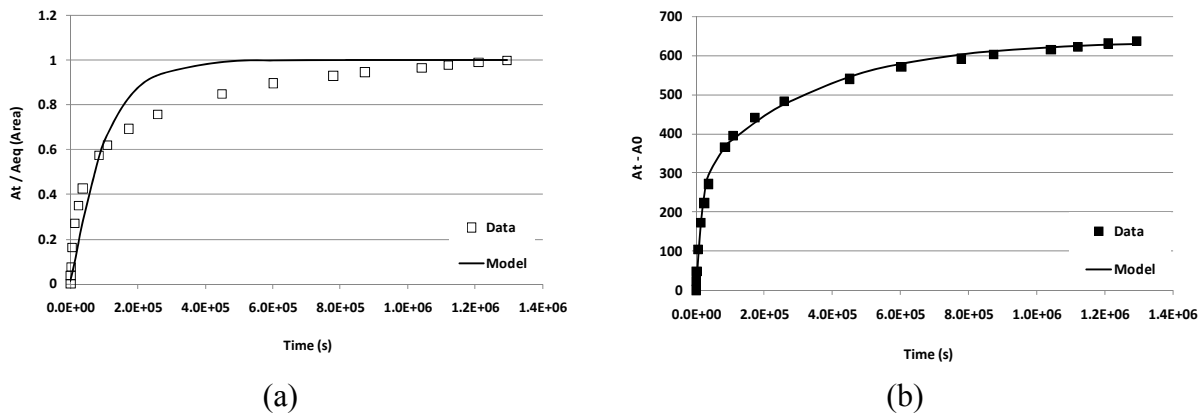


Figure M2b.1 Typical results obtained by (a) Analysis 1 (Fickian diffusion model) and (b) Analysis 2 (Dual Mode diffusion model) for asphalt AAB.

Table M2b.1 Diffusivities measured for some asphalt binders using the FTIR technique.

Asphalt	Number of Replicates	Dual Model Diffusion Values				
		$D_1(\text{nm}^2/\text{s})$	$D_2(\text{nm}^2/\text{s})$	x_1	Average $D_{\text{eff}} (\text{nm}^2/\text{s})$ [CV]	R^2 (fitting with the model)
AAB	6	23.02	0.79	0.51	12.17 [49%]	0.989
AAD	4	38.26	1.75	0.57	16.79 [37%]	0.978
ABD	6	75.07	0.40	0.53	39.82 [45%]	0.969

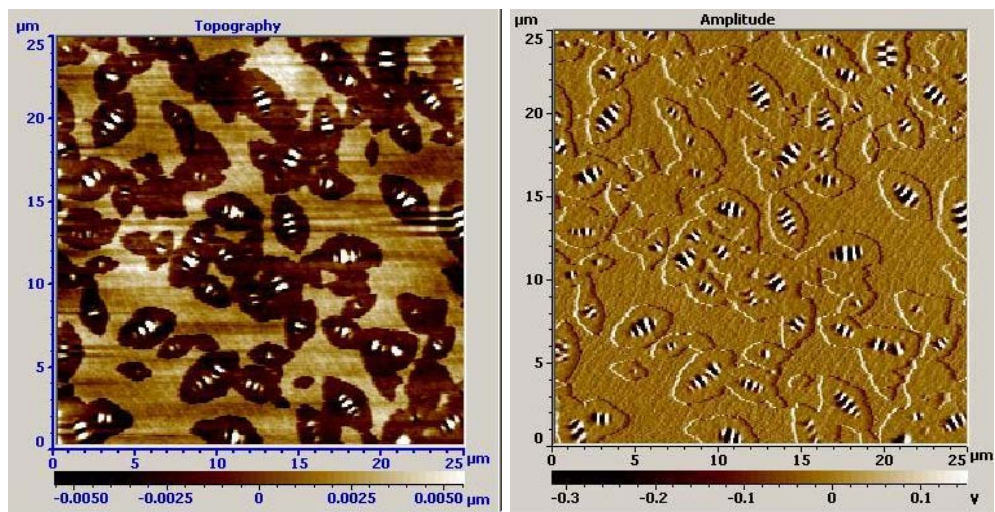
- The values of diffusivity reported in this study are much smaller than the values reported by Arambula et al. (2009) and Kassem et al. (2006). However, the values reported in this paper pertain to the diffusion of liquid water through thin films of asphalt binder which is different from diffusion of moisture through mixtures or mastics. The latter is dictated by macroscopic properties including interconnected air voids that allow moisture to travel much faster through the bulk. In contrast, the results shown in this study are relevant to the diffusion of moisture through the binder as in the case of microstructural entities that interconnect voids to the binder-aggregate interface. The impact of this could be that binders that develop a tenacious bond with aggregate surfaces and also resist moisture diffusion to the binder-aggregate interface may be more resistant to moisture damage. Further study is underway to evaluate the difference in diffusivity values when water is in liquid versus vapor form.
- The results obtained in this study are in the same order of magnitude of the results presented by Wei (2009) using the Electrochemical Impedance Spectroscopy (EIS). Wei used thin binder film on aluminum plate substrate.

The second objective of this subtask was to evaluate the influence of history of exposure to moisture on the rate of water transport in thin films of asphalt binder. This portion of the study was completed as well. Important conclusions and findings from this study are as follows:

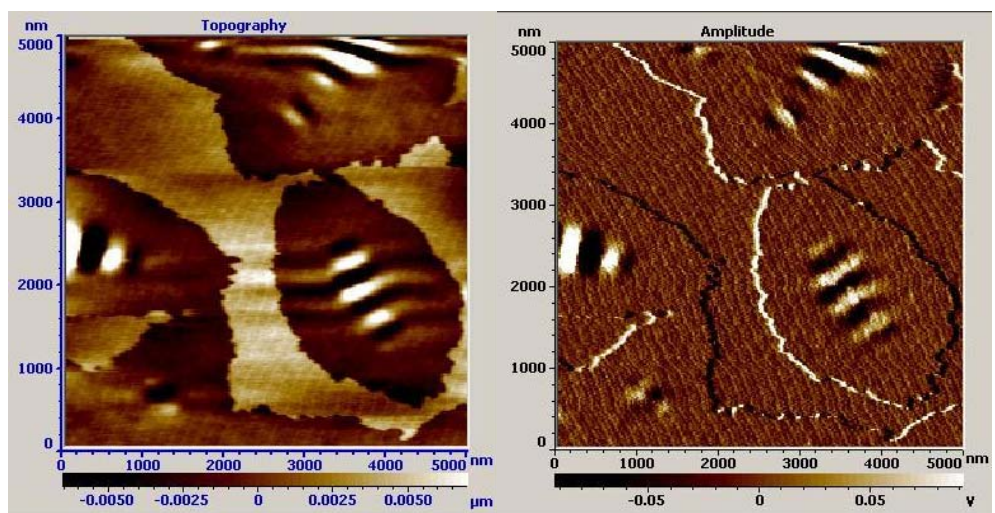
- The rate of moisture diffusion in asphalt binders depends on the history of exposure of the moisture to asphalt binder.
- In most cases, the diffusivity of moisture increased with every subsequent cycle of exposure to moisture. The increase in diffusivity was most significant after the first cycle. The change in diffusivity was dependent on the type of asphalt binder. Table M2b.2 presents some of the results indicating the history dependence of diffusivity.
- The increase in moisture diffusivity was mostly due to the change in microstructure of the asphalt binder after being exposed to the moisture. This was supported by AFM images of asphalt binder before and after being exposed to water (figure M2b.2). There was some evidence of increase in moisture trapped in the form of vapors even after dehydration that could also contribute to the increase in diffusivity.

Table M2b.2 History dependence of diffusivities measured using the FTIR technique.

Asphalt	Cycle	$D_1(\text{nm}^2/\text{s})$	$D_2(\text{nm}^2/\text{s})$	x_1	Average $D_{\text{eff}} (\text{nm}^2/\text{s})$ [CV]	R^2 (fitting with the model)
AAB	1	28.97	1.23	0.50	14.95 [29.8%]	0.992
	2	167.87	2.17	0.46	80.75 [47.3%]	0.984
	3	194.73	2.76	0.47	92.10 [20.5%]	0.984
AAD	1	41.72	1.84	0.41	16.19 [40.6%]	0.988
	2	59.90	1.04	0.48	28.22 [33.5%]	0.991
	3	102.98	1.45	0.43	41.34 [34.2%]	0.992
ABD	1	102.72	0.53	0.55	52.04 [34.6%]	0.974
	2	371.82	1.40	0.62	178.26 [50.3%]	0.906
	3	571.45	2.25	0.44	244.36 [21.6%]	0.946

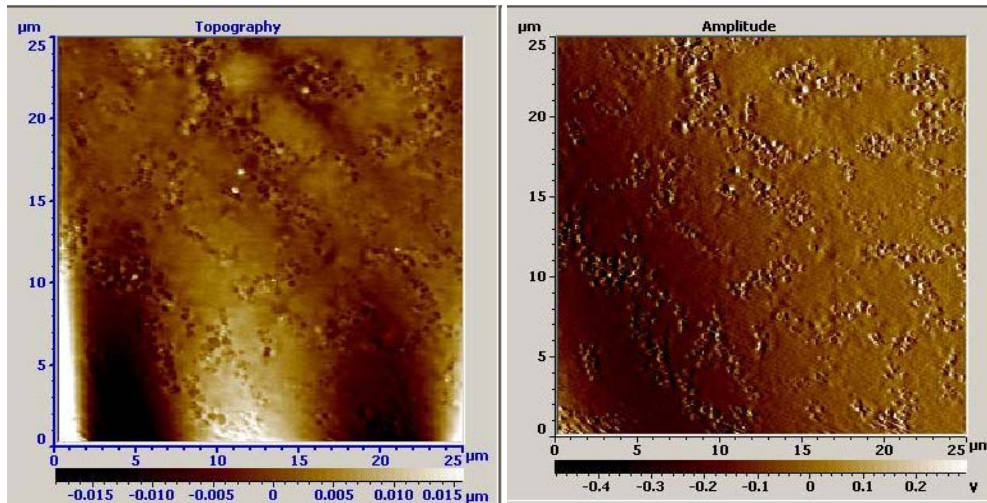


(i)

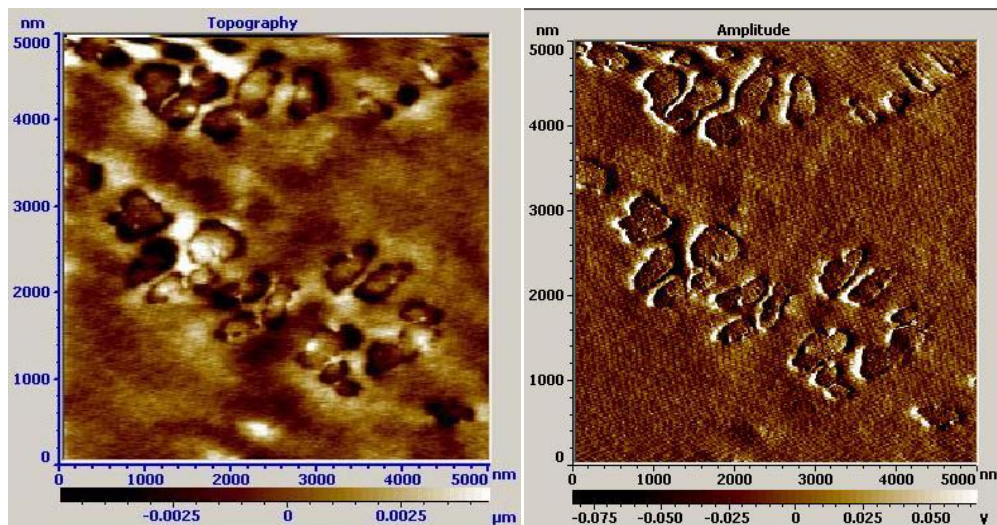


(ii)

Figure M2b.2(a). AFM images from asphalt AAD, (i) $25\mu\text{m}^2$ and (ii) $5\mu\text{m}^2$.



(i)



(ii)

Figure M2b.2(b). AFM images of asphalt AAD after 4 days of water exposure, (i) $25\mu\text{m}^2$ and (ii) $5\mu\text{m}^2$.

Significant Problems, Issues and Potential Impact on Progress

None.

Work Planned Next Quarter

The rate of debonding due to moisture at the binder-aggregate or filler interface is one of the factors that controls the overall rate of moisture damage within the asphalt mixture. In the next quarter we plan to start work on the measurement of rate of debonding at the asphalt binder-solid interface using ATR-FTIR spectroscopy. Another objective of this subtask is to validate the hypothesis that the rate or kinetics of debonding at the binder-aggregate interface is largely

dictated by the work of adhesion between these two materials (in addition to extrinsic properties such as temperature, geometry, etc). A literature review to investigate available methods to determine the rate of moisture transport at the interface (or the rate of debonding) was conducted. Findings from the literature indicate that it is possible to evaluate the rate of moisture transport at the polymer film-solid interface using spectroscopic techniques. After preliminary tests it was determined that it may not be feasible to create thin aggregate slices and measure changes at the aggregate-binder interface using the attenuated transmission mode with the FTIR. However, infrared transparent crystals such as ZnSe and KBr will be substituted for aggregates and tested with different asphalt binders. In the next quarter we will try to conduct some preliminary tests that allow simultaneous diffusion of water through the bulk and the interface.

Work Element M2c: Measuring Thin Film Cohesion and Adhesion Using the PATTI Test and the DSR (UWM)

Work Done This Quarter

A modified sample preparation procedure based on the Pneumatic Adhesion Tensile Testing Instrument (PATTI) to measure adhesion and cohesion in asphalt-aggregate systems was implemented in this quarter. The modified procedure improved repeatability and is found to be effective for measuring effect of binder modification.

The pull-out stub of the PATTI went through a series of modifications prompted by poor adhesion being observed between the stub and binders, as shown in figure M2c.1. Final modification adopted for the pull-out stub is the use of a rough metal surface rather than a smooth surface. The modification of the pull-out stub to a rough surface can prevent asphalt/stub failure by providing larger mechanical interlock and contact area between the asphalt binder and the pull-out stub. The stub used has 20 mm diameter and 800 μm thickness of the surrounding edge. A comparison between the new stub and the old one is presented in figure M2c.2.



Figure M2c.1. Photograph. Asphalt/pull-out stub failure on the stub with legs.

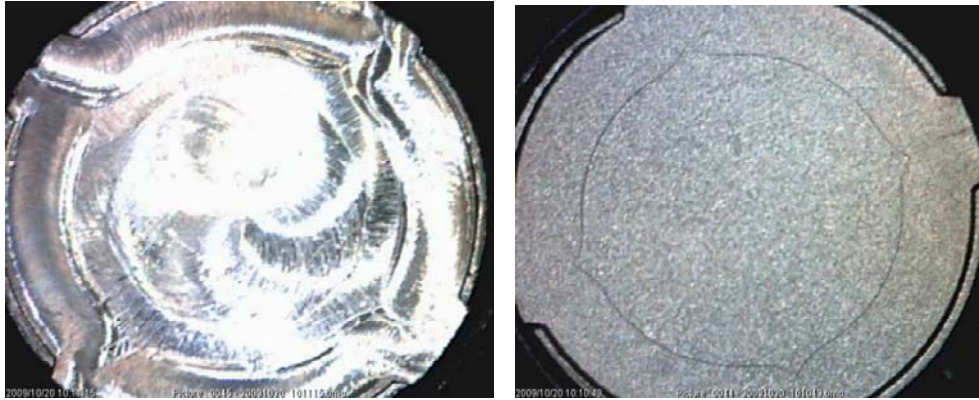


Figure M2c.2. Photograph. Comparison between the new and the old pull-out stub surface.

Significant Results

The modified PATTI test is proved to be a low-cost, simple and promising device for better characterization of moisture effect on asphalt-aggregate bond. As shown in figure M2c.3 and figure M2c.4 below, the test method is capable of discriminating between different levels of moisture effects within the same material, as well as identifying modification.

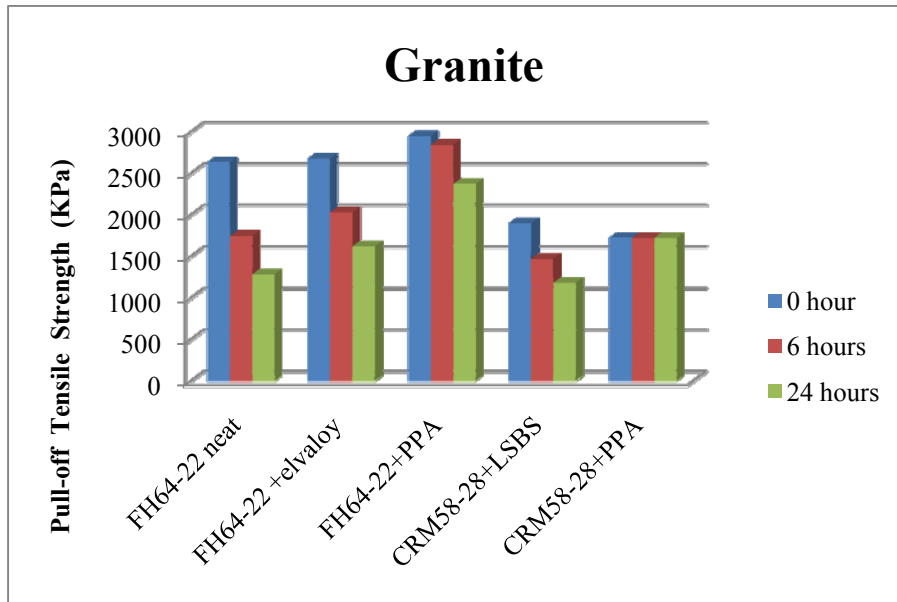


Figure M2c.3. Graph. Pull-off tensile strength values for testest performed on granite.

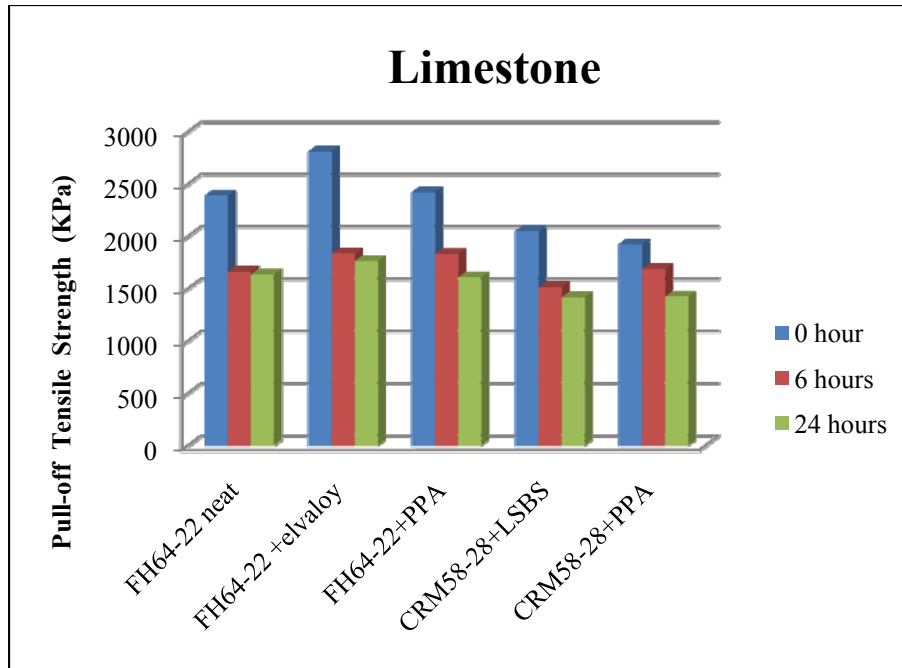


Figure M2c.4. Graph. Pull-off tensile strength values for test performed on limestone.

By comparing the results in the two figures above (figure M2c.3 and figure M2c.4), the test is also capable of detecting the influence of the aggregate's chemical composition on the moisture sensitivity of the asphalt-aggregate bond.

From the work performed in this quarter the following conclusions can be drawn:

- The modified PATTI test can be used as a practical method to measure the adhesion/cohesion properties of asphalt/aggregate systems.
- The effect of moisture conditioning on the adhesive bond between asphalt and aggregate can be quantified by the pull-off strength value.
- Modified PATTI can differentiate effects of conditioning time, conditioning solution and modification of binders. These factors show significant effect on the pull-off tensile strength.

A more comprehensive report will be published by the end of February 2010.

Significant Problems, Issues and Potential Impact on Progress

None

Work Planned Next Quarter

For next quarter the research team has decided to combine the work elements M1a (Affinity of Asphalt to Aggregate) and M2c (Thin Film Cohesion and Adhesion Using the PATTI and DSR) due to their similar objectives. All the research activities to be performed in M2c will be included in this work element for the following quarters.

CATEGORY M3: AGGREGATE SURFACE

Work Element M3a: Aggregate Surface Characterization (TAMU)

Work Done This Quarter

Physical and chemical properties of aggregates at the macro and molecular scale influence the performance of asphalt mixes. These properties control the nature and durability of the bond between aggregates and asphalt in wet and dry conditions and its resistance to moisture induced damage and fatigue cracking. Recent research by Little and colleagues have shown that surface energy of the aggregate-asphalt interface is a reliable predictor of engineering properties of the asphalt mixture. Current understanding of the aggregate and bitumen properties that control and shape surface energy is limited, limiting our ability to *a priori* predict surface energy of any given aggregate-asphalt combination.

Current tasks are organized around the (1) characterization of the chemical composition of the surfaces of reference minerals and aggregates through electron beam spectroscopies, including electron microprobe, backscatter electrons and electron-dispersive spectroscopy (EDS), (2) the characterization of the surface energies of reference minerals and aggregates through the universal sorption device and microcalorimetry, (3) quantification of surface (upper 14 nm) atomic species and chemical state with an x-ray photoelectron spectroscope (XPS), and (4) surface topography characterization with scanning electron microscopy (SEM). The results from these tasks will support the development of a predictive model of aggregate surface energies based upon the surface energies of the minerals that compose the aggregate.

Tasks completed this quarter include additional BSE imaging of the basalt (RK) in order to more accurately calculate modal mineralogy, quantitative WDS analyses of the SAz-2 montmorillonite and Georgia kaolinite, image processing of X-ray elemental distribution maps of the aggregates and reference mineral samples, and compilation and organization of the quantitative WDS analyses. Specific accomplishments are highlighted in the tables below.

Surface energy measurements for quartz, microcline, labradorite, biotite, andesine, microcline, albite, augite, hornblende, hematite, siderite, dolomite, and calcite have been collected using the universal sorption device. The components of surface energy were calculated on replicates of the samples.

Sample preparation and aggregate surface characterization tasks completed this quarter are shown in the table below.

Table M3a.1. Status of tasks associated with mineralogical and chemical characterization of aggregates.

SHRP	Name	Yr.Qtr	Thin Section Prep Status	Microprobe Analysis Status
RA	Lithonia Granite	08.1	1 aggr sample prepared, 2 more in progress	1 set of X-ray maps, 1 set of BSE images, 1 preliminary set of WDS quant analyses
		08.2	2 more aggregate samples prepared	2 sets of X-ray maps, BSE images are not needed because of grain size
		09.1		WDS quant analyses of major minerals completed
RC	Limestone (higher absorption)	08.1	2 aggr samples prepared	1 set of X-ray maps, 1 set of BSE images, 1 preliminary set of WDS quant analyses
		08.2	-	No additional analyses
RD	Limestone (low absorp.)	08.1	4 aggr samples prepared,	4 sets of X-ray maps, 1 set of BSE images, 1 preliminary set of WDS quant analyses
		08.2	-	No additional analyses
RK	Basalt	08.1	2 aggr samples prepared, 1 more in progress	2 sets of X-ray maps, 1 set of BSE images, 1 preliminary set of WDS quant analyses
		08.2	1 sample in progress	3 additional sets of X-ray maps, 13 set of BSE images, 1 set of WDS quant analyses for pyroxene, olivine, amphibole
		09.1		WDS quant analyses of feldspar, pyroxene and clay completed.
		09.2		Additional BSE images of thin sections RK1a and RK1b acquired; image processing of X-ray maps in progress
RL	Gulf Coast Gravel	08.1	5 aggr samples prepared, 9 more in progress	4 sets of X-ray maps, 1 set of BSE images, 1 preliminary set of WDS quant analyses
		08.2	9 more in progress	9 sets of X-ray maps
		09.1		WDS quant analyses of mineral grains in 9 gravel particles completed.
		09.2		Image processing of X-ray maps in progress
MM	MM Sandstone	09.1	One 25mm aggr mount prepared with > 20 fragments	1 sets of X-ray maps acquired

Sample preparation and mineral surface characterization tasks completed this quarter are shown in the tables below.

Table M3a.2. Status of tasks associated with mineralogical and chemical characterization of mineral components of aggregates.

Mineral	Group	Yr.Qtr	(1) Acquisition Status (2) Microprobe Mount Status	Microprobe Analysis Status
Quartz	Silica Mineral	08.1	(1) > 200 grams acquired (Arkansas, RNG specimen) (2) Polished microprobe mount in preparation	In progress
		08.2	In progress	In progress
Microcline	Alkali Feldspar	08.1	(1) > 160 grams acquired (G&G collection, B0434) (2) Preliminary polished mount prepared	Preliminary homogeneity and quantitative chemical analysis acquired.
		08.2	In progress	In progress
Albite	Plagioclase Feldspar	08.1	(1) > 100 grams acquired (G&G collection, B0469) (2) Polished mount to be prepared	In progress
		08.2	In progress	In progress
Oligoclase	Plagioclase Feldspar	08.3	> 100 grams acquired (G&G collection, 008)	In progress
Andesine	Plagioclase Feldspar	08.1	(1) > 65 grams acquired (G&G collection, B0513) (2) Preliminary polished mount prepared	Preliminary homogeneity and quantitative chemical analysis acquired.
		08.2	In progress	In progress
Labradorite	Plagioclase Feldspar	08.1	(1) > 160 grams acquired (Naim, Labrador; RNG specimen) (2) Preliminary polished mount prepared	Preliminary homogeneity and quantitative chemical analysis acquired.
		08.2	In progress	In progress
Anorthite	Plagioclase Feldspar	08.1	Samples to be acquired	NA
		08.2	NA	NA

Table M3.a 2. Status of tasks associated with mineralogical and chemical characterization of mineral components of aggregates (cont.).

Mineral	Group	Yr.Qtr	(1) Acquisition Status (2) Microprobe Mount Status	Microprobe Analysis Status
Hornblende	Amphibole	08.1	(1) > 350 grams acquired (G&G collection, B0545) (2) Preliminary polished mount prepared	Preliminary homogeneity and quantitative chemical analysis acquired.
		08.2	In progress	In progress
Hornblende	Amphibole	08.1	(1) > 70 grams acquired (G&G collection, Room 008) (2) Polished mount to be prepared	In progress
		08.2	In progress	In progress
		09.1	(2) Polished mount prepared	X-ray map acquired; WDS quant analyses completed.
Augite	Pyroxene	08.1	(1) > 0 (?) grams acquired (G&G collection, B1007) (2) Preliminary polished mount prepared	Preliminary homogeneity and quantitative chemical analysis acquired.
		08.2	In progress	In progress
Augite	Pyroxene	08.1	(1) > 80 grams acquired (G&G collection, Room 008) (2) Polished mount to be prepared	In progress
		08.2	In progress	In progress
		09.2		WDS quant analyses completed.
Forsteritic Olivine	Olivine	08.1	(1) > 280 grams acquired (San Carlos, AZ) (2) Polished mount to be prepared	In progress
		08.2	In progress	In progress

Table M3a.2. Status of tasks associated with mineralogical and chemical characterization of mineral components of aggregates (cont.).

Mineral	Group	Yr.Qtr	(1) Acquisition Status (2) Microprobe Mount Status	Microprobe Analysis Status
Muscovite	Mica	08.1	(1) > 65 grams acquired (G&G collection, Room 008) (2) Polished mount to be prepared	Preliminary quantitative chemical analysis acquired.
		08.2	In progress	In progress
		09.1	(2) Polished mount prepared	X-ray map acquired; WDS quant analyses completed.
Biotite	Mica	08.1	(1) > 175 grams acquired (G&G collection, B0857) (2) Polished mount to be prepared	In progress
		08.2	In progress	In progress
		09.1		WDS quant analyses completed.
Biotite	Mica	08.1	(1) > 150 grams acquired (G&G collection, Room 008) (2) Polished mount to be prepared	Preliminary quantitative chemical analysis acquired.
		08.2	In progress	In progress
Calcite	Carbonate	08.1	(1) > 100 grams acquired (Mexico; RNG specimen) (2) Polished mount to be prepared	In progress
		08.2	In progress	In progress
Dolomite	Carbonate	08.1	Samples to be acquired	NA
		08.2	NA	NA
		09.1	(2) Polished mount prepared	X-ray map acquired; WDS quant analyses completed.
Siderite	Carbonate	09.1		WDS quant analyses completed.

Table M3a.2. Status of tasks associated with mineralogical and chemical characterization of mineral components of aggregates (cont.).

Mineral	Group	Yr.Qtr	(1) Acquisition Status (2) Microprobe Mount Status	Microprobe Analysis Status
Hematite	Iron Oxide	08.1	Samples to be acquired	NA
		08.2	NA	NA
		09.1	(2) Polished mount prepared	X-ray map acquired; WDS quant analyses completed.
Magnetite	Iron Oxide	08.1	Samples to be acquired	NA
		08.2	NA	NA
Ilmenite	Iron Titanium Oxide	08.3	> 100 g sample (Ontario; RNG specimen)	NA
		09.1	(2) Polished mount prepared	X-ray map acquired; WDS quant analyses completed.
Goethite	Iron Oxyhydroxide	08.1	Samples to be acquired	NA
		08.2	NA	NA
Kaolinite (KGA-1B)	Clay Mineral	08.3	Samples acquired	NA
		08.2	Samples acquired	In progress
Kaolinite (Georgia)	Clay Mineral	08.3	Samples acquired	NA
		08.2	Samples acquired	In progress
		09.2	Unpolished flat mount prepared	WDS quant preliminary analyses completed
Montmorillonite (SAz-2)	Clay Mineral	08.3	Samples acquired	NA
		08.2	Samples acquired	In progress
		09.2	Unpolished flat mount prepared	WDS quant preliminary analyses completed
Chlorite	Clay Mineral	08.3	Samples acquired; ~25 g Calumet and New Melones (RNG)	NA
		08.2	Samples acquired	In progress

Significant Results

Establishing a Surface Energy Predictive Model

One of the first goals will be to establish a model for predicting aggregate bulk surface energies based on mineralogical composition. Improved prediction of aggregate bulk properties pertinent to moisture damage susceptibility can lead to better methods to measure material properties and moisture damage susceptibility of asphalt/aggregate mixes. Development of a simple visual field test of aggregate surface energy properties will aid in on-site evaluation of aggregate moisture damage susceptibility.

We expect the bulk/total surface energy of an aggregate to be a function of the component surface energies of its mineralogical constituents as:

$$Se_{aggregate} = \sum (Se_{Mineral} \cdot SA) + \sigma$$

where Se is surface energy, SA is surface area, and σ is the error term. A visual inspection of rock mineralogy based on percent of constituents can accurately predict total surface energy of the sample.

Methods –A Universal Sorption Device can be used to measure pure phase mineral surface energies by calculating the amount of a reference gas (water, hexane, and methylpropyl ketone in this case) sorbed to the mineral surface at various pressures. The adsorption isotherm for each reference gas is used to calculate equilibrium spreading pressure for each of the vapors along with the specific surface area (SSA) using the BET Equation. The equilibrium spreading pressure of each vapor is then used to calculate the three surface energy components using GvOC Equations. These values will then be used to establish an additive model of total surface energy for previously characterized rock samples based on percent of each constituent at the surface. The validity of the model will be tested by using the same Universal Sorption Device technique on the aggregate samples. A statistical analysis will be performed on the observed measurements versus predicted values.

Experiments – Although rock mineralogy has the capacity to be very complex it is dominated by a relatively small group of minerals of predictable variability in North America. The mineralogy of common aggregates used in hot asphalt mixes across America is outlined in the aggregate analysis data from the Strategic Highway Research Program's (SHRP) materials reference library. Pure phase minerals are being collected by Dr. Ray Guillemette based on the findings of the SHRP. These minerals are the dominant constituents in all major aggregates of the study. The chosen minerals are listed in table 1.

The surface energies of these pure phase minerals will be calculated using a Universal Sorption Device using three reference gases to determine spreading pressures. Each mineral will be crushed and passed through a number 10 sieve. Minerals will be washed with distilled water and heated for 24 hours at 80° Celsius in a Fisher Isotemp® Oven. Each reference gas will be used on a separate sample of each pure phase mineral. After the test is run each sample will be washed with distilled water and reheated at 80° C for future analysis.

After each of the pure phase mineral surface energies have been quantified the SHRP aggregate samples themselves will be crushed and analyzed on the Universal Sorption Device to statistically determine the linear additive model's validity.

Data- The data gained from this experiment will be in $erg / (cm)^2$ for each pure phase mineral and SHRP aggregate. In order to calculate mineral surface energy the isotherm for each reference gas must be calculated. To obtain a full isotherm, the aggregate is exposed to ten equal increments of partial probe vapor pressure from vacuum to saturated vapor pressure. At each stage the adsorbed mass is recorded after it reaches equilibrium. The adsorbed mass of each stage is then used to plot the isotherm. The measured isotherm for hexane is then used to calculate the specific surface area (SSA) using the Branauer, Emmett, and Teller BET equation:

$$A = \left(\frac{N_m N_0}{M} \right) \alpha$$

where N_0 =Avogadro's number; M =molecular weight of the probe vapor; α = projected area of a single molecule; and N_m =monolayer capacity of the aggregate surface. The specific surface area and each adsorption isotherm are then used to calculate three surface energy components using the GvOC equation:

$$W = 2\sqrt{\gamma_s^{lw}\gamma_v^{lw}} + 2\sqrt{\gamma_s^+\gamma_v^-} + 2\sqrt{\gamma_s^-\gamma_v^+}$$

where g^{Total} = total surface energy of the material; g^{lw} = Lifhsitz-van der Waals or dispersive component; g^{AB} = acid-base component; g^+ = Lewis acid component, and g^- = Lewis base component.

Current Results

In order to use the Universal Sorbtion Device as an appropriate measuring device for surface energy the reproducibility must first be known. In order to test the reproducibility one of the SHRP aggregates was chosen at random and the surface energy was measured on the sorption device. The aggregate was RD-7, a shaly limestone composed primarily of calcite. Hexane and methylpropyl ketone were run in triplicate and water vapor was tested four times. The results indicated that there was a good deal of internal consistency between the test runs, and the overall surface energy calculation was within a 95 percent confidence interval to previous study of the aggregate over two years ago. In total, testing of 12 minerals and two clays has either been completed or is in progress. All minerals will be tested in quadruplicate for each vapor. The results to date are included in the following chart.

Sample Surface Energies					
Aggregates	van der Waals	e- Acceptor	e- Donor	Fractional Polarity	Total
RD Limestone	49.98	0.47	469.22	0.37	78.67
MM Sandstone	45.24	2.02	310.96	0.53	95.31
RC Limestone	49.55	2.98	799.29	0.66	147.16
RL Gravel	57.50	23.00	973.00	0.84	356.80
RK Basalt	52.30	0.64	164.00	0.28	72.80
RA Granite	48.80	0.00	412.00	0.02	50.00
RB Granite	52.78	3.28	15744.19	0.90	507.3948
Minerals					
Albite	51.57	0.22	501.69	0.29	72.79
Andesine	40.64	0.40	3755.04	0.66	118.35
Augite	52.67	8.69	3890.33	0.87	420.45
Bassanite	38.27	0.30	3036.03	0.61	98.16
Biotite	52.51	0.07	809.97	0.22	67.41
Calcite	34.94	0.40	85.16	0.25	46.54
Cerussite	35.07	0.11	113.14	0.17	42.11
Dolomite	60.29	0.18	564.05	0.25	80.57
Gypsum	41.13	1.31	65.47	0.31	59.65
Gypsum Hot Deg	42.24	1.32	87.66	0.34	63.73
Hematite	48.99	2.85	558.07	0.62	128.81
Hornblende	51.92	0.91	1338.86	0.57	121.63
Ilmenite	39.76	0.35	318.90	0.35	60.89
Kaolinite	30.48	5.01	80.00	0.57	70.51
Labradorite	46.21	1.81	186.54	0.44	82.92
Microcline	44.00	0.46	202.79	0.31	63.35
Montmorillonite	42.85	1.57	80.43	0.34	65.29
Muscovite	47.55	0.55	544.68	0.42	82.07
Olivine	44.17	1.55	57.52	0.30	63.04
Quartz	50.33	0.02	365.00	0.09	55.37
Rhodochrosite	40.33	0.86	145.76	0.36	62.66
Siderite	61.39	1.59	789.63	0.54	132.18

Significant Problems, Issues and Potential Impact on Progress

No significant problems at this time.

Work Planned Next Quarter

Work planned in the next quarter includes continued analysis of the aggregates and minerals, with specific reference to surface energies.

CATEGORY M4: MODELING

Work Element M4a: Micromechanics Model (TAMU)

Work Done This Quarter

Cohesive Zone Micromechanical Model (TAMU)

During this past quarter, the cohesive zone micromechanical model was used to investigate the influence of the air void phase on the mechanical response of asphalt mixtures subjected to moisture diffusion. Two different probabilistic-based approaches were used to accomplish this objective. In the first approach, a volumetric distribution of air void sizes measured using X-Ray Computed Tomography (CT) in a dense-graded asphalt mixture was used to generate probable void structures in a microstructure of an asphalt mixture. In the second approach, a stochastic modeling technique based on random field theory was used to generate probable air void distributions of the mixture. In this second approach, the influence of the air void was accounted for by making the physical and mechanical properties of the asphalt matrix dependent on probable void distributions. Although both approaches took into consideration the characteristics of the air void phase on the mechanical response of the mixtures subjected to moist environments, the former explicitly introduced the air phase within the microstructure while the latter indirectly included its effects by modifying the material properties of the bulk matrix.

Figure M4a.2 presents the 50mm by 50mm representative volume element (RVE) that was selected in both approaches, as well as its finite element implementation. The mixture was composed by 231 coarse aggregates embedded in the fine aggregate matrix.

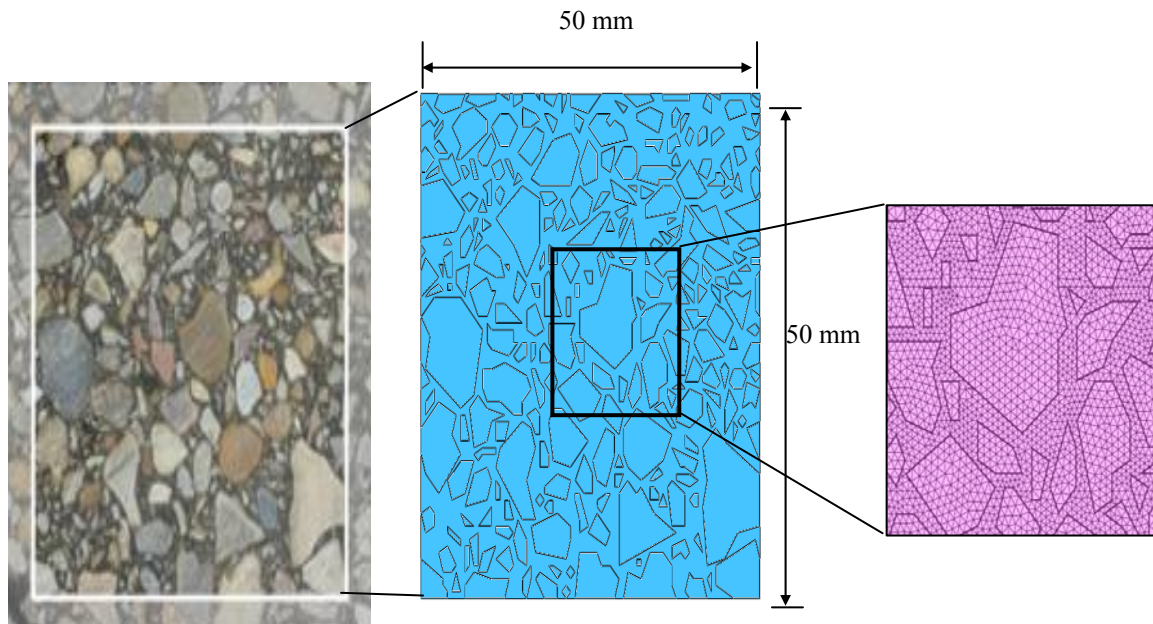


Figure M4a.2. Microstructure model used in the parametric analysis and its corresponding finite element implementation.

The results showed that an increase in the variability of the air voids content within the asphalt mixture in the field is associated with an increase in the variability of the total dissipated energy (DE) and the reduction of the stiffness of the mixture (K). Details of the stochastic approach, the material properties and the moisture diffusion and loading schemes used in the model, as well as the main results obtained from the simulations can be found in Caro et al. (2010c).

- Caro, S., Masad, E., Sanchez-Silva, M., and Little, D. (2010). "Stochastic micromechanical modeling of asphalt mixtures subjected to moisture diffusion processes." *International Journal for Numerical and Analytical Methods in Geomechanics* (submitted for evaluation).

Significant Results

None.

Significant Problems, Issues and Potential Impact on Progress

None.

Work Planned Next Quarter

Cohesive Zone Micromechanical Model

The two main tasks for the following year are:

- Incorporate the influence of moisture diffusion and the air void phase on the adhesive and cohesive fracture mechanisms within the numerical cohesive model that is currently under development by the research group at University of Nebraska, UNL (under the direction of Dr. Yong Rak Kim). This proposal will combine the results and experiences gained at TAMU in moisture induce-damage and the comprehensive micromechanical damage model developed at UNL.
- Use the experimental results on the fracture characteristics of aggregate-asphalt binder systems (work element F.1a.) to calibrate the interface fracture properties required to accurately model adhesive deterioration in the numerical coupled model.

Work Element M4b: Analytical Fatigue Model for Mixture Design

This work is addressed under Work Elements F1b-1, F3c-1, and E1a.

Work Element M4c: Unified Continuum Model

Work Done This Quarter

The moisture damage model was coupled with the viscoelastic, viscoplastic, and viscodamage model developed in work element F3c. This allowed investigating the effect of moisture on the

viscoelastic, viscoplastic, and damage response of asphalt mixes when subjected to realistic loading conditions. A parametric analysis was conducted to verify that the model captures the main effects of moisture on the response of the asphalt mixtures. In another parametric study the effect of moisture damage on permanent deformation and rutting in asphalt layers subjected to traffic loading while moisture-conditioned was studied.

Significant Results

None

Significant Problems, Issues and Potential Impact on Progress

None

Work Planned Next Quarter

The experimental verification of the moisture damage component of the unified continuum damage model and the constitutive model itself will be initiated by conducting the tests outlined in table F3c.2 after subjecting the specimens to different levels of moisture conditioning. The validated moisture law will be employed in predicting pavement distresses in the presence of the moisture based on the unified viscoelastic, viscoplastic, and viscodamage model.

CATEGORY M5: MOISTURE DAMAGE PREDICTION SYSTEM

This area is planned to start later in the project.

Moisture Damage Year 3		Year 3 (4/09-3/10)												
		4	5	6	7	8	9	10	11	12	1	2	3	
Adhesion														
M1a	Affinity of Asphalt to Aggregate - Mechanical Tests													
M1a-1	Select Materials													
M1a-2	Conduct modified DSR tests													
M1a-3	Evaluate the moisture damage of asphalt mixtures												P	
M1a-4	Correlate moisture damage between DSR and mix tests												P	P
M1a-5	Propose a Novel Testing Protocol													P
M1a-6	Standard Testing Procedure and Recommendation for Specifications													
M1b	Work of Adhesion													
M1b-1	Adhesion using Micro calorimeter and SFE							JP						
M1b-2	Evaluating adhesion at nano scale using AFM													
M1b-3	Mechanisms of water-organic molecule competition													
M1c	Quantifying Moisture Damage Using DMA													
Cohesion														
M2a	Work of Cohesion Based on Surface Energy													
M2a-1	Methods to determine SFE of saturated binders													
M2a-2	Evaluating cohesion at nano scale using AFM													
M2b	Impact of Moisture Diffusion in Asphalt													
M2b-1	Diffusion of moisture through asphalt/mastic films							JP			D			F
M2b-2	Kinetics of debonding at binder-aggregate interface													
M2c	Thin Film Rheology and Cohesion													
M2c-1	Evaluate load and deflection measurements using the modified PATTI test													
M2c-2	Evaluate effectiveness of the modified PATTI test for Detecting Modification													
M2c-3	Conduct Testing													
M2c-4	Analysis & Interpretation												See M1a	
M2c-5	Standard Testing Procedure and Recommendation for Specifications				D									
Aggregate Surface														
M3a	Impact of Surface Structure of Aggregate													
M3a-1	Aggregate surface characterization													
Modeling														
M4a	Micromechanics model development				2JP		JP							JP
M4b	Analytical fatigue model for use during mixture design													
M4c	Unified continuum model				JP		JP							JP
M5	Moisture Damage Prediction System													

LEGEND

Deliverable codes

- D: Draft Report
- F: Final Report
- M&A: Model and algorithm
- SW: Software
- JP: Journal paper
- P: Presentation
- DP: Decision Point
- [x]

Deliverable Description

- Report delivered to FHWA for 3 week review period.
- Final report delivered in compliance with FHWA publication standards
- Mathematical model and sample code
- Executable software, code and user manual
- Paper submitted to conference or journal
- Presentation for symposium, conference or other
- Time to make a decision on two parallel paths as to which is most promising to follow through
- Indicates completion of deliverable x

-  Work planned
-  Work completed
-  Parallel topic

Moisture Damage Year 2 - 5		Year 2 (4/08-3/09)				Year 3 (4/09-3/10)				Year 4 (04/10-03/11)				Year 5 (04/11-03/12)			
		Q1	Q2	Q3	Q4	Q1	Q2	Q3	Q4	Q1	Q2	Q3	Q4	Q1	Q2	Q3	Q4
Adhesion																	
M1a	Affinity of Asphalt to Aggregate - Mechanical Tests																
M1a-1	Select Materials		DP														
M1a-2	Conduct modified DSR tests		P		P												
M1a-3	Evaluate the moisture damage of asphalt mixtures				DP					P	P						
M1a-4	Correlate moisture damage between DSR and mix tests								P								
M1a-5	Propose a Novel Testing Protocol				P					P						JP, F	
M1a-6	Standard Testing Procedure and Recommendation for Specifications																
M1b	Work of Adhesion																
M1b-1	Adhesion using Micro calorimeter and SFE						JP						JP,F				
M1b-2	Evaluating adhesion at nano scale using AFM													JP			JP, F
M1b-3	Mechanisms of water-organic molecule competition				JP								JP	D	F		
M1c	Quantifying Moisture Damage Using DMA												JP	D	F		
Cohesion																	
M2a	Work of Cohesion Based on Surface Energy																
M2a-1	Methods to determine SFE of saturated binders														JP		
M2a-2	Evaluating cohesion at nano scale using AFM														JP		JP, F
M2b	Impact of Moisture Diffusion in Asphalt																
M2b-1	Diffusion of moisture through asphalt/mastic films							JP	D	F			JP	D	F		
M2b-2	Kinetics of debonding at binder-agreagte interface												JP	D	F		
M2c	Thin Film Rheology and Cohesion																
M2c-1	Evaluate load and deflection measurements using the modified PATTI test	DP	JP	D	F												
M2c-2	Evaluate effectiveness of the modified PATTI test for Detecting Modification			D	DP,F												
M2c-3	Conduct Testing																
M2c-4	Analysis & Interpretation				P							See M1a					
M2c-5	Standard Testing Procedure and Recommendation for Specifications						D										
Aggregate Surface																	
M3a	Impact of Surface Structure of Aggregate																
M3a-1	Aggregate surface characterization																
Models																	
M4a	Micromechanics model development				JP	2JP	JP		JP					M&A	D	DP	F, SW
M4b	Analytical fatigue model for use during mixture design																M&A,D
M4c	Unified continuum model					JP	JP		JP					M&A	D	DP	F, SW
M5	Moisture Damage Prediction System																

LEGEND

Deliverable codes

- D: Draft Report
- F: Final Report
- M&A: Model and algorithm
- SW: Software
- JP: Journal paper
- P: Presentation
- DP: Decision Point
- [x]

- Work planned
- Work completed
- Parallel topic

Deliverable Description

- Report delivered to FHWA for 3 week review period.
- Final report delivered in compliance with FHWA publication standards
- Mathematical model and sample code
- Executable software, code and user manual
- Paper submitted to conference or journal
- Presentation for symposium, conference or other
- Time to make a decision on two parallel paths as to which is most promising to follow through
- Indicates completion of deliverable x

PROGRAM AREA: FATIGUE

CATEGORY F1: MATERIAL AND MIXTURE PROPERTIES

Work Element F1a: Cohesive and Adhesive Properties

Subtasks F1a-1: Critical review of the literature

F1a-2: Development of test method

F1a-3: Thermodynamic work of adhesion and cohesion

F1a-4: Mechanical work of adhesion and cohesion

F1a-5: Evaluate acid base scales for surface energy calculations

Work Done This Quarter

In this quarter we completed the literature review and the portion of the experiment design related to the cohesive and adhesive properties of asphalt binders measured using a standard metal substrate. The findings were summarized in the form of a detailed technical paper that has been accepted for presentation and publication in the proceedings of the Association of Asphalt Paving Technologists.

Significant Results

The two main objectives of this task are i) to establish the relationship between practical work of adhesion or cohesion with ideal work of adhesion or cohesion, respectively and ii) to generate basic input such as the traction-separation behavior between binder/mastic-aggregate interface for inputs in the modeling effort. A test method was developed to measure these properties. Thin film specimens were created using a DSR and tested in a 5kN universal testing machine. High resolution imaging was used to measure deformation during the test. Details of the test method have been presented in previous quarterly reports and have also been summarized in a forthcoming technical paper. The summary of findings and conclusions are reiterated here.

- A range of sample thicknesses was tested to observe the effect of film thickness on the displacement and failure mode of the samples (figure F1a.1). It was found that as the sample thickness increased, the effective surface free energy of failure decreased, the maximum tensile force at failure decreased, and the displacement at failure increased.
- In general, a higher surface energy yields a higher value of fracture energy (figure F1a.2.). However, there are other material factors besides surface energy that can contribute to the fracture energy of the thin asphalt film.

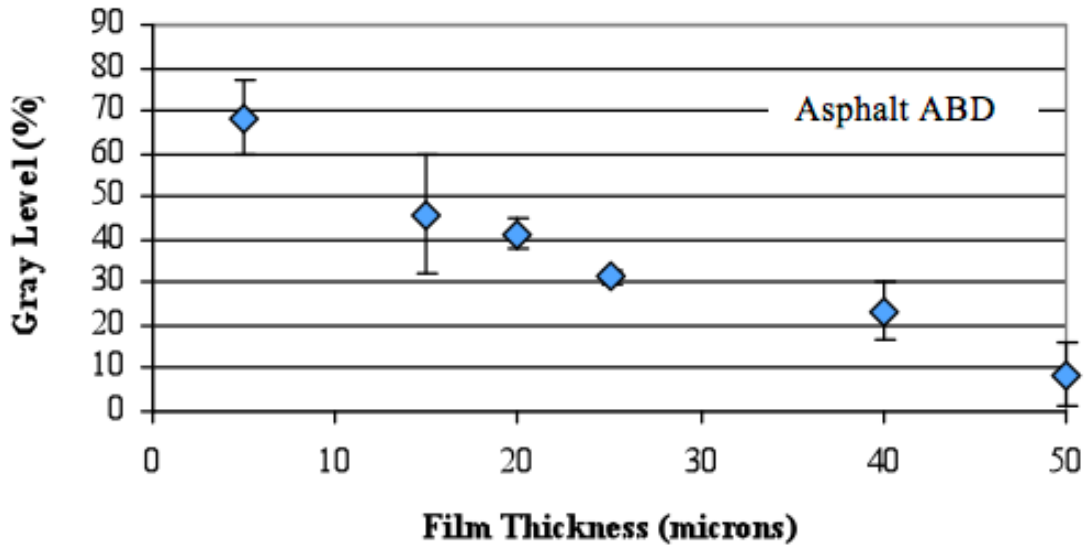


Figure F1a.1. Typical results to demonstrate influence of film thickness on tensile strength and mode of failure in asphalt binders.

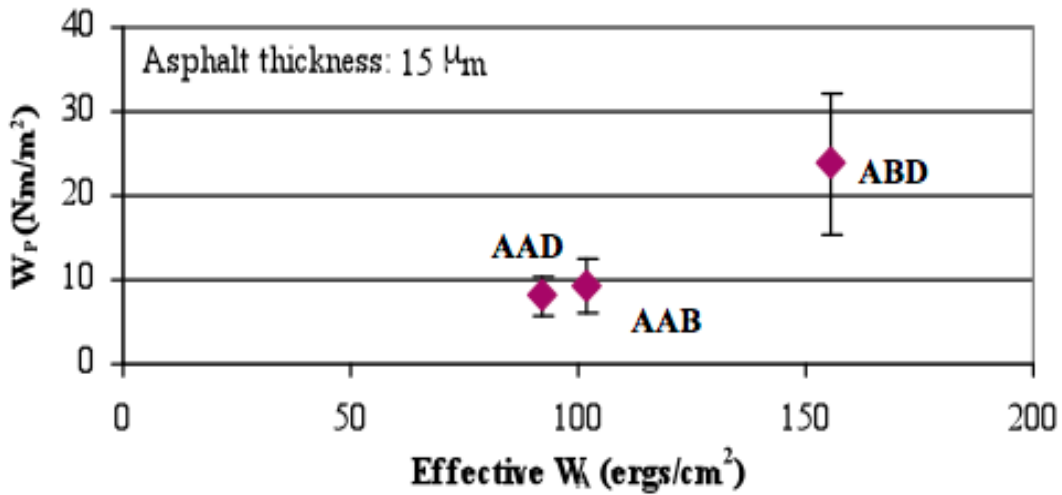


Figure F1a.2. Typical results to demonstrate relationship between practical and ideal work of cohesion for different asphalt binders at a given film thickness.

Significant Problems, Issues and Potential Impact on Progress

None.

Work Planned Next Quarter

Similar experiments to those described above will be continued in the next quarter. A significant difference from the above experiments would be the use of real aggregate substrates in lieu of a metal substrate to determine the mechanical work of adhesion and cohesion. In the next quarter we will also develop an experiment design to accommodate moisture conditioning of the test specimens and determine change in adhesive and cohesive properties as a function of moisture content.

Work Element F1b: Viscoelastic Properties (Year 1 start)

Subtask F1b-1: Viscoelastic properties under cyclic loading (TAMU)

Work Done This Quarter

The non-linear response of the viscoelastic materials can be captured using the model proposed by Schapery. However, it is also important to determine the nature of non-linearity to ensure that the aforementioned model is versatile and not dependent on the test procedure. In this quarter we furthered the investigations to determine the sources of non-linear response in asphalt materials. A summary of findings is presented below.

Significant Results

Based on some preliminary test data, it was hypothesized that the presence of a normal force leads to interaction non-linearity and consequently reduced torsional stiffness. The following approach was used to validate this hypothesis. Repeated creep-recovery tests were conducted at different stress levels on asphalt binders using the cone and plate geometry. Analysis of the test results indicated that the selected asphalt binder had a linear viscoelastic response up to stresses as high as 20 KPa. However, when the same material subjected to amplitude sweep (under sinusoidal loading) non-linear response was observed at stress amplitudes as low as 5 KPa. Close examination of the test data revealed that for the dynamic amplitude sweep test there was a build up of normal forces (figure F1b.1).

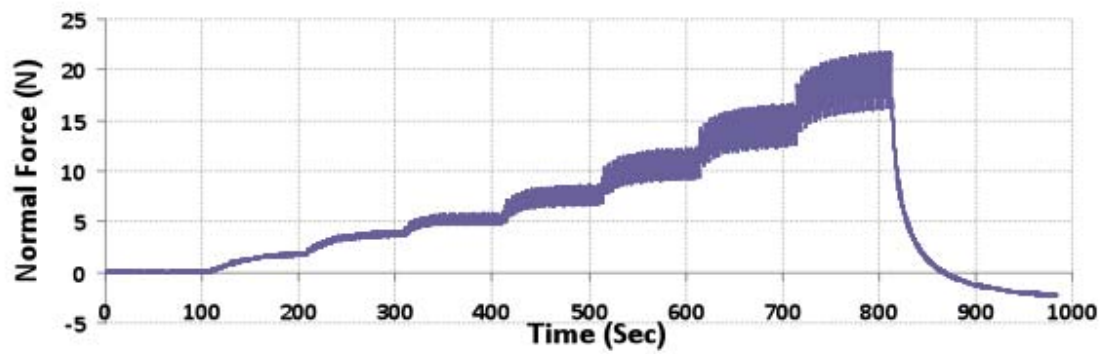
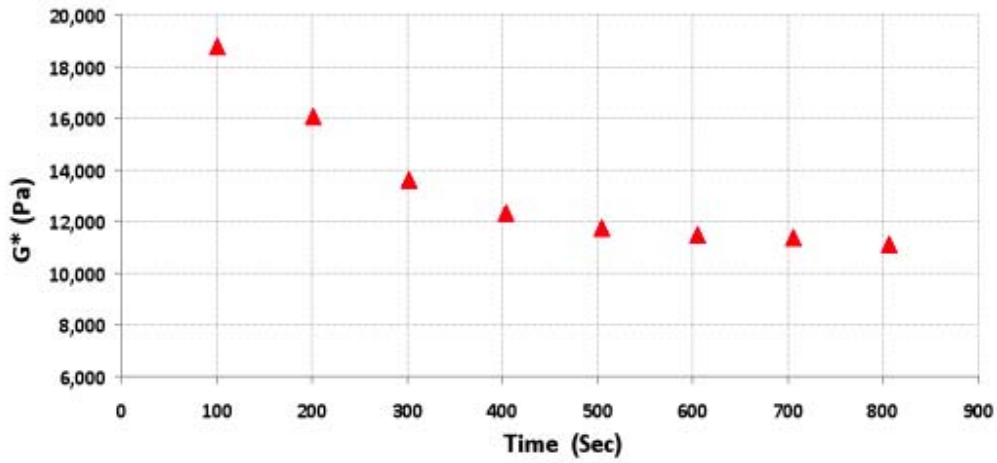
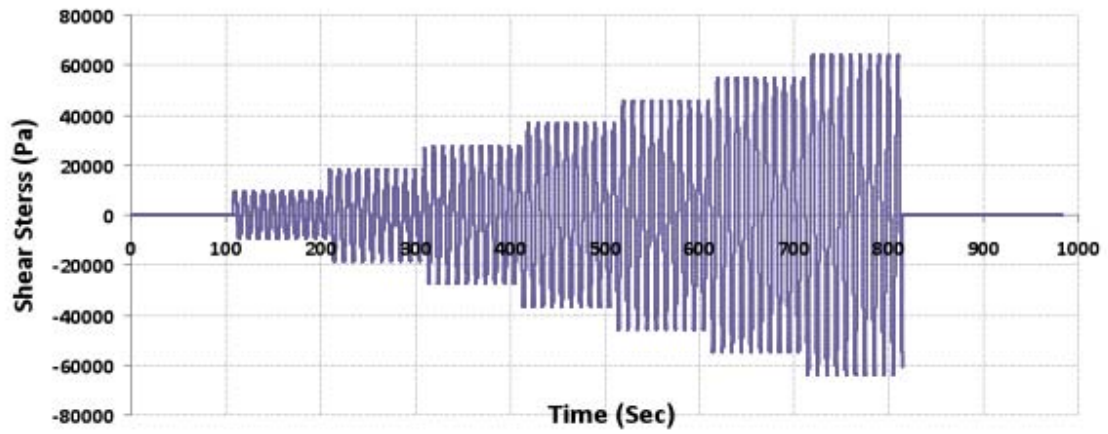


Figure F1b.1. Amplitude sweep, change in G^* and normal force for a PG grade asphalt binder tested using the DSR with cone and plate geometry.

The next step was to validate source of the normal force and quantify the amount of non-linearity induced due to the normal force. This was done by comparing the theoretical response expected from a linear viscoelastic material subjected to large deformations to the response measured using the DSR. The theoretical response was obtained using a finite element simulation of the cone and plate geometry (a closed form analytical solution could not be used because of the large deformation and specimen geometry). Figure F1b.2 illustrates the finite element analysis of the specimen in cone and plate geometry. Figure F1b.3 illustrates the difference between the results obtained from the finite element analysis and the measured values. As expected, the measured G^* was smaller than the computed G^* . The measured normal force can now be used to explain non-linearity and the difference between the measured and computed G^* values.

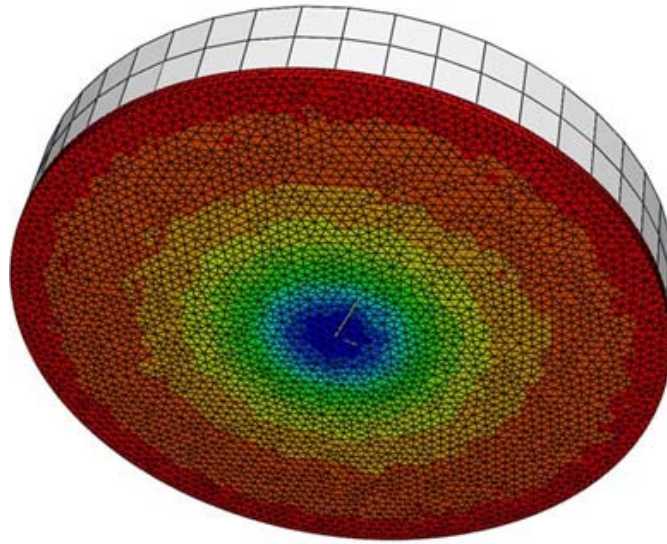


Figure F1b.2. Finite element analysis of the cone and plate geometry to determine normal force and G^* of a specimen subjected to stress amplitude sweep (colored contours show distribution of normal force).

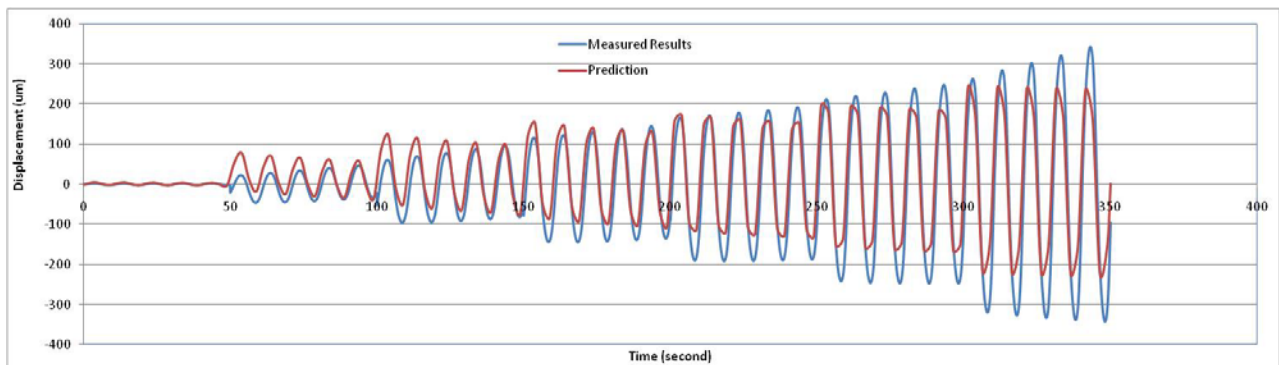


Figure F1b.3. Comparison of the computed and measured values of G^* to quantify the amount of non-linearity.

Significant Problems, Issues and Potential Impact on Progress

None.

Work Planned Next Quarter

Initial test results support the hypothesis that normal force induces a non-linear response in the material. This is also referred to as interaction non-linearity in the literature. We will continue with the investigation and modeling of this form of non-linear response. The expectation is that the findings from this subtask will result in a more robust constitutive model for the time and stress state dependent response for asphalt materials.

Subtask F1b-2: Separation of Nonlinear Viscoelastic Deformation from Fracture Energy under Repeated and Monotonic Loading

Work Done This Quarter

A technical paper, entitled “Characterization of Damage in Asphalt Mixtures Using Dissipated Pseudo Strain Energy”, was accepted for presentation in the Transportation Research Board (TRB) 89th Annual Meeting, which will be held in Washington, D.C., January 2010. This paper details the analytical formulation and test procedure to determine the dissipated pseudo strain energy (DPSE) and the recoverable pseudo strain energy (RPSE) in an asphalt mixture under destructive repeated direct tensile loading. The DPSE is separated into two categories: the DPSE for fracture and the DPSE for permanent deformation. The DPSE for fracture is used to obtain the rate of fatigue crack growth, and the RPSE is employed to determine the starting point of the crack growth that is indicated by the mean air void radius which is also called initial crack radius.

It has been found in last quarter that the RPSE (also defined as EPSE in last quarterly report) was accumulated as the number of loading cycles increased in the Repeated Direct Tension (RDT) test. At a loading cycle N , the RPSE corresponding to the current crack radius c ($c = \sum_{i=1}^n \Delta c_i$) was obtained as in equation F1b-2.1:

$$\begin{aligned} \text{Accumulated measured RPSE} &= \text{accumulated RPSE of intact material} \\ &\quad - \text{released RPSE due to growth of } c \\ &\quad + \text{stored surface energy due to growth of } c \end{aligned} \quad (\text{F1b-2.1})$$

Equation F1b-2.1 presents the energy balance between the measured energy and the actually distributed energy.

The energy balance approach was further developed in this quarter. The measured energy terms (including the DPSE and RPSE) were calculated from the measured stress and strain, which were obtained from the Viscoelastic Characterization (VEC) test and the RDT test that were detailed in previous quarterly reports. The actually distributed energy terms were computed from the true

stress and strain of the intact material around a crack. Since it was difficult to identify the true stress and strain directly from the tests as the crack grew, the volume of the intact material in which the energy changes was investigated to determine the amount of pseudo strain energy that was redistributed with each load cycle. The proposed pattern of true DPSE and true RPSE redistribution is shown in figure F1b-2.1. The stress distribution is represented by lines of force, which is illustrated by the dashed lines. Since the stress can not transmit through the crack, the lines of force are diverted around the crack, resulting in a local stress concentration (Anderson 2005). In the fracture process zone, the energy is consumed to overcome the resistance of the material, including the bond energy and plastic work. The volume from which the energy dissipates is illustrated by a toroid labeled by “1”, in which the dissipated energy consists of W_{R1} for fatigue cracking and W_{R2} for permanent deformation. In the intact material far from the crack (labeled by “2”), the lines of force are uniform, and the RPSE is stored and recovered during a loading and unloading cycle. In the area adjacent to the free surface (labeled by “3”), the RPSE of the intact material is liberated during unloading. This area is regarded as a conical region with a width of a and a height of πa (Roylance 2001). If the crack is assumed to be penny-shaped with a radius of c , a equals to $2c$ and the volume from which the energy is liberated can be calculated as:

$$V_3 = \frac{1}{3} \pi c^2 \cdot \pi c \quad (\text{F1b-2.2})$$

where V_3 is the volume in which the RPSE is liberated due to crack growth. As clarified in equation F1b-2.1, a part of the liberated RPSE is absorbed by the surface of the crack (labeled by “4”). The surface area of the crack on which the energy is stored is then calculated as follows:

$$S_4 = 2\pi c^2 \quad (\text{F1b-2.3})$$

where S_4 is the area on which the RPSE is stored due to the crack growth and the factor 2 is needed since two free surfaces have been formed.

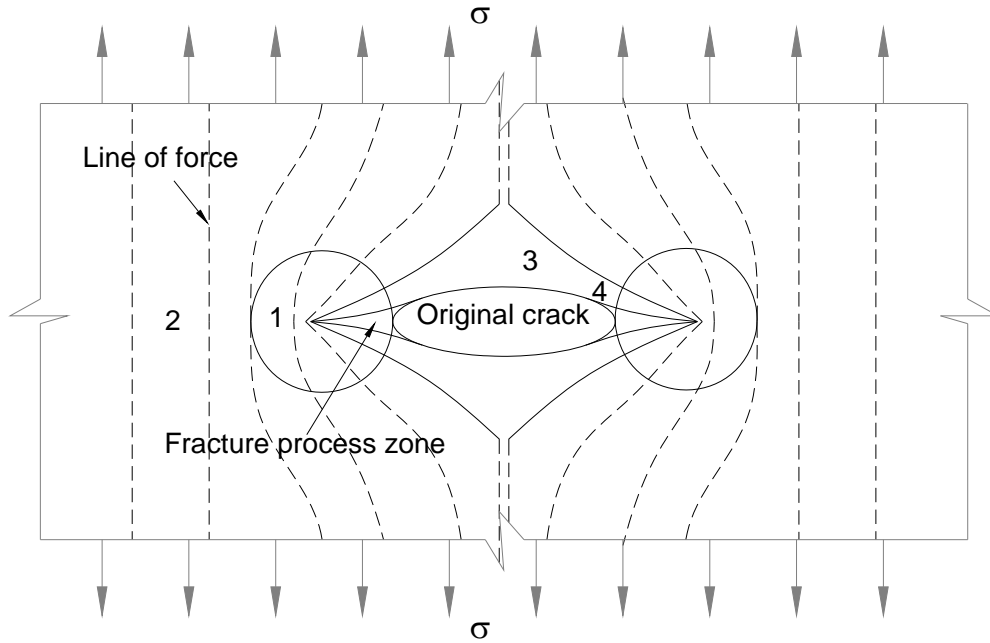


Figure F1b-2.1. Strain energy redistribution around a crack.

Based on the investigation of the strain energy redistribution around a crack, the RPSE accumulation was quantified by introducing two ratios, α and β . Then equation F1b-2.1 was revised as follows:

$$\begin{aligned} \alpha \cdot \text{apparent RPSE} &= \beta \cdot \text{RPSE of undamaged specimen} \\ &\quad - \text{released RPSE due to growth of } c \\ &\quad + \text{stored surface energy due to growth of } c \end{aligned} \quad (\text{F1b-2.4})$$

where α is the apparent accumulated RPSE ratio and β is the true accumulated RPSE ratio. These two ratios were calculated by the following equations, respectively:

$$\alpha = \frac{\sum_{i=1}^N \text{apparent RPSE}}{(\text{apparent RPSE})_{i=N}} \quad (\text{F1b-2.5})$$

$$\beta = \frac{\sum_{i=1}^N \text{RPSE of undamaged specimen}}{(\text{RPSE of undamaged specimen})_{i=N}} \quad (\text{F1b-2.6})$$

By using the two ratios α and β , the current crack radius c was determined at each loading cycle. Therefore, the whole path of the growing fatigue crack was tracked as the number of loading cycles increased.

Significant Results

An energy balance approach was developed this quarter to further investigate the strain energy redistribution around a crack in an asphalt mixture under tension loading. It was clearly explained how the energy redistributed around a crack when the crack grew. Two RPSE ratios were used in the energy balance equation so as to determine the crack radius at a certain loading cycle. Consequently, the path of the crack growing was obtained as the number of loading cycles increased.

Significant Problems, Issues and Potential Impact on Progress

The newly purchased Material Testing System (MTS) is still not ready to for testing because the software has not been fully installed. It is expected that the new MTS will be ready next quarter so more testing can be accomplished.

Work Planned Next Quarter

The current characterization of asphalt mixtures in a damaged state is based on the controlled-strain RDT test. Because the current MTS controls a single Linear Variable Differential Transformer (LVDT) in the controlled-strain test, the average reading of three axial LVDTs is not tracing a perfect sinusoidal wave. This fact introduces measurement errors to the data analysis. In order to reduce the errors caused by the machine control, a controlled-stress test will be performed on asphalt mixture samples next quarter. A corresponding data analysis method will be developed to analyze the test data from the controlled-stress test.

Cited References

Anderson, T. L., 2005, *Fracture Mechanics-Fundamentals and Applications*. 3rd ed. Boca Raton: CRC Press.

Roylance, D., 2001, *Introduction to Fracture Mechanics*. Department of Materials Science and Engineering, Massachusetts Institute of Technology, Cambridge, MA.

Work Element F1c: Aging

Subtask F1c-1: Critical Review of Binder Oxidative Aging and Its Impact on Mixtures (TAMU)

Work Done This Quarter

Studies of binder oxidation kinetics are being reviewed for the purpose of understanding the fast-rate reaction process, in support of kinetics measurements. The paper by King currently is being reviewed for its relevance in this regard.

King, G. N., 1993, Oxycyclics: Understanding Catalyzed Oxidation Mechanisms in Bitumen and Other Petroleum Products. *Fuel Science and Technology, Intl.*, 11(1), 201-238.

Significant Results

N/A

Significant Problems, Issues and Potential Impact on Progress

There are no problems or issues.

Work Planned Next Quarter

Review of literature and other work is an ongoing effort.

Subtask F1c-2: Develop Experimental Design

Work Done This Quarter

A draft experimental design has been submitted. Final selection of materials (binder and aggregate) for testing has been determined. The materials selected for the subsequent expanded experiment included two kinds of binder (Binder 1 and Binder 2, AAD-1 and AAM-1) and two types of aggregate. They are Aggregate 1 (Siliceous Conglomerate) and Aggregate 2 (Texas Limestone). A smaller experiment with Binder 1 and Aggregate 3 (Andesite), Aggregate 4 (Wyoming Limestone), Aggregate 5 (Granite), and Aggregate 6 (Gravel) was designed to study the effect of aggregate type.

Significant Results

The pilot experiment design was completed, and specimen fabrication (Subtask F1c-4) continued and was completed. While mixture testing has been delayed, pending further developing the required new mixture testing methods (Subtask F1c-4), mixture testing is now beginning.

Significant Problems, Issues and Potential Impact on Progress

Testing has been delayed, but the new protocol uses tests that take much less time than previous methods, while producing much more accurate data.

Work Planned Next Quarter

Conducting the laboratory experiments of the experimental design that use the improved testing protocol (work elements F1c-4 and F2c) has been delayed by equipment difficulties but is now underway. Also, additional field site cores for use in validation of the transport oxidation model and for evaluating the impact of binder oxidation on fatigue are being obtained.

Subtask F1c-3: Develop a Transport Model of Binder Oxidation in Pavements

Work Done This Quarter

Diffusivity is an important property that affects binder oxidation in pavements and thus is an important parameter in the transport oxidation model. Diffusivity varies with binder composition and viscosity, binder oxidation, the presence of mixture fines, and the presence of polymer. Questions being answered by fundamental measurements in this work address these impacts of polymer modification, oxidation and mixture fines.

Values of oxygen diffusivity for nine asphalts and four mastics are being measured. Diffusivities of the order of 10^{-10} to 10^{-11} m²/s have been observed as temperatures range from 60 to 80 C. Diffusivity is a function of temperature, because of its affect on the energetics of the diffusing molecules, and a function of solvent (in this case asphalt) viscosity that changes due to temperature and level of oxidation. Fundamentally, diffusivity typically is proportional to absolute temperature and inversely proportional to solvent viscosity. In fact, diffusivity/temperature (D/T) versus asphalt low shear rate limiting viscosity shows a very good linear relationship (on a log-log scale) for both base asphalts and polymer-modified asphalt. As shown in figure F1c-3.1, different correlations between D/T versus limiting viscosity have been established for base asphalts (Alon and SEM) and polymer modified asphalt (SEM + SBS).

Moreover, by using the viscosity of the base asphalt instead of the viscosity of the polymer-modified asphalt, those two correlations merge nearly together, as shown in figure F1c-3.2. These results are sparse and preliminary, but suggest that diffusing oxygen may see primarily the base asphalt. It may be that oxygen diffusion is not hindered by the polymer; it may be appropriate to view the effect of polymer on viscosity as a continuum rheological phenomenon but its effect on diffusion as a molecular scale process.

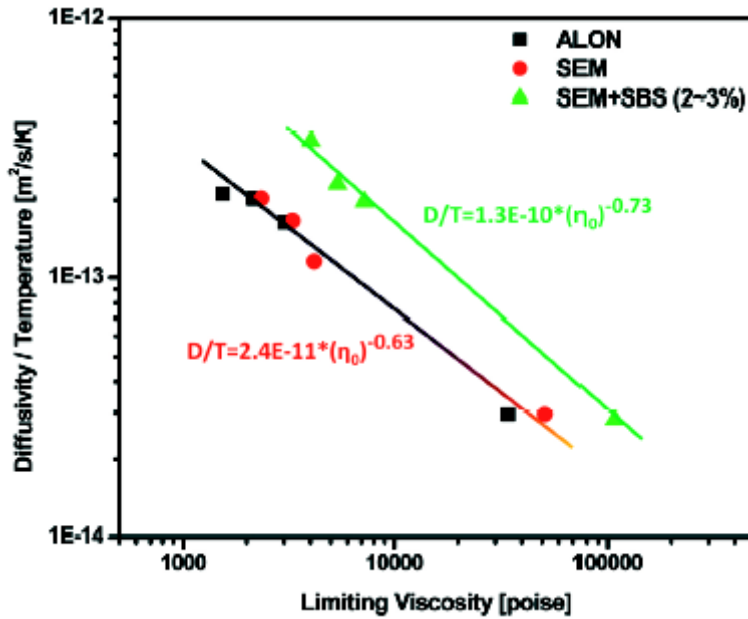


Figure F1c-3.1. Correlation between oxygen diffusivity / temperature versus limiting viscosity of asphalt.

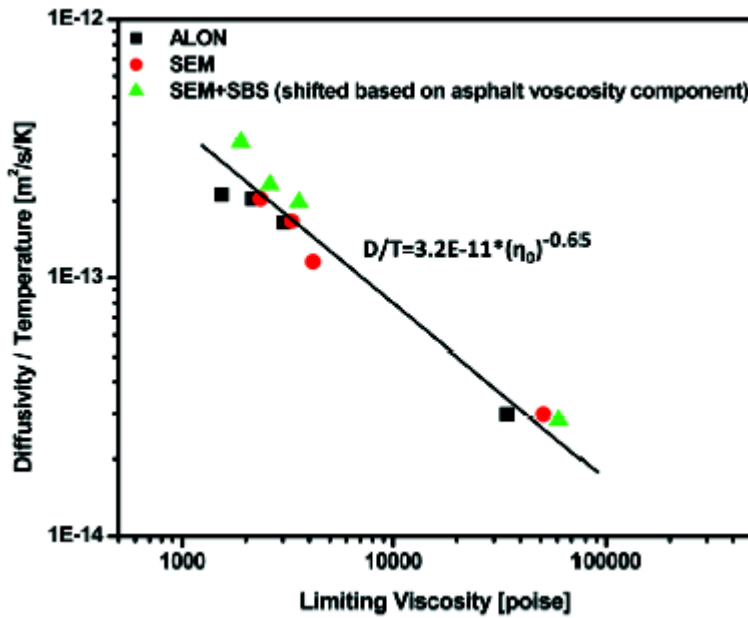


Figure F1c-3.2. Correlation between oxygen D/T versus limiting viscosity of asphalt with adjusted viscosity of SEM+SBS.

Work Planned Next Quarter

Laboratory measurement and data analysis of oxygen diffusivity in both asphalt and mastics continue in the next quarter. Correlations between D/T versus limiting viscosity of base asphalt will be further validated with data from additional asphalts. Evaluating the effect of mastic fines on diffusion will begin and theoretical relations that take into account the longer diffusion path (therefore creating a higher diffusion resistance) created by the fines will be tested.

Measurements of diffusion in specific asphalt materials, polymer-modified binders, and mastic-laden binders are important. Just as important, or even more important, is developing a fundamental understanding of the effects of polymer modification, fines, and oxidation on diffusion. Achieving this goal will facilitate accurate calculations of binder oxidation in pavements without the need for new measurements for each asphalt binder system.

Significant Problems, Issues and Potential Impact on Progress

Binder oxidation model validation remains. Due to delays in developing the testing protocol, these measurements have been delayed. However, the testing protocol is much faster and more accurate than previous methods, providing the ability to recover completely.

Work Planned Next Quarter

Actual pavement aging rates need to be compared to model calculations. Pavement cores are being tested for physical properties (subtask F1c-4) and continue in the next quarter. Cores are being sliced in half-inch increments from the surface down. Each of these slices is being tested to determine air voids, accessible air voids, binder content, binder rheology, and binder carbonyl content. These data will give binder oxidation level as a function of depth and air voids. Binder rheology, as a function of carbonyl will provide the binder hardening susceptibility for the recovered binder. Cores taken over a period of time will provide rates of oxidation in the pavement for comparison with calculations of the oxidation model. Additionally, companion cores will be measured for mixture physical properties, including fatigue. The test procedures that have been developed under subtask F1c-4 will be used on specimens cut from cores in two-inch increments, starting from the core surface. These tests will provide mixture fatigue measurements that will be compared to binder oxidative hardening.

Subtask F1c-4: The Effects of Binder Aging on Mixture Viscoelastic, Fracture, and Permanent Deformation Properties (TAMU)

Work Done This Quarter

The test protocols and data analysis method were completed to characterize the anisotropic viscoelastic properties of undamaged asphalt mixtures in compression. In the formulation of constitutive relations, six complex parameters were used to define the complete anisotropic viscoelastic properties. These six parameters were obtained by three nondestructive test scenarios, all of which are summarized in Table F2c.1 which is under Work Element F2c.

The master curves of the magnitude and phase angle of each of the six complex parameters were constructed using mathematical models listed as Equations F2c.3 through F2c.6. The master curves were then plotted to compare the tensile properties to the compressive properties in different directions. Figure F1c-4.1 shows the comparison of the master curves of the complex modulus magnitude at a reference temperature of 20°C. As can be seen from figure F1c-4.1, the compression complex modulus in the vertical direction of the asphalt mixture has a greater magnitude than that of the tensile complex modulus. As a result, it is necessary to separate the tensile modulus from the compressive modulus in the constitutive relations. Figure F1c-4.1 also shows that the magnitude of the compressive complex modulus in the vertical direction is approximately 2 – 2.5 times larger than that of the compressive complex modulus in the horizontal plane. This finding demonstrates the strong anisotropy of the asphalt mixture in compression.

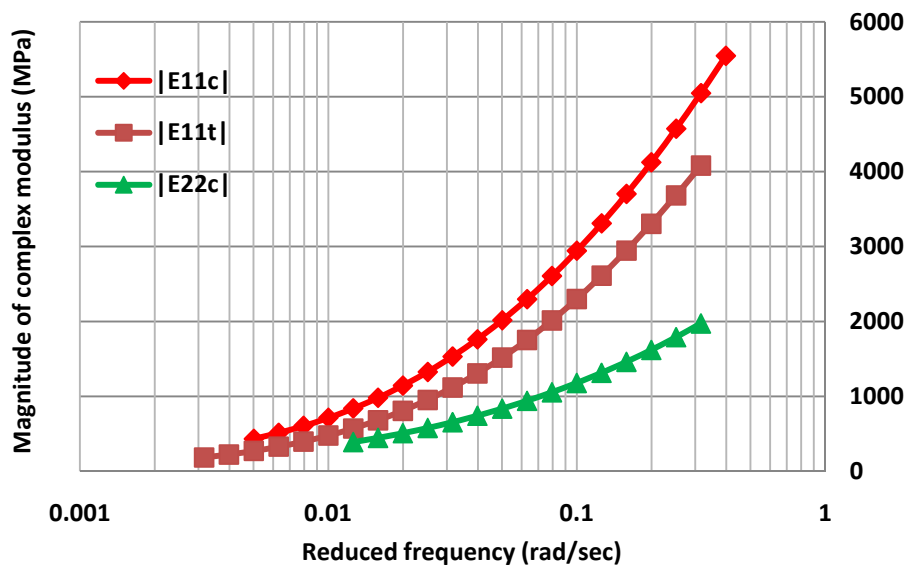


Figure F1c-4.1. Master curves of complex modulus magnitude at reference temperature 20°C.

The master curves of the complex modulus phase angle are presented in figure F1c-4.2. The phase angles of the two compressive complex moduli have close peak values, which are around 40 degrees. In contrast, the phase angle of the tensile complex modulus has a peak value of approximately 75 degrees. These findings are reasonable because when the asphalt mixture is in tension, it is mainly the asphalt binder and asphalt mastic that take the tensile load. As a result, the tensile properties of the asphalt mixture should be close to the tensile properties of the asphalt binder or asphalt mastic, which indicates a high peak value of the phase angle of the tensile modulus. When the asphalt mixture is in compression, the aggregates play an important role so the asphalt mixture is less viscoelastic. The difference in phase angle between compressive moduli and tensile modulus demonstrates again that the compressive properties of the asphalt mixtures are significantly different from the tensile properties.

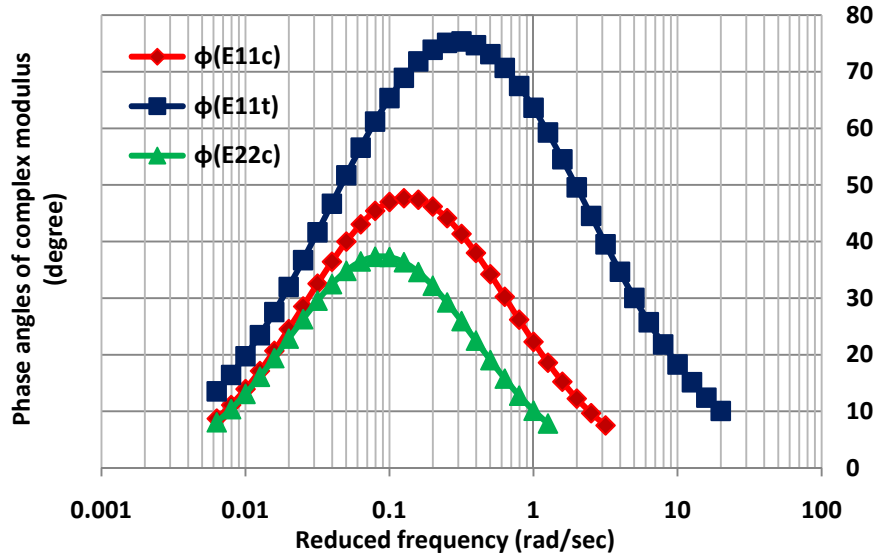


Figure F1c-4.2. Master curves of complex modulus phase angle at reference temperature 20°C.

Figures F1c-4.3 and F1c-4.4 illustrates the master curves of the magnitude and phase angle of the complex Poisson's ratios, respectively. It is reasonable for the complex Poisson's ratio to have a magnitude greater than 0.5 in this study because in anisotropic elasticity, the Poisson's ratio can range between -1 and 1.

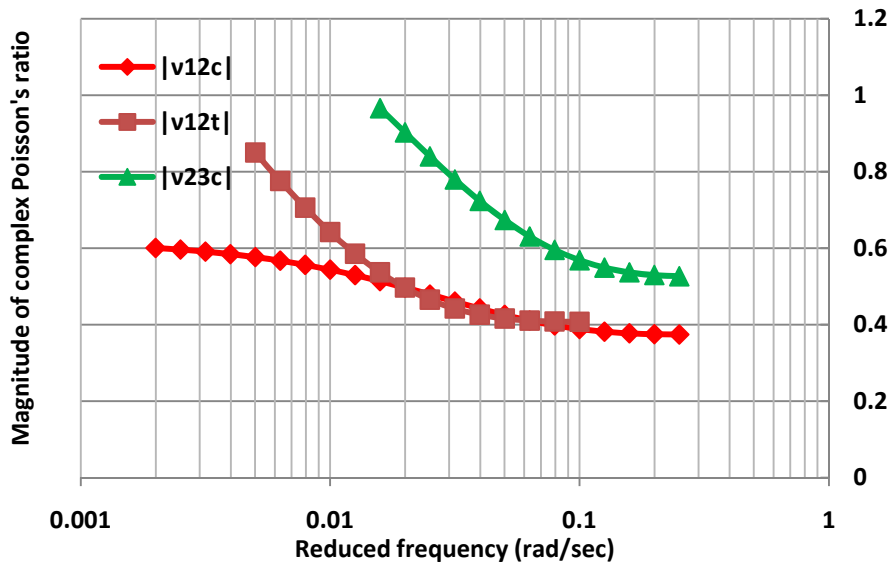


Figure F1c-4.3. Master curves of the magnitude of complex Poisson's ratio at reference temperature 20°C.

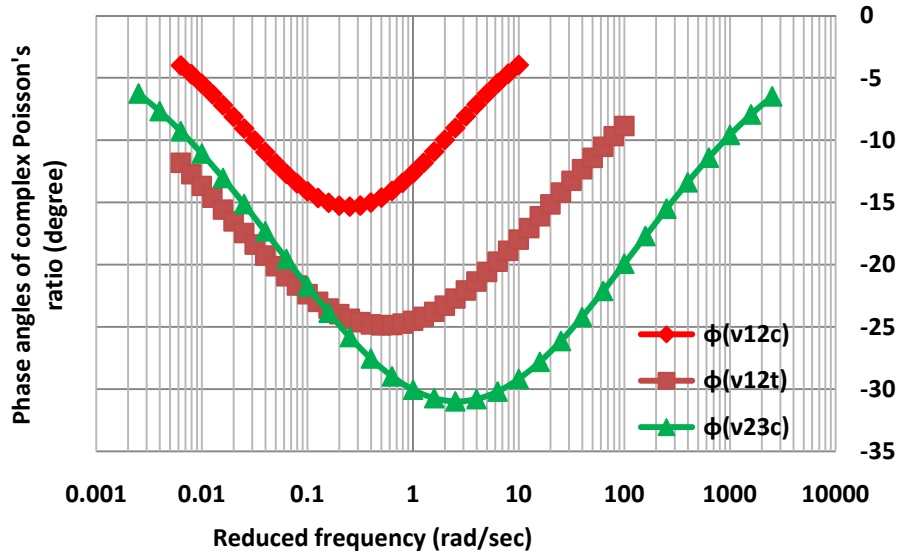


Figure F2c-4.4. Master curves of the phase angle of complex Poisson's ratio at reference temperature 20°C.

Significant Results

A new testing method was completed in this quarter to characterize the anisotropic viscoelastic properties of undamaged asphalt mixtures in compression. The newly developed test method is time-saving because the entire master curve testing process can be completed in one day. The tests used in this new method are all non-destructive so the same specimen is not damaged in the tests and can be reused in the future destructive tests for its properties in a damaged state.

The test results demonstrate that the tensile properties of the asphalt mixture are significantly different from the compressive properties. The asphalt mixture also shows a strong anisotropy when it is under compressive loading.

Significant Problems, Issues and Potential Impact on Progress

The newly purchased Material Testing System (MTS) was not ready for use yet. The software installation is expected to be complete in the next quarter.

Work Planned Next Quarter

In the next quarter, the mechanical properties of the undamaged asphalt mixture will serve as a reference state from which the damage that is introduced into the asphalt mixture can be quantified. An anisotropic viscoplastic continuum damage model will be developed to characterize the evolution of the viscoplastic deformation in the asphalt mixture. The proposed model will account for the anisotropy due to the preferential aggregate distribution, viscoplastic work hardening deformation, progressive damage evolution and simultaneous crack growth in the asphalt mixture under the increasing number of loading cycles in a destructive test.

Subtask F1c-5: Polymer Modified Asphalt Materials (TAMU)

Work Done This Quarter

In this quarter, preliminary characterizations of interactions of styrene-butadiene-styrene tri-block copolymer (SBS) with asphalt have been explored with FTIR and rheological measurements. SBS content may be quantified based on FTIR absorption of poly-butadiene at 966 cm^{-1} and polystyrene at 699 cm^{-1} (Zhang et al. 2008; Masson et al. 2001). The effect of polymer modifier on binder rheological properties can be determined by comparing rheological properties of base binder and its SBS mixture. Indexes such as the ratio between limiting viscosity (or DSR function) of polymer modified binder to limiting viscosity (or DSR function) of the base binder give an indication of polymer effectiveness in the asphalt. The DSR function would be the preferred function in the event that a low shear rate limiting viscosity does not exist for the polymer modified asphalt.

Based on those preliminary characterization methods, changes of polymer-asphalt interaction (polymer degradation) with oxidation have been investigated by oxidizing polymer modified asphalt in different temperatures at atmospheric air pressure. Figure F1c-5.1 shows changes to poly-butadiene content of SEM 70-22, indicated by its peak area at 966 cm^{-1} , at different temperatures with oxidation. These data, though not yet extensive enough, suggest a general trend of SBS degradation with oxidation. Figure F1c-5.2 shows decreases to the DSR function index (ratio of the DSR function of the polymer modified binder SEM 70-22 to the DSR function of the base binder SEM 64-22) over time due to oxidation at several temperatures. Clearly, as SBS degrades, polymer effectiveness (interaction between polymer and asphalt), as indicated by the modified binder's rheology, is reduced.

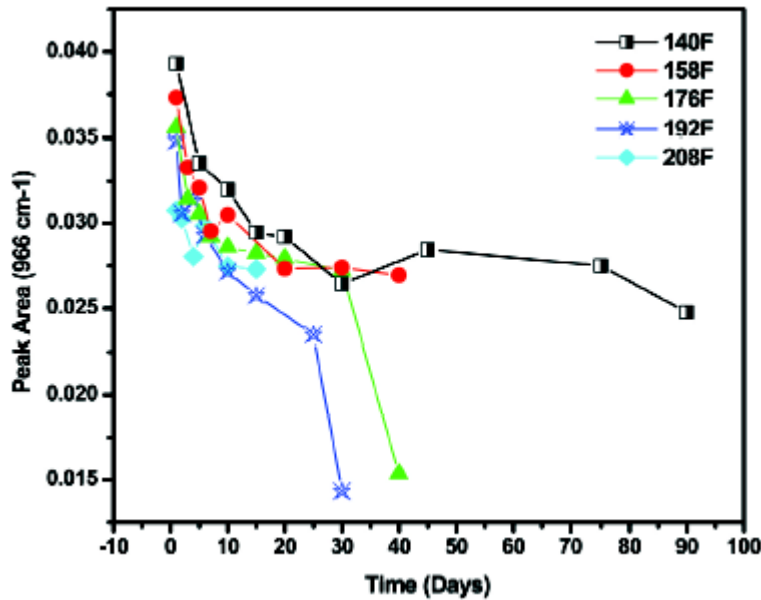


Figure F1c-5.1. Changes in poly-butadiene content (absorption at 966 cm^{-1}) with oxidation.

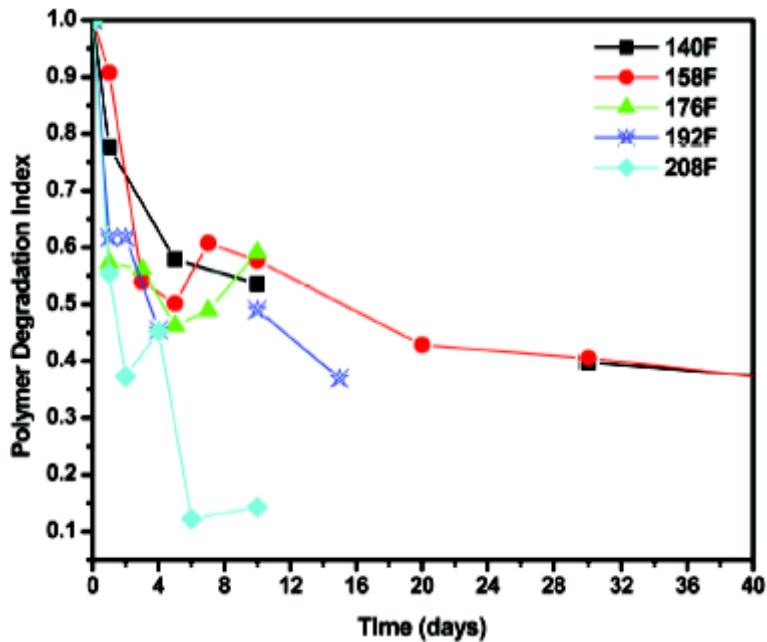


Figure F1c-5.2. Changes in DSR function index with oxidation.

Significant Results

The effectiveness of polymer in asphalts has been demonstrated to decrease with binder oxidation.

Significant Problems, Issues and Potential Impact on Progress

None.

Work Planned Next Quarter

In the next quarter, characterization methods of polymer-asphalt interaction will be further explored and improved, including morphology characterization with fluorescent microscopy and confocal microscopy. With reliable characterization methods, changes of polymer-asphalt interaction will be further investigated with studies on a number of polymer-modified asphalts to answer questions such as how polymer or polymer-asphalt interaction degrades with oxidation and how quickly the degradation occurs and its impact on mixture fatigue.

Cited References

Zhang P., J. He, and X. Zhou, 2008, An FTIR Standard Addition Method for Quantification of Bound Styrene in Its Copolymers. *Polymer Testing*, 27, 153-157.

Masson J-F., L. Pelletier, and P. Collins, 2001, Rapid FTIR Method for Quantification of Styrene-Butadiene Type Copolymers in Bitumen. *Journal of Applied Polymer Science*, 79, 1034-1041.

Work Element F1d: Healing

Subtasks F1d-1: Critical review of the literature

F1d-2: Material selection

F1d-3: Experiment design

F1d-4: Test methods to measure properties related to healing

Work Done This Quarter

Temperature dependence of intrinsic healing in asphalt binders

Intrinsic healing of asphalt binder can be determined using the DSR based test method as described above. Based on the hypothesis for the healing mechanism it is expected that the intrinsic healing of asphalt binders would be temperature dependent. In order to validate this hypothesis and quantify the rate of intrinsic healing was determined at three different temperatures using the DSR. This testing was recently completed and the data are being analyzed.

Experiment design to determine wetting characteristics of asphalt binder

The rate of wetting of asphalt binders is one of the two important components of the healing model. In order to validate the model presented in the form of equation (1) the rate of wetting and rate of intrinsic healing must be known for a given material. The DSR based test method may be used to determine the rate of intrinsic healing. However, the rate of wetting cannot be measured directly. Based on this limitation, two options were explored to validate the healing model.

The first option was to control the rate of wetting experimentally by performing a strain-controlled test in direct tension mode on sand-asphalt mixtures. In this case the rate of deformation from the peak strain to zero strain can be assumed to represent the rate of crack closure for mode I cracks formed during the fatigue cracking process. Notwithstanding the accuracy of this assumption, one confounding factor in this approach was the stress reversal as the crack is forced to close. Stress reversal from tension to compression is expected for time dependent materials subjected to cyclic loading in a displacement-controlled mode. This stress reversal would invalidate the use of intrinsic healing rates that are not measured with the specimen subjected to a compressive stress state. Based on preliminary test results and feedback collected during the FHWA Models Expert Task Group meeting in San Antonio we have decided not to pursue this option to validate the healing model.

The second option to validate the healing models is back calculate the rate of wetting using experimental data and intrinsic healing properties of the binder with equation 1. We are currently

conducting preliminary tests to validate this approach. A deconvolution process can be used to back-calculate the wetting function. The model will be validated using a randomized series of loading and rest periods. A preliminary experiment design to accomplish this was developed; this experiment design will be finalized and reported in the forthcoming quarterly reports.

Significant Problems, Issues and Potential Impact on Progress

None.

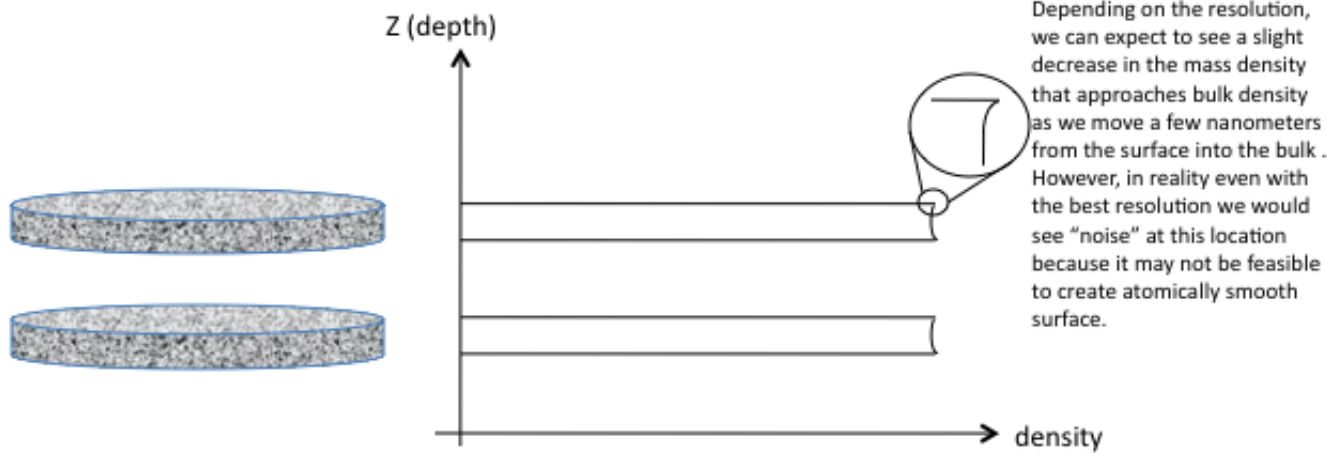
Work Planned Next Quarter

1. Validation of the healing mechanism using synchrotron experiments

Texas A&M and ARC have been offered a unique opportunity to use the Canadian Light Source Synchrotron located at the University of Saskatchewan to perform key experiments related to the process of healing. The use of beam time from the synchrotron will not cost the ARC project.

The objective of this experiment is to determine the rate at which intrinsic healing occurs across an artificially created crack interface. The integrity of the material and amount of healing is quantified in terms of the mass density of the material. The hypothesis here is that the mass density at the interface of a crack would be zero (point of singularity). However, as the material heals over time the average mass density across the interface should approach a value that is similar to the bulk mass density.

The following is the outline for the experiments that will be conducted. Two specimens of the asphalt binder will be prepared on solid substrates (figure F1d.1). The faces of these two specimens will be used to represent two faces of an ideally fractured bulk material. These two faces will be brought into intimate contact with each other and the mass density will be monitored across the interface over time (figure F1d.2).



Approximately 50 micron thin film spin cast on silica substrate (bulk specimens up to a few millimeters can also be created using molds)

Figure F1d.1. Schematic of the specimens and expected density profile.

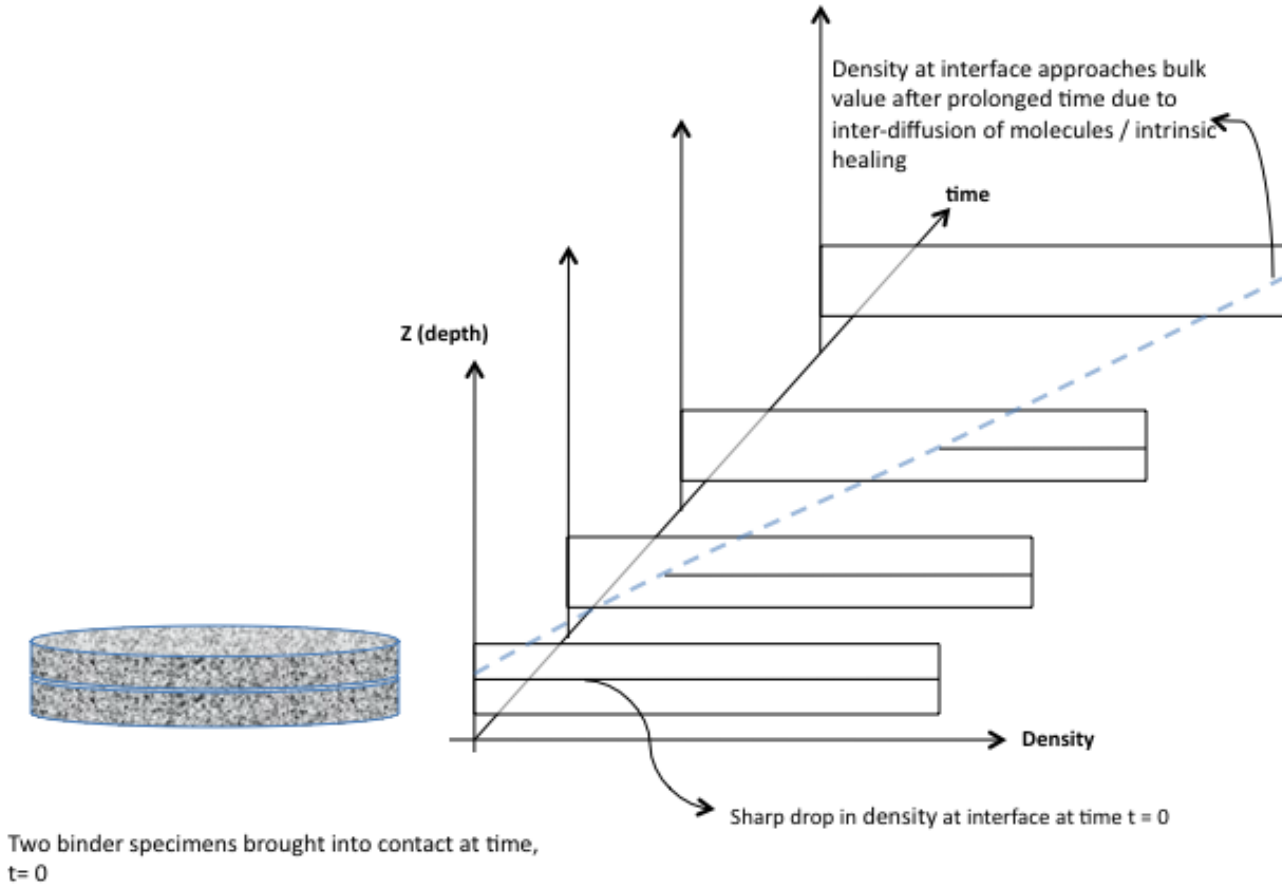


Figure F1d.2. Measurement of density across the interface over time.

2. *Determining the wetting function for the healing model for sand-asphalt or FAM mixtures and validating the model using randomized loading and rest periods*

As described in equation (1), there are two critical components for the micro-mechanical healing model. First is the rate of intrinsic healing of asphalt binders. These properties can be measured using the DSR based test method. Second, is the rate of crack wetting in a mixture that is undergoing fatigue cracking. The rate of crack wetting can be determined using material properties with the model for crack wetting that was originally developed by Schapery as shown in equation F1d.2 below.

$$\frac{d\phi(tX)}{dt} = \dot{a}_b = \beta \left[\frac{1}{D_1 k_m} \left\{ \frac{\pi W_c}{4(1-\nu^2)\sigma_b^2 \beta} D_0 \right\} \right]^{-\frac{1}{m}} \quad (\text{F1d.2})$$

In equation F1d.2, W_c is the work of cohesion; ν is the Poisson's ratio; σ_b represents the stresses at the crack surfaces; \dot{a}_b is crack closing speed; β is the healing process zone; D_0 , D_1 , and m are creep compliance parameters which can be obtained by fitting $D(t) = D_0 + D_1 t^m$; and k_m is a

□

□

material constant that can be computed from m . Material properties such as the healing process zone cannot be obtained by direct experimental measurements. Therefore, an alternate approach is to back calculate the rate of wetting of asphalt binders in sand-asphalt or full asphalt mixtures using equation (1). In other words, the overall healing of a test specimen will be measured experimentally and the wetting characteristics will be obtained using a deconvolution of equation (1), given that the rate of intrinsic healing is known a priori using the DSR test method.

A preliminary experiment design has been developed to determine the rate of wetting. Preliminary tests are currently being carried out to validate the feasibility of this experiment design. All tests are currently being carried out using the DMA in torsional shear. The final test matrix and approach will be presented in forthcoming quarterly reports. Once the rates of wetting and intrinsic healing are determined, a series of random fatigue cracking and self-healing experiments will be carried out to validate the applicability of this micromechanics model.

3. Validating the relationship between mechanical properties and wetting characteristics of the sand-asphalt mixture or FAM

The last and one the most important components of this work element will be to determine the relationship between the rate of wetting and the viscoelastic properties of the material. Rate of wetting for different materials will be obtained from the previous step. The theoretical relationship between the rate of wetting and viscoelastic properties is available in the form of equation F1d.2. The model presented in equation 2 can be partially validated using the results from this subtask.

4. New Subtask F1d-5b: Thermodynamic model for healing in asphalt binders

This is a new subtask that is being added to the work element on healing. The micromechanical model of healing described in F1d-5 addresses the healing of microcracks. As one would glean from a close analysis of the Schapery closure speed model, most of the healing is expected to occur in the β process zone. The size range of these cracks is not exactly defined but one would expect them to range from the nano scale to a few millimeters. Work by Kringos, Schmetts, Pauli and Scarpas (2009) has relied upon Atomic Force Microscope (AFM) surface topography of asphalt binders that show the evidence of phase separation within the bitumen. They postulate that if the mechanical properties, specifically stiffnesses, of the phases are significantly different then the interfaces between the phases serve as natural stress inducers. They used their finite element model CAPA 3-D to demonstrate this. The result of the TU Delft study was to demonstrate the presence of crazing that occurs among the phases at the interfaces. Kringos et al. described thermodynamic considerations and a constitutive formulation that could explain how a reversal of the crazing process could occur with the input of thermal energy and/or mechanical energy back into the system. This results in healing at a smaller length scale than the model presented in this section. The ARC team applauds the excellent work and approach being developed by the TU Delft team.

In fact, as described in the Year 2 and Year 3 work plans, ARC has designed AFM experiments aimed at investigating the properties of different phases of the bitumen at TAMU. This work has demonstrated differences in the viscoelastic properties of the phases, and this work will be continued at an accelerated rate in year 4. Two Ph.D. level students working jointly under the

supervision of Professors Rajagopal in the Mechanical Engineering Department of TAMU and Dallas Little have been trained in thermodynamic and mechanics by Professor Rajagopal for the past year and one half to address this problem. In year four they will complete the task of defining the viscoelastic properties between the phases of the asphalt binder using the AFM. Professor Rajagopal is well recognized as an expert in mechanical models based on thermodynamic natural configurations and will supervise the development of a healing model or healing parameter to address healing from this length scale. We believe we can synergistically work with our colleagues at TU Delft who have made significant development in modeling healing at this length scale, and we plan to seek their advice and collaboration in each step of this approach in order to properly recognize their excellent work and optimize the results. In fact Professors Scarpas and Little are working together on synchrotron experiments with Dr. Alexander Schmets, who has already taken steps using Spin Echo Small Angle Neutron Scattering (SESANS) to investigate whether the phase appearance at the surface of the binder identified through AFM is in fact a surface phenomenon or a bulk phenomenon.

Subtask F1d-5: Testing of Materials for model validation* (TAMU)

Work Done This Quarter

No activity this quarter.

Work Planned Next Quarter

This will begin next quarter.

Subtask F1d-6: Evaluate Relationship Between Healing and Endurance Limit of Asphalt Binders (UWM)

Work Done This Quarter

In this quarter, a strain-controlled time sweep with intermittent loading was used to evaluate the effect of healing on fatigue life. Previous efforts of the research group regarding healing characterization by means of time sweep with rest periods were unsuccessful due to poor repeatability of the testing results. However, improvements on the testing procedures, specifically during specimen preparation and trimming, resulted in highly repeatable tests. The loading sequence of the time sweep tests consisted of 10 cycles of loading followed by a rest period. The rest periods used were zero, two and four seconds. All tests were conducted with a frequency of 10 Hz, shear strain of 4%, and temperature of 25 °C. The binder tested was an unaged neat PG 64-22. Two tests were conducted for each rest period.

The number of loading cycles resulting in a 50% reduction in the complex modulus is commonly used to define fatigue life (Tsai and Monismith 2007). Figure F1d-6.1 provides the effect of healing on fatigue life based on the testing results. The figure indicates that increasing the rest period extends the fatigue life.

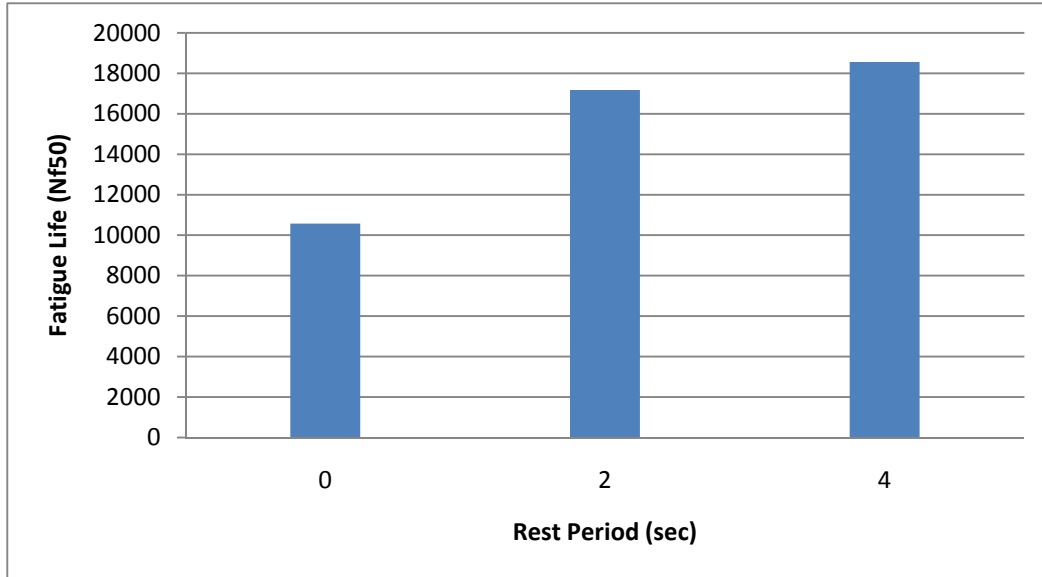


Figure F1d-6.1. Graph. Effect of healing on fatigue life.

Additionally, the ratio of dissipated energy change (RDEC) was used to evaluate fatigue and healing properties (Shen and Chiu 2009). Using dissipated energy principles to predict fatigue life has been studied extensively. A definition of dissipated energy is provided below.

$$DE = \pi \frac{\tau^2}{G^*} \sin(\delta) \quad (\text{F1d-6.1})$$

where

DE = dissipated energy

τ = shear stress

G^* = complex modulus

δ = phase angle

Shen et al. (2009) found that the change in dissipated energy under controlled-strain loading has three distinct stages. This phenomenon is shown in figure F1d-6.2. The RDEC is the slope of the dissipated energy versus number of loading cycles curve. In stage II, the RDEC is nearly constant. This constant slope is called the plateau value (PV). The PV has been proven to correlate with the fatigue life of the material (Shen and Carpenter 2005). The measured PV at all rest periods tested are included in table F1d-6.1. As shown in the table, increasing the rest period decreases the PV. This is expected as a lower PV corresponds to a higher fatigue life.

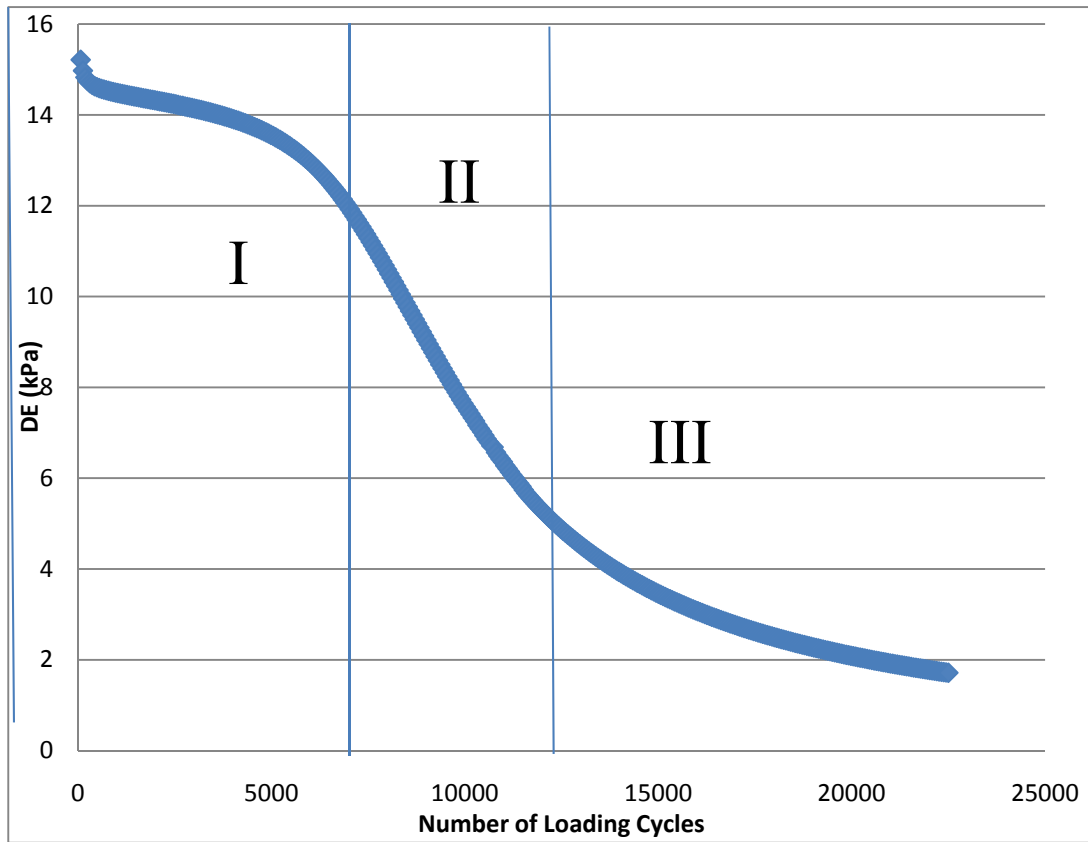


Figure F1d-6.2. Graph. Change in dissipated energy (DE) during a controlled-strain fatigue test.

Table F1d-6.1. Effect of healing on PV.

Rest Period (sec)	Run 1	Run 2	Average PV	Coefficient of Variation
0	1.51E-03	1.29E-03	1.40E-03	5.56%
2	8.71E-04	8.08E-04	8.40E-04	2.65%
4	7.12E-04	7.50E-04	7.31E-04	1.84%

It has been shown that for mixtures and binders, the PV value and fatigue life corresponding to a 50% reduction in complex modulus (i.e., Nf50) can be uniquely related using a power law function (Shen and Carpenter 2005; Shen et al. 2009). The results from the time sweep tests with rest periods indicate that a power law function adequately fits the relationship between PV and Nf50, as shown in figure F1d-6.3.

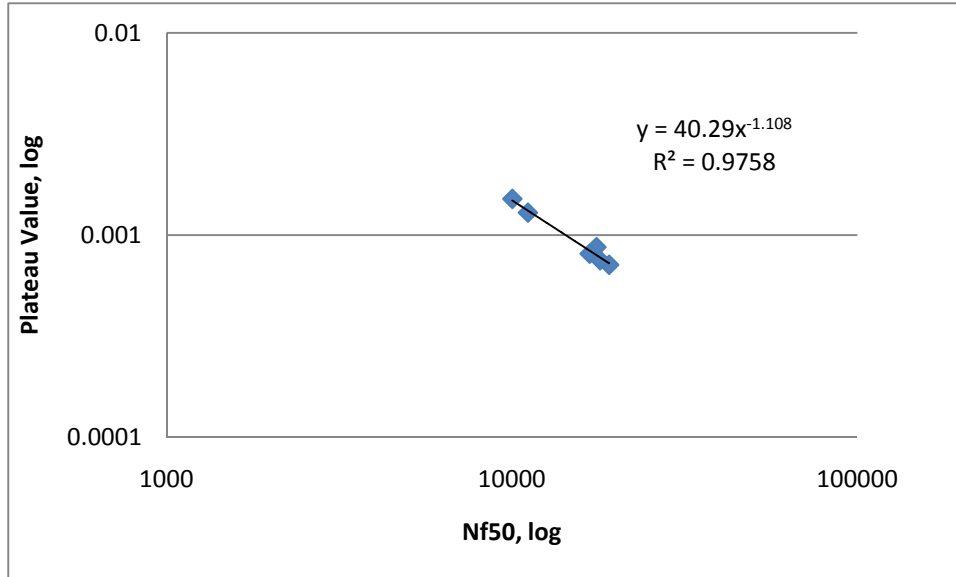


Figure F1d-6.3. Graph. PV – fatigue life relationship.

The healing rate (HR) represents the rate of energy recovery per unit of rest time and it is independent of the rest period used. The HR of a binder is defined as the slope of the PV versus rest period plus one (RP+1) curve in a log-log scale (Shen and Carpenter 2005). Figure F1d-6.4 shows the PV versus RP+1 for the binder tested. The calculated HR for the PG 64-22 binder is 0.414. The measured HR was compared to a predictive model for calculating the HR as a function of rheological properties of binders (G^*) measured at a given frequency and strain. The equation for the predictive model developed by Shen et al. (2009) is:

$$HR = 40.225\gamma^{-0.963}G^{*-0.4114}f^{-0.2853} \quad (\text{F1d-6.2})$$

where

HR = healing rate

G^* = initial complex modulus (Pa)

γ = shear strain

f = frequency (Hz)

Testing conditions of a 4% shear strain, frequency of 10 Hz, and a measured initial G^* of 3,350,000 Pa were used in the model. The predicted HR based on the model is 0.957, which is more than double the measured HR. It is important to note that the model described by equation F1d-6.2 was developed for a PG 64-28. The research team used this predictive model to determine if the magnitude of the HR obtained for the tested binder was reasonable. The team was not expecting to match the prediction exactly because the HR depends on the binder type.

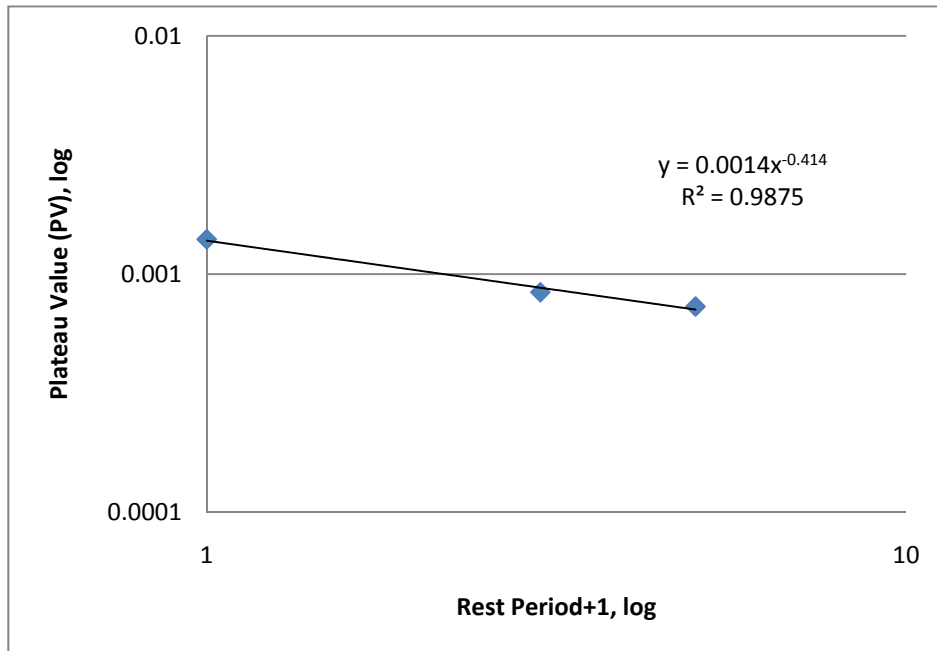


Figure F1d-6.4. Graph. PV – fatigue life relationship.

Significant Results

The research team was able to perform repeatable time sweep tests with rest periods (coefficient of variation < 6%) for an un-aged neat binder, as shown in figure F1d-6.5. Also, reasonable values of HR were obtained based on the approach of RDEC and PV proposed by Shen et al. (2009).

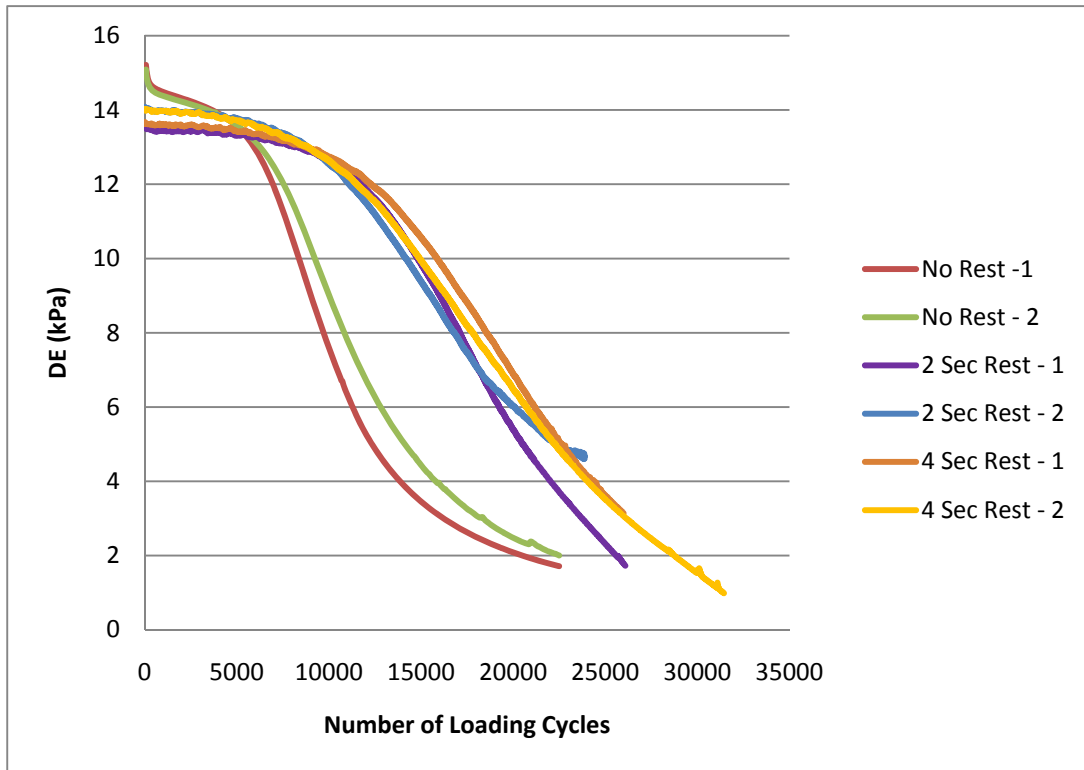


Figure F1d-6.5. Graph. Time sweep tests with rest periods.

Significant Problems, Issues and Potential Impact on Progress

The progress of this task has been delayed due to dedicating more time to the F2e work element and delays in arrival of a graduate student expected to work in this project until December 2009. The research team will focus its efforts in this work element to reduce the impact of the delay.

Work Planned Next Quarter

Next quarter, characterization of binder healing using the concepts of RDEC and PV will continue. The experimental plan presented in the Year 4 work plan has been developed and the experimental matrix includes: one base binder, four rest periods, three modifications, two strain levels, and two replicates per condition.

Cited References

Shen, S. and S. H. Carpenter, 2005, Application of the Dissipated Energy Concept in Fatigue Endurance Limit Testing. *Transportation Research Record* 1929: 165-173.

Shen, S. and H. Chiu, 2009, Fatigue and Healing in Asphalt Binders, Presented at the 88th Transportation Research Board Annual Meeting, Washington, D.C.

Shen, S., H. Chiu, and H. Huang, 2009, Characterization of Fatigue and Healing for Asphalt Binders, *ASCE Journal of Materials in Civil Engineering*, Accepted for Publication.

Tsai, B. W. and C. Monismith, 2007, Influence of Asphalt Binder Properties on the Fatigue Performance of Asphalt Concrete Pavements. *Asphalt Paving Technology: Association of Asphalt Paving Technologists-Proceedings of the Technical Sessions 74*: 733-789.

Subtask F1d-7: Coordinate with Atomic Force Microscopic (AFM) Analysis (WRI)

Work Done This Quarter

Hypothesis

In the later stages of fatigue cracking, the failing sections of pavement are often observed to form distinct crack patterns (i.e., alligator crack pattern) usually localized in the traffic wheel path, and often occurring later in the life of the pavement. By comparison, in investigations relating to metal fatigue, pattern forming cracking has been successfully correlated to the microstructure which develops in these materials during casting (Cappelli et al. 2008, Bian and Taheri 2008) corresponding to grain boundaries at the meso, micron and nanometer scale. Occurrence of grain boundaries may be a result of the heterogeneous nature of a material (Cappelli et al. 2008; Bian and Taheri 2008). Thus, this same idea (i.e., grain boundary formation) can be applied to paving materials if such pattern forming phenomena were to be observed (Robertson et al. 2005, 2006).

Experimental

Asphalts and asphalt fractions were doped with model waxes (normal paraffins). Octacosane ($C_{28}H_{58}$) and triacontane ($C_{30}H_{62}$), were purchased from Analabs, Inc. Tetratetracontane ($C_{44}H_{90}$) was purchased from Alpha Products, and pentacontane ($C_{50}H_{102}$) and hexacontane ($C_{60}H_{122}$) were purchased from Fluka Chemie. Fischer-Tropsch wax, (Sasobit®, nominal melt point, $100^{\circ}C \infty C_{60}H_{122}$) was donated by Sasol Wax North America Corp., Hayward, CA. Sample mixtures were prepared by dissolving, individually, model waxes and asphalts in toluene. Asphalt-toluene solutions were mixed with wax-toluene solutions to produce 1% to 8% by weight wax in asphalt sample thin-films. Solution mixtures (asphalts, waxes, and asphalt-wax mixtures) were spin-cast on boro-silicate glass microscope slides to produce 2-micron to 10-nm thick films. Asphalt was also doped with 1.5% by mass Fisher-Tropes wax (Sasobit®, Sasol Wax North America Corp., Hayward, CA). Sample were prepared by adding FT-wax pellets to a small can of asphalt then stirring the contents in a $130^{\circ}C$ oven equipped with a paddle mixer. Thin-film samples were prepared by smearing heat softened material on a glass slide.

Morphology of Model Wax and Wax-Doped Asphalts

Sample thin-films were prepared by doping model waxes into naturally low wax content asphalts. In these studies model paraffin waxes; octacosane ($C_{28}H_{58}$), triacontane ($C_{30}H_{62}$), tetratetracontane ($C_{44}H_{90}$), pentacontane ($C_{50}H_{102}$) and hexacontane ($C_{60}H_{122}$), and an asphalt warm mix modifier wax, Fischer-Tropsch wax, (Sasobit®, nominal melt point of $100^{\circ}C \infty C_{60}H_{122}$) were utilized. In certain cases, mixtures of these five model waxes were also prepared

and studied. Samples were generally prepared by dissolving the model paraffin wax in a solvent such as toluene or n-heptane, followed by thin-film spin casting. In most cases, at room temperature, paraffin-solvent solutions were observed to gel, thus, solutions were gently heated just prior to loading of the syringe in order to spin cast the film. Paraffin solutions (toluene) were then combined with an asphalt toluene solution (naturally low wax content asphalt AAG-1) to produce mixtures in the 1% to 8% by mass model wax concentration range. Prior to sample thin-film preparation, each solution mixture was stirred then spin-cast and finally dried in air for several minutes prior to AFM analysis. WM-AFM (topography, error and phase) images were collected for nominally 1-micron to 500-nm thick films of both wax and wax-doped samples, both before and after thermal conditioning by annealing to 80°C (10 to 20-min).

Figures F1d-7.1 through F1d-7.8 depicts topography, error or phase WM-AFM images of model wax crystal morphologies and wax-doped films of asphalt AAG-1. In all cases the wax-doped asphalt samples exhibit different microstructure development compared to the original AAG-1 sample, depicted in both figures F1d-7.1 and 8. In many cases, particularly with doped samples containing higher molecular weight waxes; tetratetracontane ($C_{44}H_{90}$), pentacontane ($C_{50}H_{102}$), hexacontane ($C_{60}H_{122}$), and Fischer-Tropsch wax, (Sasobit®), "bee" structuring is readily observed.

In figure F1d-7.1, for example, large irregular shaped agglomerations of octacosane lamella are depicted in scan-a, while after heating, half-hemispherical structures form, scan-b, and in very thin films, dendrites may be observed. By comparison, octacosane doped into AAG-1 at 2%, 6%, and 8% by mass show a transition from a flat spotty surface (scan-a), to a scroll morphology (scan-d). The morphology of this sample is similar in appearance to IEC neutral fractions of asphalt AAM-1, which was discussed in the previous quarterly report. After thermally annealing these samples, (AAG-1 doped with 1%, 2%, and 6%), differ still from their un-annealed state, as depicted in figure F1d-7.3.

Similar observations may also be made for samples of AAG-1 doped with 2% by mass tetratetracontane, pentacontane, and hexacontane, where, in each case, "bee" microstructures form. In figure F1d-7.6, AFM scans were further obtained at different locations on the sample film, thus demonstrating that microstructures differed in shape as a function of location from the center of the film. These observations suggest that wax structuring is inhomogeneous within a sample film.

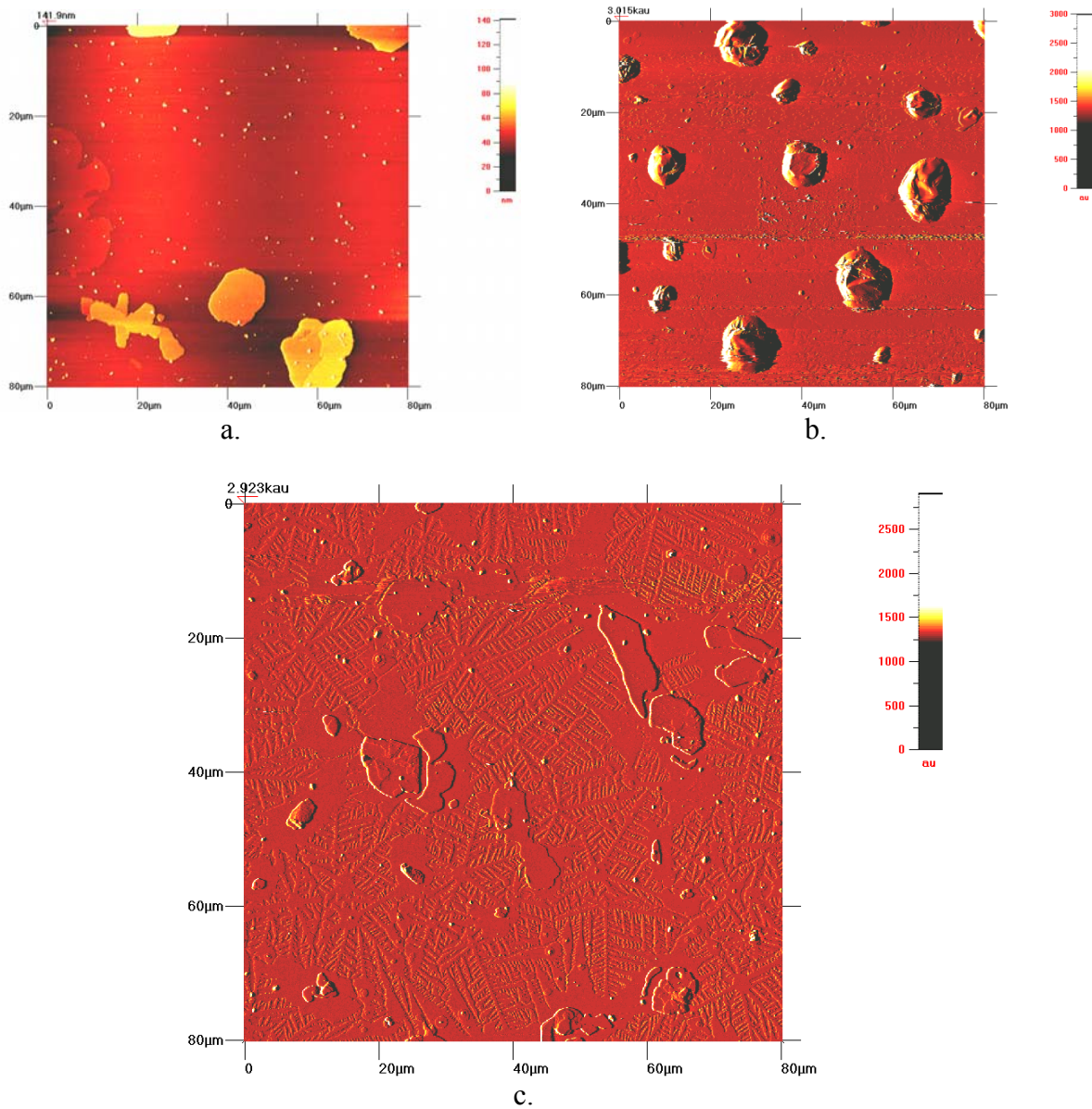
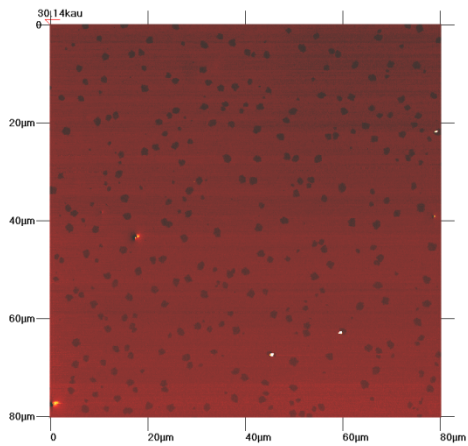
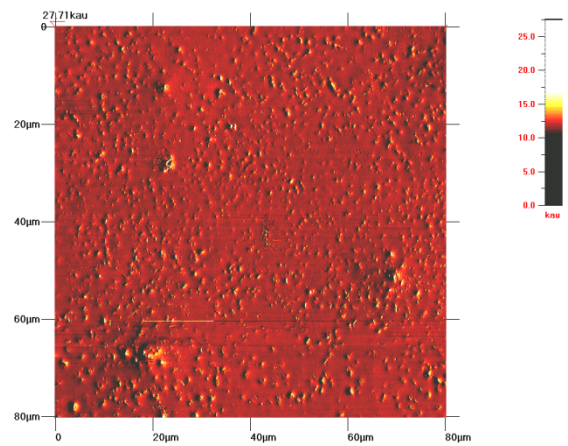


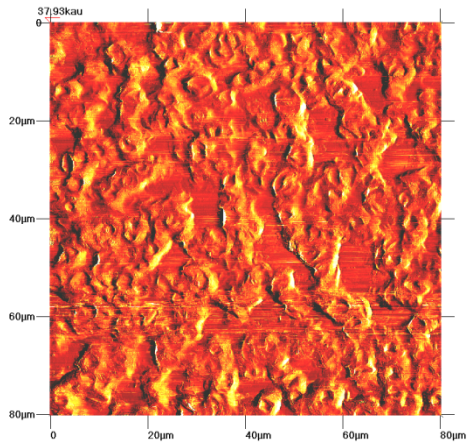
Figure F1d-7.1. Octacosane spin-cast from an n-heptane solution, a. (topography) before heat annealing, b. (error) after before heat annealing to 80°C, and c. (error) spin-cast after 10-fold dilution of original solution.



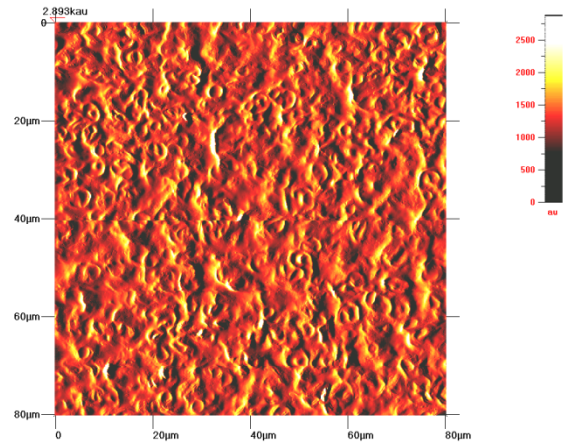
a.



b.



c.



d.

Figure F1d-7.2. AAG-1 mixed with octacosane at, a-d; 0% (phase), 2% (error), 6% (phase) and 8% (error), respectively, (imaged directly after spin casting).

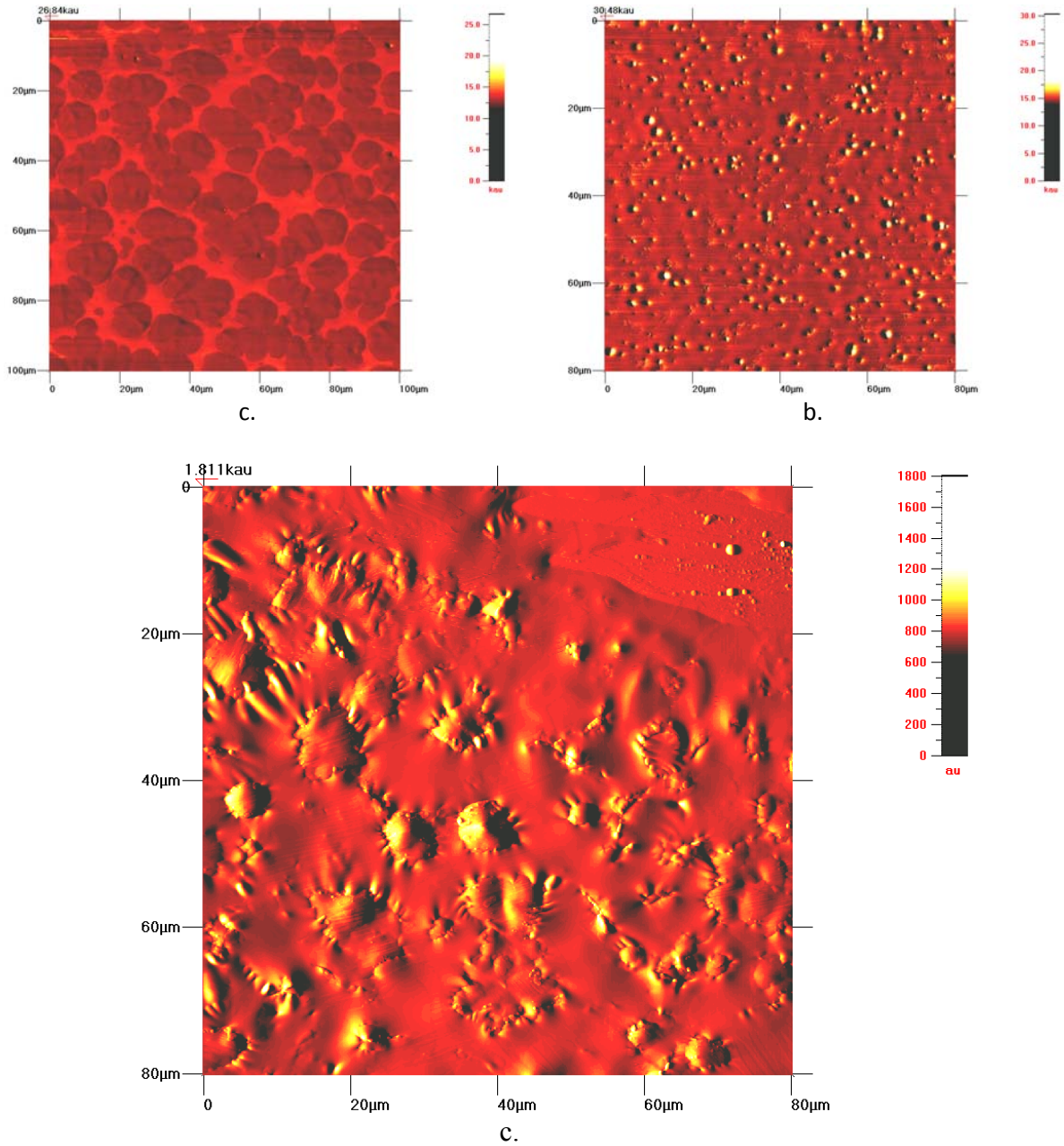


Figure F1d-7.3. AAG-1 mixed with, a-c; 1% (phase), 2% (phase) and 6% (error) octacosane, respectively, (all imaged after heat-annealing to 80°C).

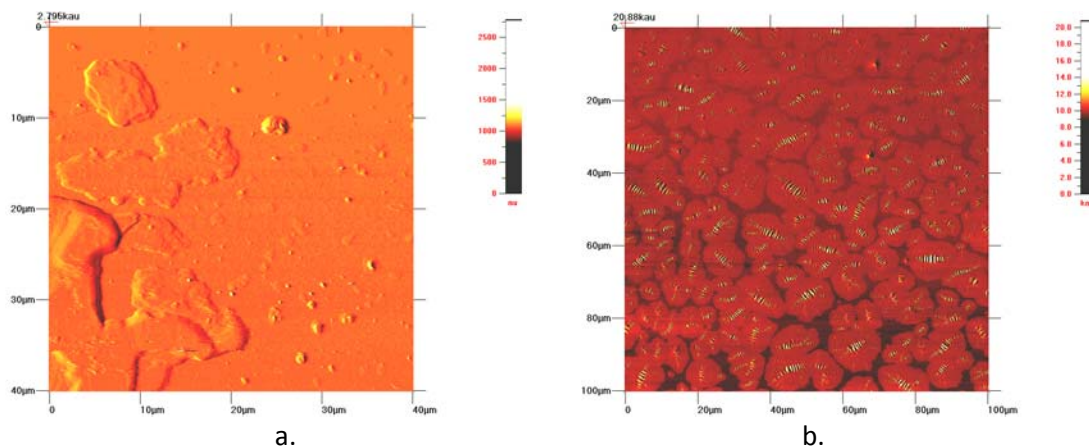


Figure F1d-7.4. a. (error) Tetratetracontane heat annealed to 80°C, and b. (phase) AAG-1 mixed with 2% (by mass) tetratetracontane heat annealed to 80°C.

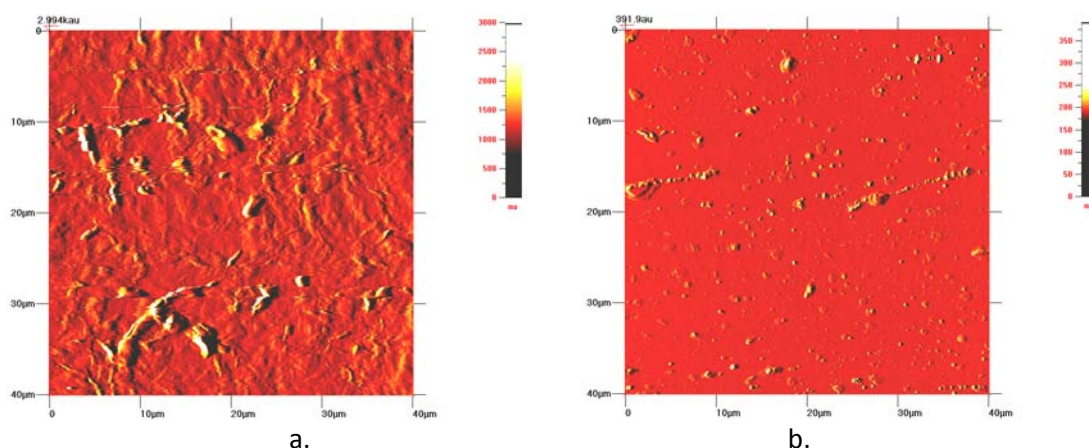


Figure F1d-7.5 a. (error) Pentacontane imaged directly of spin-casting from solution (toluene), and b. (error) pentacontane heat annealed to 80°C.

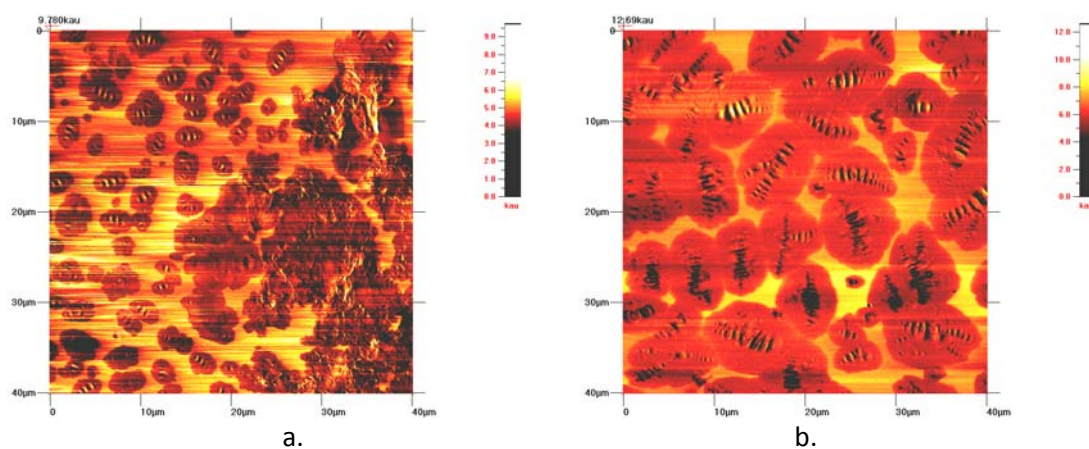


Figure F1d-7.6. a. (error, imaged at center of film) AAG-1 mixed with 2% (by mass) with pentacontane, and b. (phase, imaged midway between center and edge of film, same sample)

Finally, some of the most interesting structuring observed was associated with a wax mixture doped into AAG-1. Figure F1d-7.7, for example, depicts scans of octacosane plus hexacontane (50:50, by mass) doped at 2% by mass into AAG-1. The five pointed leaf shaped crystals that were observed have been reported elsewhere by Tsukruk and Reneker (1995), Loveinger et al. (1994), and Zhou et al. (2000).

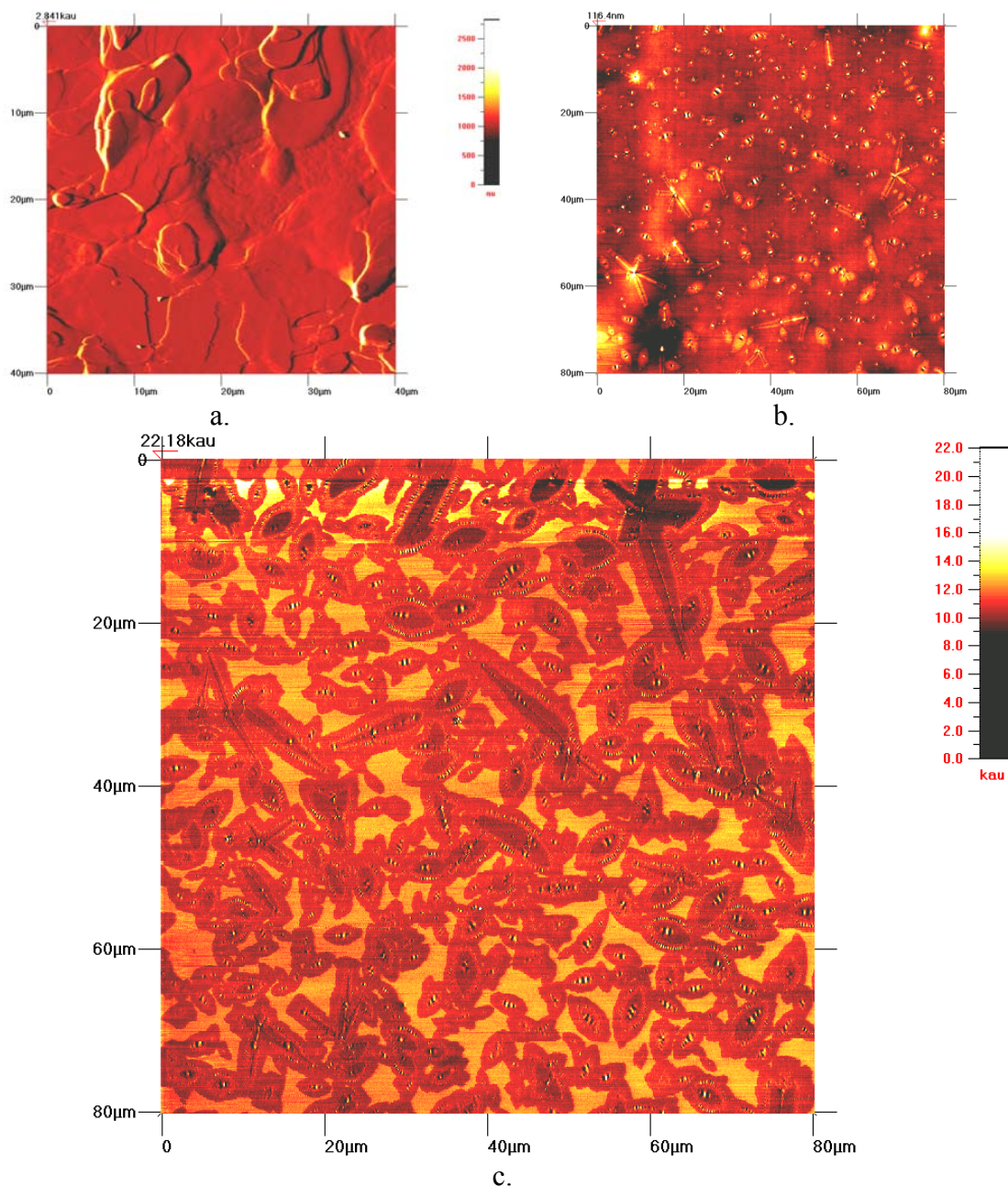


Figure F1d-7.7. a. (error) Octacosane+hexacontane (50:50, by mass) spin-cast from solution (toluene), b. (phase) AAG-1 mixed with 2% (by mass, 50:50 mixed wax blend) octacosane+hexacontane, and c. (error) AAG-1 mixed with 2% (by mass, 50:50 mixed wax blend) octacosane+hexacontane, heat annealed to 80°C.

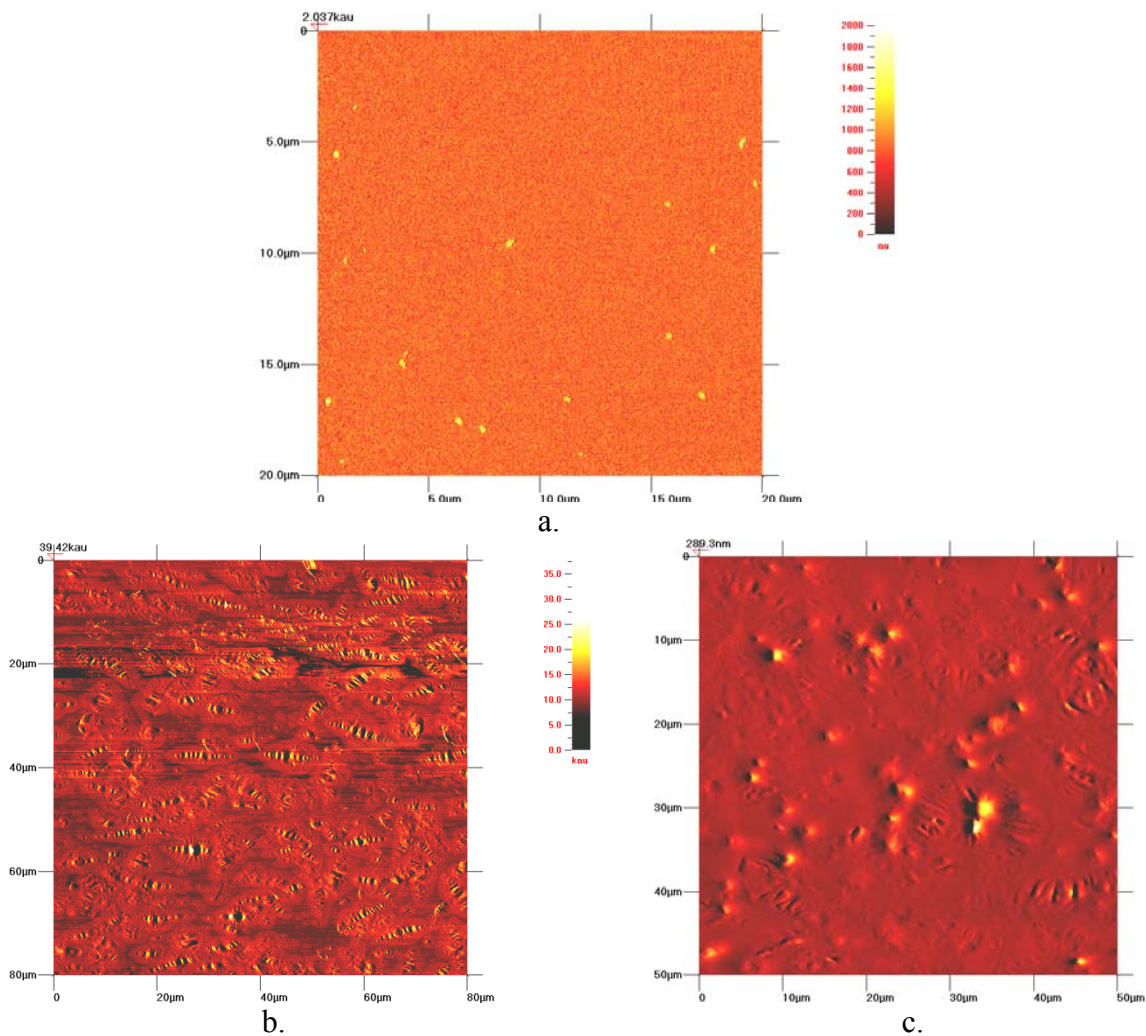


Figure F1d-7.8. a. WM-AFM phase-contrast images of AAG-1, b. AAG-1 blended with 1.5% by mass Fisher-Tropes wax, and c. topography image of AAG-1 blended with 2% by mass triacontane.

Interpretation of Findings: Paraffin Crystallization

Ferris et al. (1931), as early as 1931 observed wax crystals extracted from petroleum. Although the crystals depicted in their work are similar in shape to the structures depicted in this work, the crystals observed by Ferris et al. are comparatively orders of magnitude larger in size (macroscopic crystals). Chichakli and Jessen (1967) later studied the crystal habits of C_{22} n-alkanes mixed with heavier waxes ranging in composition from C_{26} to C_{53} , and in low concentration with SARA fractions derived from an East Texas crude oil. Paraffin crystal samples were prepared as solutions in n-heptane which were solvent evaporated on copper grids prior to imaging. These investigators reported observing orthorhombic micro-crystals by electron microscopy while crystallographic data was obtained by X-ray diffraction. Structuring depicted

in images of paraffin crystals, whether prepared in a heavier wax or SARA fractions were similar in shape and size to each other.

Toda et al. (1991) studied the lateral crystal habits of a select group of paraffins (C_n ; C_nH_{2n+2}). In these studies crystals were prepared in n-octane then deposited on glass slides between a cover plate after evaporation of the solvent. Images of the crystals obtained very close to the melting point temperature of the paraffin seemed to reveal that the single crystal habit differed based on the chain length of the paraffin where it was found that the lower molecular weight paraffins formed circular habits, ($\sim <C_{40}$: C_{19} , C_{22} , C_{24} , C_{34} , and C_{18} mixed with C_{20}), while higher molecular weight paraffins ($\sim >C_{40}$: C_{44} , C_{50} , and C_{66}) formed lenticular shaped habits. Furthermore, in certain cases, particularly with C_{18} and C_{20} n-alkanes, and C_{34} prepared in C_{19} diamond shaped habits were reported.

Dorset et al. (1990, 1993), Dorset and Annis (1996), considered single-crystal structuring in several different sizes of polymethylene systems. In many of these investigations the crystal morphology observed by electron microscopy was characterized in terms of sectorization of orthorhombic crystals. Dorset et al. (1990) specifically, reported that of some of the higher molecular weight n-paraffins, within the range $C_{36}H_{74}$ to $C_{82}H_{186}$, of which do not undergo lamellar chain folding, would otherwise form sectorized crystals, (i.e., flattened pyramidal structures with corrugations along the $\langle 130 \rangle$ plane of the crystal lamelle), while shorter n-paraffins, on the other hand, were found to not form sectors once crystallized.

Hollander et al. (2001) further observed dendrite growth in $C_{23}H_{48}$, $C_{25}H_{52}$, and $C_{32}H_{66}$, n-paraffins grown deposited from n-decane followed by recrystallization. Plomp et al. (2003) later observed dislocation movement in $C_{40}H_{82}$, n-paraffin wax structures by AFM resulting in imperfect crystal growth. In all of the studies cited thus far, on extended paraffins are assumed to form the crystals that were observed. In turn, Ungar et al. (2000) and Putra and Ungar (2003) studied the crystal habits of excessively long paraffins, n- $C_{198}H_{398}$ and n- $C_{246}H_{492}$, where it was found that the paraffin molecules could undergo at least single folding so that curved crystal growth faces are thus attributed to self-poisoning of the crystal lamella. Finally, White et al. (2002) observed cylindrical and scroll shaped lamellae in branched n-paraffins (C_{96} and C_{98}).

Tsukruk and Reneker (1995), Loveinger et al. (1994), and Zhou et al. (2000) also observed sectorization in polyethylene and polypropylene crystals. These systems are often found to product rectangular shaped crystals, often arranged in a radial patten extending from a central point where the rippling is present along the longer axis of the crystal. Kyu et al. (2000), Mehta et al. (2004a and b), and Xu et al. (2005) later reported observing the evolution of the same type of rippled morphologies in single crystals composed of syndiotactic polypropylene, which were produced from a poly(ethylene octane)- polypropylene melt, also imaged by AFM. Specifically, Kyu, Mehta and Xu (Kyu et al. 2000; Mehta et al. 2004a, 2004b; Xu et al. 2005) studied the "Growth Dynamics of Isotactic Polypropylene Single Crystals during Isothermal Crystallization from a Miscible Polymeric Solvent". In this work Mehta, Kyu and Xu employed a phase-field model to describe crystallization (solidification) processes subsequently observed by AFM in their sample films. Rippled structures in their model were considered in terms of periodic surface stresses at the crystals surface. Specifically, the authors derive a functional of the free energy contributions to crystal ordering,

$$\mathcal{F}_{crystal} = \int_{\Omega} \left(\begin{aligned} &\Phi_{\varphi} \left[\frac{\varphi^2}{2} - (1+\zeta) \frac{\varphi^3}{3} + \frac{\varphi^4}{4} \right] + \frac{1}{2} \left[\mathbf{\kappa}_{\theta} (\nabla\theta) + \varepsilon (\nabla^2\theta)^2 \right] \\ &+ \Phi_{\theta} \left[\frac{\theta^4}{2} - 4(\lambda_r - 1)\theta^2 \right] - \alpha\theta(\varphi - \varphi^2) + \frac{(\mathbf{\kappa}\nabla\varphi)^2}{2} \end{aligned} \right) d\Omega \quad (\text{F1d-7.1})$$

expressed in terms of a local free energy term

$$f_0 = \Phi_{\varphi} \left[\frac{\varphi^2}{2} - (1+\zeta) \frac{\varphi^3}{3} + \frac{\varphi^4}{4} \right] \quad (\text{F1d-7.2})$$

defined by an asymmetric double well potential function in φ , where φ is the crystal order parameter (non-conserved), and a potential field strength, Φ_{φ} . A free energy gradient term is further defined as

$$f_{\nabla} = \frac{(\mathbf{\kappa}\nabla\varphi)^2}{2} \quad (\text{F1d-7.3})$$

which quantifies the ‘‘diffuseness’’ of the liquid-solid crystal interfaces which develop during crystal formation, where $\mathbf{\kappa}$ -values are tensor components of the polarization vector in a polar crystal, and/or tensor components of the crystal-lattice symmetry (Cahn and Hilliard 1958, 1959a, 1959b). For a single crystal composed of a chain folded lamella with periodic undulations (Mehta et al. 2004a, 2004b), also included a curvature elastic free energy term,

$$f_{\theta} = \frac{1}{2} \left[\mathbf{\kappa}_{\theta} (\nabla\theta) + \varepsilon (\nabla^2\theta)^2 \right] \quad (\text{F1d-7.4})$$

and a free energy term for elastic deformation,

$$f_{\lambda} = \Phi_{\theta} \left[\frac{\theta^4}{2} - 4(\lambda_r - 1)\theta^2 \right] \quad (\text{F1d-7.5})$$

(i.e., the strain recovery potential associated with the deformation or volume contraction during crystallization), given

$$\lambda_r = \frac{\lambda}{\cos(\theta)} \quad (\text{F1d-7.6})$$

where Φ_{θ} is defined as the elastic modulus, θ is the angle of chain tilt of polymer molecules that comprise the lamella, and λ_r is the maximum recoverable strain. Finally $f_{\alpha\theta}$ is a free energy term that is added to the free energy functional expression accounting for coupling between the asymmetric double well potential and the tilt angle, expressed as

$$f_{\alpha\theta} = -\alpha\theta(\varphi - \varphi^2) \quad (\text{F1d-7.7})$$

In the results discussed here, our findings show that crystal habits of model n-paraffins match precisely with observations made by the researchers referenced herein. Specifically, lenticular, crystal habits with ripples (i.e., the "bee microstructures") were most often observed in neat asphalt base on previous work. Dendrite growth was further observed in the present studies in very thin films of octacosane, as depicted in figure F1d-7.1. Furthermore, regarding crystal habits of model paraffins doped into asphalt, bee microstructures may be generally described as spherical to lenticular in profile. We further noted that the scroll structures described by White et al. (2002) are similar to our 6% and 8% octacosane mixed with AAG-1 (figure F1d-7.2). This same morphology was also observed in the IEC neutral fractions of AAM-1. Finally, rectangular and/or leaf shaped structures (habits) with ripples, and often arranged in a radial distribution about a central point in a set of five lamellae, similar in shape to structures reported by (Kyu et al. 2000; Mehta et al. 2004a, 2004b; Xu et al. 2005) associated with crystallized syndiotactic polypropylene, as are also present in our mixed model wax systems (figure F1d-7.7). Thus, Kyu et al. (Kyu et al. 2000; Mehta et al. 2004a, 2004b; Xu et al. 2005), have proposed that this type of structuring may be a result of curvature elasticity in the single crystal lamella, and thus, may be a basis for modeling wax crystallization in asphalt.

Significant Results

The nature of the "bumble bee" microstructures that have been observed in asphalt via AFM imaging by several researchers over the past decade has been elucidated. The studies presented here clearly demonstrate that naturally low wax content asphalt doped with long chain alkane paraffins develop microstructures identical to naturally higher wax content asphalt. It is presently asserted that these structures, when they naturally occur in waxy asphalt, are most likely a result of paraffin waxes present in the asphalt in the form of single micro/nano- "liquid" crystal lamellae. These wax single-crystals which form at the surface of asphalt thin films, particularly when subjected to mild thermal agitation are readily observed by AFM techniques.

It is presently hypothesized that wax single crystals are distributed more or less evenly throughout bulk films of asphalt constituting a gel state of the material, particularly at temperatures below ambient (Senra et al. 2009; Visintin et al. 2005; Kristofer et al. 2005). This gel state would then tend to include some of the solvent phase of the asphalt at temperatures above the glass transition temperature possibly contributing to embrittlement of the binder in this temperature range. Oxidation of the binder further decreases the effective amount of the solvent phase of the asphalt by converting/promoting molecules originally associated with polar aromatic and naphthene aromatic phases to the asphaltene type molecular phase. Each of these mechanisms, if accelerated by low loading for asphalt which are most prone to these mechanisms of embrittlement could be responsible for premature fatigue and thermal cracking and reduced healing.

Significant Problems, Issues and Potential Impact on Progress

A temperature and gas environmental control chamber is presently being fabricated around the AFM instrument to control oxygen and moisture influences upon thermal-cycle imaging and nano-mechanics experiments.

Work Planned Next Quarter

Analysis of existing data will continue in the next quarter. In these analyses, morphological features observed in asphalt and asphalt chromatographic fraction thin films prepared from validation site asphalts will be compared to performance data of the field site pavements. Image analysis of AFM scans will be developed to define a roughness “lumpiness” index.

Cited References

Bian, L., and F. Taheri, 2008, Fatigue Fracture Criteria and Microstructures of Magnesium Alloy Plates. *Materials Science and Engineering A*, 48774–85.

Cahn, J. W., and J. E. Hilliard, 1958, Free Energy of a Nonuniform System. I. Interfacial Free Energy. *J. Chem. Phys.*, 28 (2): 258-267.

Cahn, J. W., and J. E. Hilliard, 1959a, Free Energy of a Nonuniform System. II. Thermodynamic Basis. *J. Chem. Phys.*, 30 (5): 1121-1124.

Cahn, J. W., and J. E. Hilliard, 1959b, Free Energy of a Nonuniform System. III. Nucleation in a Two-Component Incompressible Fluid. *J. Chem. Phys.*, 31 (3): 688-699.

Cappelli, M. D., R. L. Carlson, and G. A. Kardomateas, 2008, The Transition Between Small and Long Fatigue Crack Behavior and its Relation to Microstructure. *International Journal of Fatigue*, 30: 1473–1478.

Chichakli, M. and F. W. Jessen, 1967, Crystal Morphology in Hydrocarbon Systems. *Ind. Eng. Chem.*, 59(5): 86-98.

Dorset, D. L., and B. K. Annis, 1996, Lamellar Order and Crystallization of Linear Chain Solid Solutions. *Macromolecules*, 29: 2969-2973.

Dorset, D. L., J. Hanlon, C. H. McConnell, J. R. Fryer, B. Lotz, J. C. Wittmann, E. Beckmann, and F. Zemlin, 1990, Why do polyethylene Crystals Have Sectors. *Proc., Natl. Acad. Sci. USA*, 87: 1696-1700.

Dorset, D. L., R. G., Alamo, and L. Mandelkern, 1993, Surface Order and Sectorization of Polyethylene Lamellae. *Macromolecules*, 26: 3143-3146.

Ferris, S. W., H. C. Cowles, Jr., and L. M. Henderson, 1931, Composition and Crystal Form of the Petroleum Waxes. *Industrial and Engineering Chemistry*, 23 (6): 681-688.

Hollander, F. F. A., O. Stasse, J. van Suchtelen, and W. J. P. van Enckvort, 2001, Recrystallization Phenomena of Solution Growth Paraffin Dendrites. *J. Cryst. Growth*, 233: 868-880.

Kristofer, P., M. Senra, Y. Yi, A. M. Sastry, and H. S. Fogler, 2005, Paraffin Polydispersity Facilitates Mechanical Gelation. *Ind. Eng. Chem. Res.*, 44: 7242-7254.

Kyu, T., R. Mehta, and H-W Chin, 2000, Spatiotemporal Growth of Faceted and Curved Single Crystals. *Phys. Rev. E.*, 61(4): 4161-4170.

Loveinger, A. J., B. Lotz, D. D. David, and M. Schumacher, 1994, Morphology and Thermal Properties of Fully Syndiotactic Polypropylene. *Macromolecules*, 27: 6603-6611.

Mehta, R., W. Keawwattana, and T. Kyu, 2004a, Growth Dynamics of Isotactic Polypropylene Single Crystals During Isothermal Crystallization from a Miscible Polymeric Solvent. *J. Chem. Phys.*, 120(8): 4024-4031.

Mehta, R., W. Keawwattana, A. L. Guenther, and T. Kyu, 2004b, Role of Curvature Elasticity in Sectorization and Ripple Formation During Melt Crystallization of Polymer Single Crystals. *Phys. Rev. E.*, 69: 061802.

Plomp, M., W. J. P. van Enckvort, P. J. C. M. van Hool, and C. J. van de Streek, 2003, Morphology of and Dislocation movement in n-C40H82 Paraffin Crystals Grown from Solution. *Journal of Crystal Growth*, 249: 600-613.

Putra, E.G.R., and G. Ungar, 2003, In Situ Solution Crystallization Study of n-C246H494: Self-Poisoning and Morphology of Polyethylene Crystals. *Macromolecule*, 36: 5214-5225.

Robertson, R. E., K. P. Thomas, P. M. Harnsberger, F. P. Miknis, T. F. Turner, J. F. Branthaver, S-C. Huang, A. T. Pauli, D. A. Netzel, T. M. Bomstad, M. J. Farrar, J. F. McKay, and M. McCann. "Fundamental Properties of Asphalts and Modified Asphalts II, Final Report, Volume I: Interpretive Report," Federal Highway Administration, Contract No. DTFH61-99C-00022, Chapters 1-4 submitted for publication, November 2005.

Robertson, R. E., K. P. Thomas, P. M. Harnsberger, F. P. Miknis, T. F. Turner, J. F. Branthaver, S-C. Huang, A. T. Pauli, D. A. Netzel, T. M. Bomstad, M. J. Farrar, D. Sanchez, J. F. McKay, and M. McCann. "Fundamental Properties of Asphalts and Modified Asphalts II, Final Report, Volume I: Interpretive Report," Federal Highway Administration, Contract No. DTFH61-99C-00022, Chapters 5-7 submitted for publication, March 2006.

Senra, M., T. Scholand, C. Maxey, and H. S. Fogler, 2009, Role of Polydispersity and Cocrystallization on the Gelation of Long-Chained n-Alkanes in Solution. *Energy Fuels*, 23: 5947-5957.

Toda, A, H. Miyaji, Y. Ogawa, and K. Takamizawa, 1991, Lateral Habits of n-Alkane Single Crystals. *J. Matter. Sci.*, 26: 2793-2796.

Tsukruk, V. V., and D. H. Reneker, 1995, Surface Morphology of Syndiotactic Polypropylene Single Crystals Observed by Atomic Force Microscopy. *Macromolecules*, 28: 1370-1376.

Ungar, G., P. K. Mandal, P. G. Higgs, D. S. M. de Silva, E. Boda, and C. M. Chen, 2000, Dilution Wave and Negative-Order Crystallization Kinetics of Chain Molecules. *Phys. Rev. Lett.*, 85(20): 4397-4400.

Visintin, R. F. G., R. Lapasin, E. Vignati, P. D'Antona,† and T. P. Lockhart, 2005, Rheological Behavior and Structural Interpretation of Waxy Crude Oil Gels. *Langmuir*, 21: 6240-6249.

White, H. M., I. L., Hosier, and D. C. Bassett, 2002, Cylindrical Lamellar Habits in Monodisperse Centrally Branched Alkanes. *Macromolecules*, 35: 6763-6765.

Xu, H., R. Matkar and T. Kyu, 2005, Phase-field Modeling on Morphological Landscape of Isotactic Polystyrene Single Crystals. *Phys. Rev. E.*, 72: 011804.

Zhou, W., S. Z. D. Cheng, S. Putthanarat, R. K. Eby, D. H. Reneker, B. Lotz, S. Magonov, E. T. Hsieh, R. G. Geerts, S. J. Palackal, G. R. Hawley, and M. Bruce Welch, 2000, Crystallization, Melting and Morphology of Syndiotactic Polypropylene Fractions. 4. In Situ Lamellar Single Crystal Growth and Melting in Different Sectors. *Macromolecules*, 33 (18): 6861-6868.

Subtask F1d-8: Coordinate Form of Healing Parameter with Micromechanics and Continuum Damage Models (TAMU)

Work Done This Quarter

A continuum-based healing model is developed and integrated into the unified continuum damage model. This model postulates the existence of another thermodynamic natural configuration (the healing configuration) besides the apparent (damaged) and true (undamaged) configurations (see figure F1d-8.1). During the loading-unloading process, some new cracks and voids are nucleated and propagated and also some of the micro-cracks may have been healed. Therefore, it is found that the coupling of healing with the damage model is achieved through the following expression:

$$\sigma_{ij} = [1 - \phi(1 - h)] \bar{\sigma}_{ij}$$

where σ_{ij} is the apparent (damaged) stress tensor, $\bar{\sigma}_{ij}$ is the true (undamaged) stress tensor, $0 \leq \phi \leq 1$ is the damage (micro-cracks and micro-voids) density such that $\phi = 0$ indicates no damage and $\phi = 1$ indicates complete damage (fracture). The new variable h defines the healed micro-crack density such that $0 \leq h \leq 1$ where $h = 0$ indicates no healing and $h = 1$ indicates complete healing of existing micro-cracks.

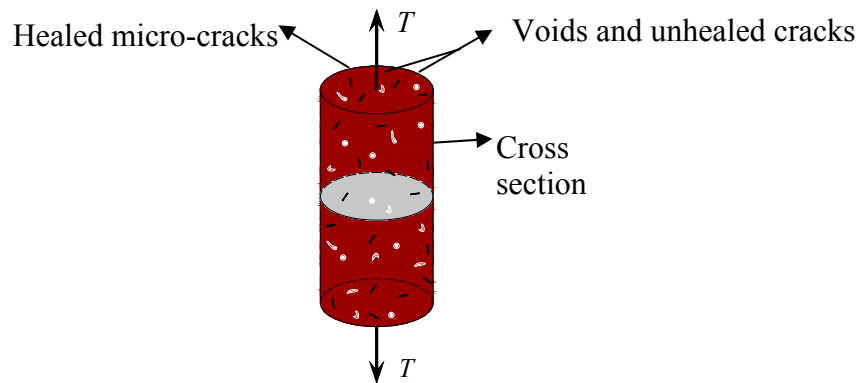


Figure F1d-8.1. Schematic representation of a cylindrical under tension and its healed and unhealed defects.

Work Planned Next Quarter

An evolution equation for the healing damage density h will be developed based on insights gained from micromechanical modeling and careful micro and nano experiments. Once developed, the healing model will be validated against asphalt mix experimental data.

CATEGORY F2: TEST METHOD DEVELOPMENT

Work Element F2a: Binder Tests and Effect of Composition (UWM)

Work Done This Quarter

Elasticity is an important property that relates to the ability of materials to recover after deformation. It has also been claimed that more elastic binders are more resistant to fatigue and that the use of elastic recovery in the PG Plus specification is a surrogate method to ensure better fatigue resistance. Work last quarter focused on simplifying the elastic recovery test method and investigating its relationship to binder fatigue.

Current methodology for measuring elastic properties of asphalts requires the use of a ductility bath, which has several disadvantages: inconsistency of the testing sample geometry, time-consuming sample preparation, and manual data collection. It is also known that manually cutting the asphalt sample and moving it back to estimate recovery is subject to operator variability. A simplified method for testing the elastic recovery of binders in the Dynamic Shear Rheometer (DSR) was developed. The results from the DSR and the ductility bath correlate very well. The use of a DSR for elastic recovery measurements has several advantages: small sample size, automated measurement, constant testing sample geometry, and quick and easy sample preparation.

Using this newly developed methodology, neat and modified binders were tested, and the results were compared with fatigue resistance properties collected from time sweep tests. The results indicate that elastic properties do not correlate with fatigue resistance data for asphalt binders measured in the DSR. This prompts the research team to question the relationship between elastic properties and fatigue resistance of binders. A DSR-based elastic recovery can replace the ductility-based test, and future work can continue on validating the relationship between elastic recovery and pavement performance using a more engineering-based test.

Significant Results

Elastic recovery tests performed in the ductility bath have been the standard for measuring elastic properties of binders for some time. However, there are numerous disadvantages associated with this method: sample preparation and testing temperature changes are time-consuming, the test employs inconsistent sample geometry, and the lack of automated data acquisition for the measurements.

A procedure has been developed for measuring the elastic recovery of binders using the DSR instrument. This procedure is better for several reasons:

- It is an automated procedure.
- It uses a much smaller sample size than the test run in the ductility bath.
- Sample preparation is quick and easy.
- The testing geometry stays constant throughout the test.
- The temperature control is fast and accurate.
- The DSR instrument is a common instrument in asphalt testing labs.
- The new procedure can give the same information as the tests run in the ductility bath.

Fatigue failure in binders can be measured by using the dissipated energy ratio (DER) concept. The N_{p20} parameter (number of cycles at which the material exhibits a 20% deviation from the line of equality between DER and number of cycles) appears to offer a good representation for fatigue performance of asphalt binders (Bonnetti et al. 2002; Delgadillo and Bahia 2005).

To investigate the relationship of elastic properties to fatigue resistance in binders, DSR elastic recovery measurements were performed alongside time sweep tests on the same set of materials containing different types of modification, and the data obtained from the two tests were compared.

Testing Procedure

The elastic recovery test in the DSR is set up to follow the ASTM D6084 testing procedure A. This test is run in the DSR instrument using the 8-mm parallel-plate geometry setup. The testing gap is 2.000 mm.

The testing procedure contains two parts:

- The first part is run in **strain-control** mode. This part imposes a constant strain rate of 2.32%/sec for 120 seconds, leading to a final maximum strain of 277.78%.
- The second part is run in **stress-control** mode. The instrument imposes a 0.0Pa shear stress for a period of 1 hour. This is the relaxation part of the test.

Figure F2a.1 represents the shear strain versus time $\gamma(t)$ for a typical elastic recovery test in the DSR, while figure F2a.2 shows a typical plot for the evolution of stress versus time in the elastic recovery test procedure for the DSR. Two replicates are shown in both figures. The example data shows how repeatable and precise the measurements are when the DSR is used. There is little doubt that such measurements, which require much less materials and can be conducted in all DSR devices used today, are better than the measurements done in the ductility bath. The 8-mm plate geometry was used for the tests and the rate of stain and maximum reached strain were selected to mimic the current elastic recovery test in the ductility bath.

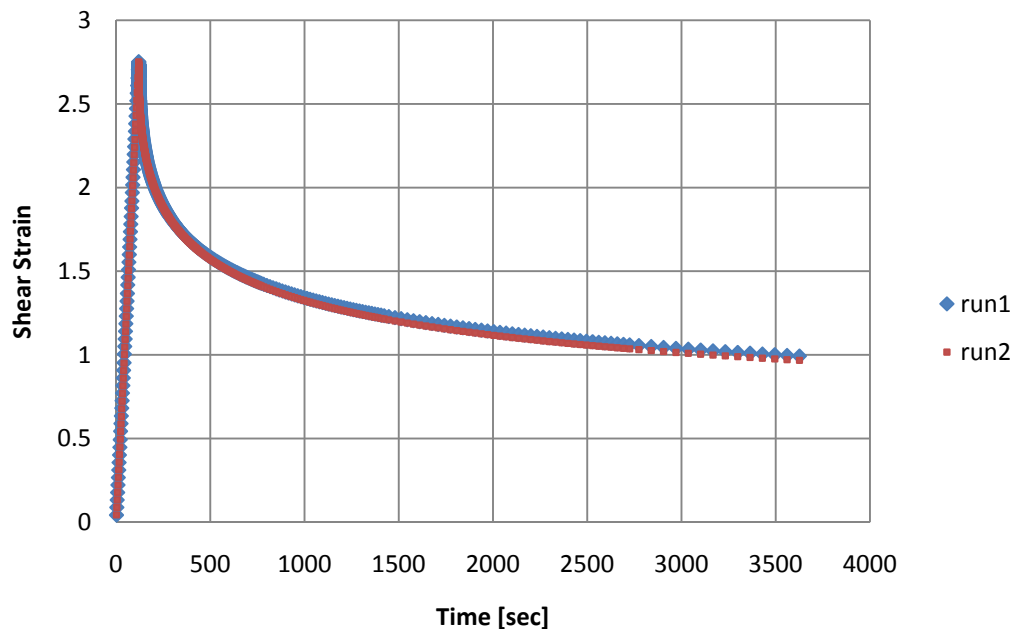


Figure F2a.1. Graph. Typical $\gamma(t)$ curve for the elastic recovery test in the DSR.

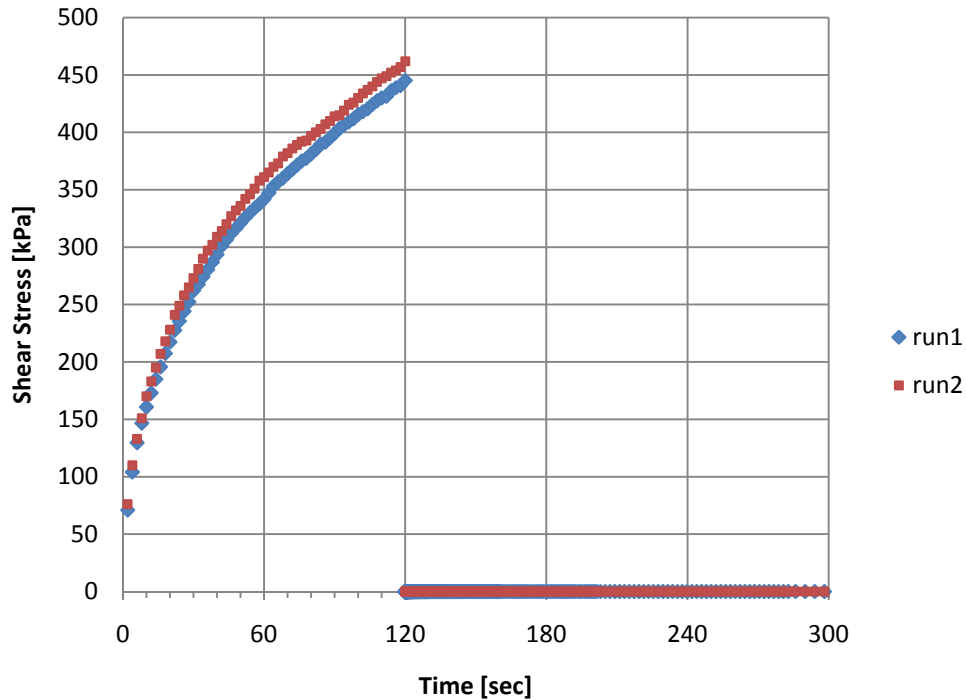


Figure F2a.2. Graph. Typical shear stress curve for the elastic recovery test in the DSR.

The curves shown in figures F2a.1 and F2a.2 can be used to calculate a number of fundamental rheological properties that are better related to binders' behavior. Precise calculations of recovery and rate of evolution of stress with loading time can be used for better ranking of binders, and possibly a stronger engineering relationship to pavement performance. This is the subject of another publication being prepared by the research team.

Tests and Materials

Three base binders and several modifiers are included in this study. The base binders range from a PG 58-28 to a PG 64-22. Some modified binders have been produced in the research team's lab while others were provided already modified by the manufacturer. All asphalts are tested after aging in the rolling thin film oven (RTFO) per AASHTO T240 specifications.

Styrene-butadiene-styrene (SBS) triblock copolymer, ethylene terpolymer (Elvaloy[®]) and polyphosphoric acid (PPA) are the modifiers used in this study. They cover a broad range of the modifier spectrum by including reactive and nonreactive elastomers, cross-linked and uncross-linked polymeric additives, and a low molecular weight acid modifier. Two levels of modification are selected for every polymer modifier used. This leads to a total of nine modified binders and three unmodified base binders included in this study, as shown in table F2a.1.

DSR elastic recovery tests are performed at 25 °C. Both strain rate (2.32%/sec) and maximum strain values (278% strain) were calculated based on the geometry and the deformation values required in the standard elastic recovery test, as described by ASTM D6084.

Table F2a.1. Materials used in the study.

Material	Grade
FH NEAT	64
FH+2 LSBS XLK	70
FH+4 LSBS XLK	76
FH+0.7 ELV+PPA	70
FH+1.5 ELV+PPA	76
VB NEAT	58
VB+CBE	64
VB+CBE+2 LSBS	70
VB+CBE+2 LSBS XLK	70
CRM NEAT	58
CRM+2 LSBS XLK	64
CRM+4 LSBS XLK	70

LSBS = linear styrene-butadiene-styrene. XLK = cross-linking. ELV = Elvaloy.

The main difference between the two tests is that while the DSR-run elastic recovery is performed in shear, the test described by the ASTM D6084 procedure is run in uniaxial tension.

Elastic Recovery Data

Data collected according to ASTM D6084 procedure A are compared with data collected using the newly developed DSR-based procedure for elastic recovery of binders. Results are summarized in table F2a.2.

Table F2a.2. Elastic recovery test results from the ductility bath and the DSR.

Material	% ER-DSR	% ER-Ductility
FH NEAT	15	25
FH+2 LSBS XLK	53	75
FH+4 LSBS XLK	73	90
FH+0.7 ELV+PPA	54	73
FH+1.5 ELV+PPA	73	88
VB NEAT	13	19
VB+CBE	19	28
VB+CBE+2 LSBS	42	54
VB+CBE+2 LSBS XLK	62	80
CRM NEAT	12	18
CRM+2 LSBS XLK	50	70
CRM+4 LSBS XLK	79	90

ER = elastic recovery.

It is clear from the data presented in table F2a.2 that both tests rank the materials similarly. The values measured by the DSR instrument are approximately 70% of the values obtained in the ductility bath. However, this does not affect the ranking or accuracy of the test. To the contrary, because the rheometer employs a constant geometry and a more accurate displacement reading, values for the coefficients of variations from the DSR data are below 3.00%. Moreover, the results obtained in the DSR show very good correlation with those obtained in the ductility bath, as shown in figure F2a.3.

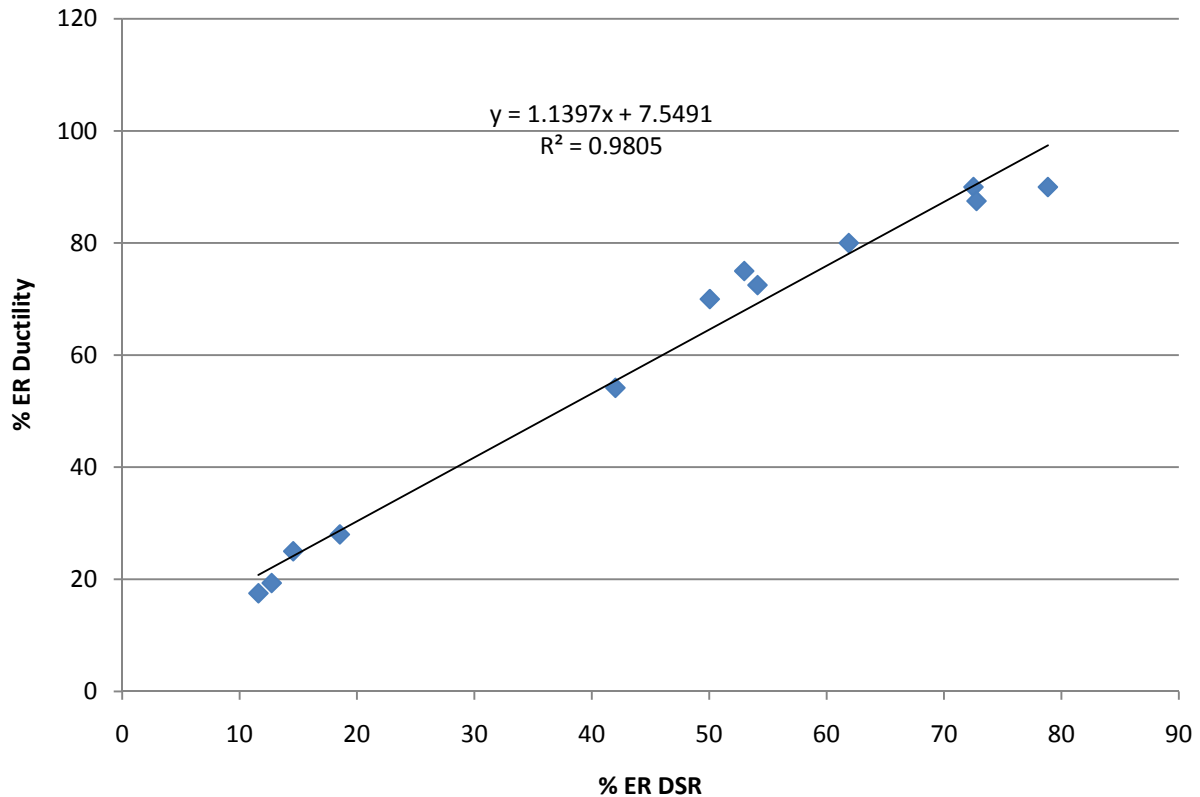


Figure F2a.3. Graph. Elastic recovery data: correlation between the ductility bath and the DSR.

The finding of good agreement between the DSR and the elastic recovery results, coupled with the ease of DSR sample preparation, excellent temperature control, and the availability of the DSR in most labs, makes a compelling case for replacing the elastic recovery measurements for binders done in the ductility bath with the procedure described for the DSR.

The N_{p20} parameter was chosen as the indicator of fatigue resistance for asphalt binders. The parameter is calculated by measuring binder fatigue under stress-controlled cyclic loading in the DSR. The results are used to plot DER as a function of cycles. The number of cycles at 20% change in the DER is determined and defined as N_{p20} (Bahia et al. 2001). By determining the N_{p20} at two stress levels, the results can be used to calculate the K_1 and K_2 model parameters from plots of the logarithmic transformation of N_{p20} versus initial dissipated energy (Bahia et al.

2001; Bonnetti et al. 2002). The model is then used to predict the N_{p20} values for any dissipated energy value (W_i). The N_{p20} for W_i values equal to 10 kPa and 30 kPa are shown in table F2a.3 for the binders tested in this study. The table also summarizes the K_1 and K_2 values.

Table F2a.3. Summary of time sweep test results.

Flint Hills	N_{p20} for $W_i=10$ kPa	N_{p20} for $W_i=30$ kPa	K_1	K_2
Neat	2.97E+05	3.30E+04	3E+13	-2.001
2% LSBS	2.82E+05	1.65E+04	6E+15	-2.582
2% LSBS XLK	7.71E+05	6.85E+04	5E+14	-2.203
4% LSBS	2.06E+05	1.01E+04	2E+16	-2.747
4% LSBS XLK	2.67E+07	1.81E+05	4E+25	-4.544
0.7% Elvaloy	1.63E+05	3.32E+04	1E+11	-1.447
1.5% Elvaloy	1.07E+05	3.58E+04	1E+09	-0.993
1% PPA	6.24E+05	5.11E+04	8E+14	-2.277

The results summarized in table F2a.3 are graphically represented in figure F2a.4, which shows clear effects of the modification type and cross-linking. The ranking changes slightly based on the W_i values, but in general modified binders vary significantly in their fatigue resistance. These fatigue properties estimated from the time sweep test results are compared with the elastic properties of the tested materials as resulted from the DSR procedure.

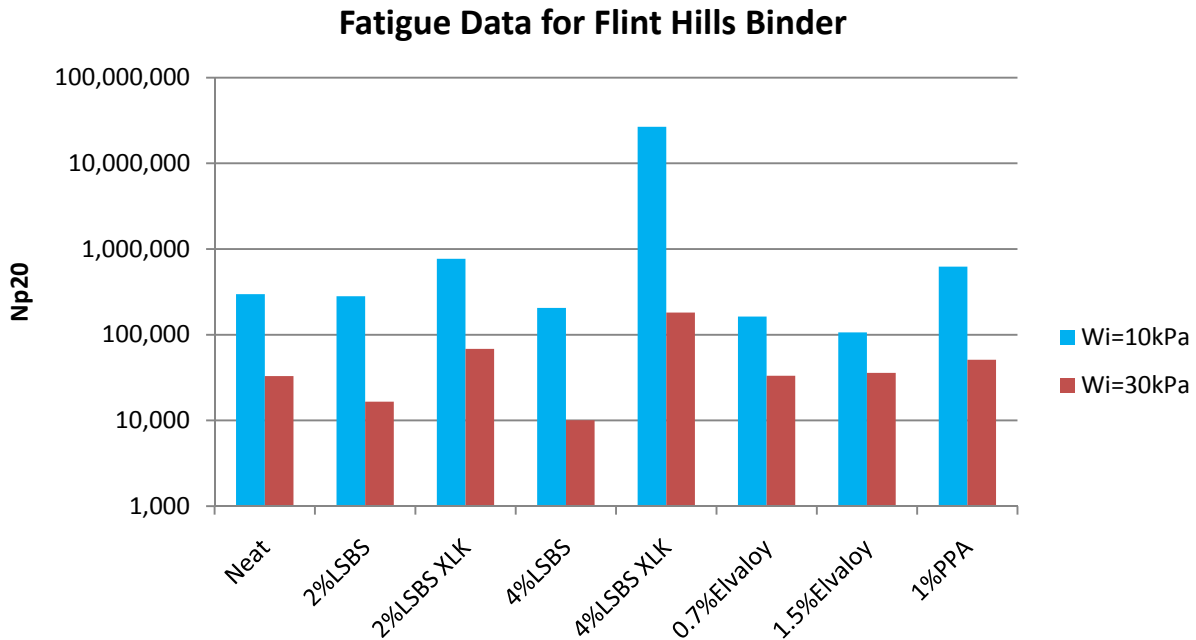


Figure F2a.4. Chart. Normalized fatigue behavior at two dissipated energy levels representative of a soft and hard binder, respectively.

SBS triblock copolymer, ethylene terpolymer and PPA are the modifiers used in this study. They cover a broad range of the modifier spectrum by including reactive and nonreactive elastomers, cross-linked and uncross-linked polymeric additives, and a low molecular weight acid modifier. Two levels of modification are selected for most of the polymer modifiers used, as shown in table F2a.4.

Table F2a.4. Materials derived from the Flint Hills base binder.

Material	Grade
Neat	PG 64
2% LSBS	PG 70
2% LSBS XLK	PG 70
4% LSBS	PG 76
4% LSBS XLK	PG 82
0.7% Elvaloy	PG 70
1.5% Elvaloy	PG 76
1% PPA	PG 70

Table F2a.5 exemplifies the testing temperature corresponding to the equistiffness testing conditions.

Table F2a.5. Temperatures for equal-stiffness conditions: $G^* = 18$ MPa.

Flint Hills	Continuous Grade Temperature
Neat	21.3 °C
2% LSBS	24.6 °C
2% LSBS XLK	21.7 °C
4% LSBS	24.5 °C
4% LSBS XLK	21.9 °C
0.7% Elvaloy	22.9 °C
1.5% Elvaloy	21.7 °C
1% PPA	22.3 °C

Using the DSR procedure, elastic recovery tests were performed on the materials described in the experimental section. The results of these tests are summarized in table F2a.6. It is noticeable that the level of modification can be well detected by the test results, but little difference is observed when comparing different modifiers at similar levels of modification (modification levels reflect increases of one or two PG grades).

Table F2a.6. Elastic recovery data from the DSR instrument for the Flint Hills binder.

Material	% Recovery
Neat	24.77
2% LSBS	42.56
2% LSBS XLK	41.14
4% LSBS	53.47
4% LSBS XLK	63.93
0.7% Elvaloy	39.41
1.5% Elvaloy	48.18
1% PPA	29.61

Correlations Between Elastic Recovery and Fatigue Testing Results

Figure F2a.5 presents the correlation between the elastic recovery data and fatigue testing results. From this graph it is apparent that no correlation exists between fatigue resistance and elastic properties of binders.

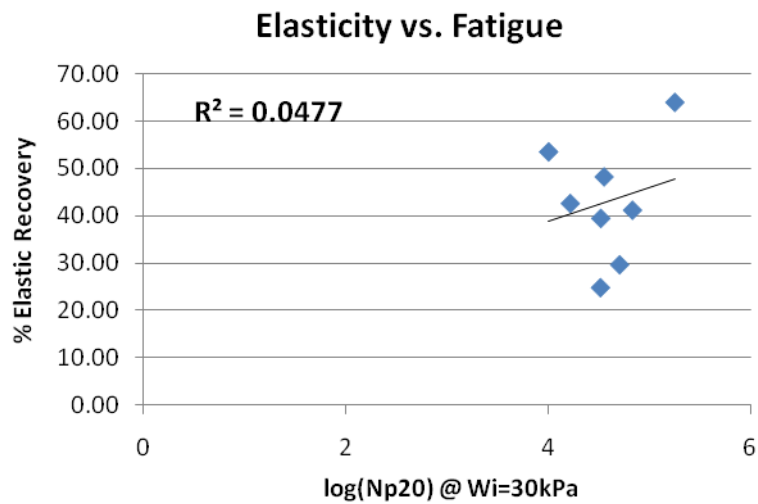


Figure F2a.5. Graph. Elastic recovery versus fatigue data.

Preliminary conclusions include the following:

- Elastic recovery data measured with a new protocol in the DSR at intermediate temperatures show good correlation with elastic recovery results collected in the ductility bath following the ASTM D6084 procedure. This finding suggests that the D6084 standard can be replaced with a simple test in the DSR. The DSR test procedure mimics the D6084 procedure in which a constant rate of deformation is imposed until a certain strain is reached, after which load is removed to allow for recovery.

- The new test in the DSR is believed to be more effective because its temperature, loading and unloading can be much better controlled than those in the ASTM D6084 procedure can. In addition, a much smaller sample is needed, and the test can be done in standard DSR devices.
- Among the advantages the research team foresees in running DSR tests in place of elastic recovery are: smaller sample size, shorter testing time, and more information—such as toughness, tenacity and elastic recovery—from one instrument.
- The elastic recovery values could not be correlated to fatigue results of binders. Therefore the question of relevance of the elastic recovery to pavement performance remains unanswered. It is critical that this question be answered because if elastic recovery cannot be found to relate to performance, it should not be used in selecting binders.

Significant Problems, Issues and Potential Impact on Progress

None.

Work Planned Next Quarter

The team will continue to develop the elastic recovery test in the DSR along with following the approved testing matrix for this work element.

Cited References

Bahia, H. U., D. I. Hanson, M. Zeng, H. Zhai, M. A. Khatri, and R. M. Anderson, 2001, *Characterization of Modified Asphalt Binders in Superpave Mix Design*. NCHRP Report 459.

Bonnetti, K. S., K. Nam, and H. U. Bahia, 2002, "Measuring and Defining Fatigue Behavior of Asphalt Binders." *Transportation Research Record*, 1810: 33-43.

Delgadillo, R. and H. Bahia, 2005, "Rational Fatigue Limits for Asphalt Binders derived from Pavement Analysis." *Journal of the Association of Asphalt Paving Technologists*, 74: 97-137.

Work Element F2b: Mastic Testing Protocol (TAMU)

The reader is referred to work element M1c where a new procedure for preparing FAM specimens were presented.

Year Four Work Plan

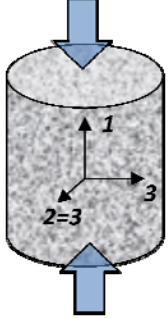
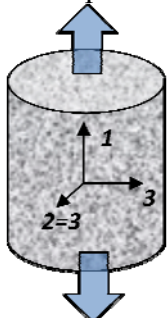
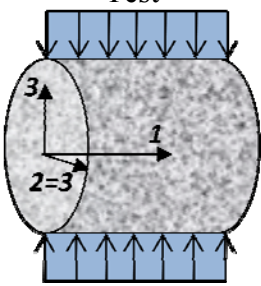
The reader is referred to the software development that was presented in work element M1c.

Work Element F2c: Mixture Testing Protocol (TAMU)

Work Done This Quarter

In this quarter, the mixture testing protocols and data analysis methods were completed to characterize the anisotropic viscoelastic properties of undamaged asphalt mixtures in compression. Mathematical models were used to construct the master curves of both magnitude and phase angle of all six complex anisotropic parameters at a reference temperature of 20°C. Table F2c.1 summarizes the testing protocols, anisotropic parameters and the master curve models.

Table F2c.1. Summary of mixture testing protocol characterizing the anisotropic viscoelastic properties of undamaged asphalt mixtures in compression.

Test Method	Anisotropic Parameter	Calculation Model	Master Curve Model
Uniaxial Compressive Creep Test 	Compressive Complex Modulus in Axial Direction $E_{11}^{C*}(\omega)$	$E_{11}^{C*}(\omega) = \left\{ s \cdot \bar{E}_{11}^C(s) \right\}_{s=i\omega}$ $= \left\{ \frac{\bar{\sigma}_{11}^{-C}(s)}{\bar{\varepsilon}_{11}^{-C}(s)} \right\}_{s=i\omega}$	Magnitude = Equation F2c.3 Phase Angle = Equation F2c.4
	Compressive Complex Poisson's Ratio in Axial Plane $\nu_{12}^{C*}(\omega)$	$\nu_{12}^{C*}(\omega) = \left\{ s \cdot \bar{\nu}_{12}^C(s) \right\}_{s=i\omega}$ $= \left\{ -\frac{\bar{\varepsilon}_{22}^{-C}(s)}{\bar{\varepsilon}_{11}^{-C}(s)} \right\}_{s=i\omega}$	Magnitude = Equation F2c.5 Phase Angle = Equation F2c.6
Uniaxial Tensile Creep Test 	Tensile Complex Modulus in Axial Direction $E_{11}^{T*}(\omega)$	$E_{11}^{T*}(\omega) = \left\{ s \cdot \bar{E}_{11}^T(s) \right\}_{s=i\omega}$ $= \left\{ \frac{\bar{\sigma}_{11}^{-T}(s)}{\bar{\varepsilon}_{11}^{-T}(s)} \right\}_{s=i\omega}$	Magnitude = Equation F2c.3 Phase Angle = Equation F2c.4
	Tensile Complex Poisson's Ratio in Axial Plane $\nu_{12}^{T*}(\omega)$	$\nu_{12}^{T*}(\omega) = \left\{ s \cdot \bar{\nu}_{12}^T(s) \right\}_{s=i\omega}$ $= \left\{ -\frac{\bar{\varepsilon}_{22}^{-T}(s)}{\bar{\varepsilon}_{11}^{-T}(s)} \right\}_{s=i\omega}$	Magnitude = Equation F2c.5 Phase Angle = Equation F2c.6
Indirect Tensile Creep Test 	Compressive Complex Modulus in Radial Direction $E_{22}^{C*}(\omega)$	$E_{22}^{C*}(\omega) = \left\{ s \cdot \bar{E}_{22}^C(s) \right\}_{s=i\omega}$ $\bar{E}_{22}^C(s) = \text{Equation F2c.1}$	Magnitude = Equation F2c.3 Phase Angle = Equation F2c.4
	Compressive Complex Poisson's Ratio in Radial Plane $\nu_{23}^{C*}(\omega)$	$\nu_{23}^{C*}(\omega) = \left\{ s \cdot \bar{\nu}_{23}^C(s) \right\}_{s=i\omega}$ $\bar{\nu}_{23}^C(s) = \text{Equation F2c.2}$	Magnitude = Equation F2c.5 Phase Angle = Equation F2c.6

The models for $\bar{E}_{22}^C(s)$ and $\bar{\nu}_{23}^C(s)$ are shown in Equations F2c.1 and F2c.2 as follows:

$$\bar{E}_{22}^C(s) = \frac{1}{s} \cdot \frac{A \cdot \bar{P} \cdot s \bar{E}_{11}^C \cdot s \bar{E}_{11}^T}{A \cdot \bar{P} \cdot s \bar{E}_{11}^T \cdot s \bar{\nu}_{12}^C \cdot s \bar{\nu}_{12}^T + \left(\bar{U}_y + \frac{h}{l} \cdot \bar{U}_z \cdot s \bar{\nu}_{12}^T \right) \cdot s \bar{E}_{11}^C \cdot s \bar{E}_{11}^T + B \cdot \bar{P} \cdot s \bar{\nu}_{12}^T (1 + s \bar{\nu}_{12}^T) \cdot s \bar{E}_{11}^C} \quad (\text{F2c.1})$$

$$\bar{v}_{23}^C(s) = \bar{E}_{22}^C \left[\frac{M \left[1 - (s\bar{v}_{12}^T)^2 \right]}{K \cdot s\bar{E}_{11}^T} - \frac{s\bar{v}_{12}^C \cdot s\bar{v}_{12}^T}{s\bar{E}_{11}^C} - \frac{r\bar{U}_z \cdot s\bar{v}_{12}^T + l\bar{U}_x}{lK\bar{P}} \right] \quad (\text{F2c.2})$$

where A , B , M , and K are testing configuration parameters in N/m; $h = r = 0.0375\text{m}$ and $l = 0.05\text{m}$; \bar{P} is the Laplace transform of a constant load P , and $\bar{P} = P/s$; \bar{E}_{11}^C , \bar{E}_{11}^T , \bar{v}_{12}^C , and \bar{v}_{12}^T are Laplace transforms of the corresponding time-dependent variables, which are determined in the uniaxial compressive creep tests and uniaxial tensile creep tests; \bar{U}_x , \bar{U}_y and \bar{U}_z are Laplace transforms of the U_x , U_y and U_z that are the radial deformation, vertical deformation and axial deformation in the indirect tensile creep test.

The mathematical model in Equation F2c.3 (Luo and Lytton 2009) was used to construct the master curves of the complex modulus magnitudes. Figure F2c.1 shows the master curves of $|E_{11}^{C*}|$, $|E_{11}^{T*}|$ and $|E_{22}^{C*}|$.

$$|E^*(\omega)| = \frac{E_g}{\left[1 + \left(\frac{\omega_{cE}}{\omega \cdot 10^{C(T-T_r)}} \right)^{R_E} \right]^{\frac{R_E}{\log 2}}} \quad (\text{F2c.3})$$

where E_g = glassy modulus of the asphalt mixture, MPa; ω_{cE} = crossover frequency of the asphalt mixture, rad/sec; R_E = rheological index for modulus; and C = slope of the temperature shift factor.

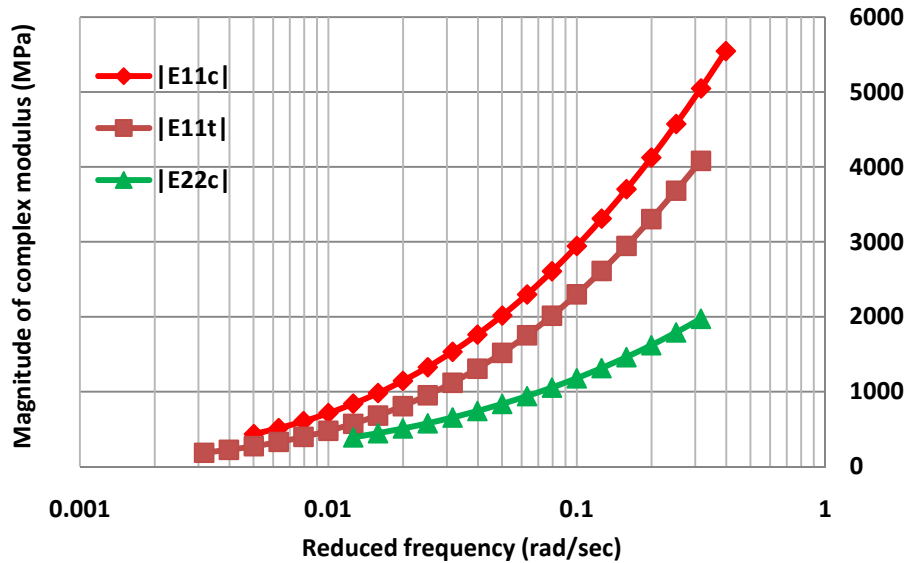


Figure F2c.1. Master curves of the magnitude of complex moduli at reference temperature 20°C.

In figure F2c.1, the master curve of $|E_{11}^{C*}|$ is above the master curve of $|E_{11}^{T*}|$, which indicates that the compressive complex modulus in the vertical direction of the asphalt mixture has a greater magnitude than that of the tensile complex modulus. This finding is reasonable and demonstrates that it is necessary to separate the tensile modulus from the compressive modulus in the constitutive relations. Figure F2c.1 also shows that $|E_{11}^{C*}|$ is about 2~2.5 times larger than $|E_{22}^{C*}|$, which proves that the asphalt mixture has a significant anisotropy in compression.

Equation F2c.4 (Bahia et al. 2001) was utilized to construct the master curves of the phase angles of the complex moduli, which are plotted in figure F2c.2.

$$\varphi_E = \frac{\varphi_{mE}}{\left[1 + \frac{\log \left(\frac{\omega_{mE}}{\frac{C_1(T-T_r)}{\omega \cdot 10^{C_2+(T-T_r)}}} \right)}{R_{\varphi E}} \right]^2}^{\frac{m}{2}} \quad (\text{F2c.4})$$

in which φ_{mE} = the maximum phase angle for modulus, degrees; ω_{mE} = the frequency where φ_{mE} occurs, rad/sec; $R_{\varphi E}$ = fitting parameters for modulus; T_r = reference temperature; and C_1 and C_2 = frequency-temperature shift constants.

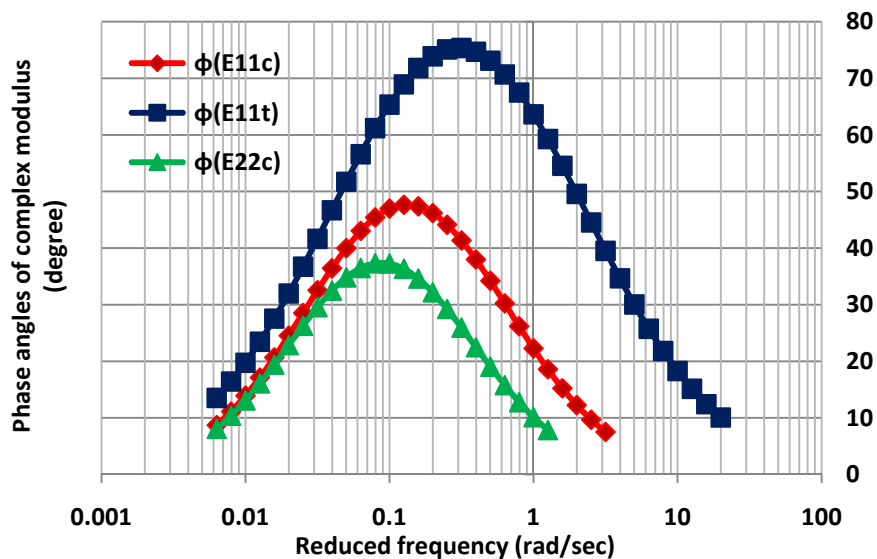


Figure F2c.2. Master curves of the phase angle of complex moduli at reference temperature 20°C.

Figure F2c.2 shows that $\phi(E_{11}^{C*})$ and $\phi(E_{22}^{C*})$ have close peak values, which are around 40 degrees, while $\phi(E_{11}^{T*})$ has a greater peak value of approximately 75 degrees. This difference demonstrates again that the tensile properties of the asphalt mixture significantly differ from its compressive properties.

Equation F2c.5 was developed to fit the master curves of the magnitude of the complex Poisson's ratio, which are shown in figure F2c.3. Equation F2c.6 was used to construct the master curves of the phase angle of the complex Poisson's ratio and shown in figure F2c.4. It is reasonable for the complex Poisson's ratio to have a magnitude greater than 0.5 in this study because in anisotropic elasticity, the Poisson's ratio can range between -1 and 1.

$$|v^*(\omega)| = \frac{\alpha}{1 + \beta e^{k[\omega \cdot 10^{C(T-T_r)}]}} \quad (\text{F2c.5})$$

$$\varphi_v = \frac{\varphi_{mv}}{\left\{ 1 + \frac{\log \left(\frac{\omega_{mv}}{\omega \cdot 10^{\frac{C_1(T_r-T)}{C_2+(T_r-T)}}} \right)}{R_{\varphi_v}} \right\}^2 \frac{m}{2}} \quad (\text{F2c.6})$$

where α , β , and k are fitting parameters; φ_{mv} = the maximum phase angle for Poisson's ratio, degrees; ω_{mv} = the frequency where φ_{mv} occurs, rad/sec; R_{φ_v} = fitting parameters for Poisson's ratio; T_r = reference temperature; and C , C_1 and C_2 = frequency-temperature shift constants.

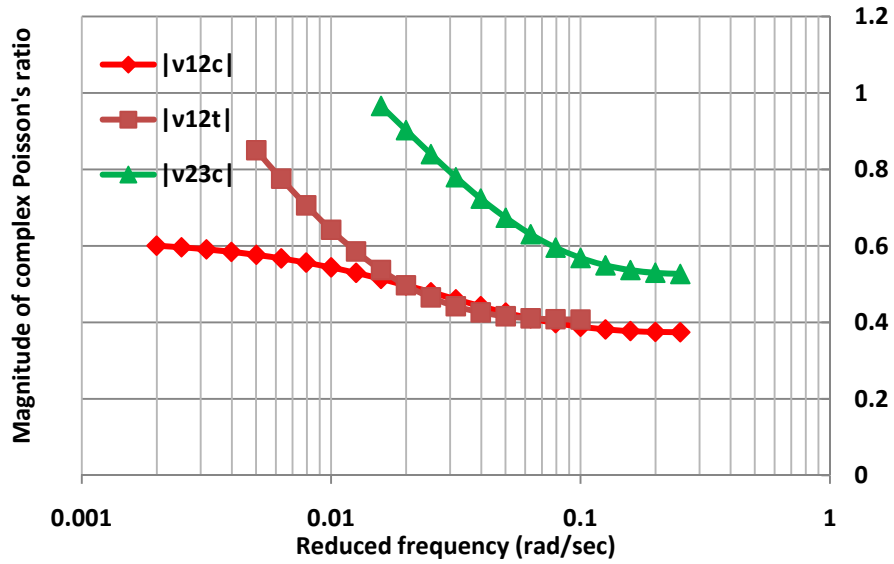


Figure F2c.3. Master curves of the magnitude of complex Poisson's ratio at reference temperature 20°C.

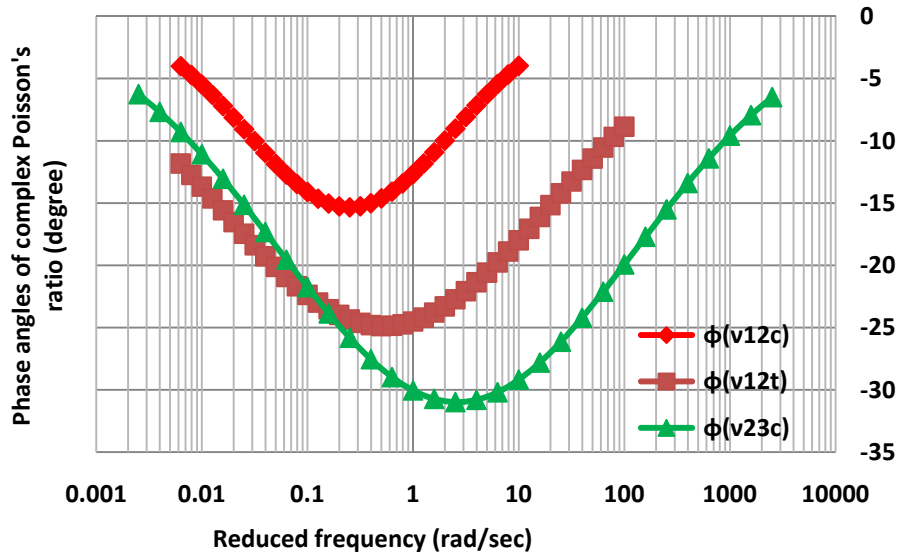


Figure F2c.4. Master curves of the phase angle of complex Poisson's ratio at reference temperature 20°C.

The magnitude and phase angle of the complex Poisson's ratio in compression and tension can be compared in figures F2c.3 and F2c.4, which demonstrate the distinct properties in different loading modes and significant anisotropy of asphalt mixtures.

Compared to the traditional anisotropic test protocols using multiple specimens cored in different directions, the newly proposed test protocols were more efficient to characterize the anisotropic viscoelastic properties of undamaged asphalt mixtures in compression. First, creep tests instead of dynamic tests were required to obtain the anisotropic complex modulus and complex Poisson's ratio. Second, only one cylindrical specimen was needed for the three tests, which eliminated the sample to sample error and reduced the quantity of the testing materials. Third, this testing protocol was time-saving because each test was finished in one minute. The entire master curve testing process was completed in one day. Finally, strains were limited to the endurance limit of 100 microstrains so no damage was introduced to the specimen. Therefore, the same specimen could be reused in the future destructive tests.

Significant Results

An efficient mixture testing protocol was completed to characterize the anisotropic viscoelastic properties of undamaged asphalt mixtures. The master curves were constructed for the magnitude and phase angle of the six complex anisotropic parameters, which indicated that the undamaged asphalt mixture exhibited significant anisotropic properties in compression. The master curves also showed that the undamaged asphalt mixture had significantly different tensile properties and compressive properties.

Significant Problems, Issues and Potential Impact on Progress

The newly purchased Material Testing System (MTS) was not ready for use yet. It is expected that the new MTS will be ready in the next quarter.

Work Planned Next Quarter

The mechanical properties of the undamaged asphalt mixture provide a good reference state from which the damage that is introduced into the asphalt mixture can be quantified. With an increasing number of loading cycles, the asphalt mixture will change from the undamaged state into the damaged state, where the physical properties are still anisotropic while the deformation will become viscoplastic. Therefore, in next quarter, an anisotropic viscoplastic continuum damage model will be developed to describe the constitutive relationship during the evolution of the viscoplastic deformation in the asphalt mixture. The proposed damaged model needs to account for the following phenomena in the asphalt mixture:

- anisotropy due to the preferential aggregate distribution,
- viscoplastic work hardening deformation,
- progressive damage evolution, and
- simultaneous crack growth.

Cited References

Bahia, H. U., D. I. Hason, M. Zeng, H. Zhai, M. A. HKhatri, and R. M. Anderson, 2001, *Characterization of Modified Asphalt Binders in Suprepave Mix Design*, Report 459. National

Cooperative Highway Research Program (NCHRP), Transportation Research Board, National Research Council, Washington, D.C.

Luo, R., and R. L. Lytton, 2009, Characterization of the Tensile Viscoelastic Properties of an Undamaged Asphalt Mixture. *Journal of Transportation Engineering, American Society of Civil Engineers (ASCE)*, Accepted for Publication.

Work Element F2d: Tomography and Microstructural Characterization (TAMU)

X-Ray Computed Tomography

Work Done This Quarter

X-Ray CT image and analysis techniques on asphalt mixtures were performed to support the efforts in work elements F2d and F3c. These methods have been developed to analyze the damage directional distribution.

Year Four Work Plan

X-ray CT will be used to scan the test specimens in work elements F2d and F3c, and the developed image and analysis techniques will be utilized to analyze damage directional distribution.

Work Element F2e: Verification of the Relationship between DSR Binder Fatigue Tests and Mixture Fatigue Performance (UWM)

Work Done This Quarter

In this quarter, the fatigue testing (i.e., time sweep, amplitude sweep and Binder Yield Energy Test (BYET)) of binders selected in previous quarterly reports was completed. The analysis of the fatigue data using the framework of viscoelastic continuum damage (VECD) of the ALF binders was completed based on the data collected for binders and the mixture data provided by FHWA. Table F2e.1 includes the testing conditions for the data sets.

The ultimate objective of the VECD analysis for both the time and amplitude sweep tests is the estimation of the fatigue life (N_f) using equation F2e.1:

$$N_f = A(\gamma_{\max})^B \quad (\text{F2e.1})$$

The coefficients A and B can be determined from amplitude or time sweep tests and γ_{\max} represents the strain level of the binder in the pavement structure.

Table F2e.1. Binder and mixture fatigue test conditions from which data was used in analysis this quarter.

Binder	BYET 0.005 – 0.01/s	Time Sweep – Strain controlled	Amplitude Sweep	Uniaxial Mix Fatigue Provided by FHWA	ALF Fatigue
Control 70-22	XXX	3, 5, 7%	XX	2@1050 micro	X
Air-Blown	XXX	3, 5, 7%	XX	3@780 micro	X
CR-TB	XXX	3, 5, 7%	XX	3@630 micro	X
Terpolymer	XXX	5, 7%	XX	2@540, 1@750 micro	X
SBS-LG	XXX	3, 5, 7%	XX	3@750 micro	X

CR-TB: terminally blended crumb rubber-modified. SBS-LG: linear-grafted styrene-butadiene-styrene polymer-modified.

The parameters A and B for the binders listed in table F2e.1 obtained from VECD analysis of the linear amplitude sweep tests are presented in table F2e.2. The parameter A is derived from the linear amplitude sweep test results, while the factor B is derived from a Dynamic Shear Rheometer (DSR) frequency sweep test. As shown in the table, the variability of factor A is relatively low. It is thus shown that the procedure shows good repeatability as indicated by the low coefficient of variation (COV) (i.e., COV <10%) of the calculated number of cycles to failure.

Table F2e.2. VECD analysis of amplitude sweep binder results.

Binder	Run 1		Run 2		Average		COV	
	A	Nf - 2.5%	A	Nf - 2.5%	A	Nf - 2.5%	A	Nf - 2.5%
Control	3.92E+06	31,149	3.85E+06	30,590	3.89E+06	30,870	1.28%	1.28%
CR-TB	2.16E+07	122,961	1.87E+07	106,889	2.02E+07	114,925	9.89%	9.89%
Elvaloy	2.69E+07	235,790	2.33E+07	204,423	2.51E+07	220,107	10.08%	10.08%
SBS-LG	9.20E+06	79,968	8.16E+06	70,900	8.68E+06	75,434	8.50%	8.50%

Table F2e.3 shows the number of cycles to failure predicted from time and amplitude sweep tests. The performance of these binders in ALF is listed in table F2e.3. Figure F2e.1 shows the relation between the parameter A and ALF cracking. Fairly good linear correlation is observed between the amplitude sweep results and ALF performance if the SBS-LG binder is not included in the analysis. The research team tested an extra replicate of the SBS binder to determine if there was an error during the amplitude sweep test of this binder. However, the results from the extra replicate were consistent with the results previously obtained. The research team will investigate why the SBS binder has a poor performance in the amplitude sweep test but shows the best performance in the time sweep test, as shown in table F2e.3.

Table F2e.3. Predicted fatigue performance and ALF results from the time sweep (TS) and linear amplitude sweep (LAS).

Binder	TS Nf - 5%	LAS Nf - 5%	TS Nf - 7%	LAS Nf - 7%	Crack Length
Control	11,770	803	4,640	136	90.6
CR-TB	51,730	2,468	12,630	370	24.9
Elvaloy	158,670	6,556	45,680	1,152	9
SBS-LG	1,167,100	2,207	236,480	386	0

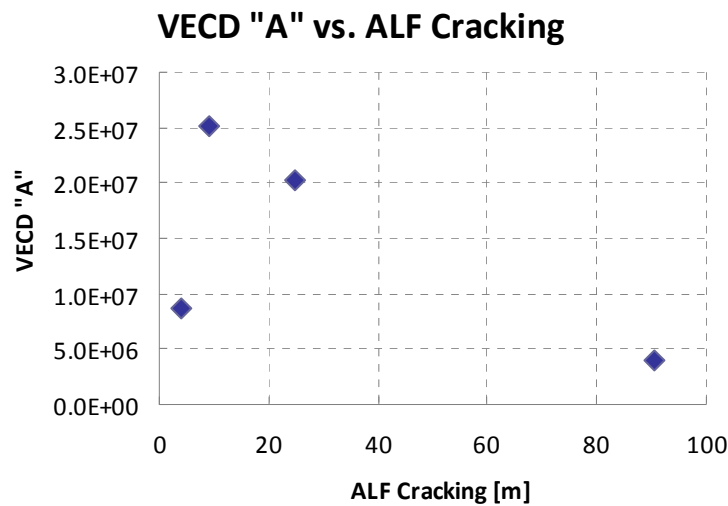


Figure F2e.1. Graph. Comparison of parameter A from VECD analysis and ALF cracking.

In this quarter, the research team completed fatigue testing of the binders from the Transportation Pooled Fund study TPF-5(146), which is being conducted by the University of Massachusetts, Dartmouth research team. The Transportation Pooled Fund study team has supplied a very good set of mixture fatigue data for validation of the linear amplitude test of binders. The test methods used and the number of replicates tested are listed in table F2e.4. The research team plans to conduct the VECD analysis of this data set next quarter.

Table F2e.4. Transportation Pooled Fund study TPF-5(146) binder fatigue testing completed.

Binder	BYET 0.01/s	BYET 0.08/s	Amplitude Sweep	Time Sweep – 5%	Time Sweep – 7%
64-28 AI	XX	XX	XX	XX	XX
64-28 PPA	XX	XX	XX	XX	XX
64-34 SemMaterials	XX	XX	XX	XX	XX
76-22 Citgo	XX	XX	XX	XXXX	XX
64-22 12% GTR	XX	XX	XX	X-	X-
64-28 AI 2% Latex	XX	XX	XX	XX	XX

AI = Asphalt Institute. PPA = polyphosphoric acid. GTR = ground tire rubber. X= number of replicates.

Significant Results

Based on the analysis of the extensive experimental matrix, the research team considers the amplitude sweep test combined with the VECD modeling a suitable method for fatigue characterization of asphalt binders.

The research team conducted an investigation on the variation of the linear amplitude sweep results due to operator and laboratory equipment. The results from amplitude sweep tests conducted in a different laboratory were very similar to the results obtained in the University of Wisconsin–Madison laboratory.

Also, the team at UW-Madison developed a draft standard for the BYET and the linear amplitude sweep procedure. The standards will be submitted to ETG for review and discussion in the February meeting.

Significant Problems, Issues and Potential Impact on Progress

None.

Work Planned Next Quarter

The research team will conduct the analysis of the amplitude sweep tests of the Transportation Pooled Fund study TPF-5(146) binders. A typical mix design with locally available aggregates will be used for the planned push-pull fatigue testing to find the relationship between mixture fatigue and the proposed linear amplitude sweep test results.

The research group will continue implementation of the amplitude sweep procedure for fatigue characterization of binders by performing a sensitivity analysis of all the parameters involved in the VECD calculation of the damage curves.

CATEGORY F3: MODELING

Work Element F3a: Asphalt Microstructural Model (WRI, URI, VT)

Work Element F3a: Asphalt Microstructural Model (University of Rhode Island)

Work Done This Quarter

The work done in the October–December 2009 quarter focused on the contributions of individual molecules to overall mechanical relaxation within molecular simulations and the relationship in rheology modeling between mechanical response and distribution of relaxation times. The molecular scale work relates to the development of model asphalts and the rheology modeling relates to the push/pull between molecular and microscopic length scales that was described in the July–September 2009 quarterly report.

Sub-subtask F3a-1.1, *Next Generation Model Asphalts*. The key conclusion finalized this quarter from analyzing pre-existing molecular-scale simulation results was that larger molecules show a decoupling between rotational and translational diffusion as temperature decreases, with rotation slowing dramatically as viscosity increases and translational diffusion slowing much less. Smaller molecules maintain a consistent relationship between rotation and translation as temperature decreases, meaning that both properties lose a correspondence with viscosity. These results indicate that asphaltenes control viscosity while moderate-size resins provide a continually evolving environment in which asphaltenes can move. A manuscript describing these results was submitted to the *Journal of Chemical Physics*.

Work was initiated during this quarter on simulating new resin molecules for next-generation model asphalts. An initial set of molecules was chosen from prior simulations of Murgich and co-workers (1999). Calculations were still in progress at the end of the quarter.

Analysis continued of the alkane crystallization event identified last quarter in a first generation model asphalt. One example of the positions of n-C₂₂ chains in an equilibrated simulation cell at 298 K is shown in the right side of figure F3a.1. The left side shows the box early in the simulation, before crystallization occurred. Box edges are connected by periodic boundary conditions, meaning that a chain exiting the right side reenters the left side, and vice versa. The same method connects the top/front and bottom/back. Asphaltene and resin molecules (not shown) fit in the spaces between images of the n-C₂₂ crystal domains. A Letter describing this crystallization event is being written. Use of these results to help with parameters for phase field calculations will be pursued as the data are analyzed.

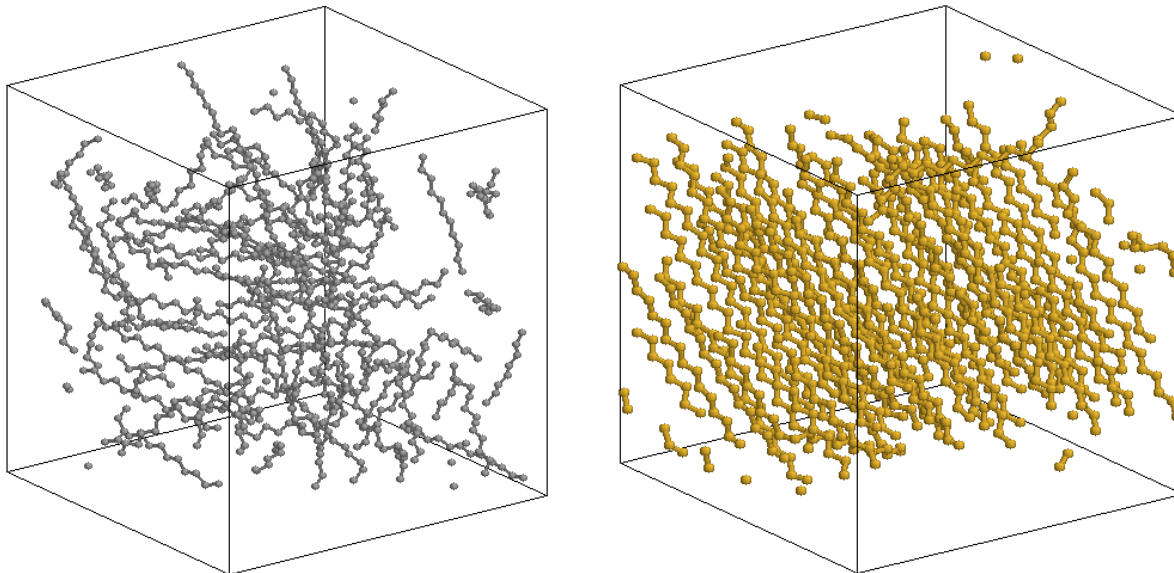


Figure F3a.1. Image of n-C₂₂ configurations in a model asphalt at 298 K earlier in the simulation (left) and after spontaneous formation of crystal domains occurred (right, approximately 14 ns later). Hydrogen atoms on the n-C₂₂ chains, asphaltene molecules, and resin molecules are present in the simulation but are omitted from the pictures for clarity. Periodic boundary conditions connect the left/right, top/bottom, front/back, making this a continuous crystal within the bulk of a model asphalt.

Sub-subtask F3a-1.2, Molecular simulation “push” and phase model “pull”. The key conclusion finalized this quarter came from a related project in rheology modeling: asphalts showing similar performance gradings can have significant differences in relaxation time distribution, which implies differences in their underlying chemistry. These asphalts have the potential to differ in their response to similar stress and stress conditions, due to their differences in relaxation time distribution. A manuscript describing these results was submitted to *Rheologica Acta*.

A literature survey on applying the SAFT equation of state (for a summary see (Muller and Gubbins 2001)) to systems that include asphaltene molecules was initiated during the quarter and continues to develop. The primary motivation in existing studies has been reproducing phase behavior that explains the precipitation of asphaltenes during crude oil production and refinement. An example is the work of Chapman and co-workers (e.g. Ting et al. 2003, Gonzalez et al. 2005), which uses a lumping scheme based on chemical families (saturates, aromatics/resins, asphaltenes) to determine SAFT parameters. Their results predict pressure-dependent density, toluene solubility, and reservoir phase behavior. The motivation to consider SAFT in this project is for it to serve as a bridge between detailed molecular simulation results and the more coarse-grained free energy models needed in phase field simulations.

Significant Problems, Issues and Potential Impact on Progress (followup to 7-9/2009 quarter)

Most research efforts this quarter were made by Prof. Greenfield, due to the difficulty cited in the prior quarter with finding a URI graduate student to bring onto the project for the Fall 2009 semester. That problem has been remedied going forward, as new URI M.S. student Derek Li will join the project. Li has prior experience simulating model asphalts from when he was a URI undergraduate, and he is expected to come up-to-speed quickly.

Cost sharing accounting is now up-to-date. Cost sharing expenses are currently far ahead of the overall 1:4 ratio compared to project expenditures. The project spending rate will increase this quarter as graduate student Derek Li joins the project. Li is a Rhode Island resident, so the prior cost sharing plan (which had assumed an Out-of-state Tuition Award that is not applicable for an in-state resident) will continue to require modifications. The changes in place have Prof. Greenfield devoting part of his sabbatical to the project, thus contributing his 50% sabbatical salary as cost share. Some rebudgeting occurred during the past quarter to account for this change in work effort and additional rebudgeting will potentially be necessary again in the coming quarters.

Work Planned Next Quarter

The next quarter will again focus on two areas: (1) next-generation model asphalts and (2) molecular/phase model connections.

Sub-subtask F3a-1.1, *Next Generation Model Asphalts.*

- Complete Letter about crystallization event and submit for publication.
- Communicate with WRI about choice of asphalts of interest and corresponding chemical characterization data (NMR, FTIR, etc.).
- Formulate model asphalts using properly sized molecules and conduct initial simulations. Additional asphaltene molecular structures will be considered as well. The choice of compounds will be pursued jointly by URI and WRI.

Sub-subtask F3a-1.2, *Molecular simulation “push” and phase model “pull”.* Additional formulation work is required to identify the detailed path for incorporating molecular simulation outputs into phase field model inputs. The following address this need.

- Complete literature survey about applications of the SAFT equation of state to asphaltenes.
- Communicate with phase-field practitioners on this project about how parameters can cross the molecule/phase field scales.

Outcomes from all discussion will be shared at a F3a team meeting.

Cited References

- Murgich, J., J. A. Abanero, and O. P. Strausz, 1999, Molecular Recognition in Aggregates Formed by Asphaltene and Resin Molecules from the Athabasca Oil Sand. *Energy Fuels*, 13:278–286.
- Muller, E. A. and K. E. Gubbins, 2001, Molecular-Based Equations of State for Associating Fluids: A Review of {SAFT} and Related Approaches. *Ind. Eng. Chem. Res.*, 40:2193–2211.
- Ting, P. D., G. J. Hirasaki, and W. G. Chapman, 2003, Modeling of Asphaltene Phase Behavior with the SAFT Equation of State. *Petrol. Sci. Tech.*, 21:641–661.
- Gonzalez, D. L., P. D. Ting, G. J. Hirasaki, and W. G. Chapman, 2005, Prediction of Asphaltene Instability under Gas Injection with the PC-SAFT Equation of State. *Energy Fuels* 19:1230–1234

Work Element F3b: Micromechanics Model (TAMU)

Subtask F3b-1: Model Development

Work Done This Quarter

Cohesive Zone Micromechanical Model

During this quarter we have mainly progressed towards three activities:

- Using the improved SCB fracture-testing system developed during the previous quarters, we have performed the SCB tests at different loading rates with specimens fabricated with different thicknesses. This effort is to provide any meaningful insights into the effects of specimen geometry and loading rates on fracture characteristics of fine aggregate matrix (FAM) specimens.
- We then determined cohesive zone fracture properties of the FAM phase at different loading rates by integrating the SCB fracture test results with finite element simulations of the SCB tests.
- Another primary task we focused on during this quarter was the implementation of the testing-analysis protocol that we have developed during the last quarters for mixing, compaction, and production of FAM specimens. This effort is to develop a more articulate and scientific protocol in mixing and compaction of the FAM phase, which produces key material properties (viscoelastic properties and cohesive zone properties of matrix phase) to accomplish the finite element-based micromechanical modeling.

Work progress and significance of each activity can be summarized as follows.

- SCB fracture testing at different loading rates with different specimen thicknesses:

The testing set-up developed in the previous quarters was used for the fracture testing of SCB specimens subjected to constant displacement rates. The first activity was to determine a proper specimen thickness to be used in the experimental fracture characterization. This was motivated by the fact that expensive three-dimensional simulations can be closely approximated by two-dimensional simulations (such as a plane stress condition) if the specimen is thin enough to be subject to the plane stress fracture condition. Thin specimens are subject to plane stress loading at the crack tip, while thick specimens experience crack-tip triaxiality in the interior of the section. The stress state in the central region is essentially plane strain at distances from the crack tip that are small compared to the plate thickness. Near the free surface, the stress triaxiality is lower, but a state of pure plane stress exists only at the free surface. Based on this fact, we attempted three specimen thicknesses (25, 38, and 50 mm) and compared test results.

Figure F3b-1.1 presents SCB test results from the three thicknesses at two different loading rates, 100 mm/min and 50 mm/min. As shown in the figure, the shift of the curve for the 38-mm-thick specimens with a shift factor of 0.66 (25/38) produced results that closely approximate the results for the 25-mm-thick specimens, while the same trend was not observed from the 50-mm-thick specimens with a shift factor of 0.50 (25/50). Test results indicate that two-dimensional simulations assuming the plane-stress condition can be performed with test results of SCB specimens less than 38-mm thick. A similar finding was also reported in a study by Li and Marasteanu (AAPT vol. 73, 2004), where simulations of the SCB test demonstrated the existence of stresses in the out-of-plane direction for the specimens with its thickness of 50 mm. Negligible out-of-plane stresses were observed from 25-mm-thick specimens. Based on test results and the similar finding by Li and Marasteanu (AAPT vol. 73, 2004), the SCB tests to characterize fracture properties of the FAM phase were conducted with 25-mm-thick specimens.

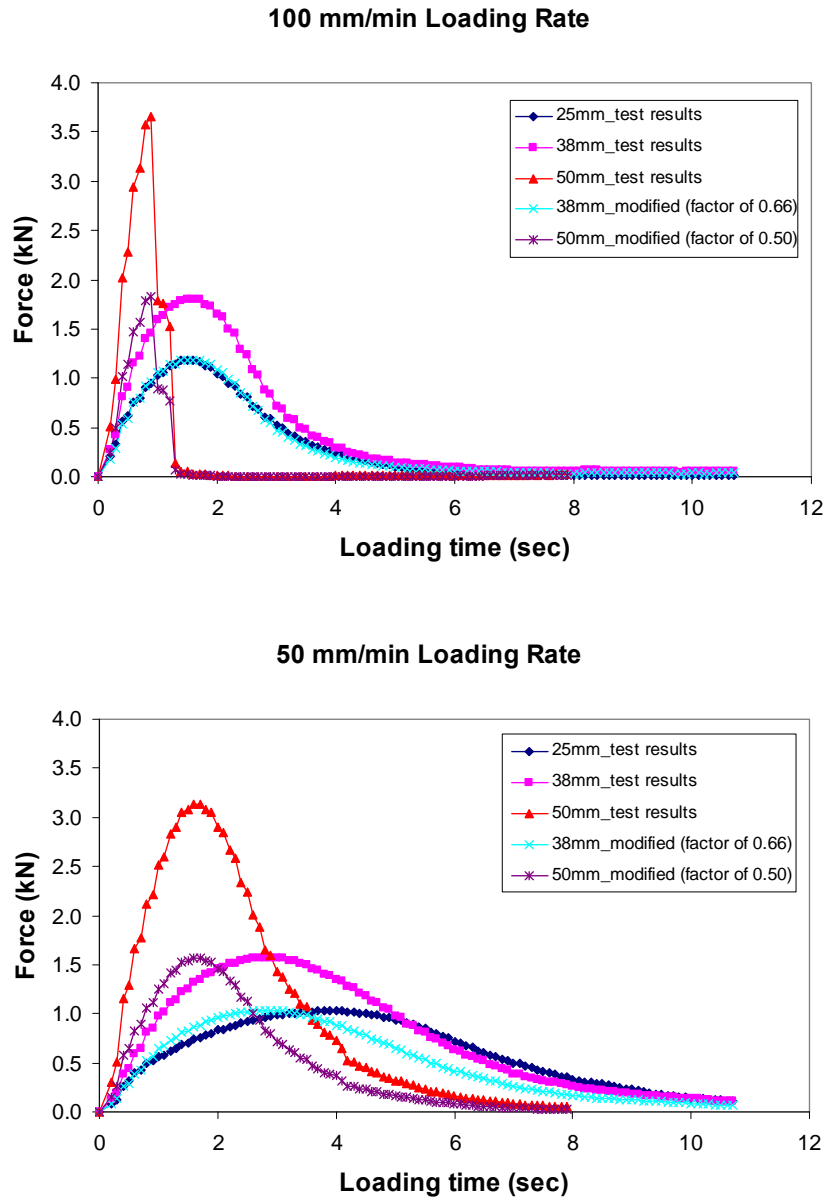


Figure F3b-1.1. SCB test results from three thicknesses at two different loading rates.

A total of 15, 25-mm-thick SCB specimens were then fabricated to investigate rate-dependent fracture characteristics of the FAM phase by applying five different loading rates (i.e., 50, 100, 200, 400, and 600 mm/min). For each loading rate, three replicates were tested. Testing was highly repeatable without large discrepancies observed among the replicates: percent deviation in peak force of each replicate with respect to the mean value from all three replicates was less than 10%.

Figure F3b-1.2 presents the SCB test results by plotting the reaction force as the loading time increased. Clearly, rate-dependent mechanical behavior is observed. Slower loading rates produce more compliant responses than faster loading rates. The rate-dependent mechanical response is related to several effects such as the viscoelasticity of the bulk matrix and the fracture process through the cohesive zone. Test results can be incorporated with numerical simulations that account for both the material viscoelasticity and the cohesive zone fracture process to identify if the rate-dependent mechanical response is related to the fracture process. Cohesive zone fracture parameters identified at each different loading rate can provide the rate-dependent fracture process, if it exists.

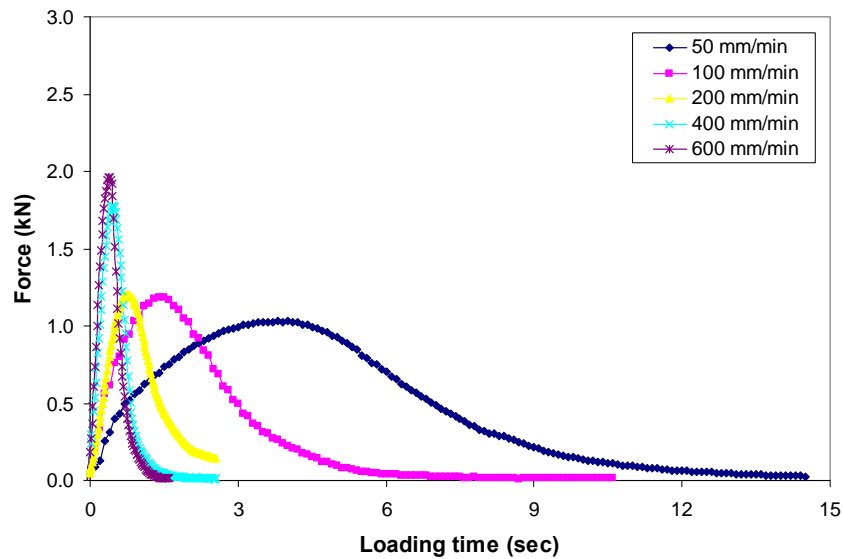
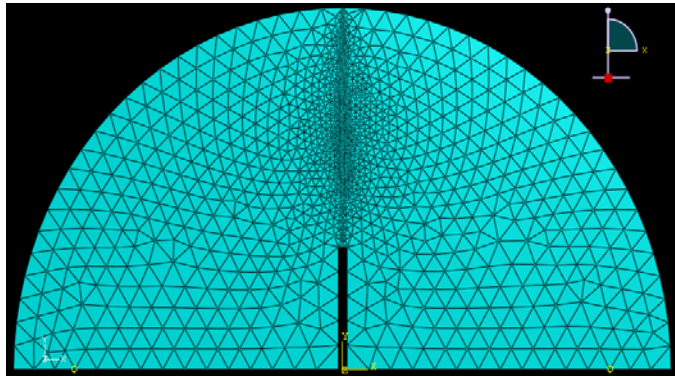


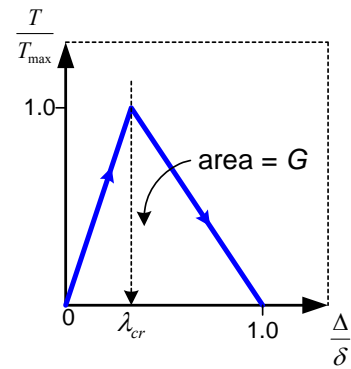
Figure F3b-1.2. SCB test results at the five different loading rates.

- Determination of cohesive zone fracture properties of the FAM phase at different loading rates by integrating the SCB fracture test results with finite element simulations of the SCB tests:

For the SCB simulations, a finite element mesh illustrated in figure F3b-1.3 was used by incorporating a bilinear intrinsic cohesive zone model, which is also presented in figure F3b-1.3. Cohesive zone elements are imbedded along the vertical ligament from the notch tip.



(a) Finite Element Mesh of the SCB Specimen



(b) Bilinear CZ Model

Figure F3b-1.3. Numerical simulation of the SCB testing.

Figure F3b-1.4 shows the experimental and numerical results obtained from the five different loading rates applied to the SCB specimens. Generally, a very good match was found between the test results and the numerical simulations. A different set of cohesive zone properties, as presented in figure F3b-1.5, was necessary to match with test results, which clearly implies that the fracture process in viscoelastic media (FAM specimens in this case) is also a rate-dependent phenomenon and must be modeled accordingly. As the loading rates become faster, the cohesive zone strength and the fracture energy necessary to initiate crack growth increase.

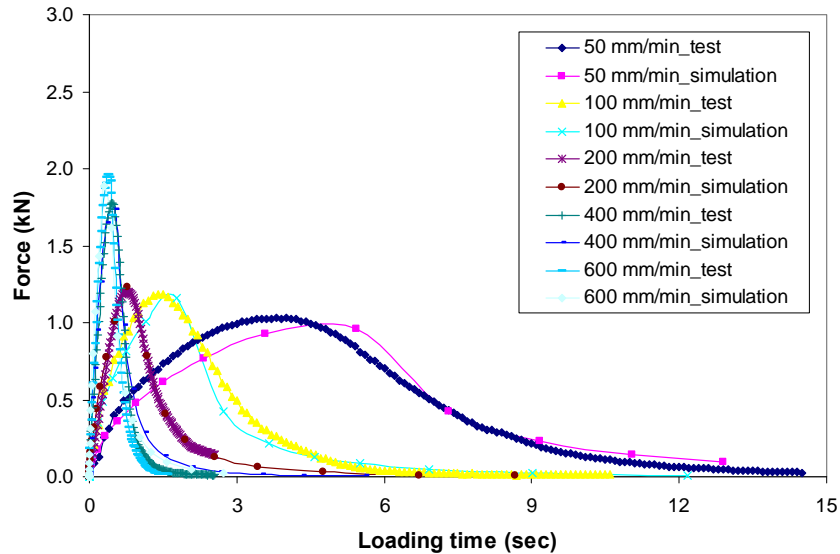


Figure F3b-1.4. SCB test results vs. numerical simulations.

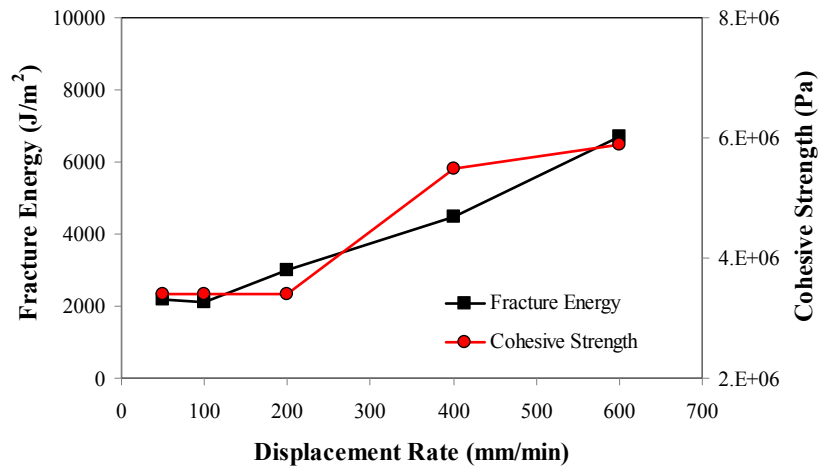


Figure F3b-1.5. Cohesive zone fracture properties at different loading rates.

- Implementation of the testing-analysis protocol for mixing, compaction, and production of FAM specimens:

We have worked on a testing-analysis protocol which includes the mix design, specimen fabrication, characteristic testing, and mechanical analyses of the FAM phase. This effort is to develop a more articulate and scientific approach in mixing and compaction of the FAM phase, which produces key material properties (viscoelastic properties and cohesive zone fracture properties) to accomplish the computational micromechanics modeling. Unlike conventional volumetric systems, the asphalt concrete has been defined to consist of two primary material phases – the elastic phase of aggregates and the viscoelastic phase of FAM, which is composed of asphalt binder, fine aggregates passing sieve No. 16 (1.19 mm), and entrained air voids. The maximum fine aggregate size of 1.19 mm in the FAM mixture was selected based on two-dimensional digital image analyses of cross sections obtained from various compacted asphalt concrete samples. The digital images could not properly capture aggregates approximately less than 1.0 mm, which is close to the mesh size of sieve number 16. The mix design of the FAM phase has been postulated on the basis of the sharing of binder by the coarse and fine aggregates in the asphalt concrete mixture. The design considered binder content that is absorbed into aggregates and that covers aggregates with a fixed binder film thickness. Algebraically, the required binder content to produce the FAM mixture was proposed as the one remaining after excluding binder absorbed in the coarse aggregates and the thin film (12 micron) of binder covering coarse aggregates from the total binder in the bulk asphalt concrete mixtures. The new protocol also incorporated the extraction of small DMA specimens out of Superpave gyratory bulk samples that were compacted with different amounts of FAM mixtures to represent different levels of air voids. Each DMA specimen was tested to characterize linear viscoelastic properties (in a form of dynamic modulus master curve) at each different level of air voids. Test results were then incorporated with the micromechanical finite element simulations to predict

linear viscoelastic dynamic moduli of the corresponding bulk asphalt concrete mixture. Simulated dynamic moduli from the micromechanical model are then finally compared to realistic dynamic moduli obtained from laboratory tests (AASHTO TP62) so that the appropriate level of compaction to produce the FAM mixture can be determined. So far, we have finished mixing, fabricating FAM specimens with different levels of air voids, DMA testing of FAM specimens, and the testing of asphalt concrete specimens for the mixture dynamic moduli. Significant findings after performing the micromechanical finite element simulations and comparisons with experimental results will be reported in the next quarter.

Lattice Micromechanical Model

In the previous quarter, efforts focused on the characterization of the quantitative aspects of the existing lattice model. The sensitivity to notch size of the previously implemented model has been investigated. One of the main problems with the previous implementation is that the effect of rate of loading could not be captured in the analysis. The current quarter's effort has focused on implementing a new model that can capture the effect of rate of loading in a lattice model.

In the previous implementation, the stress-strain curve of the lower scale was fed as the fundamental behavior to the lattice links of the next scale. Because the correspondence principle was used to acquire the viscoelastic response of the links, the rate of loading did not have any effect on the results. After some investigation into different models, the viscoelastic continuum damage (VECD) model appears to be the most suitable to address this problem.

The idea is to evaluate the damage parameter (S value) of each link in each time step and find the material integrity (C value) based on the amount of damage the material has undergone. Material integrity is a representative of material stiffness. As a result, material stiffness can be modified in each step by knowing the C value for each link. Because the amount of damage is correlated to the strain rate, the effect of the rate of loading can be captured.

Once the C vs. S relationship is available for the material, the pseudo strain (ε^R) for all the links in the lattice can be found. Using Equation (F3b-1.1) the damage parameter for each link in step $i+1$ can be found by knowing the damage parameter from the previous step.

$$S_{i+1} = S_i + \Delta t \left(-\frac{1}{2} (\varepsilon^R)^2 \frac{(\partial C)_i}{\partial S} \right)^\alpha \quad (\text{F3b-1.1})$$

Using the C vs. S relationship, C_{i+1} can be found for all the links. By knowing the C value and pseudo strain for each of the elements, the stress for each of the elements can be found, as shown in Equation (F3b-1.2).

$$\sigma_{i+1} = C_{i+1} \varepsilon^R \quad (\text{F3b-1.2})$$

Because the stress for each link is known for each time step, the reaction of the whole specimen to the applied load for all the time steps can be determined, and as a result, the stress-strain relationship for each scale up to the failure point can be found.

The C vs. S relationship can also be found for the analyzed specimen as well. This C vs. S relationship represents the continuum damage behavior of the material in the current scale and can be used as an input for the next scale.

In other words, in the new proposed method, the C vs. S curves, instead of the stress-strain curves, are used as inputs for each scale. The specimen in each scale is analyzed using the C vs. S curve obtained from the lower scale. After analysis, the C vs. S curve for the analyzed scale can be obtained and refined to be used as an input for the next scale. This procedure can be recursively performed inside a multiscale code.

The aforementioned procedure is implemented into the multiscale virtual fabrication and lattice modeling software (MS-VFLM). Preliminary results show that this method can capture the effect of rate of loading on an asphalt concrete specimen. In figure F3b-1.6, the stress-strain curves for three different loading rates are compared. As figure F3b-1.6 shows, faster loading has caused a stiffer response. The same trend has been observed in experiments.

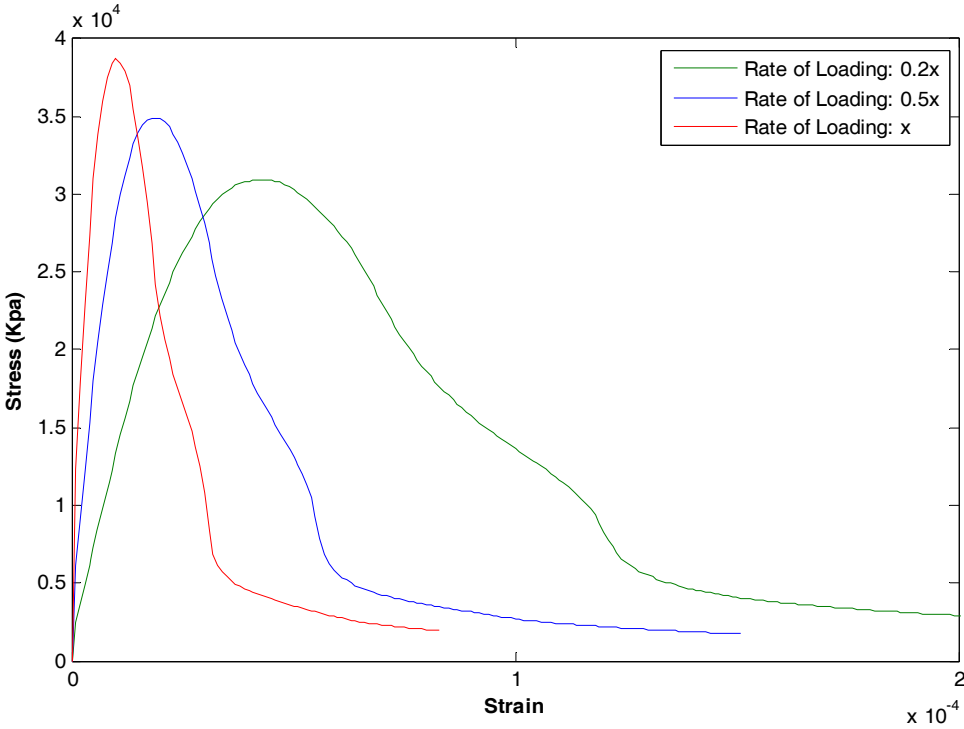
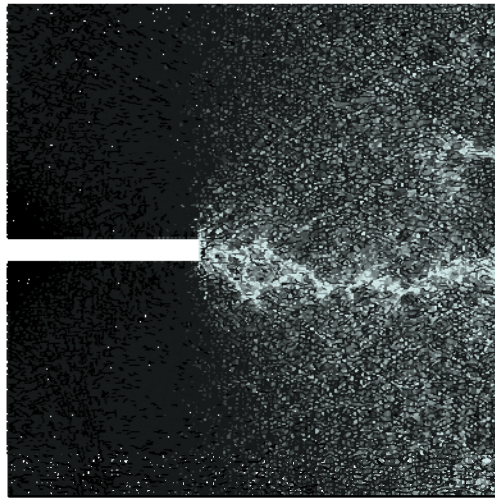
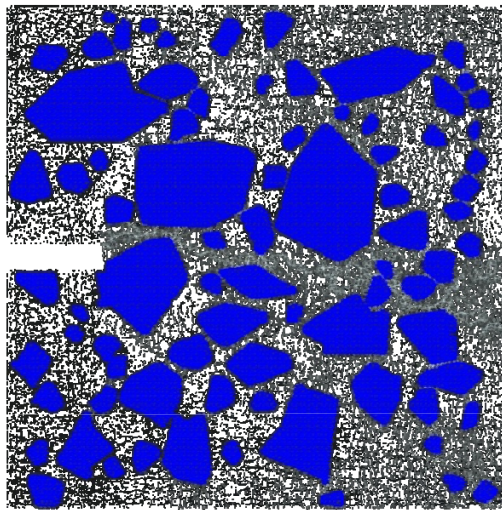


Figure F3b-1.6. Effect of loading rate on stress-strain curve.

Figure F3b-1.7 (a) and (b) shows the damage pattern of homogeneous (figure F3b-1.7a) and heterogeneous (figure F3b-1.7b) specimens obtained via the new implementation.



(a)



(b)

Figure F3b-1.7. Crack pattern: (a) homogeneous specimen; (b) heterogeneous specimen.

The new procedure has been implemented and some preliminary investigations have been undertaken. Further work must be done to quantitatively compare the results obtained from the analysis and the experiments. Work in the next quarter will focus on the following issues:

- a. C vs. S data are available at the mastic and matrix levels. The new implementation will be used and modified in order to obtain results that match the experimental data.
- b. The presence of air voids appears to affect the specimen strength significantly, and the incorporation of air void content into the lattice modeling will be investigated.

Continuum Damage to Fracture

A preliminary model that quantifies the micromechanical characteristics of damage under cyclic loading is currently under development. The model shows promise in that the macroscopic effects appear to be captured at low temperatures. The effort in the near future would focus on further refinements of the model, such as the inclusion of stress dependency and viscoelastic effects, followed by experimental verification. The ultimate goal of this effort is to understand the propagation of microcracks through localization, which is expected to facilitate the bridging of continuum damage models to localized fracture.

Significant Problems, Issues and Potential Impact on Progress

None.

Work Planned Next Quarter

Cohesive Zone Micromechanical Model

In the next quarter we will present research findings at two conferences: TRB 2010 and GeoFlorida (ASCE). Based on the research outcomes obtained so far, we will start working on the implementation of a cohesive zone model that is capable of accounting for the rate-dependent fracture process in asphaltic materials. This is a fundamental part of our work and is expected to provide important and meaningful insights into the effects of loading rates on the fracture behavior of the asphalt concrete mixtures. In addition, as mentioned earlier, any significant findings on the effort to identify proper mixing-compaction-production practices of the FMA phase will be reported in the next quarter.

Lattice Micromechanical Model

- Quantitative verification of the new continuum damage approach with experimental results.
- Preliminary implementation of air voids in lattice modeling software.

Continuum Damage to Fracture

The preliminary micromechanical model for distributed damage will be refined by including the effects of viscoelasticity, heterogeneity and stress level.

Work Element F3c: Development of Unified Continuum Model (TAMU)

Work Done This Quarter

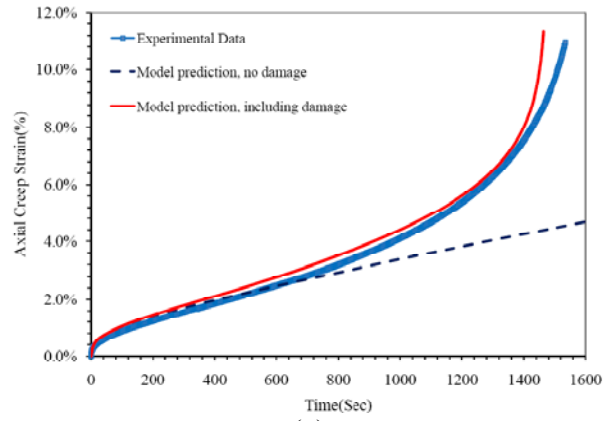
A temperature-dependent viscodamage model was developed and coupled to the existing viscoelastic and viscoplastic constitutive laws which are also enriched with temperature terms to describe the effect of mechanical damage, and temperature on the behavior of asphalt mixtures.

The thermo-viscodamage model is formulated to be a function of temperature, total effective strain, and the damage driving force which is expressed in terms of the stress invariants of the effective stress in the undamaged configuration. The proposed expression for the damage force allows for the distinction between the influence of compression and extension loading conditions on damage nucleation and growth. Furthermore, the effect of the moisture on the strength degradation of asphalt mixes is also modeled using continuum damage mechanics. Hence, different damage laws which are a function of moisture content are investigated.

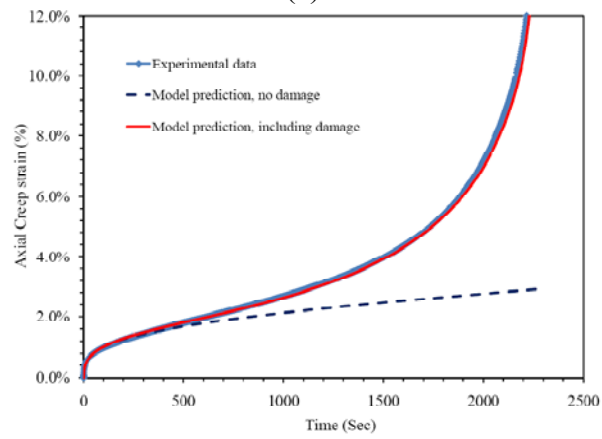
Also, a new configuration (i.e. healing configuration) is proposed in order to incorporate the effect of healing on the response of asphalt mixes subjected to repeated loading with different rest periods. This configuration can differentiate between the healed and unhealed cracks and makes the implementations very simple.

The thermo-viscoelastic-viscoplastic-viscodamage part of the TAMU mode is verified using several laboratory experiments. To this end, a systematic procedure is developed to determine model parameters as well as the temperature coupling terms. Then, the calibrated model is validated through comparing the model predictions with the experimental results for creep, creep-recovery, and constant strain rate tests over a range of temperatures, stress levels, and strain rates. Figure F3c.1 shows the comparison of the creep response between the experimental measurements from the Nottingham experimental database and model predictions when considering damage and no damage. As this figure shows, the model is capable of predicting the creep response of asphalt mixes at different temperatures and stress levels. It also shows the model capability on predicting both the shape of creep response and the time of failure over a range of temperatures and stress levels.

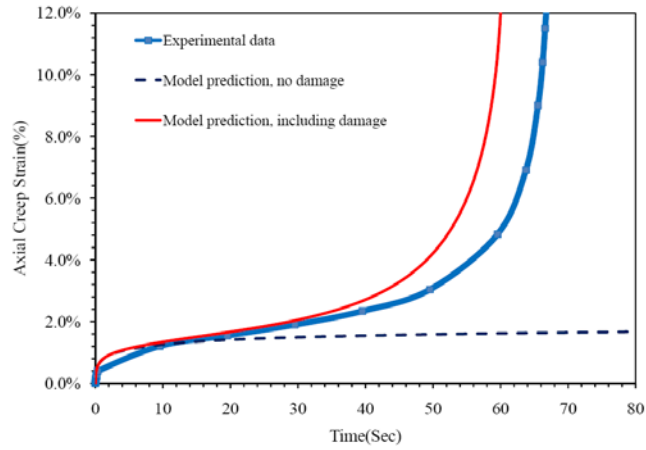
Comparisons between experimental measurements and figure F3c.2. The shaded area shows the region that experimental measurements are located whereas the dashed-lines are the model predictions. Figure F3c.2 also confirms the model capability in predicting the behavior of asphalt mixes for different stress paths.



(a)

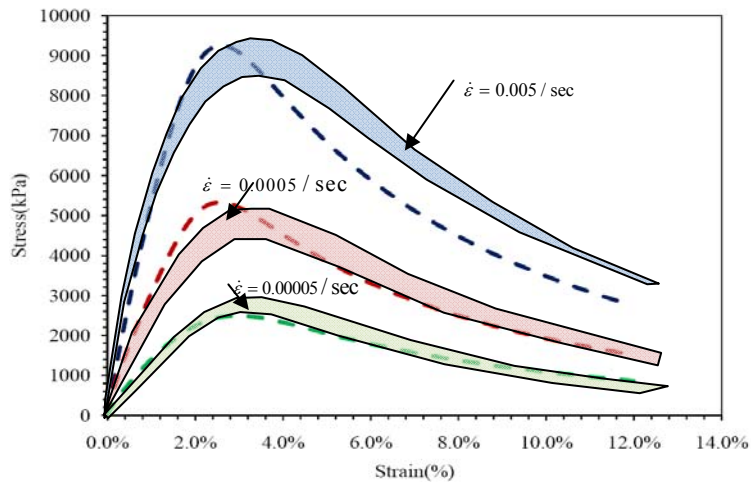


(b)

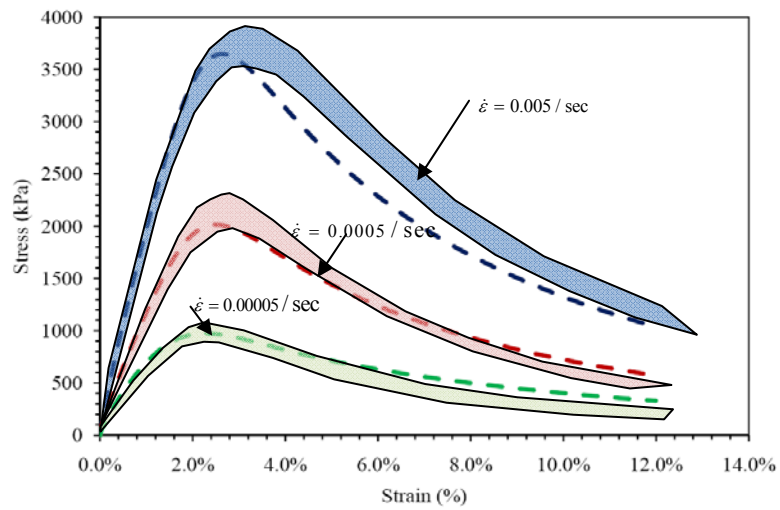


(c)

Figure F3c.1. The comparison of the creep response between experimental measurements and model prediction for: (a) $T = 10^{\circ}C$; $\sigma = 2500(KPa)$ (b) $T = 20^{\circ}C$; $\sigma = 1000(KPa)$ (c) $T = 40^{\circ}C$; $\sigma = 750(KPa)$



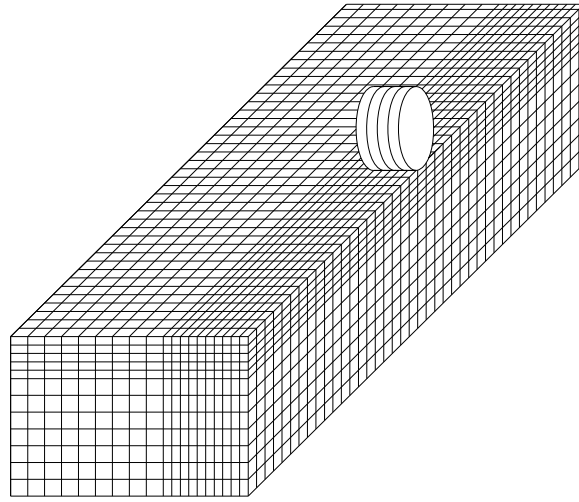
(a)



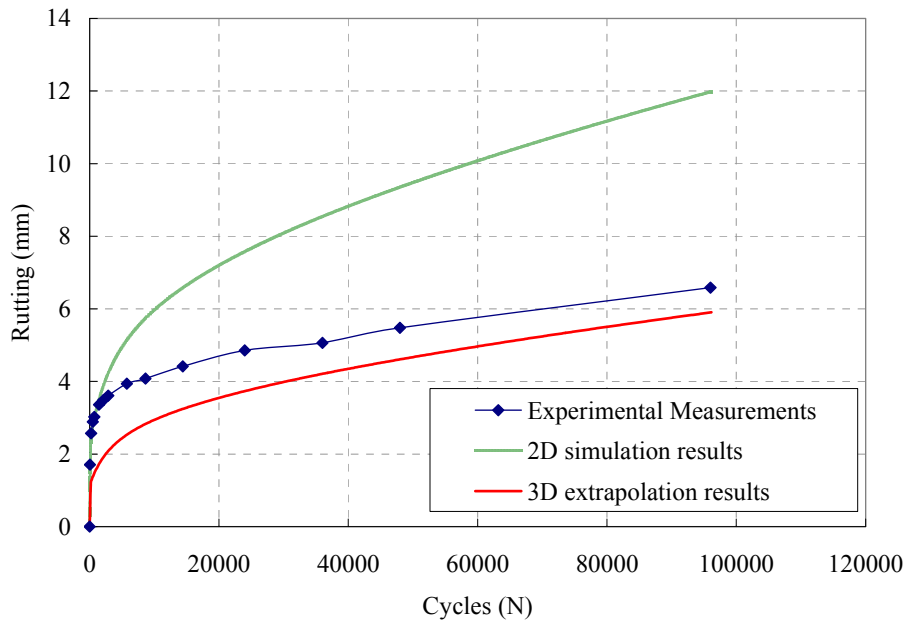
(b)

Figure F3c.2. The comparison of the stress-strain diagram between the experimental measurements and the model prediction for the constant strain rate test at:
 (a) $T = 10^{\circ}C$ (b) $T = 20^{\circ}C$

The complex nature of applied loading, huge number of loading cycles (e.g. millions of loading cycles), and complex behavior of asphaltic materials make the accurate simulation of rutting in pavements very difficult and challenging. From the numerical point of view, it is almost impossible to conduct the 3D simulation of rutting in pavements subjected to hundreds of thousands loading cycles. Hence, a thorough study on the effect of both different loading modes (e.g. pulse loading, equivalent loading, and moving loading) and type of simulation (2D and 3D) is recently conducted. Based on these studies an extrapolation technique for extrapolating the results of 3D FE analysis subjected to the realistic loading conditions based on the predicted rutting values in 2D simulation is proposed. The proposed extrapolation technique is then used for predicting the rutting in Wheel Tracking Test. The 3D finite element mesh for modeling the Wheel Tracking Test is shown in figure F3c.3(a). Figure F3c.3(b) shows the comparisons between the experimental measurements from the Nottingham experimental database and the model predictions for a Wheel Tracking Test subjected to 96000 loading cycles. In this figure, the 2D FE simulates the rutting up to 96000 cycles; while the 3D finite element only simulates the rutting up to 1000 cycles. Then, the extrapolation technique is employed to predict the rutting in 3D up to 96000 cycles. Figure F3c.3(b) shows that the final model prediction and experimental measurements are in good agreement.



(a)



(b)

Figure F3c.3. (a) the three dimensional FE mesh for modeling the Wheel Tracking Test (b) comparison of the experimental measurements and model predictions for Wheel Tracking Test; the blue line is the experimental measurements. The green line is the 2D simulation results whereas the red line is the final model predictions based on the extrapolation technique.

A major challenge in using finite element analysis of asphalt pavements is the time it takes to analyze performance under realistic moving loads. Therefore, we have investigated the influence of using more simplified loading patterns on performance. Five loading modes were simulated in three-dimensional (3D) analysis; and two loading modes were simulated in two-dimensional analysis. The permanent deformation results from these seven loading patterns simulating a wheel tracking test were compared.

Significant Results

None

Significant Problems, Issues and Potential Impact on Progress

None

Work Planned Next Quarter

The next quarter work plan for the unified continuum damage model will focus initiating extensive calibration and validation of the coupled viscoelastic, viscoplastic, and viscodamage model based on the ALF data. Detailed description of the ALF data is available in the final report of project DTFH61.05.RA.00108, which was submitted by North Carolina State University to the Federal Highway Administration on May 2008.

Work Element F3d: Calibration and Validation

This work element is planned to start later in the project.

Fatigue Year 3		Year 3 (4/09-3/10)											
		4	5	6	7	8	9	10	11	12	1	2	3
Material Properties													
F1a	Cohesive and Adhesive Properties												
F1a-1	Critical review of literature												
F1a-2	Develop experiment design												
F1a-3	Thermodynamic work of adhesion and cohesion												
F1a-4	Mechanical work of adhesion and cohesion			JP			JP			D			F
F1a-5	Evaluate acid-base scale for surface energy calculations												
F1b	Viscoelastic Properties												
F1b-1	Separation of nonlinear viscoelastic deformation from fracture energy under cyclic loading												JP
F1b-2	Separation of nonlinear viscoelastic deformation from fracture energy under monotonic loading			P, JP									JP
F1c	Aging												
F1c-1	Critical review of binder oxidative aging and its impact on mixtures												
F1c-2	Develop experiment design		F										
F1c-3	Develop transport model for binder oxidation in pavements						P, JP				P, JP		D
F1c-4	Effect of binder aging on properties and performance									D			F
F1c-5	Polymer modified asphalt materials										P		D
F1d	Healing												
F1d-1	Critical review of literature												
F1d-2	Select materials with targeted properties												
F1d-3	Develop experiment design												
F1d-4	Test methods to determine properties relevant to healing												JP
F1d-5	Testing of materials												
F1d-6	Evaluate relationship between healing and endurance limit of asphalt binders			DP			JP			DP			
F1d-7	Coordinate with AFM analysis												
F1d-8	Coordinate form of healing parameter with micromechanics and continuum damage models												
Test Methods													
F2a	Binder tests and effect of composition												
F2a-1	Analyze Existing Fatigue Data on PMA												
F2a-2	Select Virgin Binders and Modifiers and Prepare Modified Binder												
F2a-3	Laboratory Aging Procedures												
F2a-4	Collect Fatigue Test Data							P					P
F2a-5	Analyze data and propose mechanisms									P			
F2b	Mastic testing protocol												
F2b-1	Develop specimen preparation procedures												
F2b-2	Document test and analysis procedures in AASHTO format												
F2c	Mixture testing protocol												
F2d	Tomography and microstructural characterization												
F2d-1	Micro scale physicochemical and morphological changes in asphalt binders							JP					
F2e	Verify relationship between DSR binder fatigue tests and mixture fatigue performance												
F2e-1	Evaluate Binder Fatigue Correlation to Mixture Fatigue Data												
F2e-2	Selection of Testing Protocols			DP						D			F
F2e-3	Binder and Mixture Fatigue Testing												
F2e-4	Verification of Surrogate Fatigue Test												
F2e-5	Interpretation and Modeling of Data						JP				P		
F2e-6	Recommendations for Use in Unified Fatigue Damage Model												
Models													
F3a	Asphalt microstructural model												
F3b	Micromechanics model												
F3b-1	Model development												
F3b-2	Account for material microstructure and fundamental material properties												
F3c	Develop unified continuum model												
F3c-1	Analytical fatigue model for mixture design												
F3c-2	Unified continuum model			JP						JP			
F3c-3	Multi-scale modeling												

LEGEND

Deliverable codes

- D: Draft Report
- F: Final Report
- M&A: Model and algorithm
- SW: Software
- JP: Journal paper
- P: Presentation
- DP: Decision Point
- [x]

- Work planned
- Work completed
- Parallel topic

Deliverable Description

- Report delivered to FHWA for 3 week review period.
- Final report delivered in compliance with FHWA publication standards
- Mathematical model and sample code
- Executable software, code and user manual
- Paper submitted to conference or journal
- Presentation for symposium, conference or other
- Time to make a decision on two parallel paths as to which is most promising to follow through
- Indicates completion of deliverable x

Fatigue Year 2 - 5		Year 2 (4/08-3/09)				Year 3 (4/09-3/10)				Year 4 (04/10-03/11)				Year 5 (04/11-03/12)			
		Q1	Q2	Q3	Q4	Q1	Q2	Q3	Q4	Q1	Q2	Q3	Q4	Q1	Q2	Q3	Q4
Material Properties																	
F1a	Cohesive and Adhesive Properties																
F1a-1	Critical review of literature			JP													
F1a-2	Develop experiment design																
F1a-3	Thermodynamic work of adhesion and cohesion																
F1a-4	Mechanical work of adhesion and cohesion					JP	JP	D	F								
F1a-5	Evaluate acid-base scale for surface energy calculations														JP		
F1b	Viscoelastic Properties																
F1b-1	Separation of nonlinear viscoelastic deformation from fracture energy under cyclic loading			D,JP	M&A, F				JP	JP		P		JP, M&A, D		F	
F1b-2	Separation of nonlinear viscoelastic deformation from fracture energy under monotonic loading			JP	M&A, F	P,JP			JP	JP		P		JP, M&A, D		F	
F1c	Aging																
F1c-1	Critical review of binder oxidative aging and its impact on mixtures																
F1c-2	Develop experiment design			D		F											
F1c-3	Develop transport model for binder oxidation in pavements		P		P, JP		P,JP		P, JP	P		P, JP			D, M&A	F	
F1c-4	Effect of binder aging on properties and performance				JP, P			D	F					JP	D	F	
F1c-5	Polymer modified asphalt materials										P				D	F	
F1d	Healing																
F1d-1	Critical review of literature																
F1d-2	Select materials with targeted properties																
F1d-3	Develop experiment design																
F1d-4	Test methods to determine properties relevant to healing				JP				JP	D	F						
F1d-5	Testing of materials										JP			M&A, D	JP, F		
F1d-6	Evaluate relationship between healing and endurance limit of asphalt binders	DP				DP	JP	DP			JP		P	JP	D	F	
F1d-7	Coordinate with AFM analysis																
F1d-8	Coordinate form of healing parameter with micromechanics and continuum damage models											JP			JP, D	F	
Test Methods																	
F2a	Binder tests and effect of composition																
F2a-1	Analyze Existing Fatigue Data on PMA		DP														
F2a-2	Select Virgin Binders and Modifiers and Prepare Modified Binder		DP														
F2a-3	Laboratory Aging Procedures																
F2a-4	Collect Fatigue Test Data		P		JP		P		P				JP, D, F				
F2a-5	Analyze data and propose mechanisms				P			P				P		P	D	F	
F2b	Mastic testing protocol																
F2b-1	Develop specimen preparation procedures		D														
F2b-2	Document test and analysis procedures in AASHTO format		D														
F2c	Mixture testing protocol		D, JP	F													
F2d	Tomography and microstructural characterization																
F2d-1	Micro scale physicochemical and morphological changes in asphalt binders						JP				JP	M&A, D	F				
F2e	Verify relationship between DSR binder fatigue tests and mixture fatigue performance																
F2e-1	Evaluate Binder Fatigue Correlation to Mixture Fatigue Data																
F2e-2	Selection of Testing Protocols					DP		D	F								
F2e-3	Binder and Mixture Fatigue Testing																
F2e-4	Verification of Surrogate Fatigue Test												D	F, DP			
F2e-5	Interpretation and Modeling of Data		JP		P		JP		P		JP		M&A				
F2e-6	Recommendations for Use in Unified Fatigue Damage Model														D	F	
Models																	
F3a	Asphalt microstructural model							JP						JP			M&A, F
F3b	Micromechanics model																
F3b-1	Model development				JP				JP			M&A	D	DP	F, SW		
F3b-2	Account for material microstructure and fundamental material properties										JP			D		F	
F3c	Develop unified continuum model																
F3c-1	Analytical fatigue model for mixture design														M&A, D		F
F3c-2	Unified continuum model			JP		JP		JP					M&A	D	DP	F, SW	
F3c-3	Multi-scale modeling											JP	M&A	D		F	

LEGEND

Deliverable codes

- D: Draft Report
- F: Final Report
- M&A: Model and algorithm
- SW: Software
- JP: Journal paper
- P: Presentation
- DP: Decision Point
- [x]

- Work planned
- Work completed
- Parallel topic

Deliverable Description

- Report delivered to FHWA for 3 week review period.
- Final report delivered in compliance with FHWA publication standards
- Mathematical model and sample code
- Executable software, code and user manual
- Paper submitted to conference or journal
- Presentation for symposium, conference or other
- Time to make a decision on two parallel paths as to which is most promising to follow through
- Indicates completion of deliverable x

PROGRAM AREA: ENGINEERED MATERIALS

CATEGORY E1: MODELING

Work element E1a: Analytical and Micro-mechanics Models for Mechanical Behavior of Mixtures (TAMU)

Work Done This Quarter

Two technical papers, entitled “Characterization of the Tensile Viscoelastic Properties of an Undamaged Asphalt Mixture” and “Characterization of Damage in Asphalt Mixtures Using Dissipated Pseudo Strain Energy”, were accepted for presentation in the Transportation Research Board (TRB) 89th Annual Meeting. Another presentation entitled “Viscoelastic Characterization of Aged Field Asphalt Mixtures Using Direct Tension Test” was scheduled in the TRB’s Data Analysis Working Group (DAWG) meeting on January 9, 2010, in Washington, D.C.

Four field cores collected in Arizona were scanned using the X-ray Computed Tomography (CT) system to obtain the air void distribution in the cores. Each of the four field cores had two construction lifts; each construction lift was scanned separately. After the X-ray CT scanning, the cores were cut into rectangular specimens for future testing.

Further data analysis was conducted on the dummy field cores that were tested in previous quarters. A master curve was constructed for the phase angle of the complex modulus of a tested field core specimen. The mathematical model for the phase angle master curve is shown in Equation E1a.1. Figure E1a.1 illustrates the master curve of the phase angle at a reference temperature of 20°C. The time-temperature shift function used the WLF form.

$$\varphi = \frac{\varphi_m}{\left[1 + \frac{\left[\log \left(\frac{\omega_m}{\frac{C_1(T-T_r)}{\omega \cdot 10^{C_2+(T-T_r)}}} \right) \right]^2}{R_\varphi} \right]^{\frac{m}{2}}} \quad (\text{E1a.1})$$

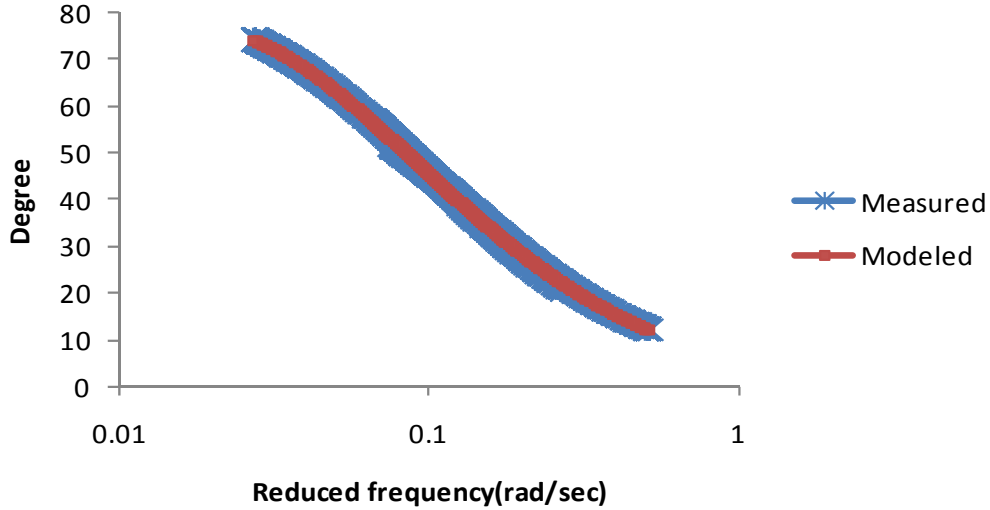


Figure E1a.1. Master curve of complex modulus phase angle of a field core specimen at reference temperature 20°C.

The tested field cores showed stiffness gradient with the pavement depth because the asphalt layer was not aged uniformly in the field. The upper layers of the pavement showed the effect of greater aging, while the lower layers were less aged. As a result, the geometric centroid of the field core specimen was different from the stiffness centroid. In the direct tension test, the Material Testing System (MTS) applied a tensile load to the geometric centroid of the specimen; the deformation of the pavement top side of the specimen was different from that of the pavement bottom side of the specimen. Because of the stiffness gradient of the field specimen, the measured strains on the different sides of the specimen were all associated with oscillations. An analytical method was developed to characterize the stiffness gradient with pavement depth of the field specimen, which was briefed in the last quarterly report. In this analytical method, two constants, n and k , were used to indicate the stiffness gradient of the field specimen as shown in Equations E1a.2 and E1a.3.

$$E(z) = E_d + (E_0 - E_d) \left(\frac{d-z}{d} \right)^n \quad (\text{E1a.2})$$

$$s\overline{E_0}(s) = ks\overline{E_d}(s) \quad (\text{E1a.3})$$

where $E(z)$ is the modulus at depth z ; E_d is the modulus at the pavement bottom side of the field specimen; E_0 is the modulus at the pavement top side of the field specimen; d is the depth of the field specimen; $\overline{E_0}(s)$ is the Laplace transform of E_0 ; $\overline{E_d}(s)$ is the Laplace transform of E_d ; s is the Laplace transform variable; and n and k are constants. The ratio of the strain amplitude at the center to the strain amplitude at the bottom was found to be:

$$\frac{\overline{\Delta\varepsilon_c}(s)}{\overline{\Delta\varepsilon_d}(s)} = \frac{2^n}{2^n - 1 + k} \quad (\text{E1a.4})$$

in which $\overline{\Delta\varepsilon_c}(s)$ is the Laplace transform of the amplitude of the strain oscillation at the middle depth of the field specimen.

Using the developed analytical method, a field core from the shoulder of US 259 was tested and analyzed. It was found this field specimen had a value of 4.07 for n and a value of 3.53 for k . The stiffness gradient curve was then determined for the top pavement layer as shown in figure E1a.2.

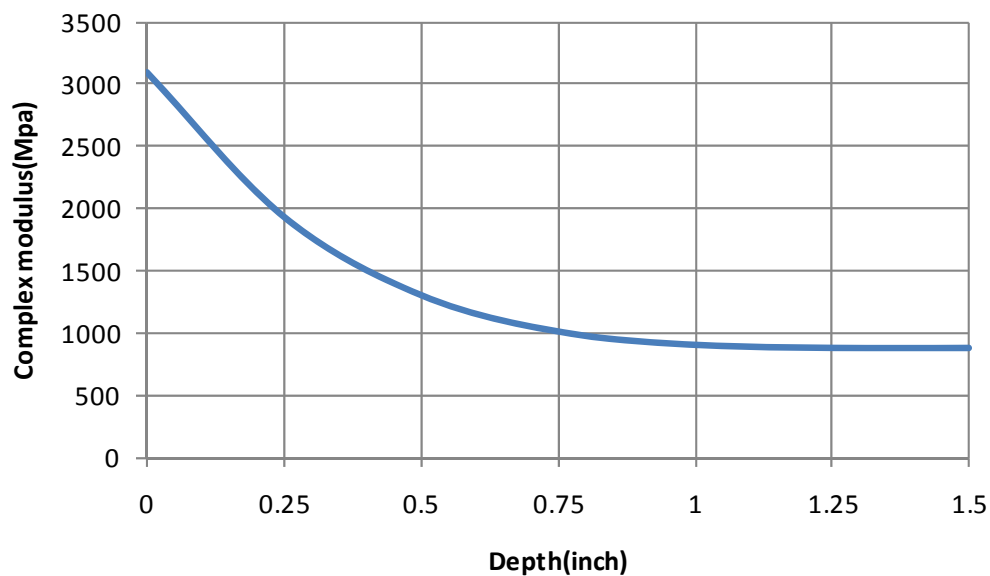


Figure E1a.2. Magnitude of complex modulus of a field core specimen with pavement depth.

Significant Results

Further data analysis was conducted on the field core specimens. The master curve was constructed for the phase angle of the complex modulus. The oscillation of the measured deformations of the field specimen was used to estimate the stiffness gradient of the field core specimens. When this method of testing and analysis is perfected, it will provide an independent means of determining the effect of field aging on as-built asphalt mixes.

Significant Problems, Issues and Potential Impact on Progress

In the controlled machine displacement direct tension test, the stress curve is significantly noisy due to the oscillation of the specimen. Therefore, instead of controlling the machine

displacement in the direct tension test, the loading rate may be controlled in the test in order to provide smoother data.

The newly purchased MTS is not ready for use. The software has not been completed installed in the MTS. The software installation is expected to be completed in the next quarter.

Work Planned Next Quarter

The analytical method to analyze the test data of the field core specimens will be further developed in the next quarter. Master curves will be constructed for the magnitude and phase angle of the complex modulus at multiple depths of the pavement layer. The stiffness gradient will be determined for more field core specimens.

Work element E1b: Binder Damage Resistance Characterization (DRC) (UWM)

Subtask E1b-1: Rutting of Asphalt Binders

Work Done This Quarter

Much of this quarter was dedicated to closer inspection of data collected during the previous two quarters, which included Multiple Stress Creep and Recovery (MSCR) testing of two modified binders and four mastics along with Repeated Creep and Recovery (RCR) of mixtures prepared with a coarse blend of granite aggregates and the aforementioned four mastics. This additional analysis was deemed necessary to determine the repercussions of the high coefficient of variation (COV) from mixture flow number (FN) results, which were seen to range from 0% to just over 40%, as reported in the previous quarterly report. Nonrecoverable creep compliance (J_{nr}) and percent recovery (%R) of binders and mastics were previously shown as curves reporting the values at each tested stress level in order to identify a trend related to stress sensitivity. Values have since been normalized to more appropriately identify the percent change in J_{nr} when increasing stress level from 0.1 kPa to 3.2 kPa. These values were also compared to determine binder influence on mastics response at testing temperatures of 64 °C and 46 °C. Mastics were then compared to mixture results to determine the relationship.

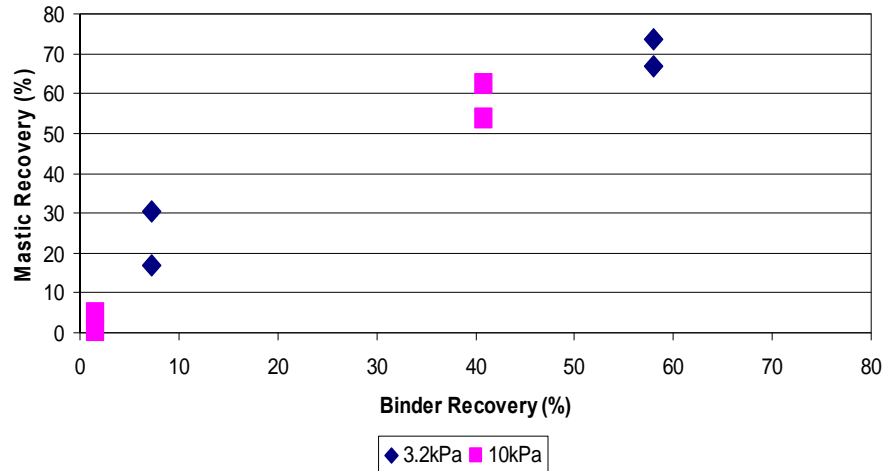
Significant Results

Percent change in J_{nr} for binders and mastics shows strong stress sensitivity as depicted in figure E1b-1.1. Binder A shows a decrease in percent change of J_{nr} when combined with either filler (granite or hydrated lime) to form mastic, while Binder B shows an increase in the percent change of J_{nr} in the mastic phase for each filler type and at both testing temperatures. The dashed line seen in figure E1b-1.1 represents a predetermined limit proposed by the Binder ETG showing where a linear response of a binder is exceeded.

Figure E1b-1.1. Graph. Stress sensitivity of binders and mastics.

When comparing binder and mastic data in terms of %R and Jnr values at 64 °C using stress levels of 3.2 kPa and 10 kPa, the relationship is found to be linear in each case, as shown in figures E1b-1.2 and E1b-1.3. However, this linearity is found for a limited data set at this time.

E1b-1.2. Graph. Comparison of binder and mastic Jnr from MSCR testing at 64 °C.



E1b-1.3. Graph. Comparison of binder and mastic MSCR recovery at 64 °C.

Recovery of the same binders and mastics showed a similar behavior to that of the Jnr values when tested at 46 °C and maintaining the same stress levels of 3.2 kPa and 10 kPa. Figure E1b-1.4 shows a linear positive relationship for the %R of binders and mastics. This relationship is not seen when comparing Jnr of the binders at 46 °C, where the relationship appears more scattered, as shown in figure E1b-1.5.

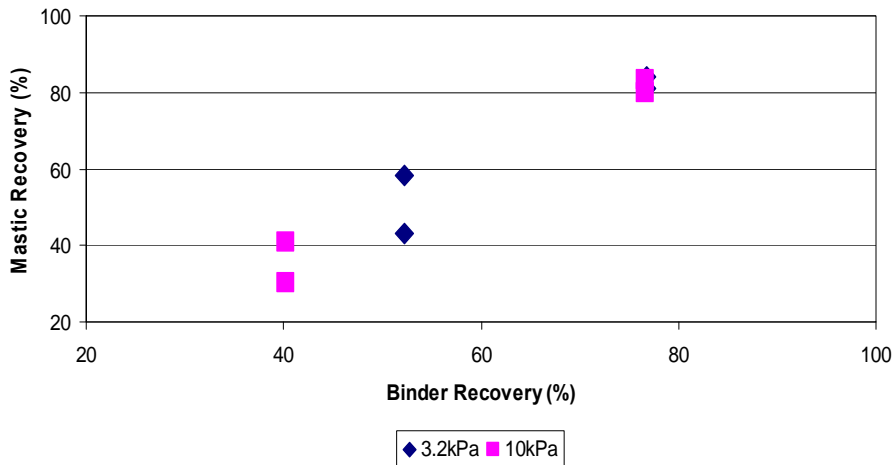


Figure E1b-1.4. Graph. Comparison of binder and mastic MSCR recovery at 46 °C.

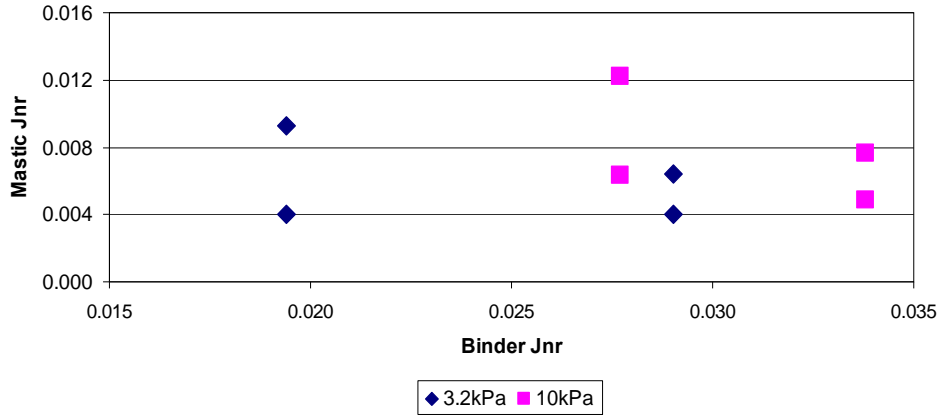


Figure E1b-1.5. Graph. Comparison of binder and mastic Jnr from MSCR testing at 46 °C.

The results of binder versus mastic appear to show a temperature dependence and variation from expectations specifically at 46 °C, which is the temperature used for mixture testing. Mixture testing was conducted at 50, 100 and 150 psi, with 100 psi determined to be the most reliable data collected thus far, as reported in the previously quarterly reports. For this reason, mastic results were plotted versus mixture data (FN of mixture versus Jnr or %R of mastic) for measurements made at 46 °C. Figure E1b-1.6 indicates that Jnr shows a scatter of data, similar to Jnr comparison of binders and mastics at 46 °C. However, figure E1b-1.7 indicates that mixture FN versus mastic %R exhibited a trend which opposes that of binder and mastic comparison at 46 °C.

Results show that binder type and the addition of mineral filler clearly influence both mastic behavior and mixture performance, though the exact causes of each require additional evaluation.

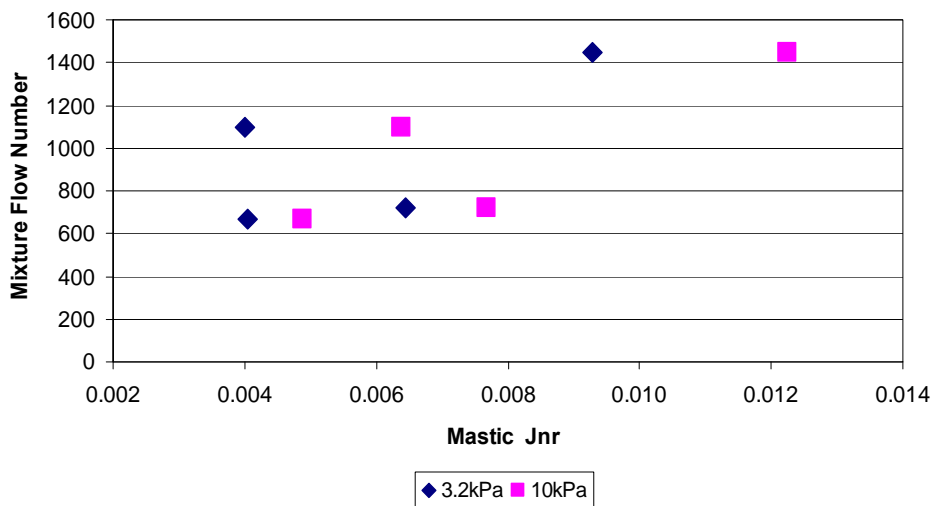


Figure E1b-1.6. Graph. Comparison of mastic Jnr (3.2 and 10 kPa) and mixture (100 psi) data at 46 °C.

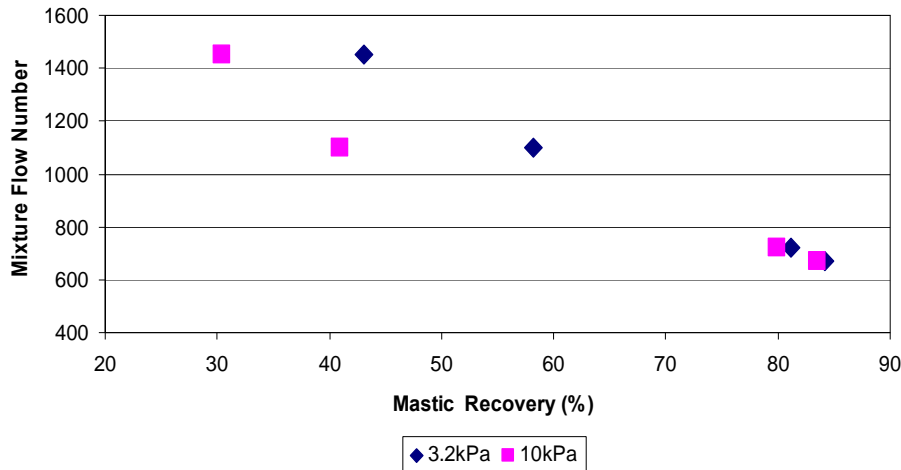


Figure E1b-1.7. Graph. Comparison of mastic %R (3.2 and 10 kPa) and mixture (100 psi) data at 46 °C.

Significant Problems, Issues and Potential Impact on Progress

The trends observed do not remain consistent from one phase to another (binder to mastic to mixture). It is suspected that the variability in these trends is caused by the limited data set thus far. To see the effect of specific variables, binder and mastic testing will continue at a designated high temperature (70 °C), as well as lower temperatures of 58 °C and 46 °C to match the temperature of mixture testing conditions. A third neat (unmodified) binder of different PG grade from the initial two binders will be added to the testing matrix. This new binder and one of the originally selected binders will be further investigated by incorporating two levels of modification into the testing plan (2% and 4% elastomer or plastomer). To offset the additional time required for this inclusion of materials, intermediate stresses have been removed from the RCR testing plan of binder and mastic. This is expected to allow the research team to retain the original time schedule.

Work Planned Next Quarter

The coming quarter is expected to yield results of additional binders and mastics and these will be carried into the mixture testing in accordance with the previously developed work plan. The additional binder incorporated in the material selection results in the following neat asphalt binders: PG 64 FH neat and PG 58 Valero neat. The first of these neat binders is to be modified with 2% and 4% elastomer and plastomer, while the second will be modified at only one level (4%) initially, resulting in:

- FH+4% CBE (plastomer).
- FH+4% styrene-butadiene-styrene (SBS) (elastomer).
- FH+2% CBE.

- FH+2% SBS.
- Valero+4% SBS.
- Valero+2% SBS.

The fillers to be combined with the above binders to produce mastics have been narrowed from three to two: hydrated lime (HL2) and pulverized granite (GH1).

MSCR and RCR testing of binders and mastics will be conducted at 70 °C, 58 °C and 46 °C, regardless of PG grade of the neat binder. This will allow for direct comparison at a high and intermediate temperature as well as temperature equivalent to mixture testing. RCR testing will be conducted at stress levels of 100, 3200 and 10000 Pa. FN testing of mixtures will continue to take place at 46 °C and stress levels of 50, 100 and 150 psi since previous results showed promising distinction between stress levels. Mixture preparation will be controlled by volumetric calculations performed per sample as opposed to a constant compaction effort. This will allow for consistent percent air voids for all mixture specimens, expected to result in greater repeatability than seen in early results.

Subtask E1b-2: Feasibility of Determining Rheological and Fracture Properties of Thin Films of Asphalt Binders and Mastics using Simple Indentation Tests

Work Done This Quarter

In this quarter the research team focused its efforts on completing the experimental testing plan and starting the finite element (FE) modeling of the indentation test.

To obtain master curves of the materials, the testing temperatures suggested in the previous quarterly report were reconsidered and reduced to 30 °C and 20 °C. This decision was made based on the high penetration rate of the indenter observed in tests performed at higher temperatures (e.g., > 40 °C).

The modified experimental plan for rheological characterization of asphalt binders at these new temperatures is shown in table E1b-2.1. Two different binders—FH 64-22 and NuStar 64-22—and three types of modifications are included to investigate if the proposed test procedure can capture broad ranges of asphalt binder performance.

Table E1b-2.1. Experimental plan.

Variables	Factors	Remarks
Temperature	2	20 °C and 30 °C
Binder	2	FH 64-22, NuStar 64-22
Size	3	Three sizes to model the size effects on creep compliance (1.7, 3.4 and 5.1cm)
Modification	3	A neat binder, elastomer (styrene-butadiene-styrene (SBS)) and plastomer modification (CBE)
Replicates	3	To determine repeatability of testing and for statistical analysis
Total Combinations		108

The progress in testing completed during this quarter is presented in table E1b-2.2. The proposed test procedure requires conditioning the samples at the specific temperature (e.g., 20 °C and 30 °C) in an environmental chamber. However, the tests are performed while the device is at room temperature. The variation of the temperature in the sample during testing was investigated by conducting a set of experiments in which temperature was measured with a thermocouple at different times and locations in the sample. The temperatures measured were found not to vary significantly within the time of the experiment. This is partly due to the fact that sample conditioning is done at temperatures closer to room temperature. Hence, losses due to thermal gradients are not pronounced.

Table E1b-2.2. Tests completed last quarter.

Binder Name	Modification	Temperature	Sample Height		
			5.1 cm	3.4 cm	1.7 cm
FH 64-22	Neat	20 °C			
		30 °C			
	SBS- Modified	20 °C			
		30 °C	X	X	X
	CBE-Modified	20 °C			
		30 °C	X	X	X
NuStar 64-22	Neat	20 °C			
		30 °C	X	X	X
	SBS-Modified	20 °C			
		30 °C	X	X	X
	CBE-Modified	20 °C			
		30 °C			

Figures E1b-2.1 and E1b-2.2 show typical indentation test results obtained from the partially completed experimental plan. It is observed from the figures that the effect of the specimen size depends on the asphalt type. The size effect is more pronounced in a less stiff (i.e., more compliant) binder, as shown in figure E1b-2.1, in comparison to a stiffer one, as shown in figure E1b-2.2. This observation is in agreement with the fact that the effect of the boundary conditions at the bottom of the specimen (i.e., rigid base) is larger for the softer binder. The research team plans to investigate the effect of the boundary conditions and specimen size on the measured creep compliance of a broad range of asphalt types by means of FE modeling.

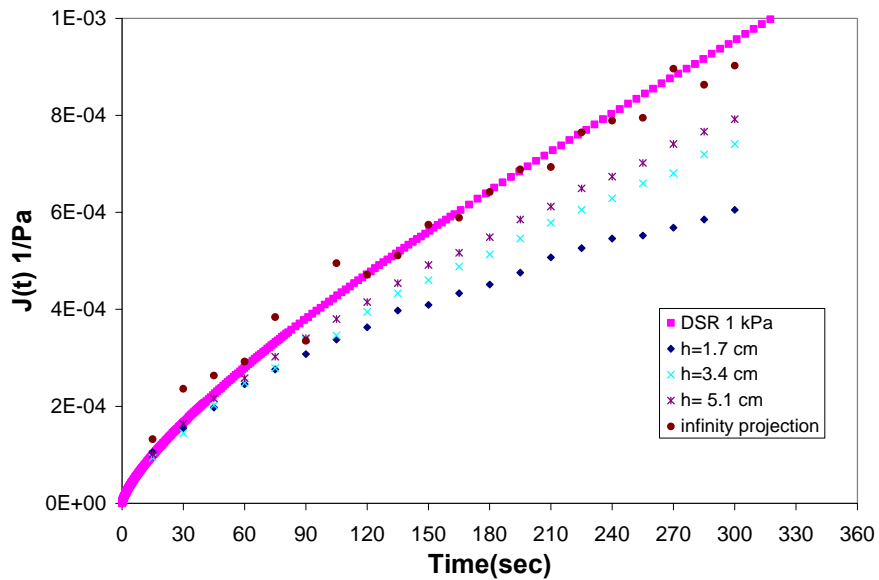


Figure E1b-2.1. Graph. Indentation results obtained for the binder NuStar 64-22 SBS. ($J(t)$ = creep compliance; DSR = Dynamic Shear Rheometer; h = depth of binder in testing container.)

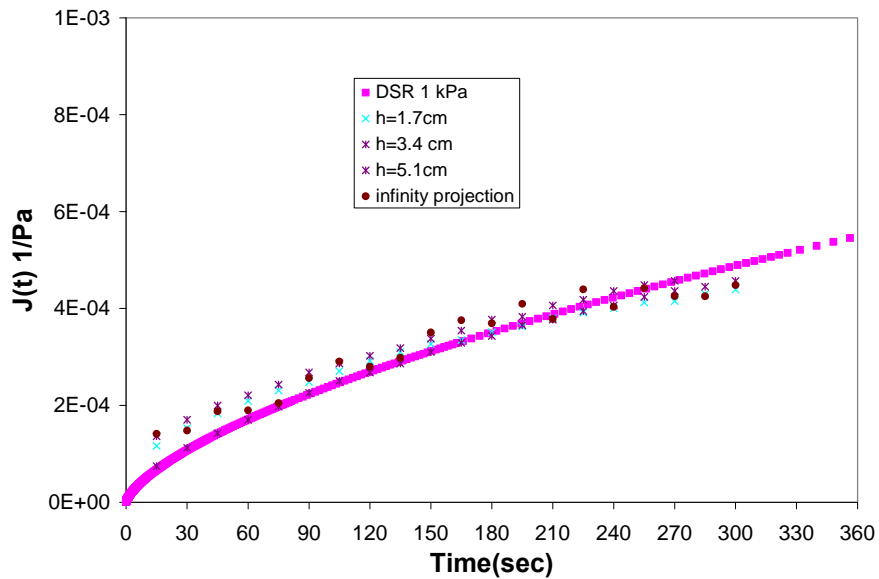


Figure E1b-2.2. Graph. Indentation results obtained for FH 64-22 SBS.

Finite Element Modeling

Preliminary testing clearly indicates the effects of specimen size and boundary conditions on the material properties obtained from indentation tests. Hence, the FE software Abaqus is used to investigate and quantify these effects. The main objective of using the numerical modeling of the indentation tests is to develop a set of correction factors for the experimentally obtained creep compliance that take into account the effects of size and boundary conditions.

In this quarter, the research team expended extensive effort to build, mesh and apply boundary conditions and run a FE model in Abaqus. The team focused on resolving issues related to the convergence of the force-controlled indentation model. The force-controlled case is more appropriate for this study, as the indentation experiment is conducted in load-controlled mode. The research team plans to solve this convergence problem next quarter.

The indentation test is modeled with Abaqus standard software using the axisymmetric option, considering the cylindrical symmetry of the sample and indenter. Eight-node quadrilateral elements are used for meshing the asphalt specimen. These elements provide a better approximation of the true solution for displacements, strains and stresses in comparison to the four-node elements. The indenter is modeled using an analytical rigid surface which is made of aluminum. Treating the indenter as a rigid surface can reduce the computational effort and also increase the accuracy of the solution of the boundary value problem. The displacement was initially modeled in two steps: In Step 1, the indenter is displaced in to the sample using a linear ramp; in Step 2, the indenter is kept at a constant displacement, as shown in figure E1b-2.3.

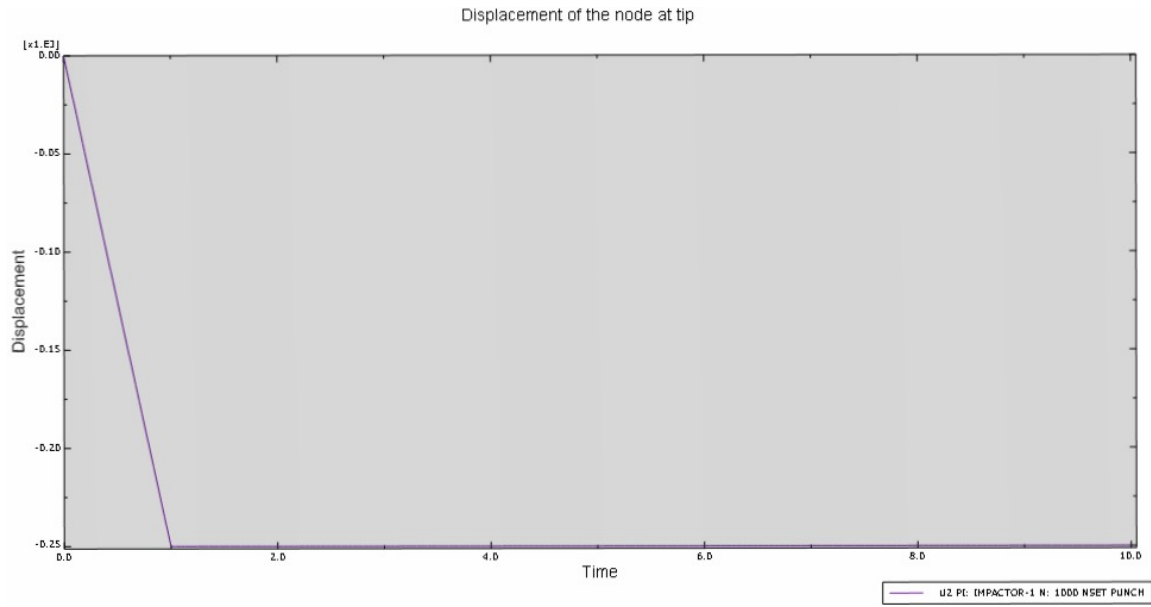


Figure E1b-2.3. Graph. Displacement versus time of the indenter.

The shape of the deformed and undeformed specimen is shown in figure E1b-2.4. The force underneath the indenter versus time is presented in figure E1b-2.5. It can be seen that the forces are relaxing with respect to time as the displacement is kept constant. Note that the initial increase in the force is due to the initial increase in the displacement with time occurring in Step 1.

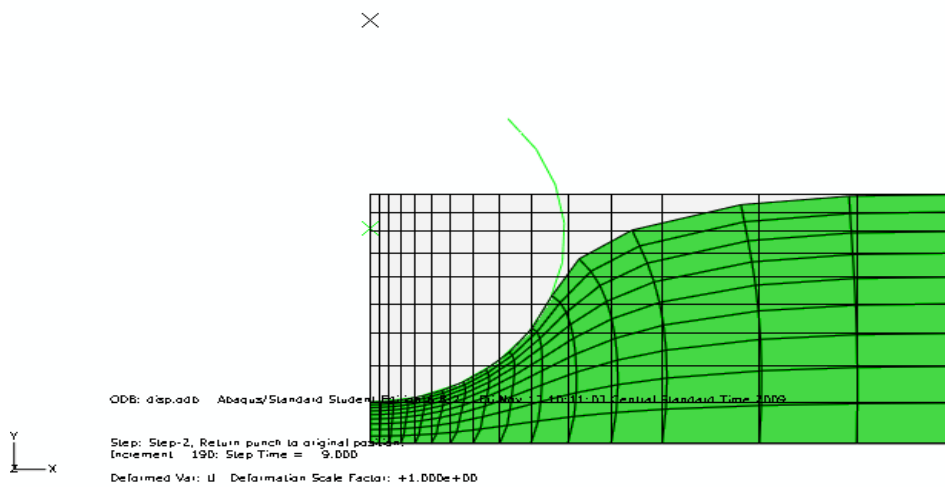


Figure E1b-2.4. Illustration. Deformed and undeformed shape of the sample.

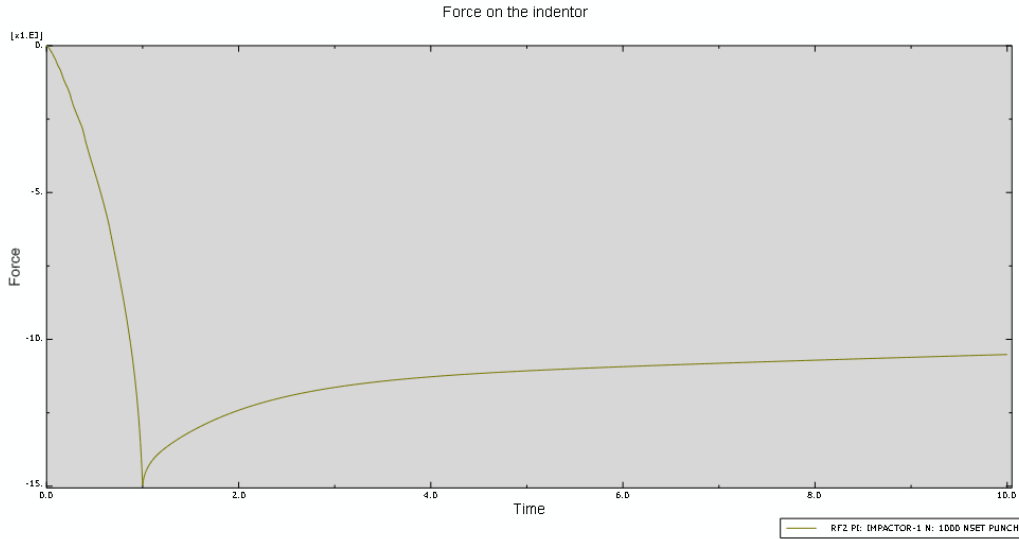


Figure E1b-2.5. Graph. Force versus time FE simulation.

Shown in figures E1b-2.6 and E1b-2.7 are the stress variation in the asphalt specimen with time. It can be seen from the figures that the stresses are not uniform throughout the sample and that stresses are relaxing with time. FE analysis could be used as a tool to investigate and understand the effect of different issues present in the experiment such as size effects and boundary conditions. Preliminary FE simulations were performed to estimate the stress state of the material under the indenter tip. The research team will be using the FE simulations to determine the magnitude of the shear stress under the indenter tip to define the stress level to be used in the DSR testing.

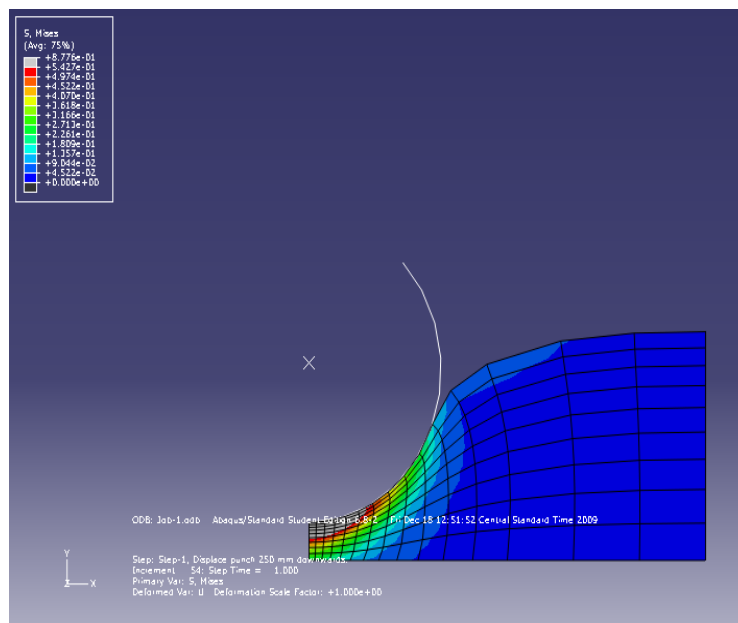


Figure E1b-2.6. Illustration. Stress variation in the sample at $t = 1$ sec.

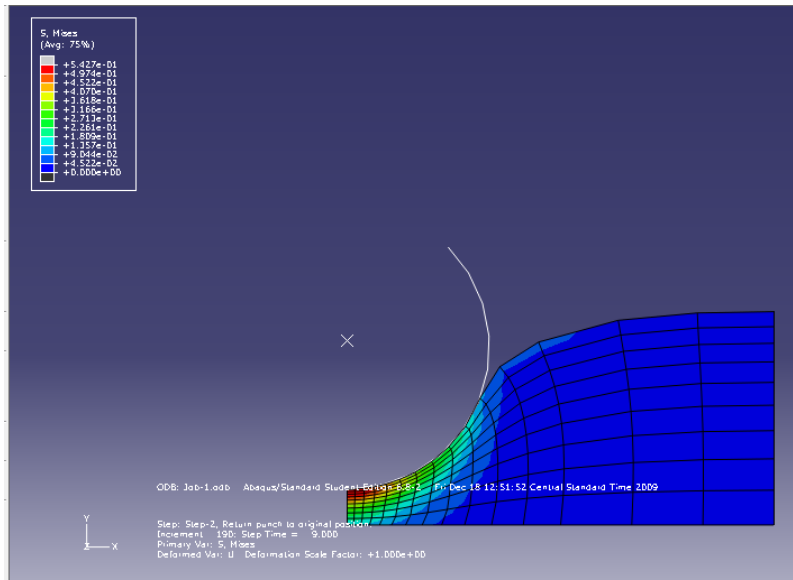


Figure E1b-2.7. Illustration. Stress variation in the sample at $t = 10$ sec.

Interconversion Methods

Interconversion methods are needed for transforming the creep compliance obtained from indentation tests to the complex modulus. In this quarter, various interconversion techniques were studied and the methods providing the most accurate transformations between linear viscoelastic properties were selected by the research team. Next quarter, the selected methods will be analyzed in detail and spreadsheets will be developed to calculate complex modulus and phase angle of asphalt binder from the creep compliance obtained in the indentation tests.

Significant Results

The creep compliance of asphalt binders at intermediate temperature can be obtained from the proposed indentation tests after corrections for specimen size. The research team made significant advances in modeling the indentation test using finite elements. The research team plans to use the results from the simulations to estimate the correction factors for the size effects.

Significant Problems, Issues and Potential Impact on Progress

During this quarter, the research team had some difficulties implementing the FE model of the indentation test in load-control mode. The main problem is related to the convergence of the numerical solution. The research team will focus its efforts on solving the convergence problem of the load-control test. The progress of this work element is not expected to be significantly affected by this modeling problem.

Minor disagreements between the legal offices at the University of Minnesota and the University of Wisconsin–Madison did not allow the research team’s research partners at the University of

Minnesota to start their work on modifications of the Bending Beam Rheometer (BBR) to run indentation tests for characterization of fracture properties at low temperature.

Work Planned Next Quarter

Next quarter, the research team will focus its efforts on completing the testing included in the experimental plan and developing the correction factors for size effects based on the FE simulations in Abaqus. A complete analysis of the interconversion methods to be used to estimate the complex modulus and phase angle from the creep compliance of the indentation test will also be derived next quarter.

Research partners at the University of Minnesota will start their work on the characterization of the fracture properties of asphalt binders at low temperature by means of indentation tests.

Work Element E1c: Warm and Cold Mixes

Subtask E1c-1: Warm Mixes

Work Done This Quarter

Work this quarter focused on further evaluation of the asphalt lubricity test that was developed and begun in the previous quarter. Two binder types were tested with and without a warm mix additive. The testing covered two normal forces, four speeds and three temperatures. Based on the testing results the research team decided to conduct a comprehensive literature review to further assess the lubricity test. Further statistical analysis was conducted to evaluate the significance of binder viscosity, binder coefficient of friction, and mixture gradation on asphalt mixture workability, as measured by the Construction Force Index (CFI) and number of gyrations to 92% G_{mm} (N92).

Finally, a significant effort was put toward the Manitoba field project as mixes workability for the binder course was measured for the binder course Bituminous C (Bit C).

Significant Results

Asphalt Binder Workability (Lubricity Testing)

Evaluating the lubricating effect of warm mix asphalt (WMA) additives on asphalt binders using the coefficient of friction (μ) measurements obtained from the Asphalt Lubricity Test continued. Figure E1c-1.1 summarizes the lubricity testing results at a speed of 50 rpm and 20 N normal force. The results show that the additive effect was up to 10% for the two binders. However, the effect of the binder grade ranged between 20% and 25%. The coefficient of friction results were also compared to conventional viscosity testing results, as shown in figure E1c-1.2. The figure indicates that there is no direct relationship between the measured friction and the viscosity. Such results motivated the research team to conduct a more comprehensive literature review to provide greater understanding of the mechanics of lubricity testing.

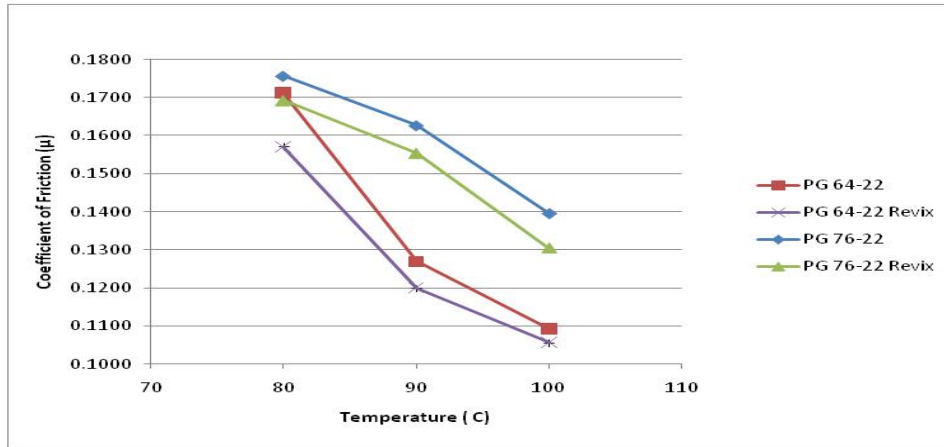


Figure E1c-1.1 Graph. Summary of lubricity test results.

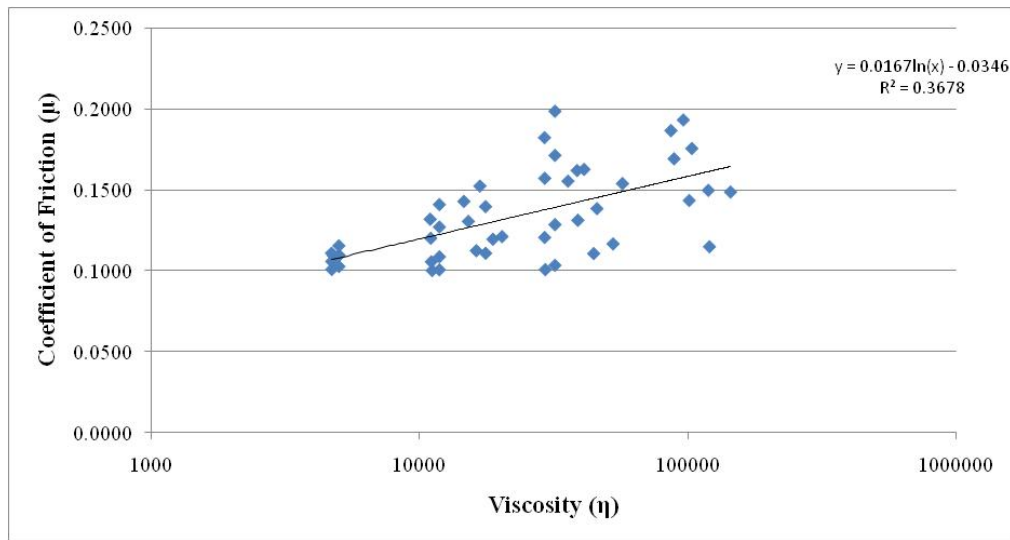


Figure E1c-1.2 Graph. Relationship between coefficient of friction and viscosity.

Based on the literature review, a conventional analysis of friction and wear for lubricant is usually done by plotting a Stribeck curve. In this curve the coefficient of friction is plotted against a Stribeck number in logarithmic scale. Stribeck number is calculated using the following equation:

$$\text{Stribeck number} = \log (R*\eta/P) \quad (\text{E1c-1.1})$$

where R is the speed, η is the viscosity, and P is the normal force.

Figure E1c-1.3(a) shows a schematic of the Stribeck curve for common lubricants. The curve defines three distinct lubrication categories—boundary lubrication, mixed lubrication and hydrodynamic lubrication—as shown in figures E1c-1.3(b), E1c-1.3(c) and E1c-1.3(d), respectively. The lubricity testing results at different speeds and normal forces, along with the viscosity measurements, were used to plot the Stribeck curve for the PG 64-22 with and without the warm mix additive Revix. Figure E1c-1.4 shows the Stribeck curve. The figure indicates that the testing conducted only covered one part of the curve (hydrodynamic range). To capture the rest of the curve, further testing is required at higher temperatures and a wider range of speeds and normal forces. The current heating system and Dynamic Shear Rheometer (DSR) machine used in this procedure has limited ranges of temperatures and normal forces. Thus, a new fixture is being developed to allow conducting the lubricity test on a different DSR which is capable of a wider range of temperature and normal force.

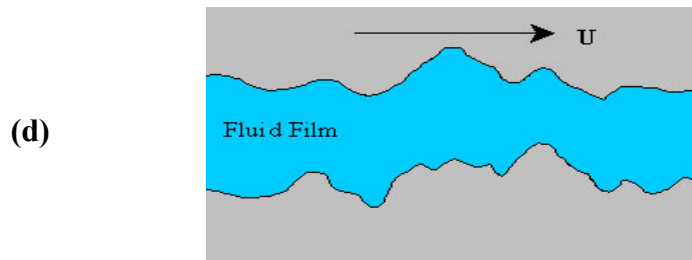
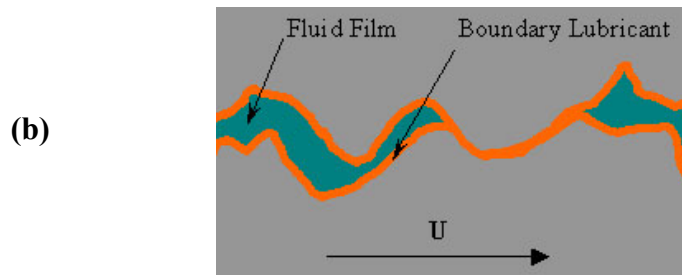
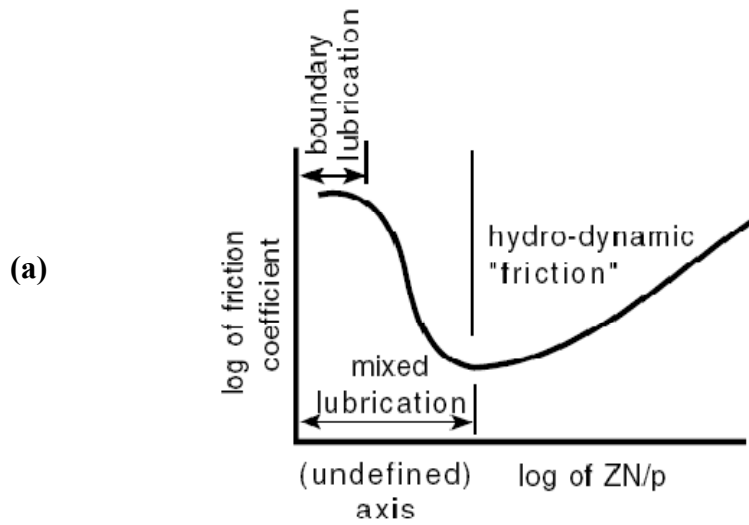


Figure E1c-1.3 Illustrations. Friction and wear analysis: (a) Stribeck curve; (b) boundary – asperities cause friction; (c) mixed (partial contact) – friction decrease as fluid pushes asperities apart; and (d) hydrodynamic (no contact) – friction increase due to viscous drag.

(Source: Modern Tribology Handbook, Bharat Bhushan, Editor, CRC Press, 2001.)

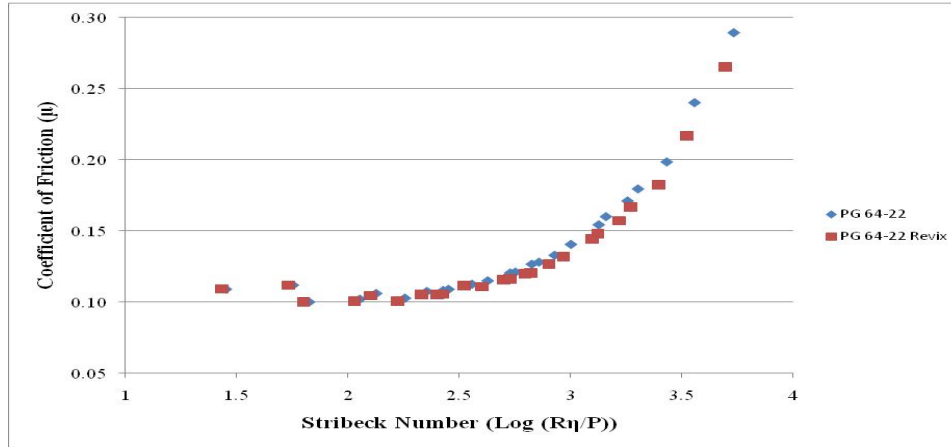


Figure E1c-1.4 Graph. Stribeck curve for PG 64-22 binder.

Asphalt Mixture Workability

Asphalt mixture workability indicators including the CFI and the number of gyrations to 92% G_{mm} (N92) were collected in the previous quarter. A statistical analysis was conducted to relate such measures to binder viscosity, binder coefficient of friction, and the mixture gradation. Mixture gradation was represented by fitting a Weibull distribution to the gradation curve. The Weibull distribution β coefficient is used as a correlation parameter. More details about the use of Weibull distribution to represent aggregate gradations can be found in the ARC Q3 2009 report for the VP2a work element.

Regression analysis of CFI and N92 are summarized in tables E1c-1.1 and E1c-1.2, respectively. Figures E1c-1.5 and E1c-1.6 show the predicted CFI versus measured CFI and predicted N92 versus measured N92, respectively. Based on the regression analysis results, the gradation β coefficient is the only significant parameter.

Table E1c-1.1 CFI regression analysis results.

Predictor	Coefficient	SE Coefficient	T	P
Constant	-450	335.1	-1.34	0.193
B	73.4	15.68	4.68	0.000
Coefficient of Friction	3321	3025	1.10	0.283
Viscosity	-0.0025	0.00502	-0.51	0.618

SE = standard error.

Table E1c-1.2 N92 regression analysis results.

Predictor	Coefficient	SE Coefficient	T	P
Constant	-59.6	25.41	-2.35	0.028
B	9.87	1.187	8.32	0.000
Coefficient of Friction	356	229	1.56	0.133
Viscosity	-0.0001	0.00038	-0.27	0.787

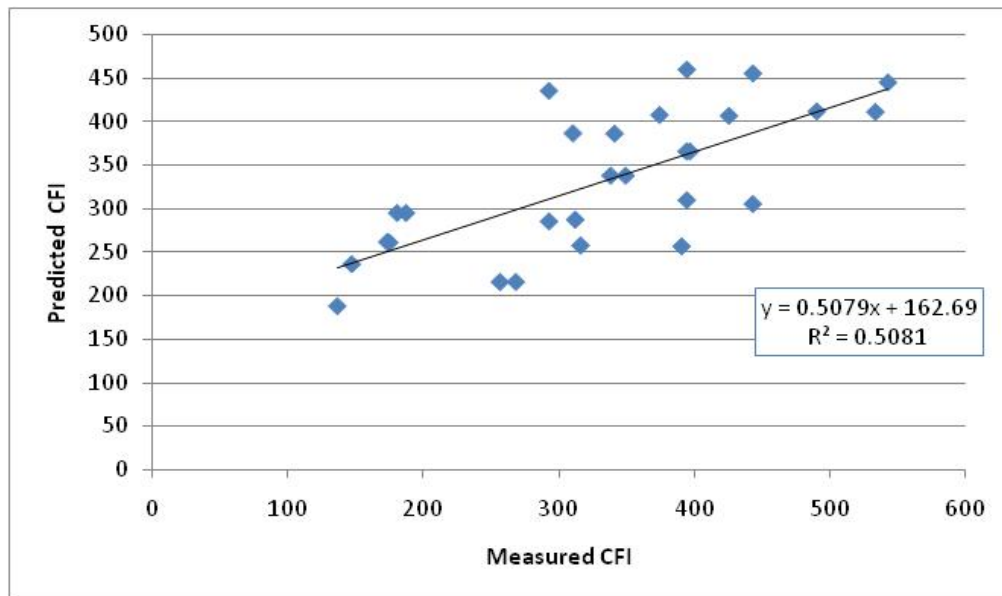


Figure E1c-1.5 Graph. Predicted CFI relationship to measured CFI.

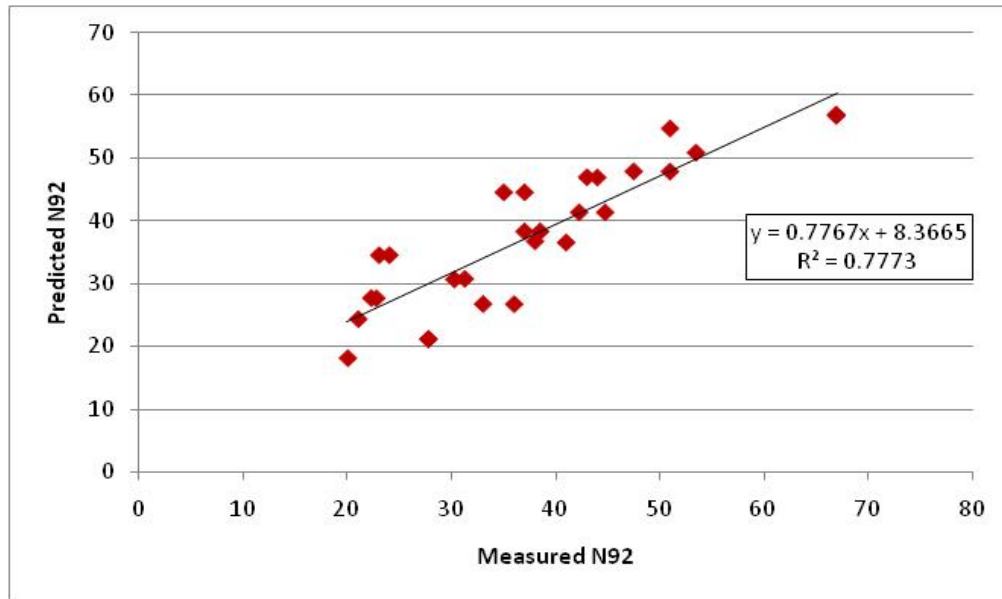


Figure E1c-1.6 Graph. Predicted N92 relationship to measured N92.

Manitoba (MIT) Field Project

The materials and mix design for the Bit C binder course was provided by MIT. HMA and WMA mixtures were evaluated in terms of aggregate coating and mixture workability to assist in providing recommendations related to appropriate mixing and compaction temperatures for the Bit C mix. A summary of the tests completed is provided in table E1c-1.3.

Table E1c-1.3. Summary of testing.

Additive	Mixing Temperature	Compaction Temperature	Mixture Workability		Aggregate Coating
			N92	CFI	
HMA	105	90	X	X	
	125	110	X	X	X
	150	135	X	X	
Advera (0.25% by wt of Mix)	105	90	X	X	
	125	110	X	X	X
	150	135	X	X	
Evotherm (0.5% by wt of binder)	105	90	X	X	
	125	110	X	X	X
	150	135	X	X	
Sasobit (1.5% by wt of binder)	105	90	X	X	
	125	110	X	X	X
	150	135	X	X	

Aggregate coating results are presented in figure E1c-1.7, with the error bars representing the pooled standard deviation of the measurements taken. Results presented in figure E1c-1.7 show values of aggregate coating ranging from 38% to 60% with the use of Evotherm and Sasobit resulting in an increase in aggregate coating of approximately 15% and 22%, respectively. Statistical analysis was conducted using Tukey’s comparison of the means at a confidence level of 95% to determine if these differences in performance were statistically different. Results of this analysis showed no effect of the WMA additives on aggregate coating. It should be noted that this could be attributed to the lack of sensitivity of the test procedure, which considers only particles 100% coated and does not allow for differentiation between particles that are almost completely coated and those with considerably more aggregate surface uncoated. Results in figure E1c-1.7 indicate that the Bit C mix prepared for this project should have a production temperature of at least 125 °C to ensure proper coating of the aggregates.

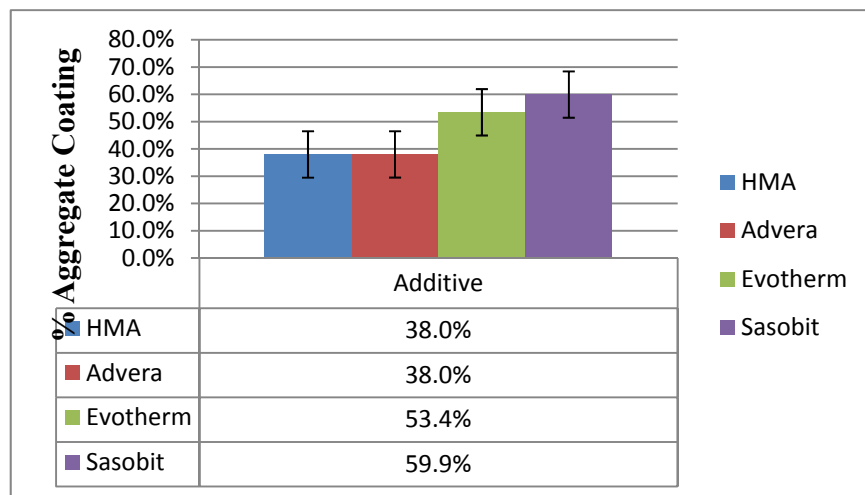


Figure E1c-1.7 Graph. Predicted summary of aggregate coating results conducted at 125 °C.

Evaluation of mixture workability was conducted on samples compacted to 160 gyrations in the Superpave gyratory compactor (SGC). All compactations were conducted at a pressure of 600 kPa. The number of gyrations was selected based on the design traffic for the project—6,600,000 equivalent single-axle loads (ESALs). This relates to a Wisconsin DOT E-10 mix. The gyration levels for this mix are provided below:

- $N_{ini} = 8$ gyrations.
- $N_{des} = 100$ gyrations.
- $N_{max} = 160$ gyrations.

Mixture workability was assessed using N9 and CFI. In addition, a sample at each compaction temperature was compacted to 495 gyrations for evaluation of mixture stability using the Traffic Force Index (TFI). This index is measured by the pressure distribution analyzer (PDA) plate and is characterized as the area under the resistive effort of the mix from 92% G_{mm} to 98% G_{mm} . These density thresholds were selected to represent the density of the mix from opening of traffic

to its terminal service life. The plots of air voids as a function of temperature are provided in figures E1c-1.8(a) and E1c-1.8(b) for N_{ini} and N_{des} , respectively.

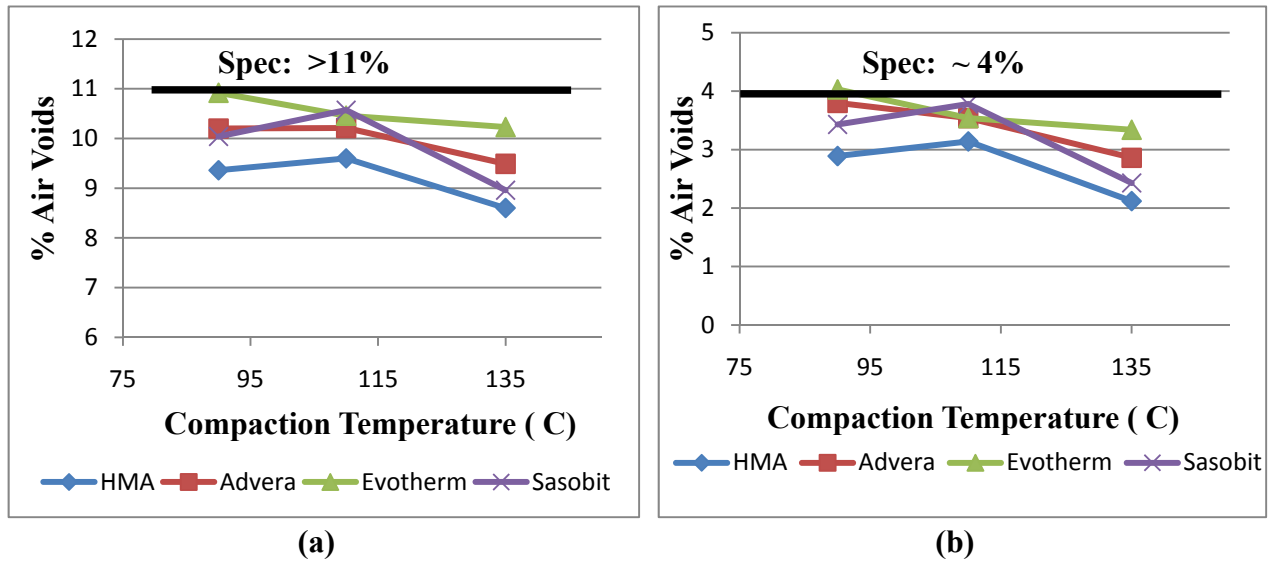


Figure E1c-1.8 Graphs. Summary of air void versus compaction temperature: (a) N_{ini} ; (b) N_{des} .

Results presented in figures E1c-1.8(a) and E1c-1.8(b) indicate that virtually all mixes compacted over the range of temperatures at both levels of gyrations exhibit air void levels below the limits set by the specification, indicating the mix is densifying more rapidly than standards allow. In both cases the mixes showed little sensitivity to temperature or to warm mix additives. These trends will be further evaluated using the aforementioned workability parameters.

Figure E1c-1.9 shows a plot of N_{92} versus compaction temperature, which indicates that there is marginal effect of temperature and WMA additives on mixture workability. In terms of temperature sensitivity, the average change in N_{92} from compaction temperatures of 135 °C to 90 °C was four gyrations—a tight range that does not allow determination of whether the change in behavior is due to material behavior or the variability related to measuring the volumetrics of the mix. Similar ranges in performance were observed when evaluating the effect of WMA additives on mixture workability. Furthermore, the HMA demonstrates more workability relative to the WMA mixes. It is hypothesized that the workability is so high due to the fine gradation and rounded gravel aggregates used that it dampens the effects of WMA additives on mixture workability.

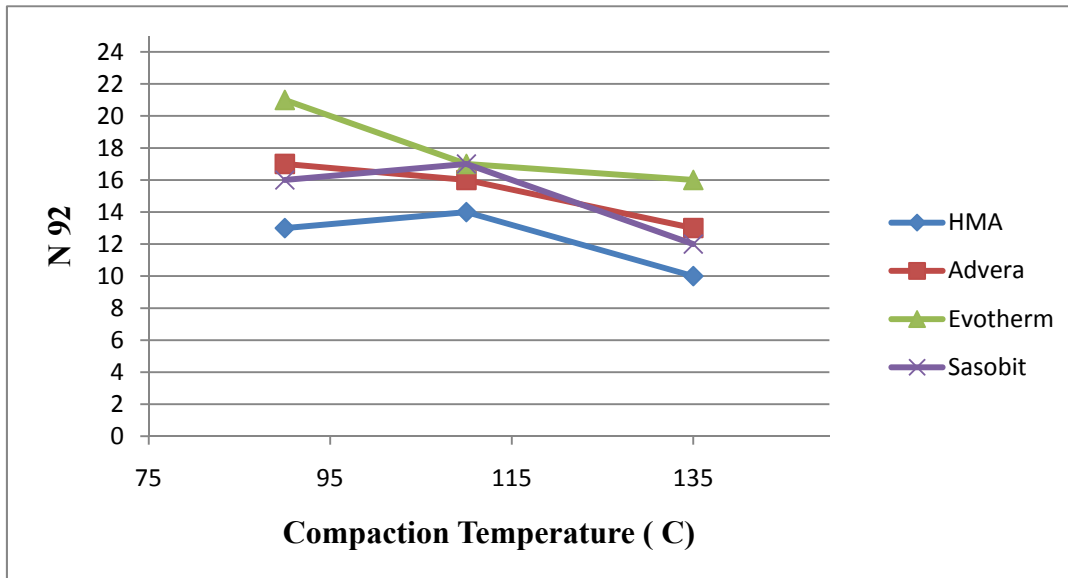


Figure E1c-1.9 Graph. Compaction temperature for Bit C HMA and WMA.

Significant Problems, Issues and Potential Impact on Progress

None.

Work Planned Next Quarter

Work next quarter will focus on the following tasks:

- *Lubricity testing.* A new experiment will be conducted to finalize the newly developed procedure. Wider ranges of temperatures, speeds and normal forces will be used on the same two binders (PG 64-22 and styrene-butadiene-styrene (SBS)-modified PG 76-22) that were used in this quarter.
- *Manitoba field project:*
 - Binder testing. This testing will include all binder testing, with viscosity and lubricity testing taking priority.
 - Mixture testing. This testing will include evaluation of mixture workability of Bituminous B (Bit B). A report will be submitted to Manitoba before construction of each lift.

Subtask E1c-2: Improvement of Emulsions' Characterization and Mixture Design for Cold Bitumen Applications

Work Done This Quarter

Research efforts this quarter continued to focus on emulsion construction properties. Binder bond strength, aggregate retention and binder viscosity characteristics were investigated using the Bitumen Bond Strength (BBS) test, strain sweep test and rotational viscometer (RV), respectively. With the latest testing results, initial performance limits may be proposed for the BBS test based on correlations to the sweep test. Correlations between viscosities measured with the RV and Saybolt-Furol viscosity are also investigated. Important findings are presented in the Significant Results section.

Significant effort was invested in refining current testing procedures for the BBS test. At a recent advisory group meeting, a draft American Association of State Highway and Transportation Officials (AASHTO) standard entitled "Determining Asphalt Binder Bond Strength by Means of the Bitumen Bond Strength (BBS) Test" was submitted for review to the FHWA's Emulsion Task Force in an effort to formalize experimental procedures and protocols. The procedure has been expanded to include both emulsified binders and hot binders and shows promise at being accepted as a standard. Revisions will continue next quarter in an effort to finalize the standard. The BBS procedure and results will be presented at the TRB 2010 Annual Meeting in a poster session.

Other efforts focused on investigating the efficacy of existing performance tests for surface seal techniques, namely the standard chip seal procedure defined by the American Society for Testing and Materials (ASTM 2008). Combinations of aggregate chips and emulsions were tested to investigate aggregate retention over time. Some samples were also subjected to the ASTM E965 test method entitled "Standard Test Method for Measuring Pavement Macrotexture Depth Using a Volumetric Technique" (ASTM 2006). Results suggest that this method, which is typically used to measure pavement macrotexture, is inadequate for characterizing chip embedment in standard sweep test samples. A literature review confirmed that construction methods rely on the concept of average least dimension (ALD) in determining application rates, a concept in need of revision. Other methods of characterizing aggregate orientation and chip embedment, including the Aggregate Imaging System (AIMS) and laser profilometer, will be investigated in Year 4 in order to improve upon the concept of ALD.

Binder viscosity was investigated using a Brookfield RV to evaluate the construction properties related to sprayability and drain-out. Current practice relies on measurement of Saybolt-Furol viscosity, a laborious measurement that has a questionable relationship to the temperatures and shear rates experienced by emulsions in the field. A procedure was developed to use the RV to investigate sprayability at high shear rates and drain-out at low shear rates. Temperatures ranging from 50 °C to 80 °C, representing typical field applications, were selected to test several binders at a range of shear rates. Preliminary results suggest that shear rate and temperature both affect a binder's rotational viscosity. Further testing concluded that the thixotropy exhibited by emulsions during initial RV testing appears to be nonrecoverable, thus the initial shearing of the material results in permanent changes to the emulsion's microstructure.

In planning to investigate energy consumption and emissions at HMA production facilities, the research team decided that such an investigation is better suited for the E1c-1 subtask. While emulsions and cold mix asphalt (CMA) must also be characterized in terms of energy consumption and emissions, at this point the effort is secondary to the evaluation of emulsion construction and performance properties and to CMA investigations with regard to subtask E1c-2.

Coordination continues with several groups. The ARC Emulsion Advisory Group meeting held in September 2009 was followed up with a face-to-face meeting in December 2009 with the Emulsion Task Force. Monthly conference calls continue with the University of Stellenbosch, South Africa, to coordinate interlab BBS testing. Relations with the American Institute of Chemical Engineers' (AIChE) Institute for Sustainability (IfS) remain strong despite limited contact over the past quarter. Other coordination efforts include regular calls with the systems automation and instrumentation company leading the effort to monitor production facility energy consumption and emissions.

Significant Results

Bitumen Bond Strength Test

Testing focused on characterizing binder adhesive properties on a variety of substrates at several curing intervals. Experimental factors for BBS testing conducted at the University of Wisconsin–Madison are shown in table E1c-2.1. BBS testing was also conducted at the University of Stellenbosch with the experimental factors shown in table E1c-2.2. Due to significant differences in sample preparation, curing conditions and emulsion types, a comparative analysis between both labs is premature. Such a comparison will be conducted in the next quarter.

Table E1c-2.1. Experimental factors for UW-Madison BBS testing.

Variable	Levels
Emulsion Type	CRS-2
	CRS-2P
Substrate Type	Dolomite
	Glass
	Granite
	Limestone
Curing Temperature (°C)	35
	45
Curing Time (hours)	2
	6
	24
	48 (selected trials only)

Table E1c-2.2. Experimental factors for University of Stellenbosch BBS testing.

Variable	Levels
Emulsion Type	CRS-65
	CRS-65 + 3% latex
	SS-66
Substrate Type	Granite
	Tillite
Curing Temperature (°C)	25
Curing Time (hours)	2
	6
	24

Comparing testing results between labs is in progress, with initial data indicating some significant differences as evident in figure E1c-2.1. Samples cured at 25 °C at the University of Stellenbosch demonstrate significantly less adhesive strength than samples cured at 35 °C and 45 °C at UW-Madison. Because the effect of testing temperature is confounded with the lab, all subsequent testing will be conducted at a standard temperature of 35 °C at both labs moving forward. The effect of increasing the curing temperature from 35 °C to 45 °C does not appear to be significant at each curing interval. Results shown in figure E1c-2.1 represent the average response for all substrate and emulsion combinations.

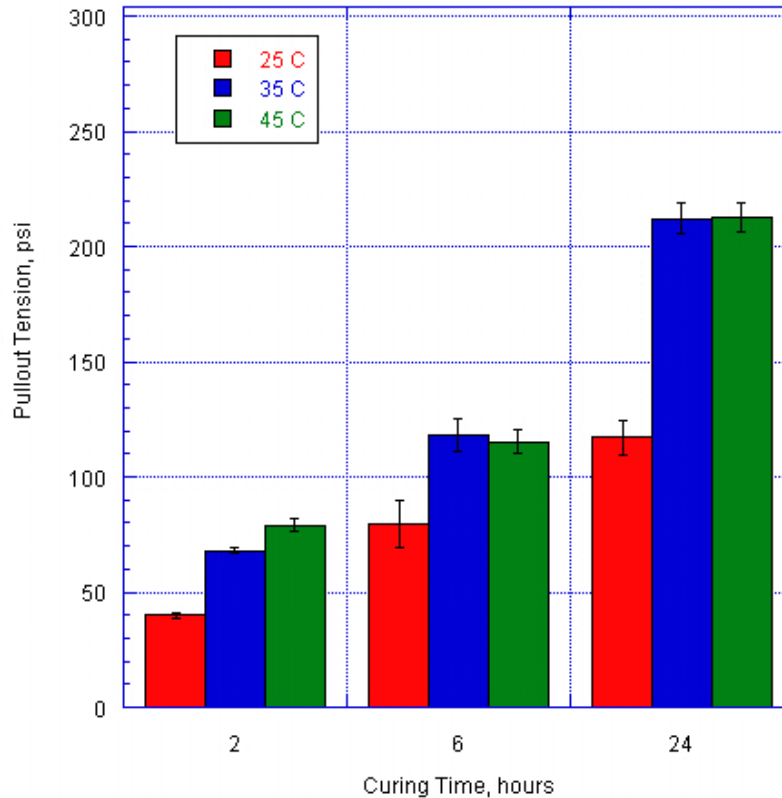


Figure E1c-2.1. Chart. Effect of curing temperature on adhesive strength.

The adhesive strength of binders can be evaluated over time in order to establish potential test specification limits. Figure E1c-2.2 displays bond strength gains over time for 16 combinations of curing temperatures, substrates and emulsions. Effect of curing time is clearly detected as the most significant factor in an analysis of variance (ANOVA). Other significant main effects at a confidence level of 95% include emulsion type and interaction of the substrate with curing temperature. At a confidence level of 90%, the interactive effect of emulsion curing time also becomes significant. Because the substrate type was not identified as a significant factor, future research will investigate possibilities for standardizing a substrate type and preparation method. Substrate options currently under consideration include portland cement concrete cylinders or gyratory-compacted HMA samples. Standardizing substrate type and preparation method may also diminish errors inherent between labs.

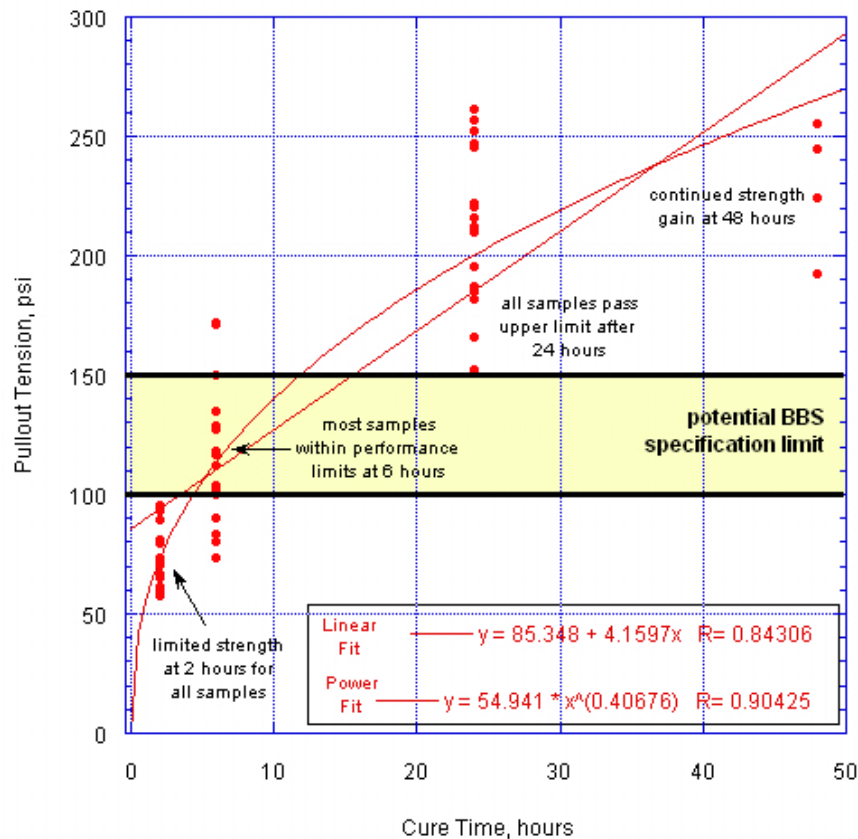


Figure E1c-2.2. Graph. Bond strength gain over time to determine specification limits.

At 2 hours curing time, all samples fail to meet the minimum proposed specification limit of 100 psi. At 6 hours curing time, 75% of samples fall within the proposed limit. All samples exceed the maximum proposed specification limit of 150 psi at 24 hours curing time. Strength gain continues at 48 hours. Both linear and power fits suggest high correlation coefficients, with $R > 0.84$ for a linear fit and $R > 0.90$ for a power fit.

Sweep Test

Sweep testing was conducted on samples collected from a local supplier and samples collected from the field projects outlined in table E1c-2.1 of the ARC July–September 2009 report. Table E1c-2.3 summarizes the experimental conditions used for preparing the sweep test samples. As with the BBS testing, independent samples are subjected to different curing times to determine aggregate retention via percent aggregate loss. Granite and limestone aggregates are combined with CRS-2 and CRS-2P emulsion for comparison to BBS test results. Field project samples are prepared according to the combinations used in the field. Sweep testing results are shown in figure E1c.2-3.

Table E1c-2.3. Experimental factors for sweep testing.

Variable	Levels
Emulsion Type	varies
Aggregate Type	varies
Aggregate Application Rate	varies (depends on aggregate specific gravity)
Emulsion Application Rate (g)	133
Curing Time (hours)	2
	6
	24
Curing Temperature (°C)	35

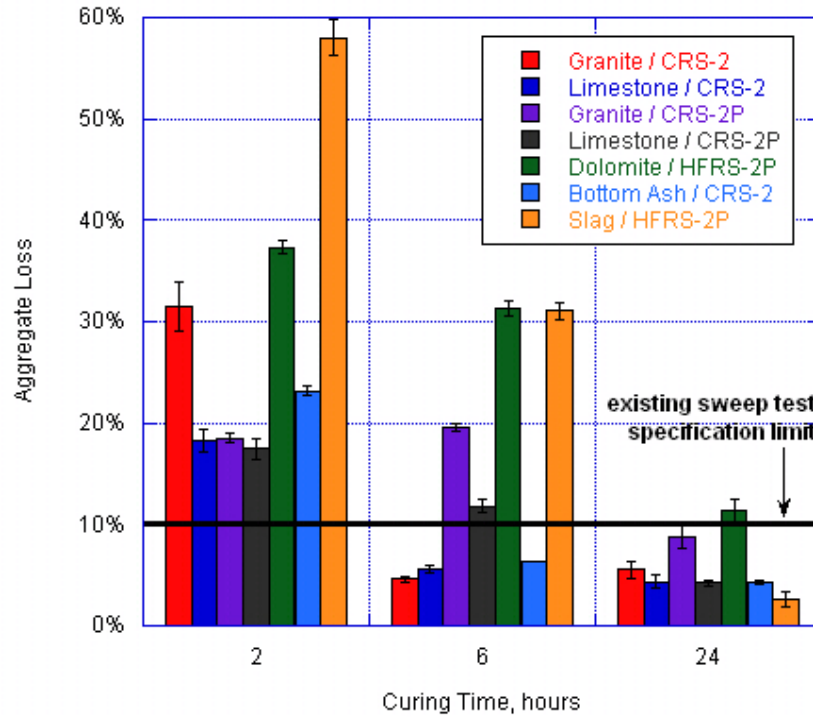


Figure E1c-2.3. Chart. Aggregate retention is investigated over time with the sweep test.

At 2 hours of curing, all sweep test samples exceed the 10% aggregate loss specification limit. Highest aggregate retention is seen for combinations of CRS-2 and CRS-2P emulsions with limestone aggregates and CRS-2P emulsion with granite aggregates at 2 hours curing. At 6 hours curing, only CRS-2 emulsion samples meet the existing performance specification, while polymer-modified samples of CRS-2 and HFRS-2 fail to meet the performance specification. With the exception of the dolomite/HFRS-2P combination, all samples meet the performance specification limit at 24 hours curing time.

For selected sweep test samples, a sand-patch procedure was developed based on the standard outlined in ASTM E965. Conditions for conducting the sand-patch procedure are given in table E1c-2.4, with experimental results shown in figure E1c-2.4.

Table E1c-2.4. Experimental factors for sand-patch testing.

Variable	Levels
Emulsion Type	CRS-2
Aggregate Type	Granite
Aggregate Application Rate (g)	450
Emulsion Application Rate (g)	133
	176
Sand Application Rate (g)	4.3
	20
Curing Time (hours)	24
Curing Temperature (°C)	35
Replicates	2

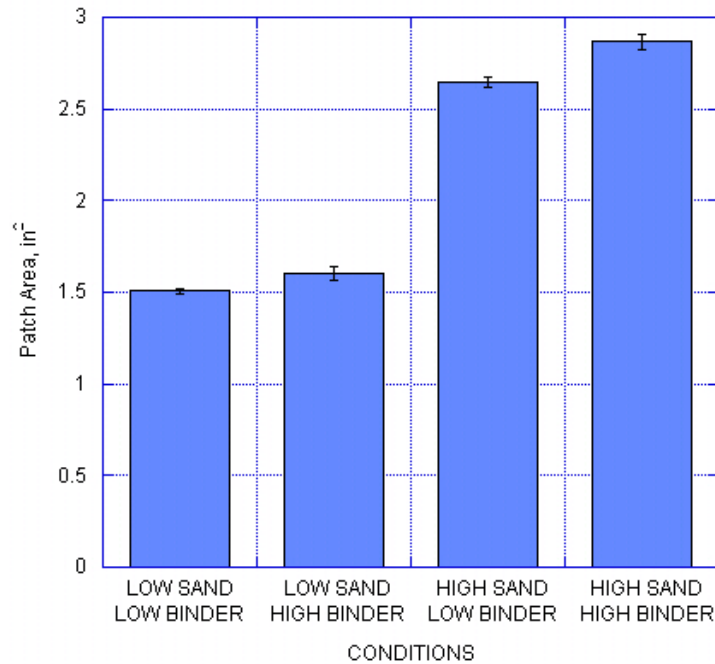


Figure E1c-2.4. Chart. Experimental results for sand-patch testing.

Results of the sand-patch test indicate that at low sand application rates, the binder application rate does not influence the size of the patch area. A significant difference in sand-patch area is seen when the sand application rate is increased. Results of this preliminary test suggest that the sand-patch procedure may not be the most appropriate for characterizing chip seal macrotexture and aggregate orientation in chip seals. Alternative methods may be considered for investigating aggregate orientation within the chip seal and overall seal macrotexture. While the concept of ALD is employed in the existing ASTM D7000 standard, the concept is in need of revision if aggregate orientation and chip embedment are to be accurately characterized. The AIMS and

laser profilometer will be investigated to assess the applicability of these systems to chip seals so that the concept of ALD may be improved.

Correlations Between the BBS Test and the Sweep Test

Results from BBS testing may be correlated to sweep test results to evaluate potential specification limits and the influence of curing time on behavior. Establishing a correlation between BBS test results and sweep test results, as shown in figure E1c-2.5, entails correlating the pullout tensile strength obtained using the BBS test to aggregate loss measured using the sweep test at identical curing and sample conditions. The correlation involves all samples cured at 35 °C. The correlation does not differentiate between emulsion types and aggregate types, as the goal in setting the specification limit is for applicability to all emulsion and aggregate types.

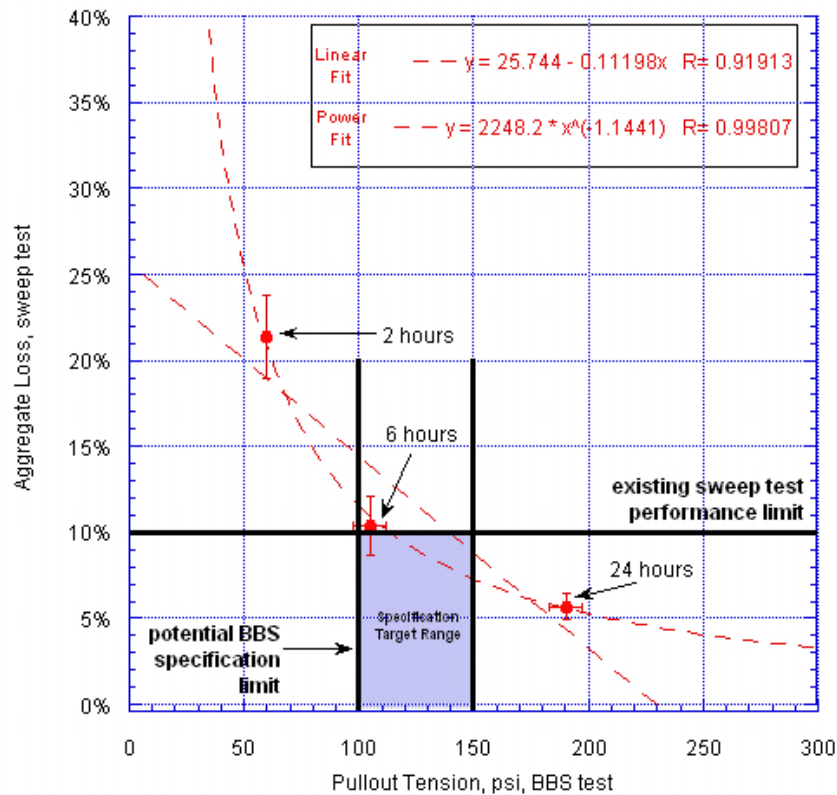


Figure E1c-2.5. Graph. Correlations between sweep test results and BBS test results are strong for linear curve fits ($R > 0.91$) and power curve fits ($R > 0.99$).

Given the existing sweep test performance limit of 10% and the proposed BBS limit of 100 to 150 psi, a specification target range may be developed for the correlation between tests. At 2 hours curing, neither the sweep test samples nor the BBS test samples fall within the specification limits. At 6 hours curing, the bond strength of binders, as measured by the BBS, falls within the potential BBS specification limit, while sweep test samples remain just beyond the existing performance limit. All samples meet the specification limits at 24 hours curing.

RV Testing

Viscosity testing using a Brookfield RV was conducted to correlate Saybolt-Furol viscosity values obtained from a local supplier to RV viscosity values, and to examine the influence of temperature and shear rate on viscosity. Testing was expanded from the initial 50-50-21 procedure outlined in the ARC July–September 2009 report to include more shear rates and higher temperatures as recommended by the Emulsion Advisory Group. Table E1c-2.5 displays the experimental factors designed for viscosity testing.

Table E1c-2.5. Experimental factors for viscosity testing.

Variable	Levels
Emulsion Type	CRS-2
	EM-8
	HFRS-2
Temperature (°C)	50
	65
	80
Shear Rate (RPM)	5
	50
	100
	150

Viscosity testing results for isothermal conditions are shown in figure E1c-2.6, with Saybolt-Furol viscosity plotted against RV viscosity. Existing specification limits are superimposed over the correlation plot (AASHTO 2001). Most samples fall within the limits for Saybolt-Furol viscosity, with only a few samples not meeting minimum viscosity requirements. Perhaps more significant is the observation that as temperature is increased from 50 °C to 65 °C to 80 °C, the slope of the regression line tends to rotate, albeit slightly, about the origin in a counterclockwise fashion. At higher temperatures, RV viscosity tends toward the Saybolt-Furol viscosity. At lower temperatures, RV viscosity values are about 50% of Saybolt-Furol viscosity.

Similar observations can be made with respect to constant shear conditions, as seen in figure E1c-2.7. Samples are tested at a variety of shear rates and correlated to Saybolt-Furol viscosity. At low shear rates of 5 rpm, the RV viscosity is approximately equal to Saybolt-Furol viscosity. As the shear rate increases to 50 rpm, the correlation line rotates about the origin in a clockwise fashion such that RV viscosity values are approximately 50% of Saybolt-Furol values. As the shear rate is increased to 100 rpm and 150 rpm, the correlation line continues to rotate clockwise about the origin. Thus, it appears that shearing rate has a more significant effect on the correlation between RV viscosity and Saybolt-Furol viscosity than temperature.

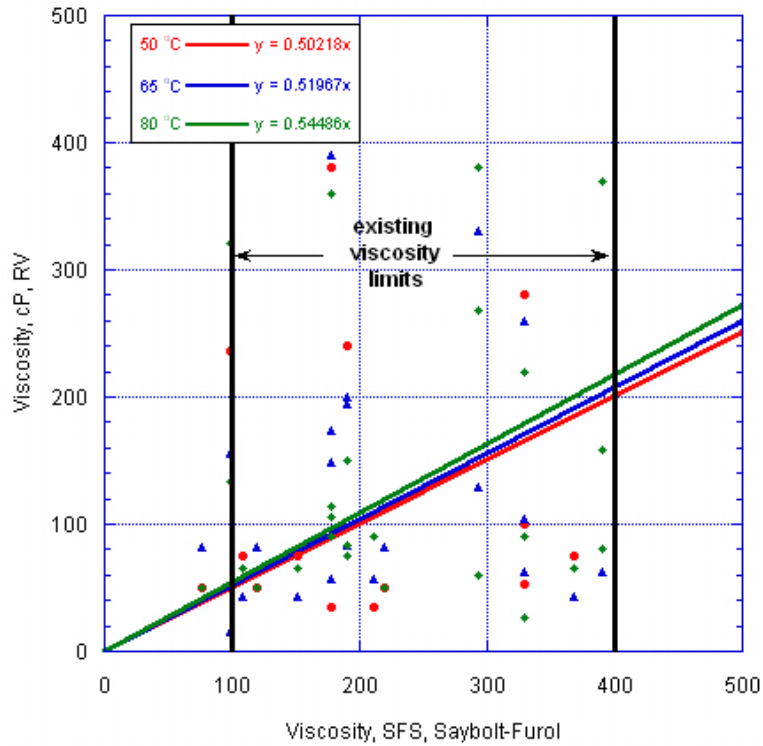


Figure E1c-2.6. Graph. Viscosity testing under isothermal conditions. (SFS = Saybolt-Furol seconds.)

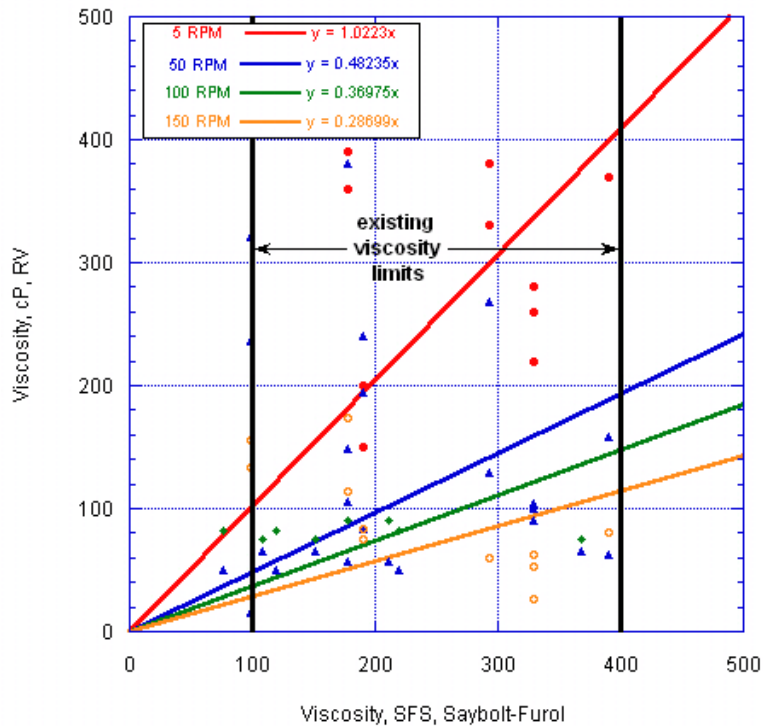


Figure E1c-2.7. Graph. Viscosity under constant shear conditions.

The effect of rest periods on viscosity is also examined. In practice, emulsion samples are likely to stagnate in various storage vessels for short or long periods of time, depending on production conditions. Pumping subjects emulsion samples to different shear histories. Preliminary data demonstrating the effect of rest periods on viscosity is shown in figure E1c-2.8 for an EM-8-type emulsion tested at 50 °C and 150 rpm. In the figure, viscosity is seen to drop rapidly during the first test interval. Following a 10-minute rest period, viscosity is seen to diminish further, though not as quickly. The viscosity appears to stabilize at an equilibrium value prior to the 100-minute rest period, after which viscosity instability becomes apparent at later shearing stages. Following the 250-minute and 500-minute rest periods, the sample seems to have completed the breaking process, resulting in permanent damage to the emulsion's microstructure.

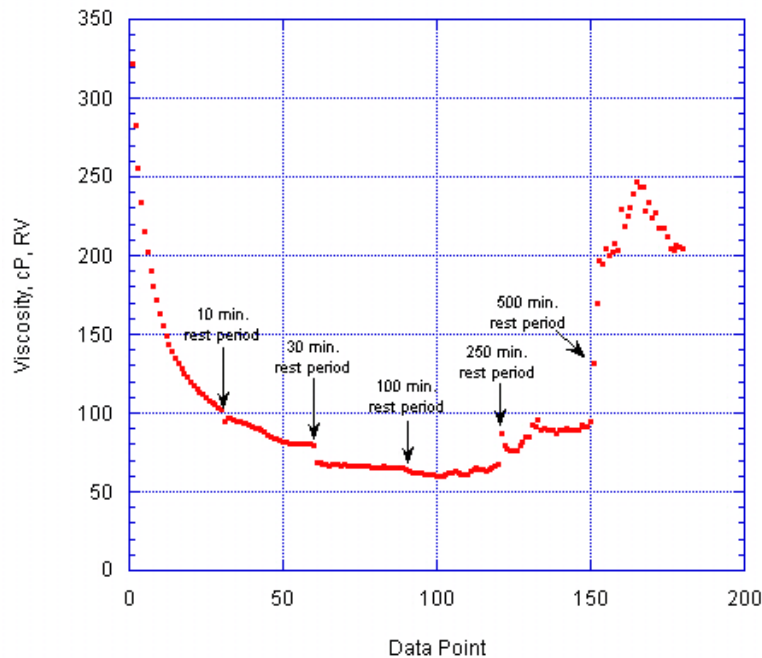


Figure E1c-2.8. Graph. The effect of rest periods on viscosity is shown for an EM-8-type emulsion tested at 50 °C and 150 rpm.

A similar investigation for examining the influence of shear rate on equilibrium viscosity is shown in figure E1c-2.9. At low shear rates like 5 rpm, the sample fails to reach an equilibrium viscosity after 30 minutes of testing. Following a 10-minute rest period, the sample is subjected to 50 rpm shearing, which further diminishes the viscosity. The sample appears to reach an equilibrium viscosity at 150 rpm after nearly 3 hours of testing. After a final 10-minute rest period, a low shear rate of 5 rpm causes the equilibrium viscosity to increase slightly to a stable value. Further testing is needed to compare different emulsion types and shear histories before drawing definitive conclusions.

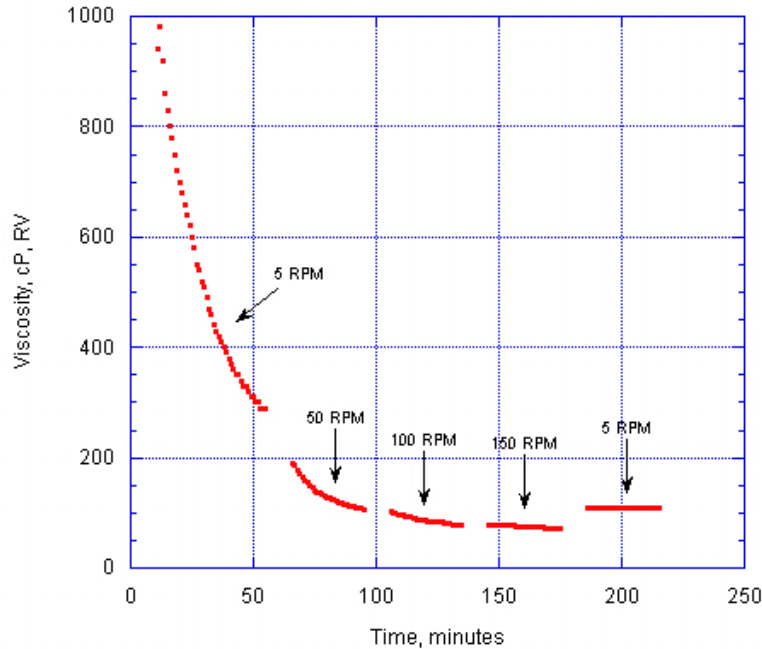


Figure E1c-2.9. Graph. The effect of different shear rates on viscosity is shown for an EM-8-type emulsion tested at 50 °C and various shear rates.

Significant Problems, Issues and Potential Impact on Progress

No significant problems were encountered in the last quarter.

Work Planned Next Quarter

Work next quarter will focus on the following tasks:

- *Emulsion construction properties.* The research team will continue to analyze emulsion construction properties using the BBS test, sweep test and Brookfield RV. BBS testing will focus on standardizing a substrate preparation procedure in order to validate interlab testing. Sweep testing will focus on developing a procedure using advanced optical instruments to characterize the effect of binder and aggregate application rates on aggregate orientation and chip embedment. RV testing will involve a further study on shear rate and temperature dependence. Storage stability procedures will be reviewed to initiate preliminary testing.
- *Emulsion residue properties.* Experimental plans and testing protocols for the evaluation of emulsion residues will be developed. Recovered residues may be tested at high surface temperatures using the Multiple Stress Creep and Recovery (MSCR) procedure to evaluate nonrecoverable creep compliance and stress sensitivity and examine resistance to bleeding. Resistance to early and late raveling may be evaluated with recovered and aged residues using Dynamic Shear Rheometer (DSR) strain sweep procedures to investigate reductions in the complex shear modulus G^* . Pressure aging vessel (PAV)-

aged residues may be tested using DSR frequency sweep procedures to evaluate resistance to fatigue cracking. Thermal cracking resistance of PAV-aged residues may be analyzed using DSR frequency sweep procedures to estimate low-temperature Bending Beam Rheometer (BBR) properties. Recovered residues may also be analyzed using MSCR and elastic recovery methods to identify the effects of polymer modification.

- *Cold mix asphalt.* A mix design method will be developed for dense CMA mixtures. The mix design method will be consistent with the Superpave volumetric mix design method for HMA. The Superpave gyratory compactor will be modified as necessary to be applicable for the design of CMA mixtures. The developed mix design method will take into consideration the unique features of CMA mixtures in terms of workability, short- and long-term stability, and long-term performance.
- *ARC Project Advisory Group and Emulsion Task Force activities.* The research team will continue to hold advisory group meetings and support Emulsion Task Force activities.

Cited References

AASHTO, 2001, AASHTO M208 Standard Specification for Cationic Emulsified Asphalt, American Association of State Highway and Transportation Officials. Washington, DC.

ASTM, 2008, ASTM D7000-08 Standard test method for sweep test of bituminous emulsion surface treatment samples, American Society of Testing and Materials. West Conshohocken, PA.

ASTM, 2006, ASTM E965-06 Standard test method for measuring pavement macrotexture depth using a volumetric technique, American Society of Testing and Materials. West Conshohocken, PA.

CATEGORY E2: DESIGN GUIDANCE

Work element E2a: Comparison of Modification Techniques (UWM)

Work Done This Quarter

During this quarter the research team continued testing the binders included in the material library developed for this study. This library includes 17 materials from six sources, five base binder grades and 12 modified binder grades. The material's testing follows the approved testing matrix. Tests performed to date are Dynamic Shear Rheometer (DSR)-run rheological measurements according to AASHTO TP5, Multiple Stress Creep and Recovery (MSCR) tests according to ASTM D7405-08a, and storage stability tests according to ASTM D7173-05. The collected binders are also subjected to laboratory aging techniques such as rolling thin film oven (RTFO) (AASHTO T240) and pressure aging vessel (PAV) (AASHTO R28).

Significant Results

Table E2a.1 shows the continuous grade for the binders included in the material library.

Table E2a.1. Continuous grade for material library binders.

Material #	Base	Modifier	Class of Modifier	Expected Grade	Continuous Grade
1	A0	None	None	PG 64	65.1
2	A1	Functionalized PE	Plastomer: Nonreactive	PG 70	71.1
3	A2	Functionalized PE	Plastomer: Nonreactive	PG 76	77.4
4	A3	SBS with cross-linking	Elastomer: Reactive	PG 70	70.8
5	A4	SBS with cross-linking	Elastomer: Reactive	PG 76	77.2
6	B0	None	None	PG 58	58.5
7	B1	Terpolymer	Elastomer: Reactive	PG 64	65.2
8	B2	Terpolymer	Elastomer: Reactive	PG 70	71.9
9	C0	None	None	PG 58	60.0
10	C1	PPA	Chemical: Reactive	PG 64	64.7
11	C2	PPA+SBS+cross-linking	Elastomer: Reactive	PG 70	72.9
12	D0	None	None	PG 58	61.2
13	D1	Functionalized PE+ SBS	Hybrid: Reactive	PG 64	65.8
14	D2	Functionalized PE+ SBS	Hybrid: Reactive	PG 70	72.1
15	E0	None	None	PG 64	66.2
16	E1	SBS with cross-linking	Elastomer: Reactive	PG 70	72.4
17	E2	SBS with cross-linking	Elastomer: Reactive	PG 76	76.1

PE = polyethylene. SBS = styrene-butadiene-styrene. PPA = polyphosphoric acid.

MSCR test results are shown in figure E2a.1. From these summary results, very different responses can be clearly observed for the binders tested based on composition, type and level of modification, and base binder. This type of information enables the research team to better understand how different modification techniques influence the behavior of asphalt binders, and how different modifiers improve different properties from the large spectrum of asphalt binder requirements.

The MSCR test results offer a very good indication of a material's resistance to rutting, as well as good insight into the elastic properties of the binders tested. This type of information, coupled with information collected from fatigue-type tests and direct elastic recovery measurements, will enable the research team to understand the connection, if any, between elasticity and fatigue life of binders.

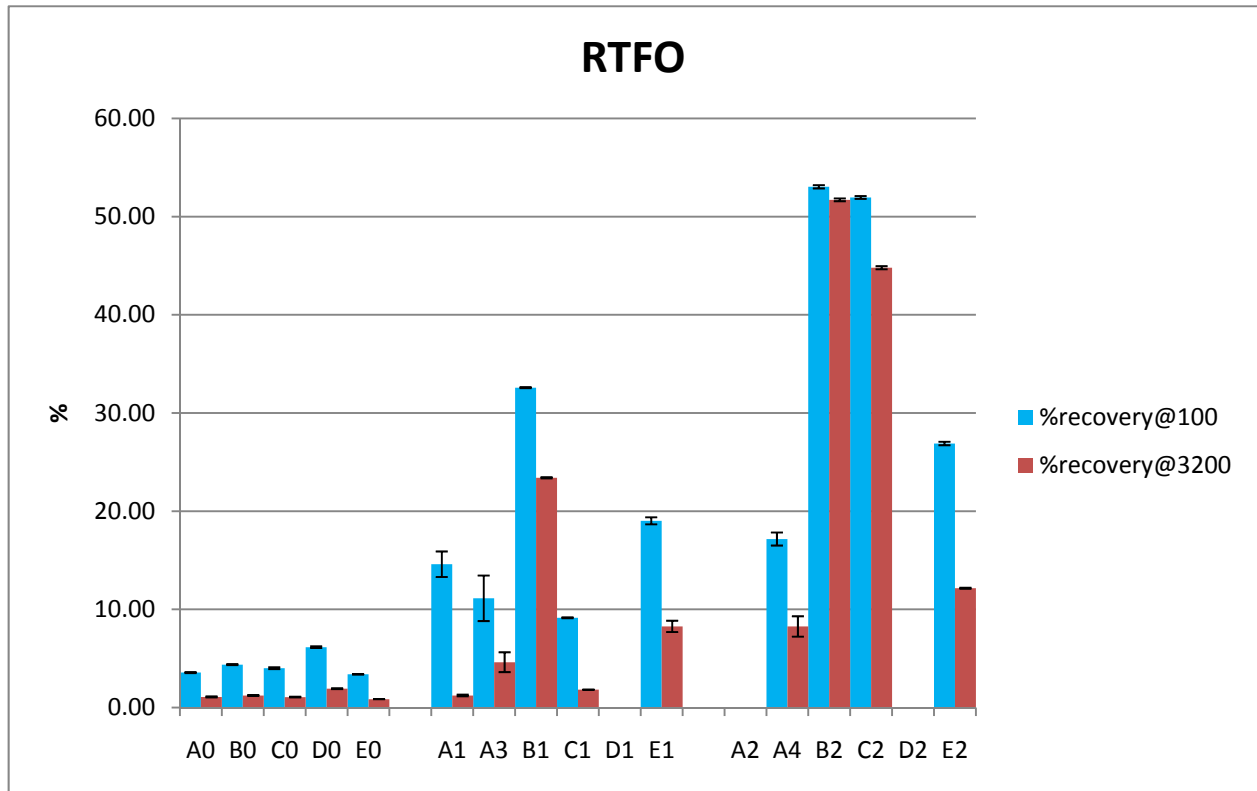


Figure E2a.1. Graph. Typical percent recovery from the MSCR test collected at the high binder grade temperature.

Significant Problems, Issues and Potential Impact on Progress

None.

Work Planned Next Quarter

Next quarter, the research team will continue aging and testing binders included in the materials database.

Work element E2b: Design System for HMA Containing a High Percentage of RAP Materials (UNR)

Work Done This Quarter

This work element is a joint project between University of Nevada, Reno and University of Wisconsin–Madison. Under subtask E2b-1.a, the impact of the current extraction techniques (i.e. ignition, centrifuge, and reflux) on the properties of the extracted RAP aggregates experiment was completed. A paper presenting the impact of the findings of this subtask on voids in mineral

aggregates (VMA) of HMA mixes containing RAP has been accepted for publication in the Journal of the Transportation Research Board.

Under subtask E2b-1.b, the testing and analysis procedure for determining the intermediate- and high-temperature properties of binders in recycled asphalt pavement (RAP) using the Dynamic Shear Rheometer (DSR) was finalized and testing has started at typical intermediate- and high-temperature levels. The analysis spreadsheet for estimating binder properties from mortar testing was modified to include low-, intermediate- and high-temperature analyses in a single workbook in order to present a complete RAP analysis on one sheet. The analysis workbook provides RAP binder true grading estimates in addition to estimated RAP binder parameters (stiffness, dynamic modulus, etc.). This sheet can be used either as a blending chart for RAP binder and fresh binder, or as a tool to estimate the allowable percentage of RAP in a mix to target a specific PG grade.

Under subtask E2b-5, a new comparative pavement performance site was constructed in Manitoba, Canada. The project is on provincial highway 8 between Gimli and Hnaua. The total project length is about 28 km (17 miles), with the ARC comparative pavement site accounting for 14 km (8.7 miles) of the project. The existing pavement is being recycled using a ratio of 50% RAP and 50% new material in the two bottom 50 mm lifts. The ARC sections were constructed over the 50% RAP material, using two 50 mm lifts with conventional hot-mix, 15% RAP, and 50% RAP, with no grade change for the new asphalt and 50% RAP with a grade change.

Western Research Institute is leading the field construction of the comparative sections, and the University of Nevada, Reno and University of Wisconsin, Madison are performing the laboratory testing. Materials have been collected from the project during production and testing is undergoing.

The physical properties of the sampled RAP materials as well as the mechanical properties of the virgin and RAP-containing HMA mixtures are under evaluation. The extracted/recovered RAP binder and the extracted/recovered blended asphalt binder from the RAP-containing HMA mixtures are being evaluated for rheological properties. The testing matrix includes laboratory mixed laboratory compacted (LMLC) samples as well as field mixed laboratory compacted (FMLC) samples. Table E2b.1 summarizes the mixtures that are under evaluation for this project. The long-term performance of the field test sections will be monitored in cooperation with MIT and the data will be used to validate the design and evaluation systems developed under ARC.

Table E2b.1. Mixtures evaluated in the Manitoba Field Section.

Bottom Lift /North Bound Lane				Bottom Lift /South Bound Lane			
RAP	Oil used	St. Station	End Station	RAP	Oil used	St. Station	End Station
50%	200/300	113+80	89+50	50%	200/300	113+80	98+00
50%	150/200	89+50	62+60	50%	150/200	98+00	62+60
15%	150/200	62+60	36+80	15%	150/200	62+60	37+80
0%	150/200	36+80	13+60	0%	150/200	37+80	13+60
Top Lift /North Bound Lane				Top Lift /South Bound Lane			
RAP	Oil used	St. Station	End Station	RAP	Oil used	St. Station	End Station
50%	200/300	102+60	90+20	50%	200/300	101+60	88+40
50%	150/200	90+20	76+60	50%	150/200	88+40	76+60
10%	150/200	76+60	52+00	10%	150/200	76+60	52+00
15%	150/200	52+00	36+37	15%	150/200	52+00	35+70
0%	150/200	36+37	13+60	0%	150/200	35+70	13+60
3rd and 4th Lift/Northbound Lane				3rd and 4th Lift/Southbound Lane			
RAP	Oil used	St. Station	End Station	RAP	Oil used	St. Station	End Station
50%	200/300	102+60	90+20	50%	200/300	101+60	98+00
50%	150/200	89+50	76+60	50%	150/200	88+40	76+60
15%	150/200	52+00	36+80	15%	150/200	52+00	37+80
0%	150/200	36+37	13+60	0%	150/200	35+70	13+60

Significant Results

Intermediate- and High-Temperature Testing and Analysis Procedure

Using the DSR in a frequency sweep protocol, the same testing methodology used with the low-temperature analysis is applied to intermediate and high temperatures. Mortar and binder samples are prepared similar to the low-temperature Bending Beam Rheometer (BBR) procedure. For example, DSR samples are taken after fresh binder is mixed with the selective aggregate, after rolling thin film oven (RTFO) binder is mixed with the selective aggregate, and after the samples have aged in the pressure aging vessel (PAV).

Using a frequency sweep with six distinct frequencies, encompassing 10 rad/sec, samples of binders and mortars are tested to obtain $G^* \sin(\delta)$ for intermediate temperatures and $G^*/\sin(\delta)$ for high temperatures. Binder properties are correlated to the mortar properties using the same methodology used for the low-temperature BBR analysis. PG binder grading limits are applied to the appropriate corresponding results and the analysis follows the low-temperature procedure to estimate allowable percentages of RAP material at selected PG grade temperatures.

RAP Binder True Grade Calculations

True grade calculations were added to the spreadsheet for the three testing temperature levels to allow for a blending chart-type procedure in lieu of the estimation of allowable percentage RAP in a mix. Figure E2b.1 demonstrates the procedure for determining the RAP binder true grade for low-temperature analysis. Using a linear relationship between log stiffness and temperature,

limiting values can be inserted (log 300 MPa), and the true grade can be calculated. Similar analysis can be conducted at intermediate and high temperatures using the appropriate limiting parameters.

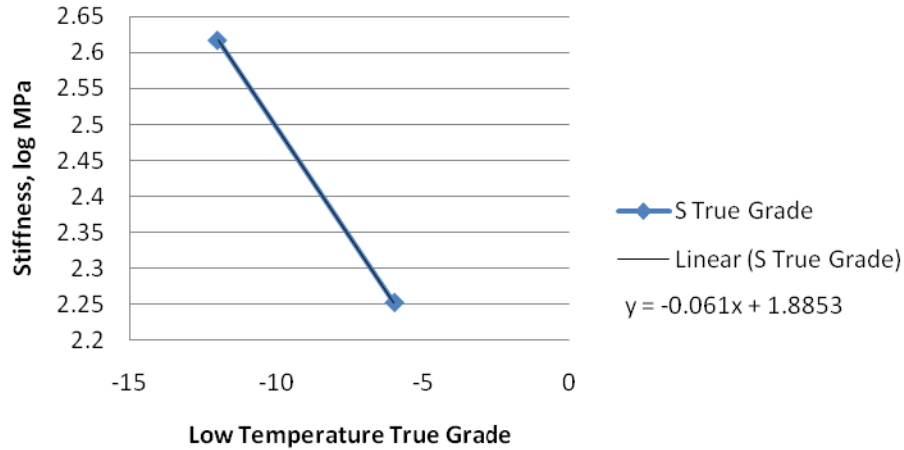


Figure E2b.1. Low-temperature true grade specification.

The analysis Excel spreadsheet contains two summary charts. The first chart includes the estimates of the PG temperatures (low, intermediate and high) for different percentages of RAP binder of the total blended binder, as shown in figure E2b.2. The second chart includes the estimates for the allowable percent of RAP material in the total mix at different PG grades, as shown in figure E2b.3.

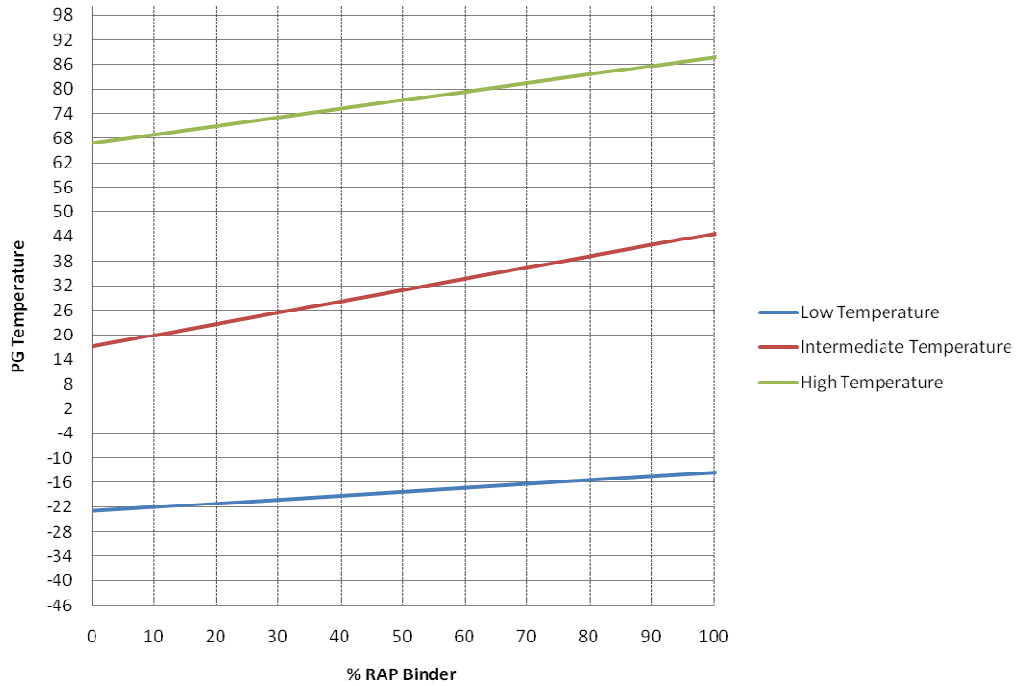


Figure E2b.2. Graph. Total blended binder true grade temperature as a function of percent RAP binder.

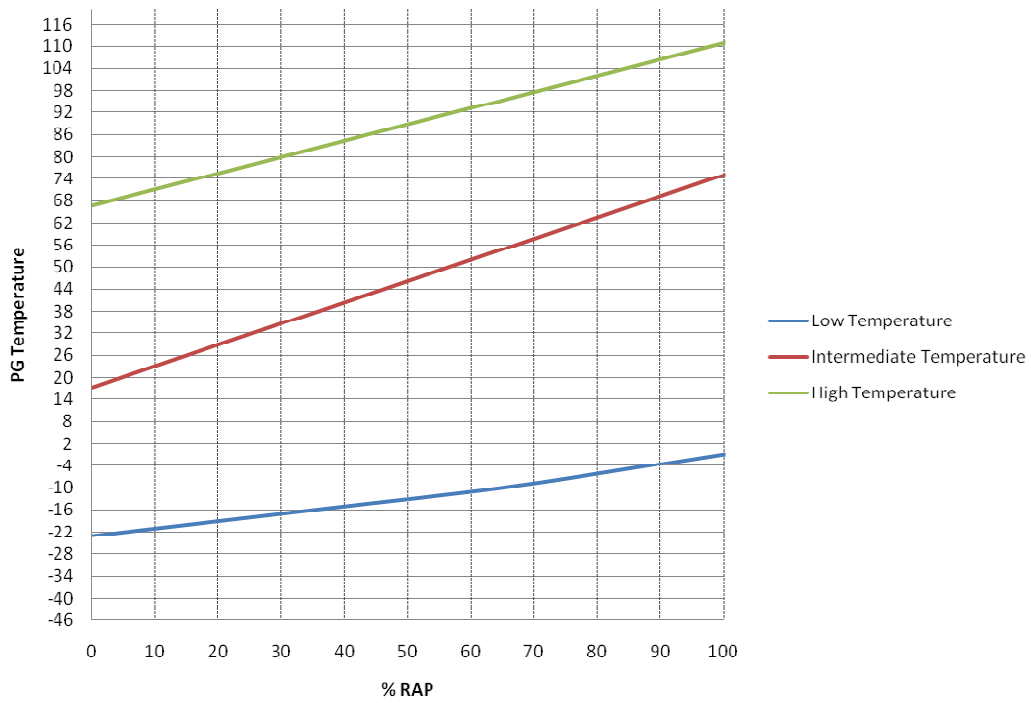


Figure E2b.3. Total blended binder true grade as a function of percent RAP included in the HMA mix.

Significant Problems, Issues and Potential Impact on Progress

None.

Work Planned Next Quarter

Verification of the low-, intermediate- and high-temperature procedures will be conducted for multiple artificial RAPs to ensure validity of the procedure. By extreme aging (40-hour PAV) of binder and blending it with selected aggregates, artificial RAP will be prepared and tested using the developed procedure. In the verification procedure, the properties of the RAP binder are now known and can be compared to the spreadsheet's estimated values. After verification, testing will continue with multiple binder grades and aggregate sources to ensure repeatability. Furthermore, the selected aggregates will be analyzed to determine if R100 material is representative of the RAP source.

Present Preliminary test results for the evaluated Manitoba mixes at the March meeting with the Manitoba Infrastructure & Transportation (MIT) in Manitoba, Canada.

Work on the experimental plan for subtask E2b-3 "Develop a Mix Design Procedure." The objective of the experimental plan is to develop a laboratory mixing process that closely simulates the actual conditions in the field under which the RAP materials are incorporated into the mixing of HMA mixtures.

Work element E2c: Critically Designed HMA Mixtures (UNR)

Work Done This Quarter

An extensive database of computed stress histories of three different asphalt pavement structures subjected to moving traffic loads at various speeds and under braking and non-braking conditions using the 3D-Move was completed.

Work continued to evaluate the applicability of the recommended deviator and confining stresses for the flow number test.

Significant Results

The characteristics of the pulse were determined by best-fitting a haversine wave shape for the equivalent triaxial deviator stress pulse that was calculated from the octahedral shear stress (τ_{oct}) at 2-inch below pavement surface under a moving 18-wheel truck at different speeds and temperatures. It was found that the haversine pulse duration is a function of the vehicle speed and pavement temperature. In all evaluated cases, neither pavement thickness nor mixture properties significantly impacted the pulse duration at 2 inches below the pavement surface. Prediction equations for estimating the anticipated deviator pulse duration as a function of pavement temperature, and vehicle speed have been developed with fitting parameters (R^2) of

0.983 and 0.999 for the non-braking and braking conditions, respectively. Figure E2c.1 shows the predicted versus the calculated pulse duration for non-braking condition.

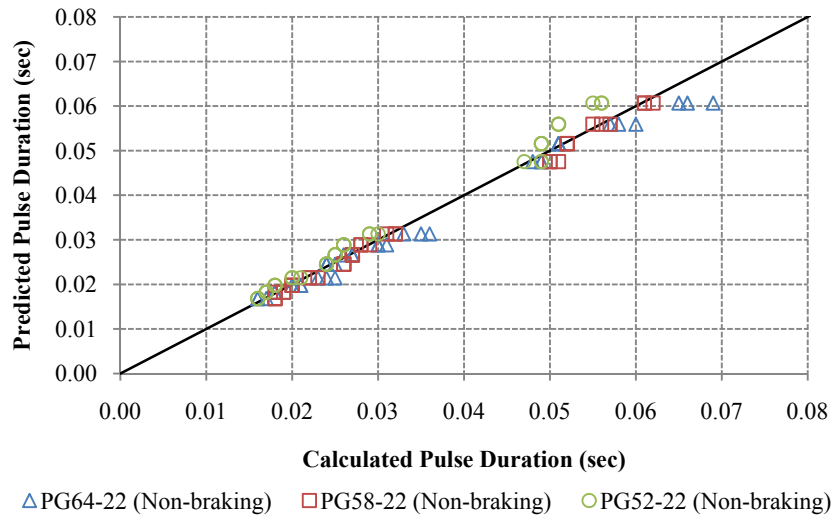


Figure E2c.1. Predicted versus calculated pulse duration – without braking condition.

The magnitude of σ_d and σ_c were determined by converting the stress tensor computed in the HMA layer at 2 inch below pavement surface under a moving 18-wheel truck using the octahedral normal and shear stresses. The amplitude of the equivalent triaxial deviator and confining stresses were found to be highly affected by the mixture's dynamic modulus, $|E^*|$, and vehicle speed and independent of the pavement structure. Under no braking conditions, the magnitude of the deviator and confining stresses ranged from 69-102 psi and 27-47 psi, respectively. In the case of braking, the magnitude of the deviator and confining stresses ranged from 108-132 psi and 30-47 psi, respectively. On average, the imposed additional shear stresses generated by the braking of the vehicle at stopping areas resulted in a 40% increase in the deviator stress (from 85 to 119 psi) and a slight increase (5%) in the confining stress. Additionally, higher deviator stresses coupled with similar or lower confining stresses were observed in the 4" HMA layer when compared to the 8" HMA layer.

Generalized equations for estimating the triaxial deviator and confining stresses for a given pavement structure and temperature and under a given vehicle speed have been provided. Overall, good correlations between the calculated and predicted stresses were found. Figure E2c.2 shows the predicted versus the computed maximum deviator and confining stresses for the three evaluated HMA mixes. Two papers have been submitted for publication to present the findings of subtask E2c.1 (Hajj et al. 2010a, Hajj et al. 2010b).

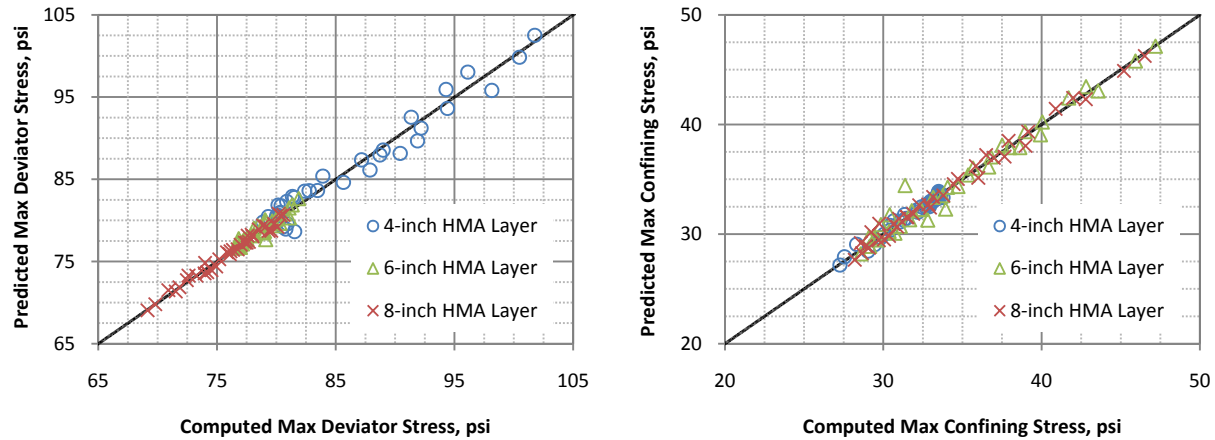


Figure E2c.2. Predicted versus computed maximum deviator and confining stress.

An excel spreadsheet that incorporates the findings of subtasks E2c.1 was developed. The spreadsheet (figure E2c.3) helps identify the repeated load triaxial / flow number test conditions at a specified temperature. The following inputs are needed in order to determine the testing conditions:

- Selection of **Braking** (e.g. at intersection ...) or **Non-Braking** condition.
- **Effective pavement temperature** in °C at 2 inch below pavement surface.
- **Vehicle operating speed** in mph.
- **Asphalt mixture stiffness** in ksi at the effective pavement temperature and loading frequency at 2 inch below the pavement surface. A given/selected stiffness can be provided or it can be calculated using the dynamic modulus parameters (including shift factors) for the determined loading time and temperature.
- **Asphalt layer thickness** in inches.

The example in figure E2c.3 is for a PG64-22 dense graded asphalt mixture where the effective pavement temperature at 2 inch below pavement surface is 60°C and the vehicle operational speed is 20 mph. The dynamic modulus data was used to determine the stiffness of the mix. Figure E2c.3 shows that to simulate a truck travelling at 20 mph the following testing conditions needs to be implemented in the laboratory for an effective pavement temperature of 60°C:

- Loading Pulse Time: 0.05 seconds
- Deviator Stress: 78 psi
- Confining Stress: 32 psi



Repeated Load Triaxial Loading Conditions

Date: 04/30/09

Project: ARC - Critical Mix	Binder Source: Paramount Asphalt	Aggregate Source: Granite - Lockwood
Mix Design: Lockwood-64-22	Binder Grade: PG64-22	Other:

Step 1: Loading Pulse Time at 2-inch Below Pavement Surface

Select Braking Condition:	No Braking
Select Effective Pavement Temperature (°C):	60
Select Operating Speed (mph):	20

$\log(\text{pulse time}) = -0.6654 - 0.00353(T) - 0.0236(S) + 0.00015414(S^2)$

Loading Pulse Time at 2-inch Below Pavement Surface (seconds)	0.052
---	-------

Step 2: Asphalt Mixture Stiffness

Select Method for Asphalt Mixture Stiffness: Dynamic Modulus Data

Dynamic Modulus Data (Ksi): 52.2

$\log(|E^*|) = \delta + \alpha / [1 + \exp(\beta + \gamma \times \log t)]$ $\log(a_T) = a \times T^2 + b \times T + c$ *Note: |E*| in ksi and Temperature in °F*

δ	α	β	γ	a	b	c
0.2697	3.0491	-1.5350	0.5640	0.0003	-0.1225	7.1458

Step 3: Deviator and Confining Stresses at 2 inches Below Pavement Surface

Select Asphalt Layer Thickness (inches): 6.0

Deviator Stress at 2-inch Below Pavement Surface (psi)	78
Confining Stress at 2-inch Below Pavement Surface (psi)	32

Step 4: Recommended Testing Conditions

Loading Pulse Time at 2-inch Below Pavement Surface:	0.052 seconds
Deviator Stress at 2-inch Below Pavement Surface:	78 psi
Confining Stress at 2-inch Below Pavement Surface:	32 psi

Figure E2c.3. Snapshot for triaxial testing loading conditions spreadsheet.

Under subtask E2c.2, an investigation was carried out in an attempt to evaluate the applicability of the recommended pulse time and deviator and confining stresses. Repeated load flow number testing was performed for the WesTrack Cell 55 plant mixture. The laboratory determined critical temperature showed consistency with the rutting field performance of the mix where an increase in rutting was observed at a given ESALs range along with an increase in the maximum pavement temperature during seven consecutive days from 40°C to 46°C.

Significant Problems, Issues and Potential Impact on Progress

None

Work Planned for Next Quarter

The calculations of the 3D-Move model will continue to cover all the loading conditions that were described in the experimental plan for this work element.

Evaluate the permanent deformation characteristics of laboratory-produced and field-produced mixtures under the testing conditions identified in Subtask E2c-1. The impact of air-voids, gradation, and binder type on the asphalt mixture critical temperature will also be evaluated.

Cited References

Hajj, E. Y., Ullao, A., Siddharthan, R., and P. E. Sebaaly. "Estimation of Stress Conditions for the Flow Number Simple Performance Test," Accepted for publication in Transportation Research Record, TRB, National Research Council, Washington, D.C., 2010.

Hajj, E. Y., Ullao, A., Siddharthan, R., and P. E. Sebaaly. "Characteristics of the Loading Pulse for the Flow Number Performance Test," to appear in AAPT Journal Volume 79, 2010.

Work element E2d: Thermal Cracking Resistant Mixes for Intermountain States (UNR & UWM)

Work Done This Quarter

This work element is a joint project between University of Nevada Reno and University of Wisconsin–Madison.

The UNR team has been writing a draft report summarizing the work completed under Subtask E2d-1 that is related to the analyses of the air and pavement temperature profiles data from the LTPP Seasonal Monitoring Program (SMP) and Westrack pavement sections.

The long-term oven aging process continued for the binders as described in the experimental plan for this work element. Table E2d.1 shows the work progress for the binder aging. Additionally, the completed aged binders are under testing for their rheological properties.

Table E2d.1. Binder aging matrix.

Aging Temp (°C)	Aging Period Unit	Aging Period	Binder Grade/Type				
			PG64-22	PG64-28NV	PG64-22 +10%Lime	PG64-22 +20%Lime	PG64-22+3% SBS
135	hours	8	AC	AC	AC	AC	AC
		15	AC	AC	AC	AC	AC
		30	AC	AC	AC	AC	AC
		44	AC	AC	AC	AC	AC
100	hours	44	AC	AC	AC	AC	AC
		90	AC	AC	AC	AC	AC
		150	AC	AC	AC	AC	AC
		240	AC	AC	AC	AC	AC
85	days	7.5	AC	AC	AC	AC	AC
		15	AC	AC	AC	AC	AC
		25	AC	AC	AC	AC	AC
		40	AC	AC	AC	AC	AC
60	days	30	AC	AC			
		60	AC	AC			
		100	AC	AC			
		160	AC	AC			
50	days	60	AC	AC			
		120	AC	AC			
		200	AC	AC			
		320	AC	AC			
AC =	Aging Completed						

Significant improvements to the dilatometric test device of binders were completed this quarter. As shown in figure E2d.1, new dilatometric cells were designed and improved o-rings with military specifications were selected to minimize the effect of rubber contraction on the test results. Figure E2d.2 shows the calibration curve for the new dilatometric cell with the improved o-ring. As shown in figure E2d.2, the influence of the contraction of the rubber is minimized and the contraction of the dilatometric cell with a dummy metal sample, for the temperature range of 30 °C to -50 °C, is negligible. Therefore, no volumetric corrections are needed for the dilatometric test results of binders for this temperature range.

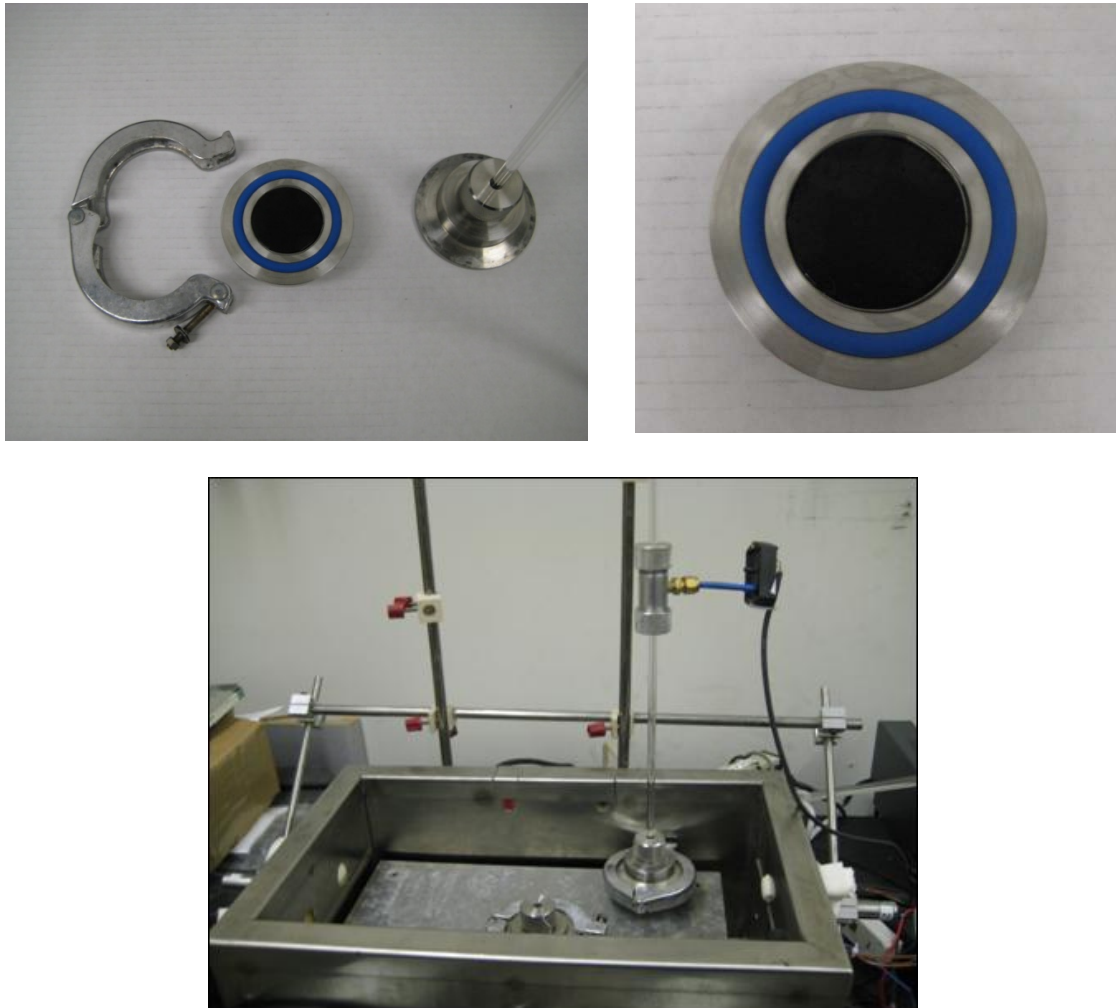


Figure E2d.1. New dilatometric cell with military o-ring for glass transition temperature (T_g) testing of binders.

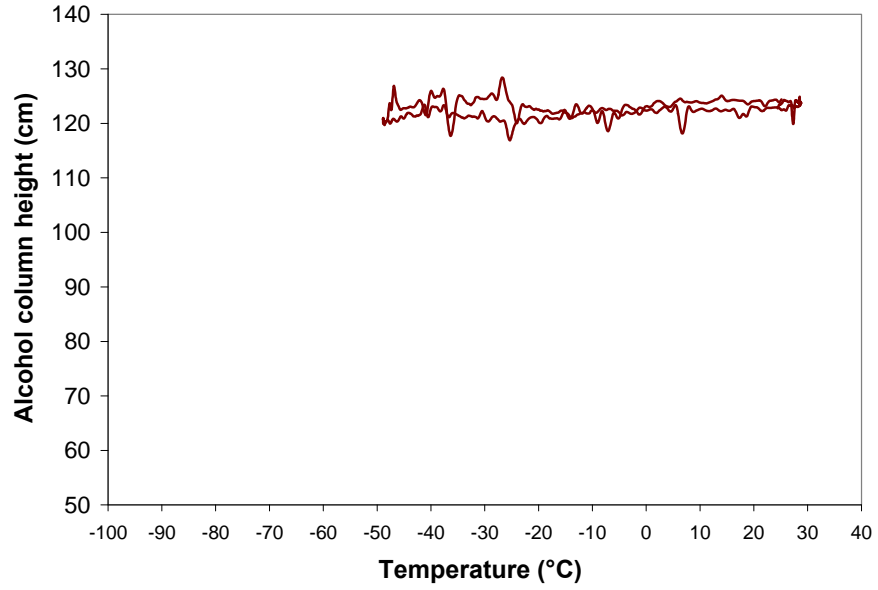


Figure E2d.2. Dilatometric cell calibration with military o-ring and metal sample.

An example of the dilatometric test performed with the new cell for two binders with different T_g is presented in figure E2d.3. The T_g and the coefficient of thermal contraction/expansion below and above the T_g are consistent with measurements reported in the literature during the SHRP project (Bahia 1991).

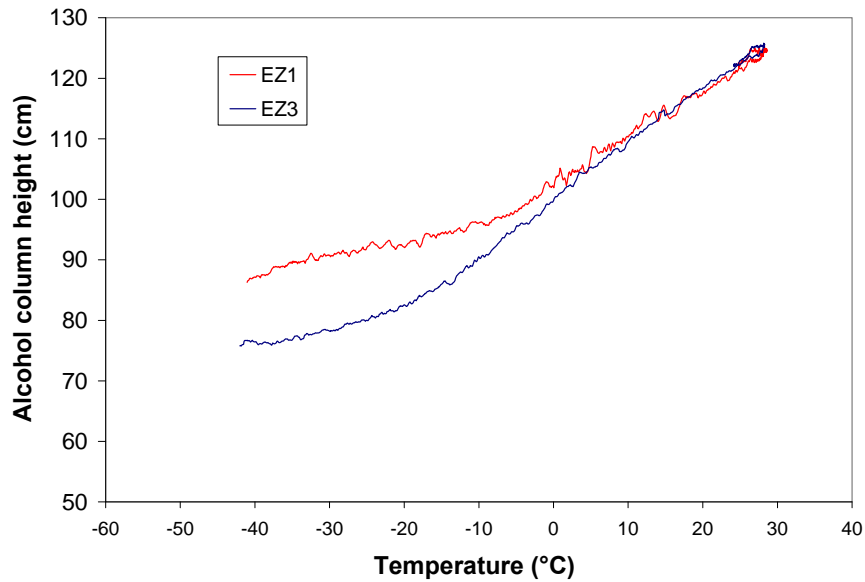


Figure E2d.3. T_g testing of binders.

An example of how the raw data obtained from the dilatometric test is fitted to the nonlinear model, as proposed in previous quarterly reports, is shown in figure E2d.4. It can be seen that the model adequately describes the experimental results ($R^2=0.98$).

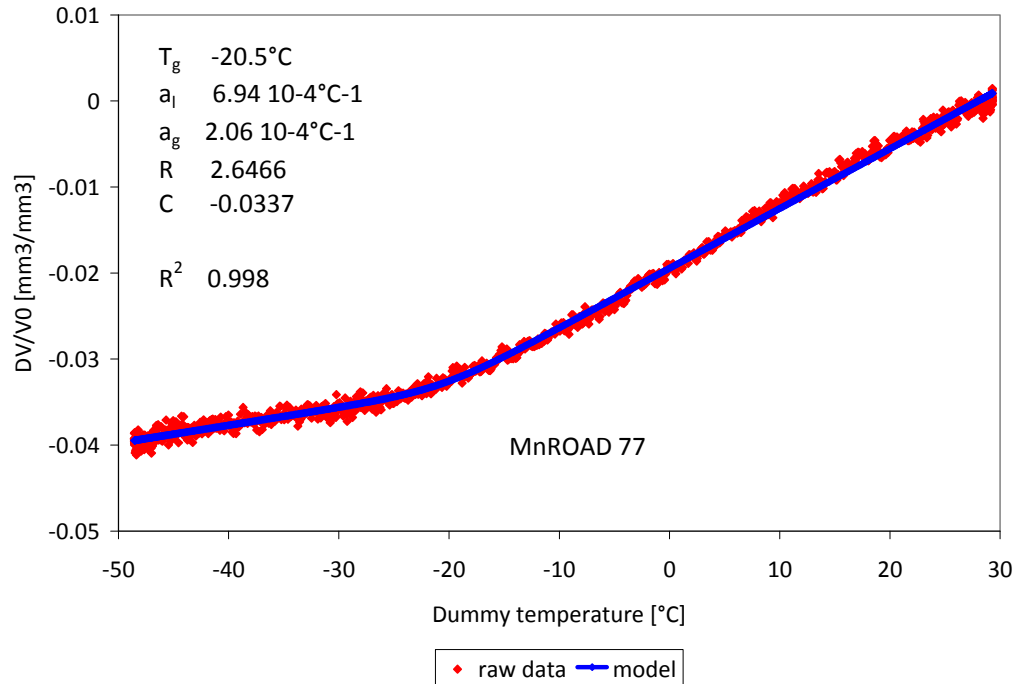


Figure E2d.4. Typical calculation of T_g and coefficients of thermal expansion/contraction above and below T_g .

The T_g for these binders were compared to the critical cracking temperature obtained from Asphalt Binder Cracking Device (ABCD) testing, as shown in table E2d.2. It can be seen that binders with lower T_g temperature have better low-temperature cracking performance.

Table E2d.2. Comparison between T_g and ABCD results.

Binder	T_g (°C) Dilatometric	T_{cr} (°C) ABCD
EZ1	-5	-29.4
EZ3	-18	-39.2

Preliminary cyclic tests with the new dilatometric cell were performed this quarter. Figure E2d.5 shows the dilatometric cyclic test performed to a binder extracted from MnROAD cell 77. Three cycles were applied to the specimen and there are no significant changes observed in the T_g and coefficients of thermal expansion/contraction after each cycle. Figure E2d.5 indicates that the area inside the volume-temperature loop increases with each cycle. Further tests and analyses are

needed to statistically measure the changes of the T_g and coefficient of thermal expansion of binders due to thermal cycling.

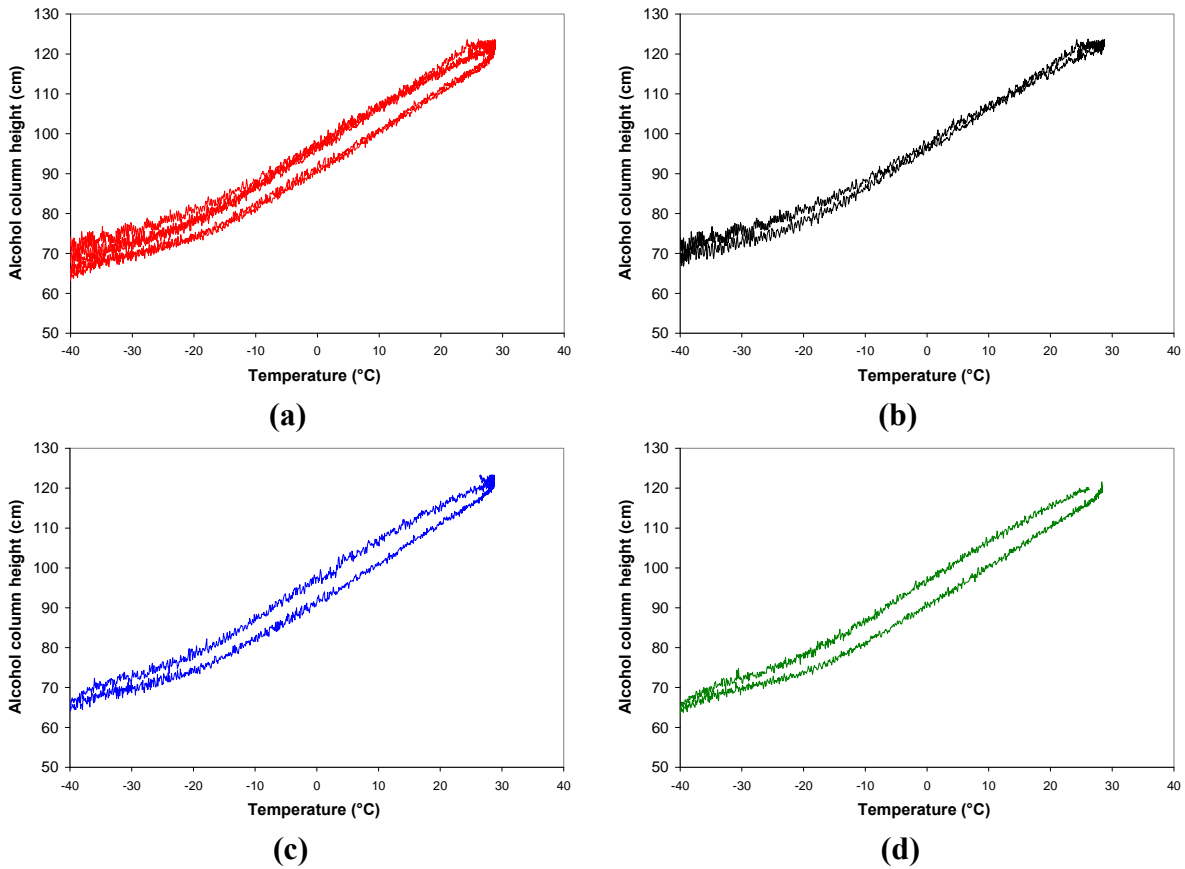


Figure E2d.5. Cyclic dilatometric (T_g) test: (a) all cycles; (b) cycle 1; (c) cycle 2; (d) cycle 3.

A Single-Edge Notched Bending (SENB) testing system with an independent cooling bath was set up in this quarter, as shown in figure E2d.6. The friction in the loading shaft previously reported was resolved. Figure E2d.7 shows the SENB results for an NCHRP Flint Hills asphalt binder tested at $-12\text{ }^\circ\text{C}$. There is an excellent repeatability of the SENB test results for this binder.

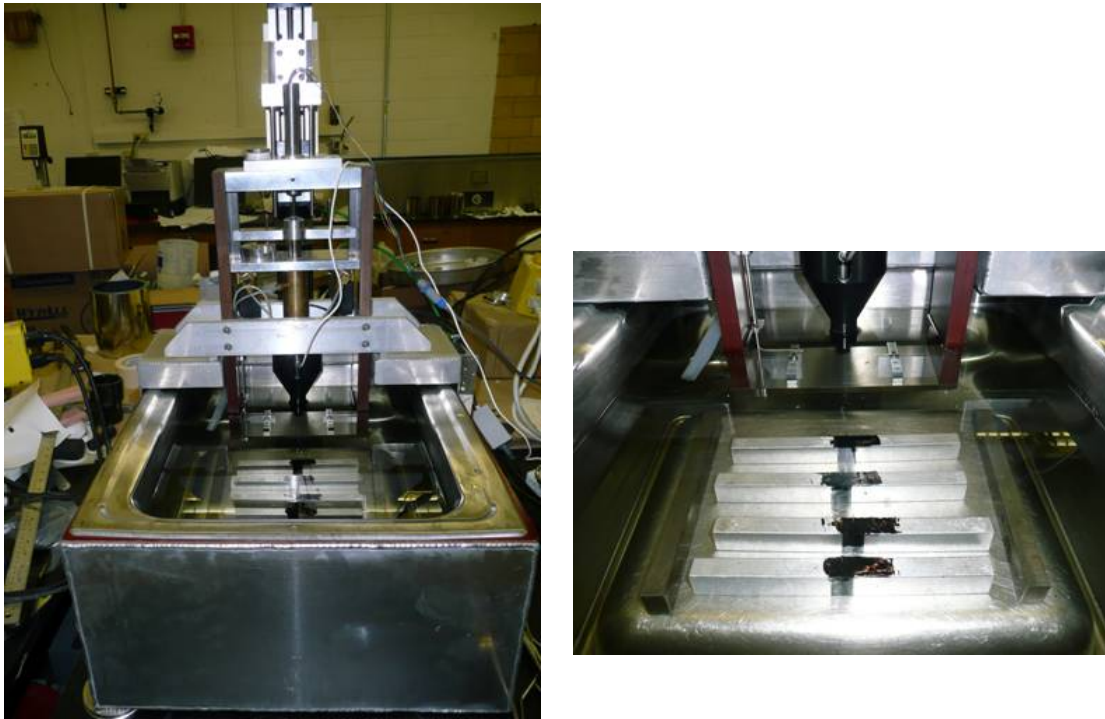


Figure E2d.6. SENB testing system.

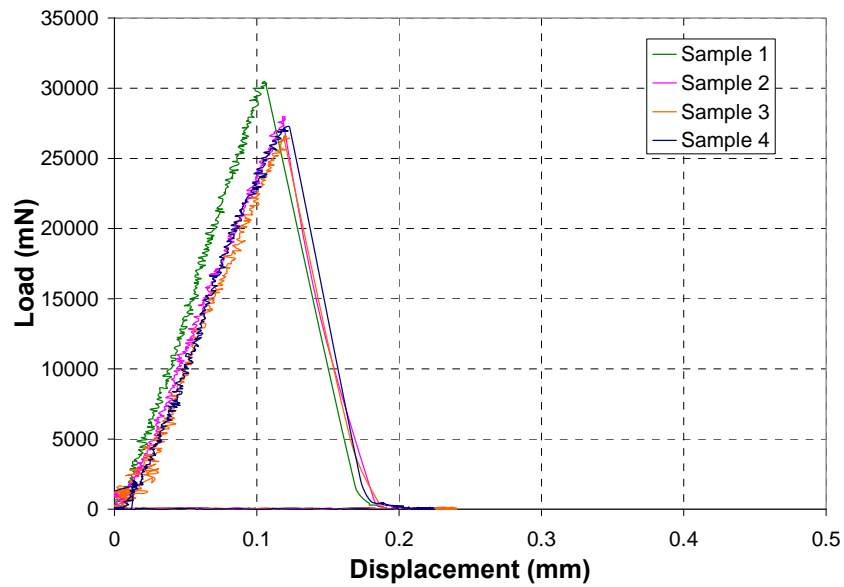


Figure E2d.7. SENB results for NCHRP Flint Hills pressure aging vessel (PAV) asphalt binder.

Under Subtask E2d-3.b and c, significant progress has been made in sample production. All of the mix designs for both tasks are complete, and nearly half of the samples have completed the laboratory aging. The remaining half is at various points throughout the aging process. Approximately third of the samples have been tested for E^* in compression. Further implementation is required for the E^* in tension testing. Figure E2d.8 shows the E^* in compression for the Lockwood and Colorado mixes at different aging conditions.

Following the mix testing, the binder is extracted and recovered for DSR and FTIR testing. This testing has begun, with a few results being available. A brief outline of the work plan was presented at TRB 2010 in January.

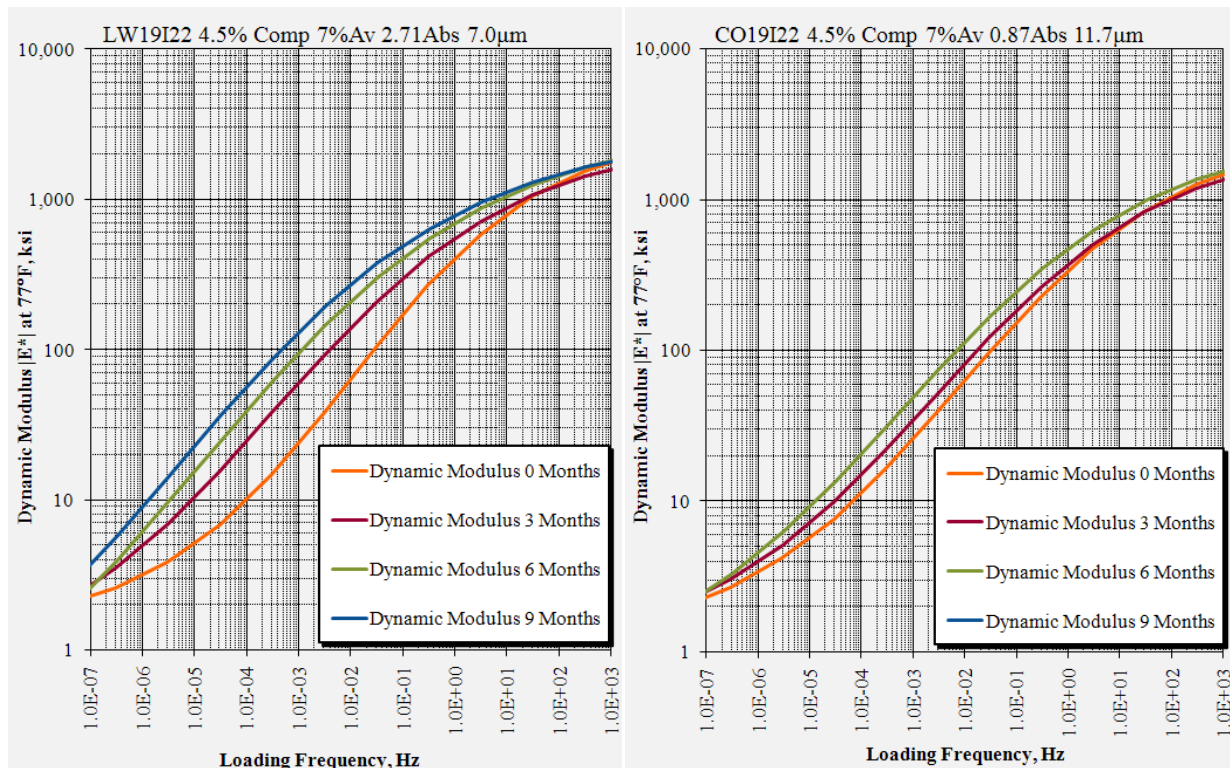


Figure E2d.8. Dynamic modulus of mixtures at different aging stages.

Significant Results

The dilatometric test for binders was successfully modified and used to collect measurements that agree with previous studies. Preliminary cyclic dilatometric tests were performed and the results are very encouraging. Problems with friction in the SENB system were also resolved in this quarter. The SENB test is capable of differentiating between the low-temperature performances of different binders, as validated by comparing results from other testing procedures.

Significant Problems, Issues and Potential Impact on Progress

The research team was not able to perform SENB tests on a polyphosphoric acid (PPA)-modified binder due to adhesion problems between the binder and the metal bars, as shown in figures E2d.8 and E2d.9. Furthermore, asphalt mastic samples prepared with a similar binder showed the same adhesion problem. The research team is planning to modify the specimen preparation procedure and the surface of the metal pieces to avoid having adhesion failures between the binder and the metal bars. The research team is not expecting a major impact on the progress of this work element due to this adhesion problem.

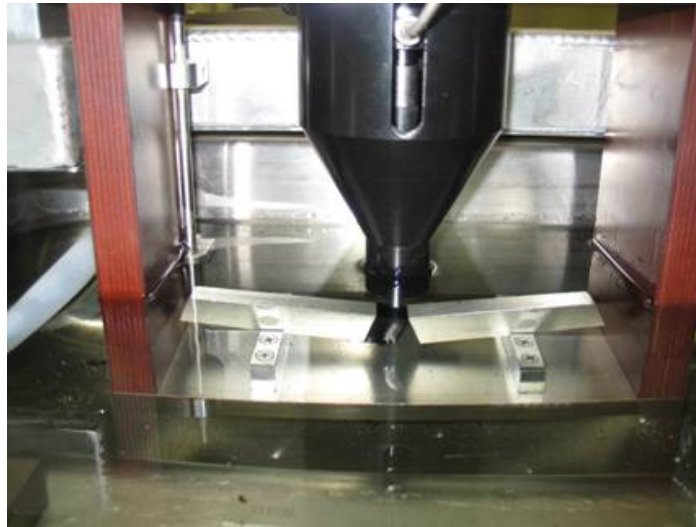


Figure E2d.8. Wall failure in SENB testing for PPA NCHRP Flint Hills binder.



Figure E2d.9. Adhesion issues with PPA-modified Flint Hills binder.

Work Planned Next Quarter

Continue the experiment to evaluate the aging characteristics (oxidation and hardening kinetics) of asphalt binders when aged in forced convection (horizontal airflow) ovens.

The research team plans to start the testing planned for in the original experimental matrix for T_g and thermal expansion/contraction for binders and mixtures. Adjustments to the SENB specimen

preparation procedure will be made to resolve the adhesion problems observed in this quarter. The research team will also begin conducting the test matrix for SENB of asphalt binders and mastics.

The team also plans to start work on incorporating the Thermal Stress Restrained Specimen Test (TSRST) fixture into the T_g device. This will allow for a unified system that characterizes both binders and mixtures in terms of T_g and strength for estimation of resistance to thermal cracking.

Continue the work on the impact of aggregate absorption and gradation on the aging of the asphalt binder. Activities on the mixtures will include continuation of sample aging in ovens, E^* testing in compression, and implementation of E^* tension testing. Following the mixture tests, the samples will then be extracted and recovered for DSR and FTIR testing.

Cited References

Bahia, H. U., 1991, *Low Temperature Isothermal Physical Hardening of Asphalt Cements*. Ph.D. thesis, The Pennsylvania State University, College Station, PA.

Work element E2e: Design Guidance for Fatigue and Rut Resistance Mixtures (AAT)

Work Done This Quarter

Dr. Christensen evaluated the effect of loading frequency on the reduced loading cycles/endurance limit approach to continuum damage fatigue analysis (CD-RC/EL) in support of work being done by AAT in Work Element TD2 to implement the testing and analysis in the Asphalt Mixture Performance Tester (AMPT). From these analyses it was determined that the fatigue testing could be done at 1 Hz which can easily be controlled with the standard servo controllers and actuators used in the AMPT. Control of tension-compression loading at 10 Hz is much more difficult and may require modifications to the AMPT equipment.

Dr. Christensen further refined the CD-RC/EL analysis using data collected with the AMPT at 1 Hz on mixtures from the Minnesota and Arizona validation sites along with previously collected data. These refinements investigated various methods for collapsing the damage data into a continuous function.

AAT's laboratory staff identified in-house mixtures that can be used in the various experiments to refine the NCHRP 9-25/9-31 models:

- Hirsch model
- Resistivity/Rutting Model
- Continuum Damage Fatigue Model

These are mixtures that AAT has used on various other projects that are available in sufficient quantity for the required testing. These mixtures will be supplemented with core the ARC core materials as they become available.

Significant Results

A comprehensive CD-RC/EL model was developed. A damage function was developed based on this model that can be easily implemented in LEA pavement design software was developed.

Significant Problems, Issues and Potential Impact on Progress

None.

Work Planned Next Quarter

As experimental data is gathered in laboratory fatigue testing, the CD-RC/EL model will be evaluated and refined as needed. The CD-RC/EL damage function will be put into EVERSTRESS and plots of damage evolution for typical HMA pavement structures developed to determine if this approach produces reasonable results.

Engineered Materials Year 3	Year 3 (4/2009-3/2010)												Team
	4	5	6	7	8	9	10	11	12	1	2	3	
(1) High Performance Asphalt Materials													
E1a: Analytical and Micro-mechanics Models for Mechanical behavior of mixtures													TAMU
E1a-1: Analytical Micromechanical Models of Binder Properties												JP	
E1a-2: Analytical Micromechanical Models of Modified Mastic Systems													
E1a-3: Analytical Models of Mechanical Properties of Asphalt Mixtures			JP	P	JP(2)				P(2)				M&A
E1a-4: Analytical Model of Asphalt Mixture Response and Damage				P	JP(2)				P(3)				
E1b: Binder Damage Resistance Characterization													UWM
E1b-1: Rutting of Asphalt Binders													
E1b-1-i. Literature review													
E1b-1-ii. Select Materials & Develop Work Plan													
E1b-1-iii. Conduct Testing					JP							P	
E1b-1-iv. Analysis & Interpretation					JP							P	
E1b-1-v. Standard Testing Procedure and Recommendation for Specifications													
E1b-2: Feasibility of determining rheological and fracture properties of asphalt binders and mastics using simple indentation tests (modified title)													UWM
E1b-2-i. Literature Review													
E1b-2-ii. Proposed SuperPave testing modifications						P							
E1b-2-iii. Preliminary testing and correlation of results										D			
E1b-2-iv. Feasibility of using indentation tests for fracture and rheological properties										D	P	JP	
E2a: Comparison of Modification Techniques													UWM
E2a-1: Identify modification targets and material suppliers					DP								
E2a-2: Test material properties												P	
E2a-3: Develop model to estimate level of modification needed and cost index													
E2a-4: Write asphalt modification guideline/report on modifier impact over binder properties													
E2c: Critically Designed HMA Mixtures													UNR
E2c-1: Identify the Critical Conditions					JP		D					F	
E2c-2: Conduct Mixtures Evaluations												D	
E2c-3: Develop a Simple Test													
E2c-4: Develop Standard Test Procedure													
E2c-5: Evaluate the Impact of Mix Characteristics													
E2d: Thermal Cracking Resistant Mixes for Intermountain States													UWM/UNR
E2d-1: Identify Field Sections									D				
E2d-2: Identify the Causes of the Thermal Cracking			D										
E2d-3: Identify an Evaluation and Testing System	DP							DP		D			JP
E2d-4: Modeling and Validation of the Developed System													
E2d-5: Develop a Standard													
E2e: Design Guidance for Fatigue and Rut Resistance Mixtures													AAT
E2e-1: Identify Model Improvements													
E2e-2: Design and Execute Laboratory Testing Program												P	
E2e-3: Perform Engineering and Statistical Analysis to Refine Models													
E2e-4: Validate Refined Models													
E2e-5: Prepare Design Guidance													
(2) Green Asphalt Materials													
E2b: Design System for HMA Containing a High Percentage of RAP Material													UNR
E2b-1: Develop a System to Evaluate the Properties of RAP Materials	D				JP					F	P		
E2b-2: Compatibility of RAP and Virgin Binders													
E2b-3: Develop a Mix Design Procedure											D		
E2b-4: Impact of RAP Materials on Performance of Mixtures													
E2b-5: Field Trials													
E1c: Warm and Cold Mixes													UWM
E1c-1: Warm Mixes													
E1c-1-i. Effects of Warm Mix Additives on Rheological Properties of Binders													
E1c-1-ii. Effects of Warm Mix Additives on Mixture Workability and Stability					JP								
E1c-1-iii. Mixture Performance Testing											P		DP
E1c-1-iv. Develop Revised Mix Design Procedures													
E1c-1-v. Field Evaluation of Mix Design Procedures and Performance Recommendations													
E1c-2: Improvement of Emulsions' Characterization and Mixture Design for Cold Bitumen Applications													UWM/UNR
E1c-2-i. Review of Literature and Standards	D1						D3						
E1c-2-ii. Creation of Advisory Group													
E1c-2-iii. Identify Tests and Develop Experimental Plan	D1									D5			
E1c-2-iv. Develop Material Library and Collect Materials													
E1c-2-v. Conduct Testing Plan													
E1c-2-vi. Develop Performance Selection Guidelines					JP		D4					P	
E1c-2-vii. Validate Performance Guidelines													
E1c-2-viii. Develop CMA Mix Design Guidelines					D2								
E1c-2-ix. Develop CMA Performance Guidelines													

Deliverable codes
D: Draft Report
F: Final Report
M&A: Model and algorithm
SW: Software
JP: Journal paper
P: Presentation
DP: Decision Point

Deliverable Description
Report delivered to FHWA for 3 week review period.
Final report delivered in compliance with FHWA publication standards
Mathematical model and sample code
Executable software, code and user manual
Paper submitted to conference or journal
Presentation for symposium, conference or other
Time to make a decision on two parallel paths as to which is most promising to follow through

Work planned
Work completed
Parallel topic

Engineered Materials Year 2 - 5	Year 2 (4/08-3/09)				Year 3 (4/09-3/10)				Year 4 (04/10-03/11)				Year 5 (04/11-03/12)				Team	
	Q1	Q2	Q3	Q4	Q1	Q2	Q3	Q4	Q1	Q2	Q3	Q4	Q1	Q2	Q3	Q4		
(1) High Performance Asphalt Materials																		
E1a: Analytical and Micro-mechanics Models for Mechanical behavior of mixtures																	TAMU	
E1a-1: Analytical Micromechanical Models of Binder Properties				P, JP	JP	P	P	JP	M&A	D	F, SW							
E1a-2: Analytical Micromechanical Models of Modified Mastic Systems				P, JP	JP	P	P		M&A	JP	D	F, SW						
E1a-3: Analytical Models of Mechanical Properties of Asphalt Mixtures	P	P, JP		P, JP	JP	P	P	M&A		D	SW, JP	F						
E1a-4: Analytical Model of Asphalt Mixture Response and Damage				P, JP	JP	P	P		M&A	D	F, JP	SW						
E1b: Binder Damage Resistance Characterization																	UWM	
E1b-1: Rutting of Asphalt Binders																		
E1b-1-1: Literature review																		
E1b1-2: Select Materials & Develop Work Plan	DP, P		P															
E1b1-3: Conduct Testing			P			JP		P										
E1b1-4: Analysis & Interpretation			JP	P	JP		JP		P			JP						
E1b1-5: Standard Testing Procedure and Recommendation for Specifications										P		JP	DP	P	D	JP	F	
E1b-2: Feasibility of Determining rheological and fracture properties of asphalt binders and mastics using simple indentation tests (modified title)																		
E1b-2i: Literature Review																		
E1b-2ii: Proposed SuperPave testing modifications or new testing devices						P												
E1b-2iii: Preliminary testing and correlation of results									D									
E1b-2iv: Feasibility of using indentation tests for fracture and rheological properties									D, P, JP		F							
E2a: Comparison of Modification Techniques																		UWM
E2a-1: Identify modification targets and material suppliers				DP		DP												
E2a-2: Test material properties								P										
E2a-3: Develop model to estimate level of modification needed and cost index																		
E2a-4: Write asphalt modification guideline/report on modifier impact over binder properties																		
E2c: Critically Designed HMA Mixtures																		UNR
E2c-1: Identify the Critical Conditions		JP		D, F		JP	D	F										
E2c-2: Conduct Mixtures Evaluations								D	D, F	JP								
E2c-3: Develop a Simple Test													D, F	JP				
E2c-4: Develop Standard Test Procedure														D, F				
E2c-5: Evaluate the Impact of Mix Characteristics																	D, F	
E2d: Thermal Cracking Resistant Mixes for Intermountain States																		UWM/UNR
E2d-1: Identify Field Sections			D, F	D, F			D											
E2d-2: Identify the Causes of the Thermal Cracking					D				D, F	JP			D, F	JP				
E2d-3: Identify an Evaluation and Testing System					DP	JP	DP, D						D, F	JP				
E2d-4: Modeling and Validation of the Developed System																	D, F	
E2d-5: Develop a Standard																	D, F	
E2e: Design Guidance for Fatigue and Rut Resistance Mixtures																		AAT
E2e-1: Identify Model Improvements																		
E2e-2: Design and Execute Laboratory Testing Program								P										
E2e-3: Perform Engineering and Statistical Analysis to Refine Models						JP		P		JP		P, D, F						
E2e-4: Validate Refined Models										JP				JP				
E2e-5: Prepare Design Guidance															M&A	P, D, F		
(2) Green Asphalt Materials																		
E2b: Design System for HMA Containing a High Percentage of RAP Material																		UNR
E2b-1: Develop a System to Evaluate the Properties of RAP Materials		JP		P	D	JP	F	P										
E2b-2: Compatibility of RAP and Virgin Binders															D, F	JP		
E2b-3: Develop a Mix Design Procedure									D						D, F	JP		
E2b-4: Impact of RAP Materials on Performance of Mixtures																	D, F	
E2b-5: Field Trials																	D, F	
E1c: Warm and Cold Mixes																		
E1c-1: Warm Mixes																		
E1c-1i: Effects of Warm Mix Additives on Rheological Properties of Binders																		UWM
E1c-1iii: Effects of Warm Mix Additives on Mixture Workability and Stability		P	D	F, DP		JP												UWM
E1c-1iii: Mixture Performance Testing								P, DP										UWM/UNR
E1c-1iv: Develop Revised Mix Design Procedures										JP	P							UWM/UNR
E1c-1v: Field Evaluation of Mix Design Procedures and Performance Recommendations														JP	D	P, F		UWM/UNR
E1c-2: Improvement of Emulsions' Characterization and Mixture Design for Cold Bitumen Applications																		UWM
E1c-2i: Review of Literature and Standards		JP, P, D	F		D1	D3												
E1c-2ii: Creation of Advisory Group																		
E1c-2ii: Identify Tests and Develop Experimental Plan				P, DP	D1	D5												
E1c-2iv: Develop Material Library and Collect Materials																		
E1c-2v: Conduct Testing Plan						JP	D4	P										
E1c-2iv: Develop Performance Selection Guidelines									JP	D	P, F							
E1c-2vii: Validate Guidelines						D2									JP	P		
E1c-2viii: Develop CMA Mix Design Procedure												P						
E1c-2ix: Develop CMA Performance Guidelines														JP	D	F		

Deliverable codes
D: Draft Report
F: Final Report
M&A: Model and algorithm
SW: Software
JP: Journal paper
P: Presentation
DP: Decision Point

Deliverable Description
Report delivered to FHWA for 3 week review period.
Final report delivered in compliance with FHWA publication standards.
Mathematical model and sample code
Executable software, code and user manual
Paper submitted to conference or journal
Presentation for symposium, conference or other
Time to make a decision on two parallel paths as to which is most promising to follow through

Work planned
Work completed
Parallel topic
Delayed

PROGRAM AREA: VEHICLE-PAVEMENT INTERACTION

CATEGORY VP1: WORKSHOP

Work element VP1a: Workshop on Super-Single Tires

This work element is complete.

CATEGORY VP2: DESIGN GUIDANCE

Work element VP2a: Mixture Design to Enhance Safety and Reduce Noise of HMA (UWM)

Work Done This Quarter

Work focused on selecting an appropriate laser profilometer and noise absorption measuring device. A laser device was purchased and a frame was built on which to mount the laser. The laser profilometer is ready to be used and produce raw data of distance and elevation measurements. Profile measurements on gyratory samples were conducted at the University of Pisa, Italy, as part of the collaboration between the University of Wisconsin–Madison and the asphalt research group at the University of Pisa.

Significant Results

Four gyratory samples of different gradations were shipped to the University of Pisa for laser profilometer measurements. The different gradations used in the samples tested are summarized in figure VP2a.1. (Gradation 3 is a porous, gap-graded mix.) Laser profile measurements are shown in figure VP2a.2. The plots show the capability of the laser device to measure the texture profile of the different samples, as well as capture the difference in the surface texture among the different gradations. The figure clearly shows how the porous mix—Gradation 3—has a more pronounced surface texture than the other three mixes.

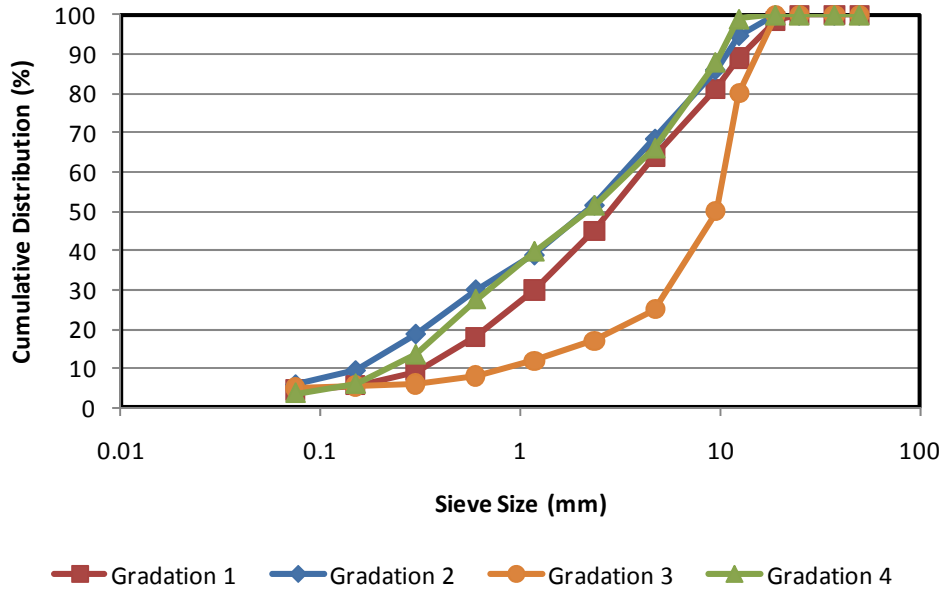


Figure VP2a.1. Graph. Selected gradations for laser profile measurements.

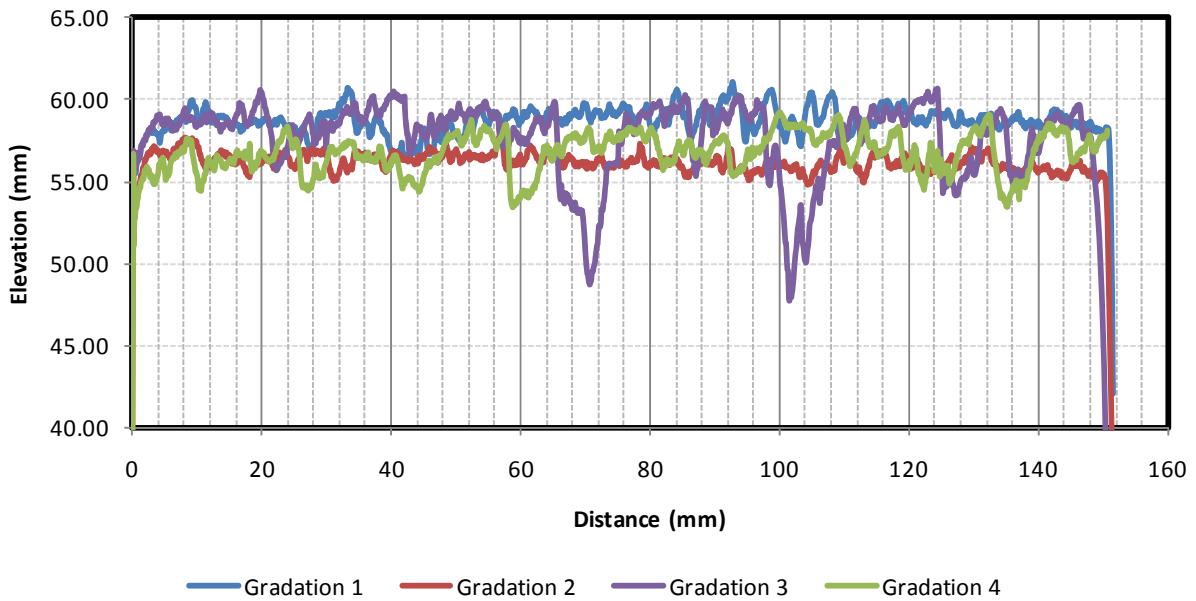


Figure VP2a.2. Graph. Laser profile measurements.

Preliminary testing of the laser profilometer at UW-Madison was completed. Three asphalt samples were measured: a dense-graded mix and two stone matrix asphalt (SMA) mixes with aggregate maximum nominal sizes of 9.5 and 12.5 mm. The collected profiles, shown in figure VP2a.3, indicate that the system is capable of measuring the surface texture profile. The system also differentiated between the dense-graded and SMA mixes, and between the two SMA mixes.

The profiles indicate that the 12.5-mm SMA has more surface texture than the other two mixes, which is expected. To check accuracy, the research team will measure the profile of certain samples and ship them to the University of Pisa for confirmation of profile measurements.

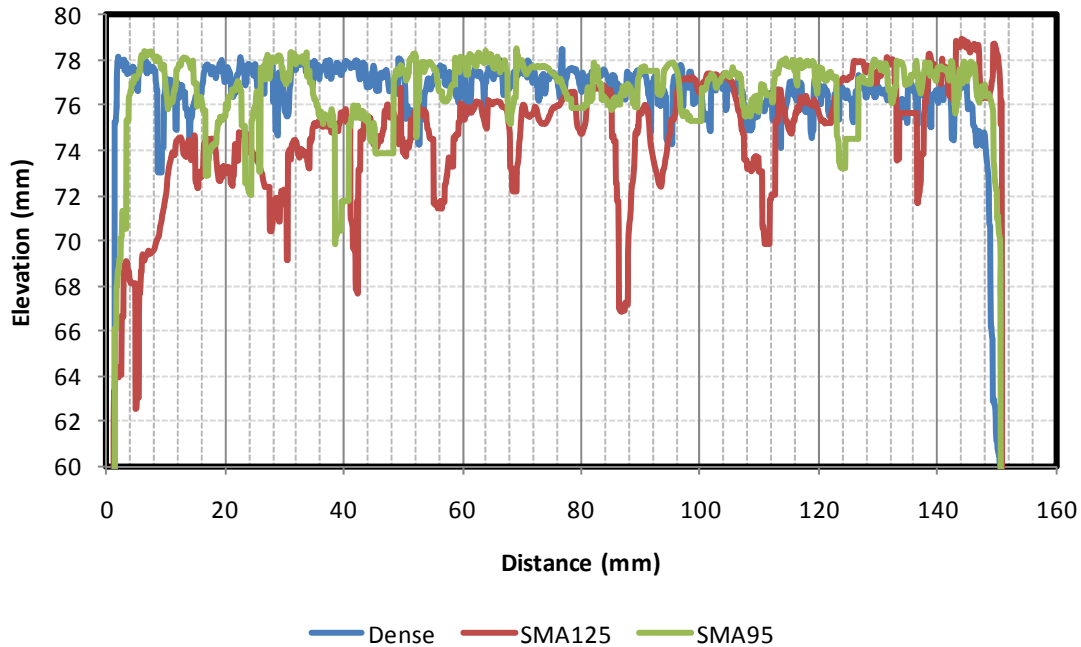


Figure VP2a.3. Graph. Laser profile measurements (UW-Madison).

Significant Problems, Issues and Potential Impact on Progress

The progress in this task was slightly delayed. The process of purchasing the laser device and the impedance tube took much longer than the research team expected. However, the two systems are now ready to be used, and the research team expects that progress should catch up in the next quarter.

Work Planned Next Quarter

Next quarter, the research team will focus on measuring the noise absorption properties and the surface macrotexture properties using the laser profilometer. Samples will be selected to cover a wide range of mix properties such as gradation and air voids. The research team will also review the literature and consult with the research group at the University of Pisa to decide if additional gradations should be considered.

The Excel analysis spreadsheet will be finalized to accommodate the raw data produced by the laser profilometer and produce the texture spectrum levels and mean texture depth following the ISO 13473-1 procedure. The calibration and measurement procedure for the impedance tube will also be finalized.

CATEGORY VP3: MODELING

Work element VP3a: Pavement Response Model to Dynamic Loads (UNR)

Work Done This Quarter

Continued the work on the 3D-Move model to make it a menu-driven software to integrate the post-processing forms. Continued the testing of the alpha-version of the 3D-Move model.

Significant Results

One of the important components of an analysis package is post-processing. The post-processing generally involves user-friendly documentation of the results and portability of the results to other platforms. For wider acceptance, steps should be taken to allow for portability as it is often required to integrate the results of the 3D-Move to other platforms, such as Word documents and Excel worksheets.

Figure VP3a.1 shows the main menu associated with 3D-Move using which all aspects of the program can be controlled. Many aspects of the input have already been addressed in our past Quarterly Reports. The topic discussed here is the post-processing of the 3D-Move output results. As shown in figure VP3a.1, the output can be viewed using:

- (1) Text Mode,
- (2) Tabular Mode (Microsoft Excel), and
- (3) Graphical Mode.

To illustrate samples of each of these options, it is necessary to review the locations where the results are needed. By clicking on Input Summary – Response Data Points (highlighted in figure VP3a.1), the coordinates of the response points of interest, which have been input before the initiation of the 3D-Move run are revealed figure VP3a.2). It can be seen that the sample problem is a three layer problem and responses at as many as 15 points have been requested. Four points are at the surface ($z = 0$) and others are interior points. The response locations relative to pavement layers and tire imprint can be interpreted from data and sketch shown on the right.

Figures VP3a.1 through VP3a.5 present the initial output windows associated with all three options of the output results. The initial screen of the Text Mode option is shown in figures VP3a.3. This figure along with data input such as Load Case and Load Type, and Vehicle Speed, gives a partial list of the normal stresses at the response data point 1 ($Y = 0; Z = 0$). The user has the option to select other responses such as shear stresses, strains (normal shear), displacement, velocity and acceleration. The complete output (i.e., subsequent screens) will contain all requested responses at all 15 response points listed on the table in figures VP3a.2. Since this is a Text Mode output, it can be easily saved and edited (insert, cut, paste etc.).

The output results under Tabular Mode (Microsoft Excel) option are shown in figures VP3a.4. Each output entry is assigned a cell and in this sample a partial list of normal and shear stresses

at a surface location ($Y = 0; Z = 0$) is presented. Subsequently, figure VP3a.5 shows a plot of normal strain in the x- direction (ϵ_{xx}), at the bottom of the HMA layer (Layer 1) developed using the Graphical Mode option. This component of strain has been selected from drop-box options shown on top left of the figure. The strain history plot shown in the figure gives maximum and minimum response values along with when they occurred. In addition, the Format Graph button shown at the bottom corner can be used to format the graph. Modifications such as labeling to axes (X and Y), graph title, color and bordering etc. can be accomplished by clicking on this button.

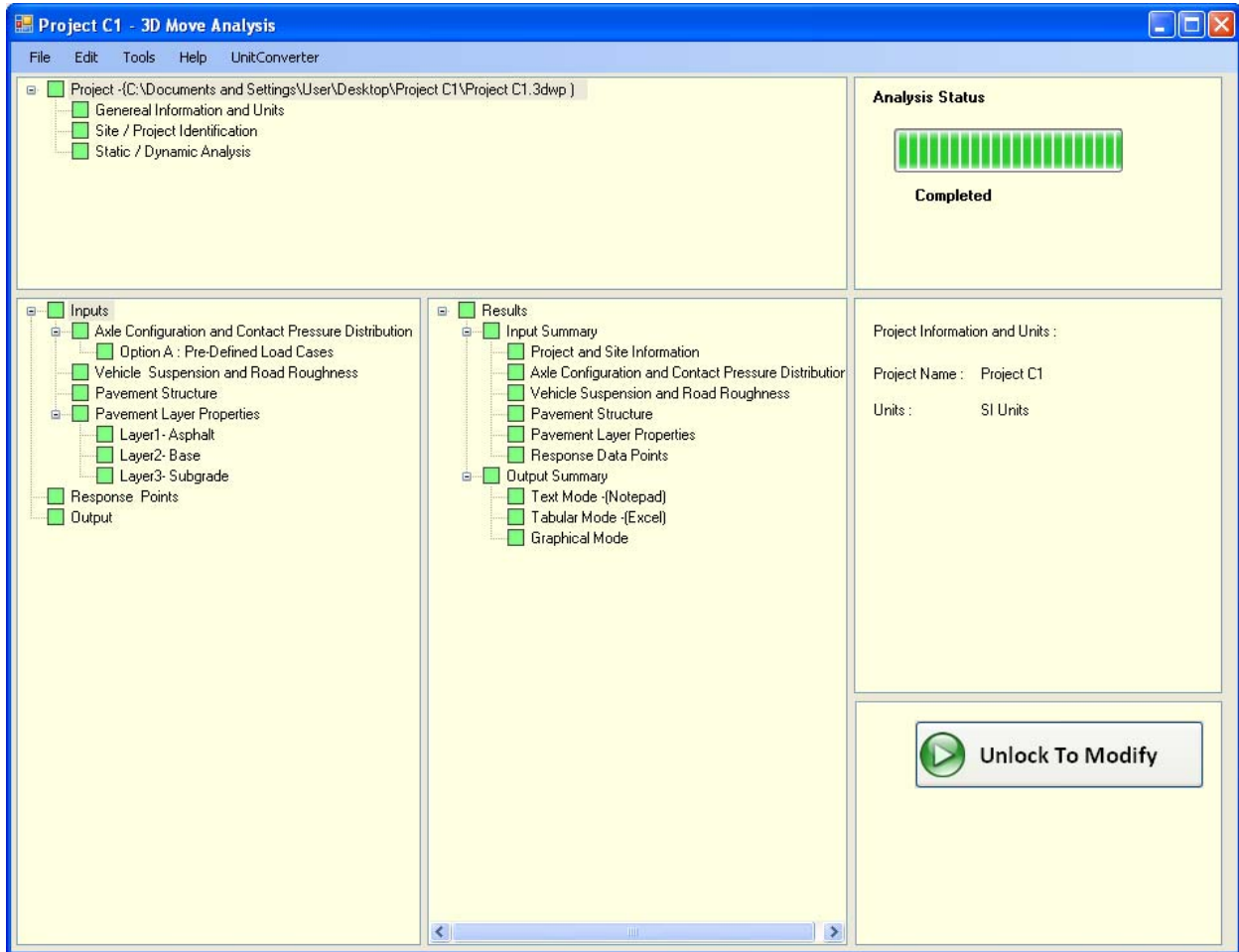


Figure VP3a.1. Main window for the input and output for 3D-Move.

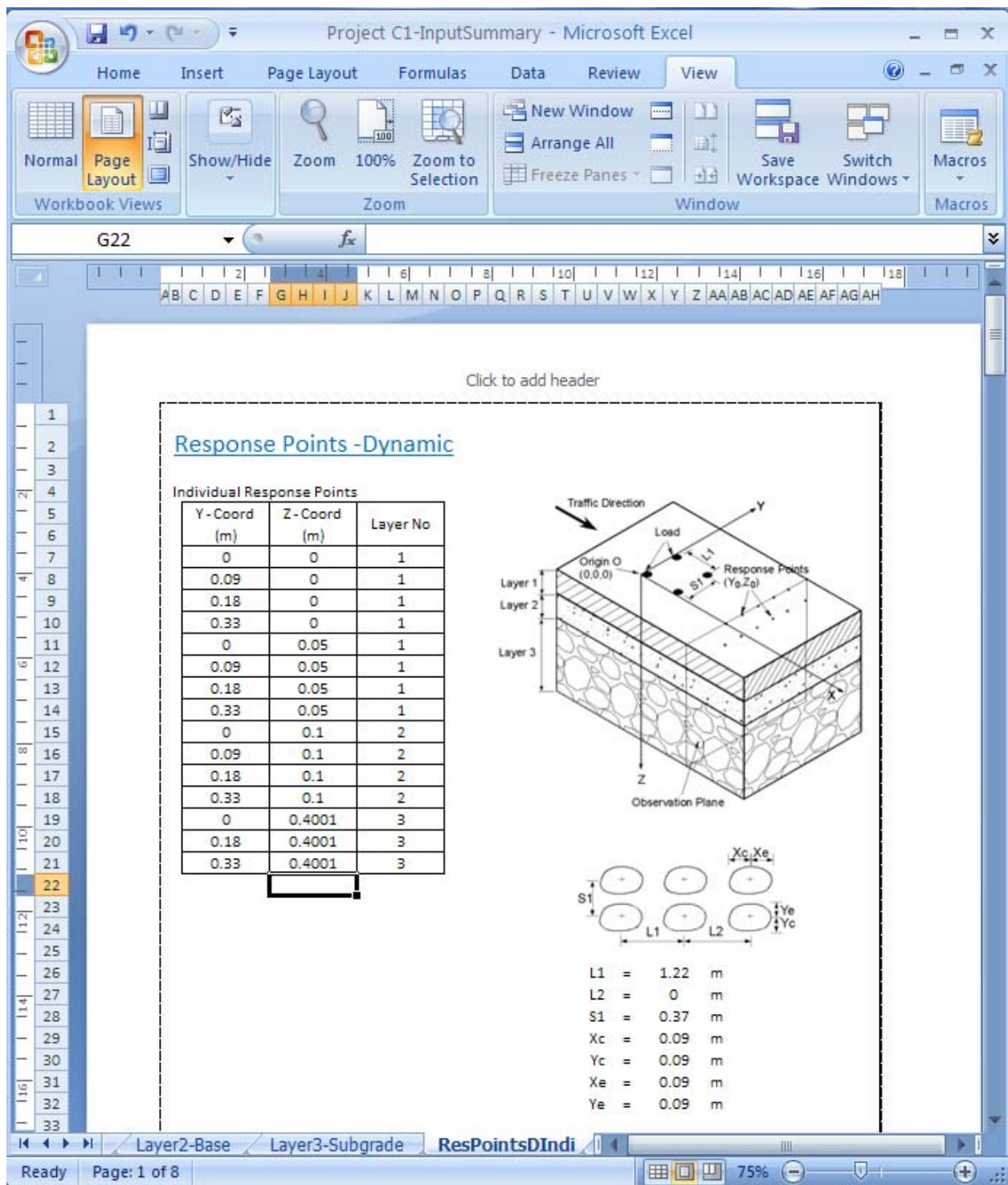


Figure VP3a.2. List of response points where 3D-Move Responses are needed.

```

Project C1_NStress - Notepad
File Edit Format View Help

*****
**
**          L O A D   C A S E   N U M B E R       1          **
**          L O A D   T Y P E   N U M B E R       1          **
**          V E H I C L E   S P E E D           11.11 (m/s)  **
**          *****                                     **

** DATA POINT NUMBER :    1
** LAYER NUMBER          :    1
** COORDINATES ( .0000E+00, .0000E+00)

-----
TIME          SXX          SYX          SZZ
0.00000E+00  -0.56114E+02    0.69422E+01   -0.10274E-05
0.90000E-03  -0.56114E+02    0.69442E+01   -0.10202E-05
0.18000E-02  -0.56114E+02    0.69513E+01   -0.10133E-05
0.27000E-02  -0.56120E+02    0.69624E+01   -0.10043E-05
0.36000E-02  -0.56130E+02    0.69770E+01   -0.99654E-06
0.45000E-02  -0.56140E+02    0.69961E+01   -0.98744E-06
0.54000E-02  -0.56161E+02    0.70201E+01   -0.98291E-06
0.63000E-02  -0.56181E+02    0.70482E+01   -0.98060E-06
0.72000E-02  -0.56204E+02    0.70804E+01   -0.97852E-06
0.81000E-02  -0.56222E+02    0.71174E+01   -0.97521E-06
0.90000E-02  -0.56253E+02    0.71581E+01   -0.97381E-06
0.99000E-02  -0.56283E+02    0.72040E+01   -0.96021E-06
0.10800E-01  -0.56311E+02    0.72541E+01   -0.95052E-06
0.11700E-01  -0.56342E+02    0.73084E+01   -0.94434E-06
0.12600E-01  -0.56384E+02    0.73672E+01   -0.94811E-06
0.13500E-01  -0.56422E+02    0.74314E+01   -0.95592E-06
0.14400E-01  -0.56472E+02    0.74983E+01   -0.94983E-06

```

Figure VP3a.3. Output results – text mode option.

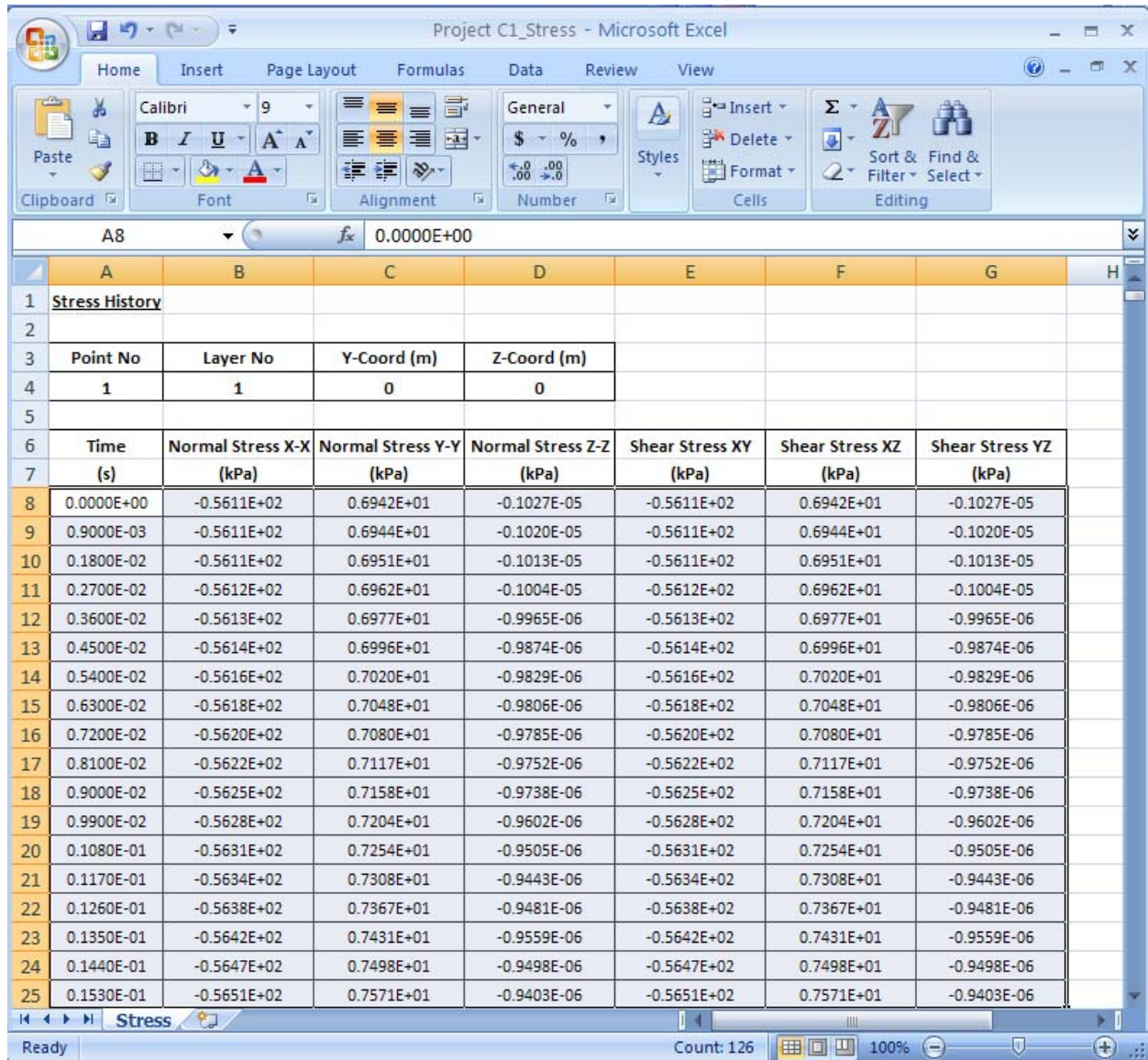


Figure VP3a.4. Output results – tabular mode (Microsoft Excel) option.

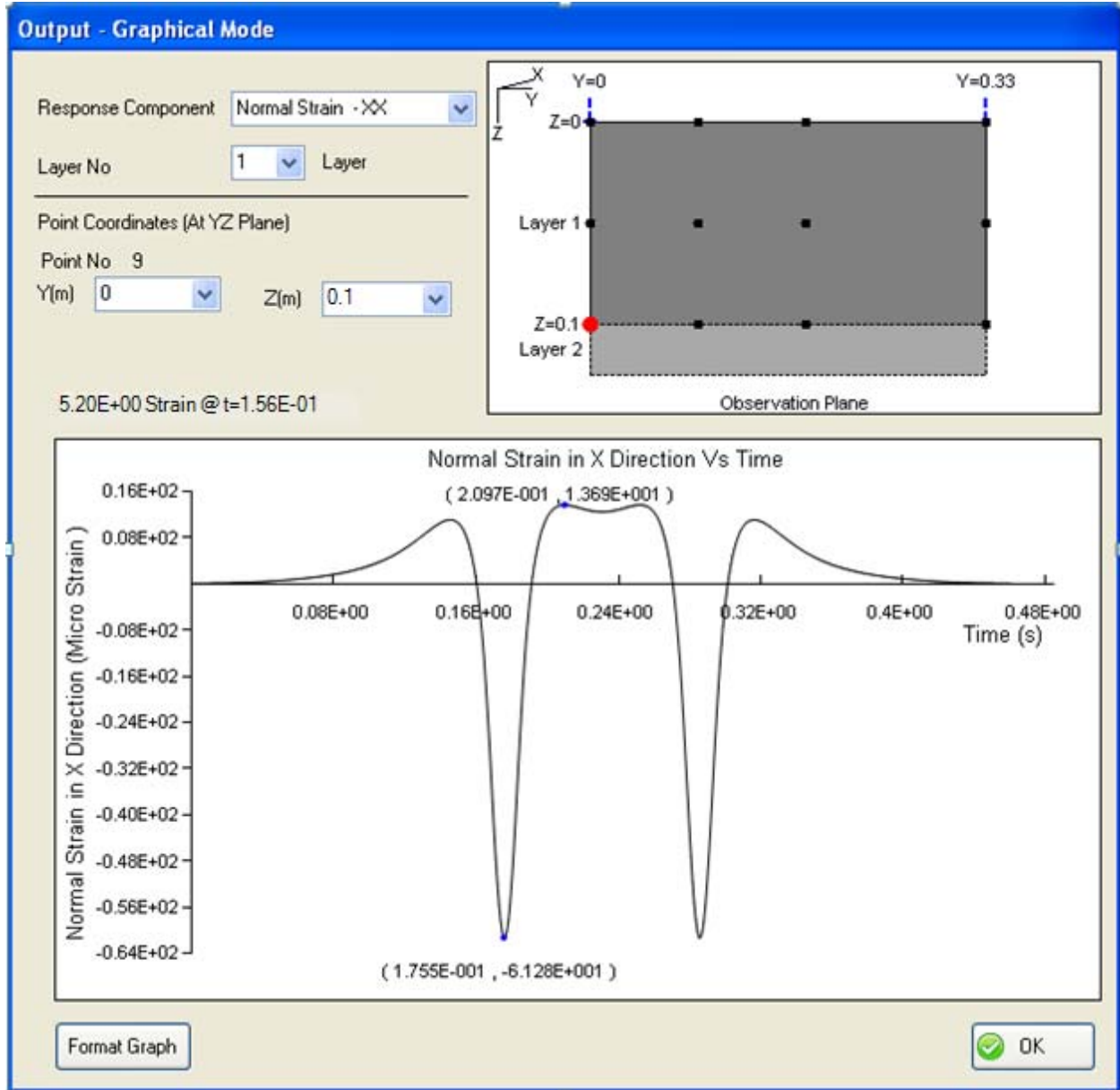


Figure VP3a.4. Output results – Graphical mode option.

Significant Problems, Issues and Potential Impact on Progress

None

Work Planned Next Quarter

Continue working on the 3D-Move model to make it a menu-driven software. Evaluate the beta version for 3D-Move.

Vehicle-Pavement Interaction Year 3	Year 3 (4/2009-3/2010)												Team	
	4	5	6	7	8	9	10	11	12	1	2	3		
(1) Workshop														
VP1a: Workshop on Super-Single Tires														UNR
(2) Design Guidance														
VP2a: Mixture Design to Enhance Safety and Reduce Noise of HMA														UWM
VP2a-1: Evaluate common physical and mechanical properties of asphalt mixtures with enhanced frictional skid characteristics														
VP2a-2: Evaluate pavement macro- and micro-textures and their relation to tire and pavement noise-generation mechanisms														
VP2a-3: Develop a laboratory testing protocol for the rapid evaluation of the macro and micro-texture of pavements														
VP2a-4: Run parametric studies on tire-pavement noise and skid response					JP									M&A,D
VP2a-5: Establish collaboration with established national and international laboratories specialized in transportation noise measurements. Gather expertise on measurements and analysis														
VP2a-6: Model and correlate acoustic response of tested tire-pavement systems														
VP2a-7: Proposed optimal guideline for design to include noise reduction, durability, safety and costs														
(3) Pavement Response Model Based on Dynamic Analyses														
VP3a: Pavement Response Model to Dynamic Loads														UNR
VP3a-1: Dynamic Loads														
VP3a-2: Stress Distribution at the Tire-Pavement Interface														
VP3a-3: Pavement Response Model												SW, v.β		
VP3a-4: Overall Model														

Deliverable codes

- D: Draft Report
- F: Final Report
- M&A: Model and algorithm
- SW: Software
- JP: Journal paper
- P: Presentation
- DP: Decision Point

Deliverable Description

- Report delivered to FHWA for 3 week review period.
- Final report delivered in compliance with FHWA publication standards
- Mathematical model and sample code
- Executable software, code and user manual
- Paper submitted to conference or journal
- Presentation for symposium, conference or other
- Time to make a decision on two parallel paths as to which is most promising to follow through

	Work planned
	Work completed
	Parallel topic

Vehicle-Pavement Interaction Years 2 - 5

	Year 2 (4/08-3/09)				Year 3 (4/09-3/10)				Year 4 (04/10-03/11)				Year 5 (04/11-03/12)				Team
	Q1	Q2	Q3	Q4	Q1	Q2	Q3	Q4	Q1	Q2	Q3	Q4	Q1	Q2	Q3	Q4	
(1) Workshop																	
VP1a: Workshop on Super-Single Tires																	UNR
(2) Design Guidance																	
VP2a: Mixture Design to Enhance Safety and Reduce Noise of HMA																	UWM
VP2a-1: Evaluate common physical and mechanical properties of asphalt mixtures with enhanced frictional skid characteristics				DP													
VP2a-2: Evaluate pavement macro- and micro-textures and their relation to tire and pavement noise-generation mechanisms				DP													
VP2a-3: Develop a laboratory testing protocol for the rapid evaluation of the macro and micro-texture of pavements		M&A		P													
VP2a-4: Run parametric studies on tire-pavement noise and skid response			JP			JP		M&A, D									
VP2a-5: Establish collaboration with established national laboratories specialized in transportation noise measurements. Gather expertise on measurements and analysis																	
VP2a-6: Model and correlate acoustic response of tested tire-pavement systems									JP	D	F						
VP2a-7: Proposed optimal guideline for design to include noise reduction, durability, safety and costs										D	P, F						
(3) Pavement Response Model Based on Dynamic Analyses																	
VP3a: Pavement Response Model to Dynamic Loads																	UNR
VP3a-1: Dynamic Loads			JP							D, F	JP						
VP3a-2: Stress Distribution at the Tire-Pavement Interface										D, F	JP						
VP3a-3: Pavement Response Model								SW, v, β					SW, JP				
VP3a-4: Overall Model													D	F			

Deliverable codes

- D: Draft Report
- F: Final Report
- M&A: Model and algorithm
- SW: Software
- JP: Journal paper
- P: Presentation
- DP: Decision Point

Deliverable Description

- Report delivered to FHWA for 3 week review period.
- Final report delivered in compliance with FHWA publication standards
- Mathematical model and sample code
- Executable software, code and user manual
- Paper submitted to conference or journal
- Presentation for symposium, conference or other
- Time to make a decision on two parallel paths as to which is most promising to follow through

	Work planned
	Work completed
	Parallel topic

PROGRAM AREA: VALIDATION

CATEGORY V1: FIELD VALIDATION

Work element V1a: Use and Monitoring of Warm Mix Asphalt Sections (Year 1 start)

Work Done This Quarter

The small samples obtained from the Yellowstone sections using a masonry drill bit are being analyzed to determine if this is a viable method to obtain pavement aging properties as compared with traditional core samples. Preliminary work has shown that the sampling method may induce some oxidation to the samples on fairly new pavements. Additional comparisons are underway.

Significant Results

None.

Significant Problems, Issues and Potential Impact on Progress

None.

Work Planned Next Quarter

Work will continue to assess the small sampling method.

Work element V1b: Construction and Monitoring of additional Comparative Pavement Validation sites (Year 1 start)

Work Done This Quarter

Laboratory work on samples from the Manitoba RAP sections was begun. The samples are being used (along with others) in the RAP compatibility study being done in Work Element E2b-2. This work is also investigating the blending of RAP and virgin binder as well as the composition of the blended components.

Significant Results

A new comparative pavement performance site using high RAP content, moderate RAP content, and conventional hot-mix was constructed in Manitoba, Canada. This site should provide valuable performance data, especially on the effect of RAP on low temperature properties.

Significant Problems, Issues and Potential Impact on Progress

Partial construction of the warm-mix site in Manitoba Canada was not as planned. The effect of the comparison of materials is to be determined. Resumption of the construction of the warm mix sections is one of the subjects of discussion to be held with Manitoba officials in a meeting on March 3, 2010.

Work Planned Next Quarter

It is planned to continue to analyze the Manitoba samples. A meeting with Manitoba Infrastructure and Transportation officials is planned for March 3, 2010 to discuss the laboratory results obtained to date on the Manitoba RAP sections and to discuss the plans for the warm mix sections planned to be completed in 2010.

CATEGORY V2: ACCELERATED PAVEMENT TESTING

Work element V2a: Accelerated Pavement Testing including Scale Model Load Simulation on Small Test Track (Later start)

Work Done This Quarter

No activity this quarter.

Significant Results

None.

Significant Problems, Issues and Potential Impact on Progress

None.

Work Planned Next Quarter

No accelerated (field) testing is planned.

Work element V2b: Construction of Validation Sections at the Pecos Research & Testing Center (Later start)

This work element is included to indicate that this may be a possibility for accelerated pavement testing for ARC research because it is a facility in the TAMU system.

CATEGORY V3: R&D VALIDATION

Work element V3a: Continual Assessment of Specifications (UWM)

Work Done This Quarter

Work this quarter focused on round-robin testing of binders used in pavements in the 2009 construction region of the Rocky Mountains. The binders were provided by the Western Cooperative Testing Group (WCTG). A database for measured binder, mixture and pavement properties was established. The database will be used to compare new and current PG Plus tests with actual pavement performance, and determine which tests are ultimately more useful in predicting pavement performance.

After discussions with the WCTG board members, letters were drafted to be sent to suppliers and WCTG members requesting relevant project information. The purpose of the letters is to connect the binders tested with a specific project or pavement section so that as much useful information as possible can be collected and added to the database, and to obtain feedback regarding the information that should be included and excluded from the database.

A new elastic recovery (ER) test using the Dynamic Shear Rheometer (DSR) was developed with the goal of replacing the current AASHTO T301 ductility bath procedure. The T301 procedure is very prone to operator variability and inconsistent sample geometry, so an analogous test on the DSR was desired to eliminate these problems. The DSR test has several distinct advantages:

- Automated procedure.
- Smaller sample size.
- Quick and easy sample preparation.
- Testing geometry stays constant throughout the test.
- Temperature control is fast and accurate.
- Strong correlation with T301.

Significant Results

The newly established database will include all the measured binder properties on the WCTG test report, which appears in the ARC Q3 2009 report, along with the coefficient of variation for each property. In addition to binder properties, the database will be expanded to include the following information:

- Mixture information.
 - Nominal maximum aggregate size.
 - Aggregate type.
 - Gradation type.
 - Asphalt content.

- Design equivalent single-axle loads (ESALs).
- Mixture design testing results.
 - Gyration to 92% G_{mm} .
 - Dynamic modulus.
 - Flow number.
 - Deformation rate.
- Project information.
 - Project code.
 - Pavement section (mile post).
 - ESAL (to date).
 - Construction date.
- Pavement performance indicators.
 - Rut depth.
 - Alligator cracking.
 - Transverse cracking.

The drafted letters to suppliers will establish a line of communication to begin collecting this additional data. The letters to WCTG members also proposed additional information to be considered for inclusion in the database, including:

- Mixture testing.
 - LA Wear (AAHTO T96).
 - Soundness (AASHTO T 104).
 - Freeze/thaw (AASHTO T 103).
 - Fractured faces (ASTM 5821).
 - Flat and elongated (ASTM D4791).
 - Fine aggregate angularity (AASHTO T304, method A).
 - Sand equivalency (AASHTO T 176).
 - Gyration compaction: N_{ini} , N_{des} , N_{max} .
 - Air voids, $\%V_a$ ($\%G_{mm}$ @ N_{des}).
 - $\%G_{mm}$ @ N_{ini} .
 - $\%G_{mm}$ @ N_{max} .
 - Dust-to-binder ratio.
 - Voids filled with binder.
 - Tensile Strength Ratio (ASTM 4867).
 - Draindown at production temperature (%).
- Pavement information.
 - Base type.

- Subgrade type.
- Pavement lift thickness.
- Base thickness.
- Pavement performance.
 - Location of rutting.
 - Location of alligator cracking.
 - Location of transverse cracking.

The procedure for the new ER test using the DSR was set up to correlate closely with the current AASHTO T301 ductility bath ER test. Therefore, the following parameters were used:

- Strain rate = 2.32% per second (based on 5-cm elongation per minute).
- Maximum strain = 278% (based on 10-cm elongation).
- Pressure aging vessel (PAV)-aged binder.
- Tests at equal stiffness temperatures, $G^* = 18$ MPa.

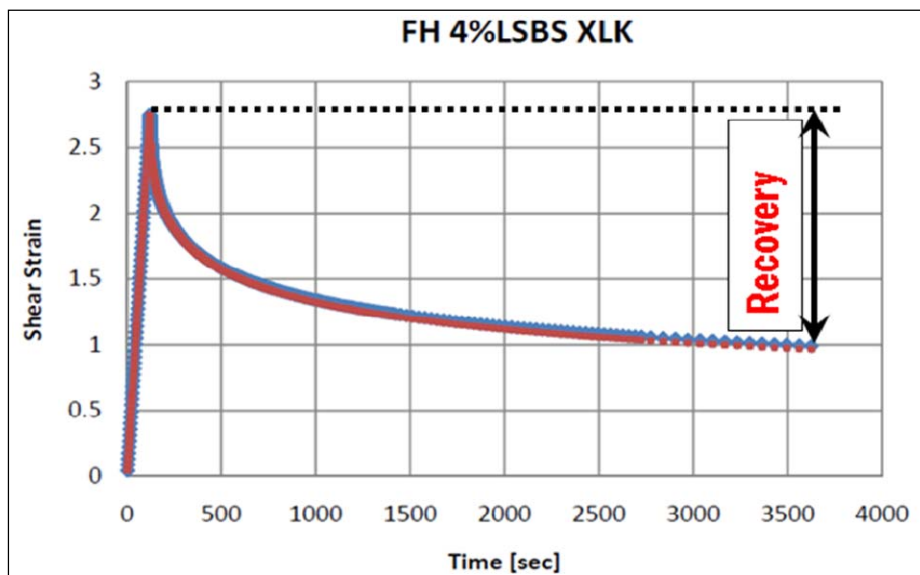


Figure V3a.1. Graph. DSR ER test of an SBS-modified binder. (SBS = styrene-butadiene-styrene; LSBS = linear styrene-butadiene-styrene.)

As figure V3a.1 shows, the data collected using the DSR are very precise and complete. The main difference between the two tests is that the DSR test is performed in shear, whereas T301 is performed in uniaxial tension. Also unlike T301, there is no pause between loading and relaxation in the DSR test.

To validate the results of the new DSR test, a set of four binders modified with different elastomers and plastomers was tested. Two replicates from each binder were tested in the DSR, and the results were compared with those from the traditional T301 test. This comparison is shown in figure V3a.2.

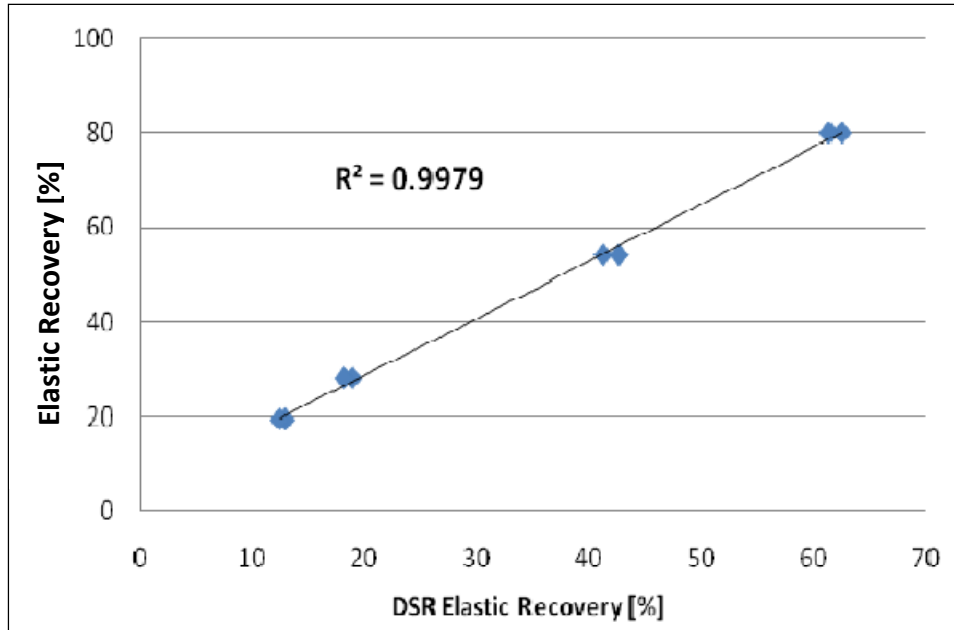


Figure V3a.2. Graph. Correlation of DSR and ductility bath ER test results.

Significant Problems, Issues and Potential Impact on Progress

None.

Work Planned Next Quarter

Round-robin binder testing will continue next quarter. The database, currently hosted by WCTG, will be transferred to University of Wisconsin–Madison in the next quarter. UW-Madison will be responsible for collecting lab results for the database and will host the online database for member access.

A poster session about the new DSR elastic recovery test will take place at the 2010 TRB Annual Meeting.

Work element V3b: Validation of the MEPDG Asphalt Materials Models Using New MEPDG Sites and Selected LTPP Sites (UNR, UWM)

Subtask V3b-1: Design and Build Sections (Start Year 1, Year 2, and Year 3)

Work Done This Quarter

None

Significant Results

None

Significant Problems, Issues and Potential Impact on Progress

Only two agencies have committed to the construction of MEPDG sites: the Washoe RTC in northern Nevada in 2008, The South Dakota DOT in 2009/2010. The researchers are facing significant hesitation from the DOTs to use the MEPDG to design and construct HMA pavements. The level of this work element has been reduced.

Work Planned Next Quarter

Continue discussions with the states to select field sections for the MEPDG validations sites.

Subtask V3b-2: Additional Testing (Start Year 2, Year 3, and Year 4)

Work Done This Quarter

None.

Work Planned Next Quarter

No work planned.

Subtask V3b-3: Select LTPP Sections (Start Year 1 thru Year 5)

Work Done This Quarter

In this quarter, the research group completed the Binder Yield Energy Test (BYET) and the linear amplitude sweep testing of the LTPP binders. Two replicates were tested for each LTPP binder, as shown in table V3b-3.1.

Table V3b-3.1. LTPP binders used for validation of BYET and amplitude sweep tests.

SHRP ID	PG HT [°C]	PG LT [-°C]	Climate*	Fatigue Cracking (m²)	Test Temp	BYET	Amplitude Sweep
04-B901	76	10	DN	328	37	XX	XX
09-0902	64	28	WF	0	22	XX	XX
09-0961	58	34	WF	2.1	16	XX	XX
34-0901	64	22	WF	49.5	25	XX	XX
34-0961	78	28	WF	178.8	28	XX	XX
35-0902	64	22	DN	32	25	XX	XX
37-0962	76	22	WN	0	31	XX	XX
89-A902	52	40	WN	6.7	10	XX	XX

HT = high temperature. LT = low temperature. DN = dry-nonfreeze. WF = wet-freeze. WN = wet-nonfreeze. X = number of replicates.

The stress-strain curves obtained from the BYET tests for the LTPP binders are presented in figure V3b-3.1. From these stress-strain curves two parameters, yield energy (YE) and shear strain at maximum shear stress (GTM) were calculated following the methodology explained in previous quarterly reports.

Figures V3b-3.1 and V3b-3.2 show the relation between the YE and GTM with fatigue cracking, respectively. YE and fatigue cracking have a fairly good correlation if sections 09-0902 and 37-0962 are not included in the calculation of the correlation. To determine if these two sections were outliers, an extra replicate for each section was tested. However, the three replicates tested were repeatable and low coefficient of variation was obtained for the YE and GTM of these two sections. Also, if sections 09-0902 and 37-0962 are not included in the analysis of GTM versus fatigue cracking, a threshold for the maximum GTM allowed can be proposed to minimize fatigue cracking, as shown in figure V3b-3.2. It is important to note that there are several factors (e.g., traffic and structure) that are neglected in this analysis that may contribute to the correlation observed.

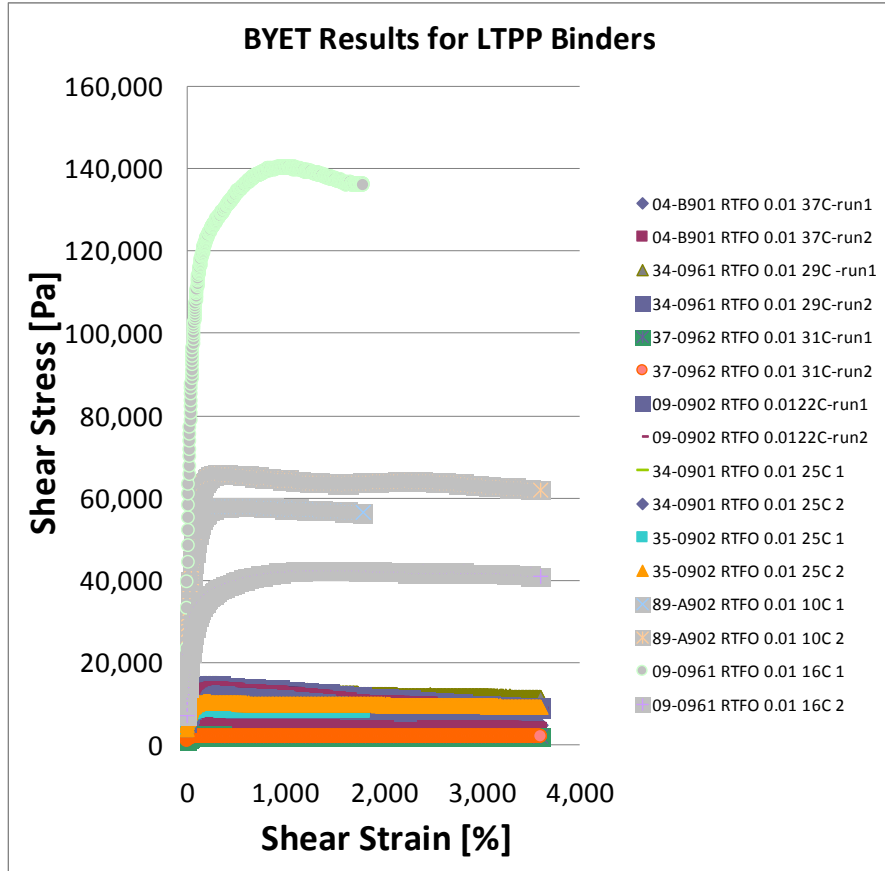


Figure V3b-3.1. Graph. BYET tests for LTPP binders. (RTFO = rolling thin film oven.)

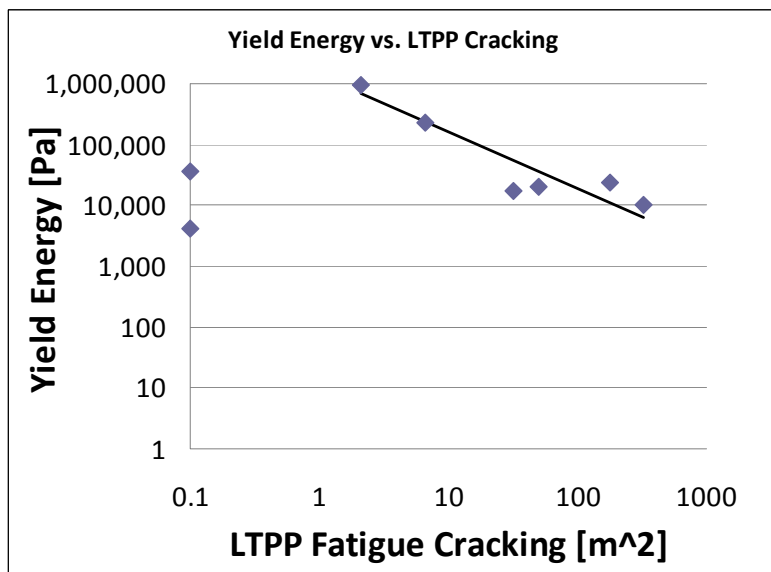


Figure V3b-3.2. Graph. Comparison between fatigue cracking and YE from BYET test of LTPP binders.

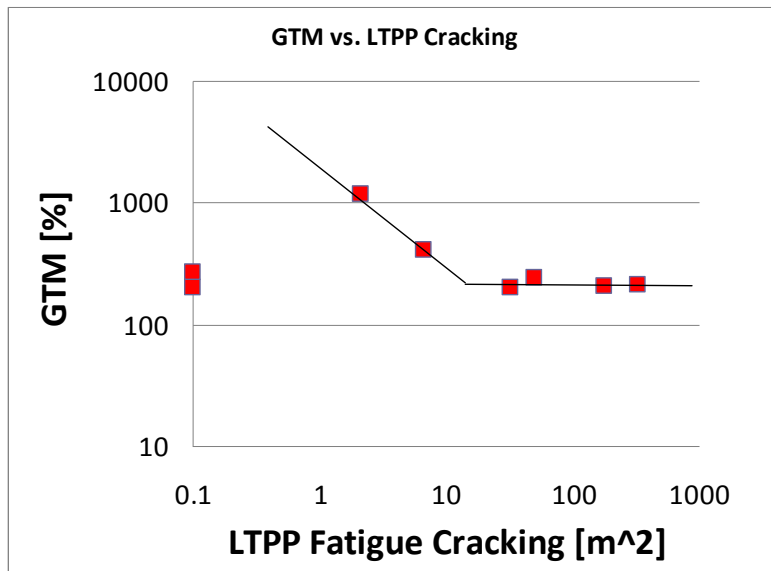


Figure V3b-3.3. Graph. Comparison between fatigue cracking and shear strain at GTM from BYET test of LTPP binders.

The amplitude sweep tests for the LTPP binders are presented in figure V3b-3.4. Good repeatability is observed for all LTPP binders. Results for the amplitude sweep tests were analyzed following the methodology explained in previous quarterly reports and using viscoelastic continuum damage (VECD) theory. The relaxation tests required to estimate (α) were not available this quarter; therefore, the A and B factors could not be calculated. An α value of 2.5 was assumed for all LTPP binders for the preliminary analysis. The research team plans to perform the relaxation or frequency sweep tests for each binder in order to complete the amplitude sweep analysis.

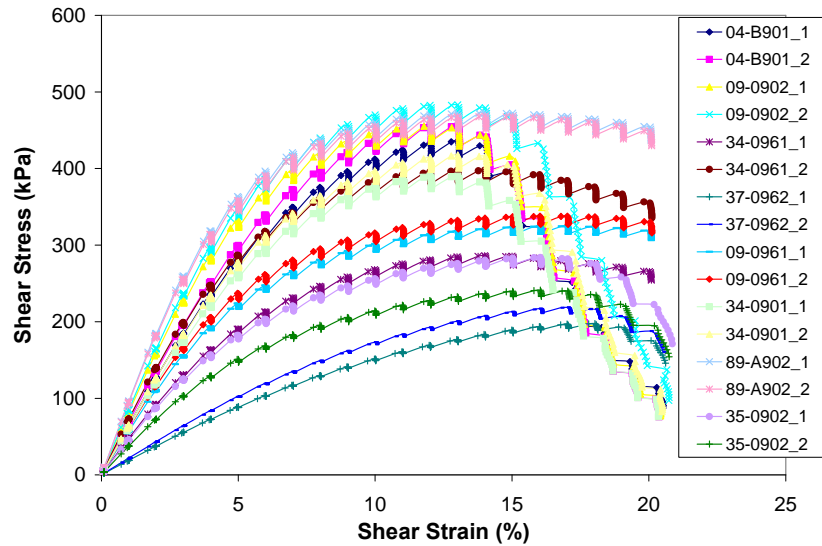


Figure V3b-3.4. Graph. Amplitude sweep tests of LTPP binders.

Table V3b-3.2 presents the results for the VECD analysis of the LTPP binders. The parameter B is not listed because it was assumed to be constant and equal for all binders (B is only a function of α). The coefficient A is directly related to the number of cycles to failure and used to determine correlations with field performance.

Table V3b-3.2. Amplitude sweep tests results for LTPP binders.

Sample	PG	Climate	Test Temperature (°C)	A	N (2.5%)	N (5%)	Fatigue Cracking (m ²)
04-B901_1	76-10	DN	37	3.40E+07	348620	10894	328
04-B901_2	76-10	DN	37	2.73E+07	279292	8728	328
09-0902_1	64-28	WF	22	1.97E+07	201387	6293	0
09-0902_2	64-28	WF	22	1.84E+07	188126	5879	0
34-0961_1	78-28	WF	28	2.03E+07	207939	6498	178.8
34-0961_2	78-28	WF	28	1.75E+07	178891	5590	178.8
37-0962_1	76-22	WN	31	3.49E+08	3571890	111622	0
37-0962_2	76-22	WN	31	2.74E+08	2801490	87547	0
09-0961_1	58-34	WF	16	2.61E+07	267526	8360	2.1
09-0961_2	58-34	WF	16	2.50E+07	256090	8003	2.1
34-0901_1	64-22	WF	25	2.65E+07	271581	8487	49.5
34-0901_2	64-22	WF	25	2.98E+07	305070	9533	49.5
89-A902_1	52-40	WN	10	1.55E+07	159205	4975	6.7
89-A902_2	52-40	WN	10	1.71E+07	175610	5488	6.7
35-0902_1	64-22	DN	25	3.57E+07	365292	11415	32
35-0902_2	64-22	DN	25	3.53E+07	361103	11284	32

Figure V3b-3.5 compares the fatigue cracking observed in the field with the calculated parameter A obtained from amplitude sweep tests and viscoelastic continuum damage theory. There is no clear trend observed between the field performance and the results from the amplitude sweep tests. However, there are important factors such as traffic that are not considered yet in this analysis. Moreover, the assumption of the α values may have a significant impact on the estimation of the parameters of the model and therefore on the prediction of the number of cycles to failure. The research team plans to perform frequency sweep or relaxation tests to determine the α values for better analysis of the results.

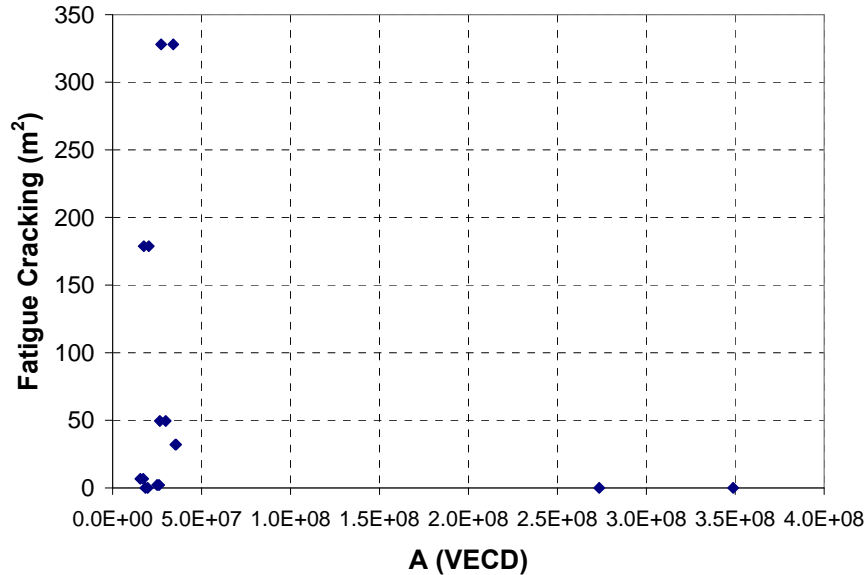


Figure V3b-3.5. Graph. Comparison between fatigue performance and amplitude sweep results of LTPP binders.

Significant Results

The BYET test parameters (i.e., YE and GTM) have a fairly good correlation with the fatigue performance of the pavements, but there are some outliers. The comparison between the fatigue performance and the linear amplitude sweep results do not show a clear relationship yet. However, one of the parameters that define the VECD model was assumed for all binders. Further analysis will be performed to determine the correlation between the VECD parameters and field performance.

Significant Problems, Issues and Potential Impact on Progress

None.

Work Planned Next Quarter

The research group plans to complete the relaxation or frequency sweep tests for the calculation of the α values for the VECD analysis of the amplitude sweep tests. The results from the Double-Edge Notched Tension (DENT) tests performed at Turner-Fairbank Highway Research Center (TFHRC) are expected to be delivered to the research team at the University of Wisconsin–Madison.

The research team will also start working on selecting LTPP sections for which low-temperature cracking and moisture damage (i.e., stripping) performance is available. Based on the asphalt binders and mixtures selected, an experimental plan for validation of the testing procedures of the thermal cracking and affinity of aggregate-binder work elements will be proposed.

Subtask V3b-4: Testing of Extracted Binders from LTPP Sections (Start Year 1)

Work Done This Quarter

None.

Work Planned Next Quarter

No work planned.

Subtask V3b-5: Review and Revisions of Materials Models (Start Year 2, Year 3, Year 4, and Year 5)

Work Done This Quarter

No work planned.

Subtask V3b-6: Evaluate the Impact of Moisture and Aging (Start Year 3, Year 4, and Year 5)

No activity to date.

Validation Year 3	Year 3 (4/2009-3/2010)											Team	
	4	5	6	7	8	9	10	11	12	1	2		3
(1) Field Validation													
V1a: Use and Monitoring of Warm Mix Asphalt Sections													WRI
V1b: Construction and Monitoring of additional Comparative Pavement Validation sites													WRI
(2) Accelerated Pavement Testing													
V2a: Accelerated Pavement Testing including Scale Model Load Simulation on small test track (This work element will include all accelerated pavement testing)													WRI
V2b: Construction of validation sections at the Pecos Research & Testing Center													WRI
(3) R&D Validation													
V3a: Continual Assessment of Specification													UWM
V3a-1: Evaluation of the PG-Plus practices and the motivations for selecting the "plus" tests.													
V3a-2: Detailed analysis of all PG-Plus tests being proposed or in use today, documentation of benefits and costs of these tests, and comparison with new tests			D										
V3a-3: Development of protocols for new binder tests and database for properties measured					JP								
V3a-4: Development of specification criteria for new tests based on field evaluation of construction and performance						D					P		
V3a-5: Interviews and surveys for soliciting feedback on binder tests and specifications													
V3b: Validation of the MEPDG Asphalt Materials Models and Early Verification of Technologies Developed by ARC using new MEPDG Sites and Selected LTPP sites													UNR/UWM/WRI
V3b-1: Design and Build Sections													UNR
V3b-2: Additional Testing (if needed)													
V3b-3: Select LTPP Sites to Validate New Binder Testing Procedures							DP				P		UWM
V3b-4: Testing of Extracted Binders from LTPP Sections													
V3b-5: Review and Revisions of Materials Models													
V3b-6: Evaluate the Impact of Moisture and Aging													

Deliverable codes

- D: Draft Report
- F: Final Report
- M&A: Model and algorithm
- SW: Software
- JP: Journal paper
- P: Presentation
- DP: Decision Point

Deliverable Description

- Report delivered to FHWA for 3 week review period.
- Final report delivered in compliance with FHWA publication standards
- Mathematical model and sample code
- Executable software, code and user manual
- Paper submitted to conference or journal
- Presentation for symposium, conference or other
- Time to make a decision on two parallel paths as to which is most promising to follow through

- Work planned
- Work completed
- Parallel topic

Validation Years 2 - 5	Year 2 (4/08-3/09)				Year 3 (4/09-3/10)				Year 4 (04/10-03/11)				Year 5 (04/11-03/12)				Team
	Q1	Q2	Q3	Q4	Q1	Q2	Q3	Q4	Q1	Q2	Q3	Q4	Q1	Q2	Q3	Q4	
(1) Field Validation																	
V1a: Use and Monitoring of Warm Mix Asphalt Sections																	WRI
V1b: Construction and Monitoring of additional Comparative Pavement Validation sites																	WRI
(2) Accelerated Pavement Testing																	
V2a: Accelerated Pavement Testing including Scale Model Load Simulation on small test track																	WRI
V2b: Construction of validation sections at the Pecos Research & Testing Center																	WRI
(3) R&D Validation																	
V3a: Continual Assessment of Specification																	UWM
V3a-1: Evaluation of the PG-Plus practices and the motivations for selecting the "plus" tests.		P	D,F														
V3a-2: Detailed analysis of all PG-Plus tests being proposed or in use today, documentation of benefits and costs of these tests, and comparison with new tests				P	D												
V3a-3: Development of protocols for new binder tests and database for properties measured						JP				P							
V3a-4: Development of specification criteria for new tests based on field evaluation of construction and performance						D		P	P			JP	P		JP		
V3a-5: Interviews and surveys for soliciting feedback on binder tests and specifications									P		JP		P		D	F	
V3b: Validation of the MEPDG Asphalt Materials Models and Early Verification of Technologies Developed by ARC using new MEPDG Sites and Selected LTPP sites																	UNR/UWM
V3b-1: Design and Build Sections										D, F							
V3b-2: Additional Testing (if needed)																	
V3b-3: Select LTPP Sites to Validate New Binder Testing Procedures						DP		P		JP		P			D	F	
V3b-4: Testing of Extracted Binders from LTPP Sections																	
V3b-5: Review and Revisions of Materials Models																	D, F
V3b-6: Evaluate the Impact of Moisture and Aging																	D, F

Deliverable codes

D: Draft Report
 F: Final Report
 M&A: Model and algorithm
 SW: Software
 JP: Journal paper
 P: Presentation
 DP: Decision Point

Deliverable Description

Report delivered to FHWA for 3 week review period.
 Final report delivered in compliance with FHWA publication standards
 Mathematical model and sample code
 Executable software, code and user manual
 Paper submitted to conference or journal
 Presentation for symposium, conference or other
 Time to make a decision on two parallel paths as to which is most promising to follow through

 Work planned
 Work completed
 Parallel topic

PROGRAM AREA: TECHNOLOGY DEVELOPMENT

Work element TD1: Prioritize and Select Products for Early Development (Year 1)

Work Done This Quarter

None. This work element has been completed.

Significant Results

Six early technology development projects have been identified and all have received favorable ratings from the ETGs.

Work element TD2: Develop Early Products (Year 3)

Work Done This Quarter

AAT received the completed hardware and software to implement the continuum damage test in the Asphalt Mixture Performance Tester from Interlaken Technology Corporation (ITC). The hardware includes: (1) 16 tension loading platens, (2) tension clamps, and (3) a gluing fixture to glue four specimens at one time. The software includes control and data acquisition to conduct cyclic tension-compression in controlled strain with minimal permanent deformation.

Initial testing with this hardware and software was conducted before accepting the work. This testing revealed slipping problems with the tension clamps originally supplied by ITC. AAT assisted ITC with the design of improved clamps, which eliminated the slipping problems. Further testing with the improved clamps indicated backlash when going through zero probably due to the combination of the small commanded movement of the actuator and clearance in the seals in the actuator. The servo controller of the AMPT machine is capable of adjusting for this backlash at 1 Hz, and slower, but not at 10 Hz. AAT reviewed the continuum damage reduced cycles derivation to determine what modifications would be needed to perform the fatigue testing at 1 Hz. This analysis confirmed that the continuum damage reduced cycles testing can be performed at any frequency. Considering the both the flexible of the analysis and the ease of future implementation, AAT decided the fatigue test should be implemented in the AMPT using 1 Hz loading. The draft standard test method for the AMPT was modified to use 1 Hz loading.

Significant Results

A complete continuum damage fatigue system has been assembled for the Interlaken AMPT owned by the NCHRP. An Excel spreadsheet to perform the reduced cycles analysis has been developed. A draft standard test method for performing fatigue testing and analyzing the data using the reduced cycles analysis has been prepared.

Significant Problems, Issues and Potential Impact on Progress

None.

Work Planned Next Quarter

The test method and equipment will be applied to fatigue data from several mixtures. A ruggedness testing plan for the simplified continuum damage fatigue test will be developed.

Work element TD3: Identify Products for Mid-Term and Long-Term Development (Years 2, 3, and 4)

Work Done This Quarter

The research team continued to review interim research products to identify potential mid-term and long-term development projects.

Significant Results

None

Work Planned Next Quarter

The research team will continue to review interim research products to identify potential mid-term and long-term development projects.

Work Element TD4: Develop Mid-Term and Long-Term Products (Years 3, 4, and 5)

This activity is planned for later in the project.

PROGRAM AREA: TECHNOLOGY TRANSFER

CATEGORY TT1: OUTREACH AND DATABASES

Work element TT1a: Development and Maintenance of Consortium Website (Duration: Year 1 through Year 5)

Work Done This Quarter

The ARC website was maintained and updated. The ARC quarterly technical progress report, Jul 1- Sept 30, was uploaded to the ARC website. Information on the intensive course on “Advanced Constitutive Modeling and Characterization of Asphaltic Materials” was added to the ARC website.

Significant Results

None

Significant Problems, Issues and Potential Impact on Progress

None

Work Planned Next Quarter

Continue maintaining and updating the ARC website.

Work element TT1b: Communications (Duration: Year 1 through Year 5)

Work Done This Quarter

None

Significant Results

None

Significant Problems, Issues and Potential Impact on Progress

None

Work Planned Next Quarter

Prepare and publish the sixth ARC Newsletter.

Work element TT1c: Prepare Presentations and Publications

Presentations

Bahia, H. U., A. Hanz, T. Miller, and P. Johannes. “Emulsion Task Force Update: Improvement of Emulsions’ Characterization and Mixture Design for Cold Bitumen Applications.” Emulsion Task Force, Scottsdale, Arizona, December 14, 2009.

Bahia, H. U., E. Mahmoud, and A. Hanz, “Quantifying the Effects of Warm Mix Additives on Workability of Mixtures using the Gyrotory Compactor and Asphalt Lubricity Test,” WMA Technical Working Group, Seattle, Washington, December 16, 2009.

Bahia, H. U., S. Mangiafico, and R. Velasquez, “Low Temperature Pooled Fund Study Phase II: Physical Hardening of Binders,” Low-Temperature Pooled Fund Project Meeting, Minneapolis, Minnesota, November 18, 2009.

Faheem, A. F., and H. U. Bahia, “Evaluation of PG Plus Testing Methods by the Asphalt Research Consortium,” Annual Meeting of the Rocky Mountain Asphalt User Producer Group, Denver, Colorado, October 20, 2009.

Faheem, A. F., and H. U. Bahia, “Evaluation of Rutting Characterization Testing Methods by the Asphalt Research Consortium,” Annual Meeting of the Rocky Mountain Asphalt User Producer Group, Denver, Colorado, October 20, 2009.

Miller, T. and H. U. Bahia. “Establishing a Framework for Analyzing Asphalt Pavement Sustainability.” ENVIROAD Conference 2009, Warsaw, Poland, October 15, 2009.

Publications

Hanz, A., Z. Arega, and H. U. Bahia, 2009, “Rheological Behavior of Emulsion Residues Produced by an Evaporative Recovery Method.” *Transportation Research Board 89th Annual Meeting*, accepted.

Hanz, A., A. F. Faheem, E. Mahmoud, and H. U. Bahia, 2009, “Measuring Effects of Warm-Mix Additives Using a Newly Developed Asphalt Binder Lubricity Test for DSR.” *Transportation Research Board 89th Annual Meeting*, accepted.

Ma, T., E. Mahmoud, and H. U. Bahia, 2009, “Development of Testing Procedure for Estimation of RAP Binder Low-Temperature Properties Without Extraction.” *Transportation Research Board 89th Annual Meeting*, accepted.

Ma, T., H.U. Bahia, E. Mahmoud, and E. Hajj, 2009, “Estimating Allowable RAP in Asphalt Mixes to Meet Target Low Temperature PG Requirements.” *Association of Asphalt Paving Technologists 85th Annual Meeting*, accepted.

Miller, T. and H. U. Bahia, 2009, “Establishing a Framework for Analyzing Asphalt Pavement Sustainability.” *International Journal of Pavement Research and Technology*, accepted.

Prapaitrakul, Nikornpon, Rongbin Han, and Charles J. Glover (2009). “A Transport Model of Asphalt Binder Oxidation in Pavements.” *Road Materials and Pavement Design*, 10 (Special Issue): 95-113.

Work element TT1d: Development of Materials Database (Duration: Year 2 through Year 5)

Work Done This Quarter

Development continued on the ARC database project this quarter. Development and testing of the database also continued this quarter. New forms have been added to the database or enhanced. This includes a form to edit materials and validation sites and to filter selection criteria.

Significant Results

The work task hierarchy has been incorporated into the database and the materials editor. Subtasks are linked to materials, reports, and validation sites, which allows for filtering of records based on the related work. For instance, a user will be able to view reports or materials related to a given Subtask, Work Element, etc. figure TT1d.1 shows the Materials form along with newly enhanced filtering of materials based on primary organization and source. This filtering will be increasing useful as the number of records grows.

The Measures Editor has been expanded to manage validation site information. The database is expected to hold validation site information sufficient to locate specific field tests. Each layer and section of a site can be recorded. A layer has a corresponding material in the database, which can be assigned one or many properties. A validation material may have any number of core samples associated, and each property of the material may have a measure corresponding to a sample. Figure TT1d.2 shows the user interface for validation site detail.

The ability to attach property measures to materials is now fully functional. Both lab and validation site measures may be stored, the only difference being that lab measures don't have site and field sample records attached. Figure TT1.d3 shows the completed filtering and viewing options for property measures. Because each material may have any number of measures associated with it, a user might wish to narrow down the results by date range, organization, or user.

Asphalt Research Consortium

Home Outreach Project Team Research Publications Workshops Newsletters Contacts Links

Logout tweetj

Materials Database

Home Page
Property Group
Materials
Properties
Measures
Material Types
Manage Tasks
Transfer Files
My Account
Manage Roles
Manage Users
Manage Organizations
Manage Suppliers

MESSAGES

Help

Select Material To Edit From Tree:

Filters: Material Type Material Category Primary Organization Source

Work Tasks Aggregate ▾ [ALL] ▾ University of Nevada, Reno ▾ Lockwood ▾

Program Area:	Engineered Materials (E) ▾
Category:	E1: Modeling ▾
Work Element:	E1a: Analytical and Micro-mechanics Models for Mechanical Behavior of Mixtures ▾
Subtask:	E1a-1: Analytical Micromechanical Models of Binder Properties ▾

xyz UNR (Lockwood)

Detach Component Fr...

Figure TT1d.1. Work task filters.

Asphalt Research Consortium

Home Outreach Project Team Research Publications Workshops Newsletters Contacts Links

Logout tweetj

Materials Database

Home Page
Property Group
Materials
Properties
Measures
Material Types
Manage Tasks
Transfer Files
My Account
Manage Roles
Manage Users
Manage Organizations
Manage Suppliers

MESSAGES

Access selector is for testing and demonstration purposes

Admin

SELECTOR

Lab Measures Field Measures

Select Validation Item

Select Validation Site Test Site

Site Description	Test Site
Site Code	xx
Contractor	Test Contractor 1
Contact	Joe Smith
Comment	comment

[Edit](#) [New](#) [Delete](#)

Select Validation Section Section 1

Section Description	Section 1
Start Location	1000
End Location	3000
Location Units	Meters

[Edit](#) [New](#) [Delete](#)

Select Layer 2

Layer	2
Pour Date	12/10/2009 12:00:00 AM
Material	xyz UNR (Lockwood)

[Edit](#) [New](#) [Delete](#)

Select Field Sample Core Sample 1

Sample Description	Core Sample 1
Sample Date	12/31/2009 12:00:00 AM
Sample Type	Core
Diameter	
Depth	

[Edit](#) [New](#) [Delete](#)

Figure TT1d.2. Validation site editor.

Filters

Organization: University of Nevada, Reno User: [ALL]

Select Date Range

Start Date

December 2009								
<	Sun	Mon	Tue	Wed	Thu	Fri	Sat	>
	29	30	1	2	3	4	5	
	6	7	8	9	10	11	12	
	13	14	15	16	17	18	19	
	20	21	22	23	24	25	26	
	27	28	29	30	31	1	2	
	3	4	5	6	7	8	9	

End Date

January 2010								
<	Sun	Mon	Tue	Wed	Thu	Fri	Sat	>
	27	28	29	30	31	1	2	
	3	4	5	6	7	8	9	
	10	11	12	13	14	15	16	
	17	18	19	20	21	22	23	
	24	25	26	27	28	29	30	
	31	1	2	3	4	5	6	

Views

Measure Browser Quantitative Properties Hide Empty Properties

Bulk Editor (Under Construction) Qualitative Properties

Figure TT1d.3. Property measures filter.

Figure TT1d.4 shows a sample view of property measures generated by the selections made in figures TT1d.2 and TT1d.3. The Measure Browser view is shown, with both quantitative and qualitative properties visible. The Measure Browser is designed to allow easy navigation and visualization of properties which have multiple measures. Each property of a material can be expanded to display a grid showing all related measures. Each property may have a unit of measure associated with it, which is applied in this view to determine the numeric format and display symbol. While all measure editing functions can be performed in this view and are now operational, a spreadsheet-like Bulk Editor view is also being developed to allow rapid data entry by consortium members where only a single measure is relevant for each property.

Quantitative Properties

AGG_SIEVE				Expand All
Property	Σ	Most Recent Value (toggle group or row to view all)		
PASSING_3/4	1	90.00	%	New
PASSING_1/2	6	70.00	%	New
PASSING_No4	1	55.55	%	New
PASSING_No200	1	25.00	%	New
AGG_COARSE_BSG				Expand All
Property	Σ	Most Recent Value (toggle group or row to view all)		
BSG_DRY	1	10.00		New
BSG_SSD	1	20.00		New
BSG_APP	1	30.00		New
ABS	1	40.00	%	New

Qualitative Properties

AGG_TYPE				Expand All
Property	Σ	Most Recent Value (toggle group or row to view all)		
	1	Test Value 1		New

Figure TT1d.4. Sample view of property measures.

The prototype system created last quarter to upload and download research reports and other files has been enhanced. Authenticated users can upload files from to the ARC database and download research reports. Authorized users can upload a report thereby submitting it for approval. The user interface has been expanded so that a second category of authorized users can approve research reports for consumption by public users.

A messages section has been added to all of the user interface forms so as to communicate diagnostic and error messages back to the end user. This enhancement provides a consistent user interface with which to communicate data back to the end user.

Work has started for the application's Help system. Each form has a Help button which with the user will be able to get usage help for a particular form or application feature. At present, the structure of the Help system is in place. Help content will continue to be developed this quarter. Formatting of the end-user forms has been improved through the consistent use of cascading style sheets. As new forms are created or modified, these cascading style sheets will simplify the process of formatting.

Significant Problems, Issues and Potential Impact on Progress

None

Work Planned Next Quarter

- Continued development of property measurement interface.
- Creation of the framework and user interface to enter material source records.
- Creation of a graphical navigator for validation second grid to aid visualization and ease of use.
- Using the role-based infrastructure already created; restrict access to specific forms and functions as defined by the project coordinator.
- Complete transactional logging system.
- Create and provide initial training for ARC Consortium users.

Work element TT1e: Development of Research Database (Duration: Year 2 through Year 5)

Work Done This Quarter

Uploaded the quarterly technical progress report to the ARC website.

Significant Results

None

Significant Problems, Issues and Potential Impact on Progress

None

Work Planned Next Quarter

Upload the ARC quarterly technical progress report to the ARC website.

Work Element TT1f: Workshops and Training

Work Done This Quarter

No activity this quarter.

Significant Results

None

Significant Problems, Issues and Potential Impact on Progress

None

Work Planned Next Quarter

A Database initial training workshop for ARC Consortium users will be held on March 11, 2010 at UNR campus.

Technology Transfer Year 3	Year 3 (4/2009-3/2010)												Team
	4	5	6	7	8	9	10	11	12	1	2	3	
(1) Outreach and Databases													
TT1a: Development and Maintenance of Consortium Website													UNR
TT1b: Communications													UNR
TT1c: Prepare presentations and publications													UNR
TT1d: Development of Materials Database													UNR
TT1d-1: Identify the overall Features of the Web Application													
TT1d-2: Identify Materials Properties to Include in the Materials Database													
TT1d-3: Define the Structure of the Database													
TT1d-4: Create and Populate the Database									SW, v, β			SW	
TT1e: Development of Research Database													UNR
TT1e-1: Identify the Information to Include in the Research Database													
TT1e-2: Define the Structure of the Database													
TT1e-3: Create and Populate the Database													
TT1f: Workshops and Training													UNR

Deliverable codes

- D: Draft Report
- F: Final Report
- M&A: Model and algorithm
- SW: Software
- JP: Journal paper
- P: Presentation
- DP: Decision Point

Deliverable Description

- Report delivered to FHWA for 3 week review period.
- Final report delivered in compliance with FHWA publication standards
- Mathematical model and sample code
- Executable software, code and user manual
- Paper submitted to conference or journal
- Presentation for symposium, conference or other
- Time to make a decision on two parallel paths as to which is most promising to follow through

- Work planned
- Work completed
- Parallel topic

Technology Transfer Years 2 - 5

	Year 2 (4/08-3/09)				Year 3 (4/09-3/10)				Year 4 (04/10-03/11)				Year 5 (04/11-03/12)				Team
	Q1	Q2	Q3	Q4	Q1	Q2	Q3	Q4	Q1	Q2	Q3	Q4	Q1	Q2	Q3	Q4	
(1) Outreach and Databases																	
TT1a: Development and Maintenance of Consortium Website																	UNR
TT1b: Communications																	UNR
TT1c: Prepare presentations and publications																	ALL
TT1d: Development of Materials Database																	UNR
TT1d-1: Identify the overall Features of the Web Application																	
TT1d-2: Identify Materials Properties to Include in the Materials Database																	
TT1d-3: Define the Structure of the Database																	
TT1d-4: Create and Populate the Database								SW, v, β	SW								
TT1e: Development of Research Database																	UNR
TT1e-1: Identify the Information to Include in the Research Database																	
TT1e-2: Define the Structure of the Database																	
TT1e-3: Create and Populate the Database																	
TT1f: Workshops and Training																	UNR

Deliverable codes

D: Draft Report
 F: Final Report
 M&A: Model and algorithm
 SW: Software
 JP: Journal paper
 P: Presentation
 DP: Decision Point

Deliverable Description

Report delivered to FHWA for 3 week review period.
 Final report delivered in compliance with FHWA publication standards
 Mathematical model and sample code
 Executable software, code and user manual
 Paper submitted to conference or journal
 Presentation for symposium, conference or other
 Time to make a decision on two parallel paths as to which is most promising to follow through

 Work planned
 Work completed